Fabrication, Characterization of Zeolite-Ceramic Composite Membranes and Their Application in Separation of Metal Ions from Aqueous Solution

Thesis submitted in partial fulfillment of the requirements for the degree of

DOCTOR OF PHILOSOPHY

by

Ashim Kumar Basumatary

Department of Chemical Engineering

Indian Institute Technology, Guwahati

Guwahati-781039, India

August 2015

Fabrication, Characterization of Zeolite-Ceramic Composite Membranes and Their Application in Separation of Metal Ions from Aqueous Solution

Thesis submitted in partial fulfillment of the requirements for the degree of

DOCTOR OF PHILOSOPHY

by

Ashim Kumar Basumatary

Roll No.126107031

Department of Chemical Engineering

Indian Institute Technology, Guwahati

Guwahati-781039, India

August 2015

Dedicated

To

My Parents

Department of Chemical Engineering

Indian Institute of Technology Guwahati

Guwahati-781039, India

Certificate

This is to certify that the thesis entitled "**Fabrication, Characterization of Zeolite-Ceramic Composite Membranes and Their Application in Separation of Metal Ions from Aqueous Solution**" being submitted by **Mr. Ashim Kumar Basumatary** for the award of PhD degree has been carried out under my guidance and supervision. The work documented in this thesis has not been submitted to any other University or Institute for the award of any degree or diploma.

_____

(Signature of Thesis Supervisor)

Dr. G. Pugazhenthi

Professor

Department of Chemical Engineering

Indian Institute of Technology Guwahati

Guwahati-781039, Assam, India

Date:

Abstract

This work reports the fabrication and characterization of MCM-41, MCM-48, Faujasite (FAU) and Analcime-C zeolite-ceramic composite membrane on porous circular shaped ceramic support by hydrothermal synthesis method. A facile uni-axial compaction method was employed for the preparation of ceramic support from low-cost clay materials such as quartz, kaolin, ball clay, feldspar, pyrophyllite and calcium carbonate, and sintered at 950 °C. The hydrothermal synthesis reaction was carried out with ceramic support in Teflon coated stainless steel autoclave reactor using gel composition (molar) of 1TEOS:0.1CTAB:0.3NaOH:60H_2O, 1TEOS:0.25Na_2O:0.65CTAB:0.62H_2O, 70Na_2O:Al_2O_3:20SiO_2:2000H_2O and 4.2Na_2O:Al_2O_3:21.3SiO_2:340H_2O:2.2TEA for the preparation of MCM-41, MCM-48, FAU and Analcime-C membranes. The synthesized zeolite powders and zeolite-ceramic composite membranes were systematically characterized by X-ray diffraction (XRD), thermogravimetric analysis (TGA), nitrogen adsorption-desorption isotherm (BET), Fourier transform infrared spectroscopy (FTIR), zeta potential measurement, field emission scanning electron microscopy (FESEM), porosity, pure water and solvent permeability tests. The formation as well as structure of MCM-41, MCM-48, FAU and Analcime-C zeolite are verified by XRD analysis. The mechanism of template removal and necessary calcination temperature for the fabrication of zeolite membranes are identified from the TGA profile of as-synthesized MCM-41, MCM-48 and Analcime-C samples. Accordingly, MCM-41 and MCM-48 membranes were calcined at 550 ^oC while analcime-C membrane was calcined at 400 ^oC. In addition, the disappearance of C-H stretching band corresponding to the hydrocarbon chain of surfactant molecules in the FTIR spectra confirms the removal of surfactant (template) from the calcined MCM-41, MCM-48 and Analcime-C samples. N_2 adsorption/desorption isotherm of MCM-41 and MCM-48 powder corresponds to typical type IV isotherm and exhibits capillary condensation steps

indicating the characteristic of the mesoporous material. The isoelectric point of MCM-41, MCM-48, FAU and Analcime-C is found to be 3.9, 3.2, 3.8 and 5.6, which are determined by zeta potential measurement. The porosity of the ceramic support reduces from 47 to 23, 22, 33, 24%, with the deposition of MCM-41, MCM-48, FAU, Analcime-C zeolite, respectively and the average pore size of the support also decreases from 1.0 to 0.173, 0.142, 0.153, 0.155 μm. It is evident from FESEM images that the surface of the ceramic support is completely covered with zeolite particles of perfect morphology and no defects and pinholes are noticed. Solvent permeation studies through the MCM-41 and MCM-48-ceramic composite membrane disclose that non polar solvents are more permeable than the polar solvents and the chemical nature of liquids is the main controlling factor for the transport of solvents. The pure water permeability of ceramic support, MCM-41, MCM-48, FAU and Analcime-C zeolite composite membrane is found to be 3.63×10^{-6}, 6.05×10^{-8}, 4.18×10^{-8}, 6.09×10^{-8}, 4.53×10^{-8} $m^3m^{-2}s^{-1}$ kPa, respectively. The fabricated zeolite-ceramic composite membranes were subjected to investigate their potential for the separation of metal ions from aqueous solution using dead-end and cross flow ultrafiltration (UF). The influence of various parameters such as applied pressure, feed concentration and pH of the solutions on the rejection and flux of Cr (VI) and trivalent metal ions (Fe^{3+} and Al^{3+}) was examined. The rejection and permeate flux behavior of metal ions are found to be mainly dependent on the electrostatic interaction between charged molecules and the zeolite-ceramic composite membranes. The dead-end filtration experiments for the separation of Cr (VI) show the maximum rejection of 80, 81, 83, 80% with permeate flux of 1.10×10^{-5}, 5.31×10^{-6}, 1.29×10^{-5}, 5.96×10^{-6} $m^3m^{-2}s^{-1}$, respectively for MCM-41, MCM-48, FAU and Analcime-C zeolite membrane at acidic pH with the feed concentration of 1000 ppm and an applied pressure of 207 kPa. The prepared composite membranes demonstrate two to four order of higher

permeation flux in comparison with other membranes reported in literature. In cross flow mode operation, the highest rejection of Cr (VI) is found to be 82, 77 and 75% with FAU, MCM-48 and MCM-41 zeolite composite membrane, respectively. MCM-41, MCM-48 and FAU zeolite membranes display the best rejection of 82, 81 and 75% for $AlCl_3$ and 83, 86 and 81% for $FeCl_3$, respectively with the feed concentration of 250 ppm and lower pH. In cross flow operation, MCM-41, MCM-48 and FAU zeolite membranes demonstrate ~86, 87, and 88% rejection for $FeCl_3$ and 82, 83 and 83% rejection for $AlCl_3$, respectively. In cross flow ultrafiltration, no flux decline is observed during the separation process of Cr (VI) and trivalent metal ions with all zeolite composite membranes. Overall, it can be concluded that among the studied zeolite membranes, FAU zeolite membrane is the finest due to higher removal efficiency, lower synthesize time and temperature (24 h and 75 °C), cheaper raw materials used for the synthesis and no calcination process involved that leads to the reduction of fabrication cost.

Acknowledgements

First of all I wish to express my deepest gratitude and heartfelt thanks to **Prof. G. Pugazhenthi** providing me opportunity to work, continuous inspiration, guiding throughout the entire course of work, for his patient in correcting, giving the useful comments and explanation to complete my experiments and thesis manuscript. I am highly indebted to **Prof. G. Pugazhenthi** for constant encouragement entire tenure of the thesis, guiding me to write in journal article and improve its quality which tremendously contributed to the writing of my thesis.

Secondly, I sincerely thanks to my doctorial committee, chairman **Prof. K. Mohanty**, DC member **Dr. C. Das**, Department of Chemical Engineering and **Prof. P. K. Ghosh**, Department of Civil Engineering for their valuable inputs and suggestions which contributed enormously to enhance the quality of my research work. I would like to thank **Prof. A. K. Ghoshal** for his help, encouragement and giving valuable suggestion.

I express my heartfelt thanks to old and new HODs of IITG and all faculty members of Chemical Engineering Department. I would like to convey my sincere gratitude to non teaching and laboratory staffs for their help to carry out the experiment throughout the work.

I would like to acknowledge Central instrument facility (CIF) HOC of IITG and staff Prof. G. Krishnamoorthy, Dr. K. K. Senapati, Mr. Chandan Borgahain, Mr. Singh and Mr. Madhurjya Borah. I would appreciate SUSPOL for proving to do contact angle instrument used in this work. Last but not the least; I would like to express my sincere gratitude to QIP cell of IITG and Assam Engineering College, Department of Chemical Engineering, giving opportunity and providing me to do research under QIP program. Special thanks to all teaching and non teaching staffs of

Acknowledgements

Chemical Engineering Department, Assam Engineering College for allowing and supporting me to do research work.

I would like to thank lab mates and lab groups Vinoth, Vikram, Kunal, Partha, Kanchapogu, Kelothu, Manish, and nearby all lab groups. Special thanks to the several people who had helped me in different ways to complete my research works.

I am forever indebted to my parents, brothers and sisters for their endless patience and encouragement. The most lovely thanks, I would like to give to my friends, NS, brother-in-laws and relatives who are always supporting entire course of my thesis work.

Lastly, I would like to special thank many other people not mentioned who have been constantly encouraging and helping to accomplish my doctorial study.

Guwahati, August 2015

Ashim Kumar Basumatary

(akbiitg@gmail.com)

Content

Content

List of Tables

List of Figures

List of Figures

List of Figures

Abbreviations

BET	brunauer-emmet-teller
BJH	barrett-joyner-halenda
CTAB	cetyltrimethylammonium bromide
MCM	mobile crystalline matter
FAU	faujasite
FESEM	field emission scanning electron microscope
TEOS	tetraethyl orthosilicate
TFC	thin film composite
XRD	x-ray diffraction
FTIR	fourier transforms infrared spectroscopy
TGA	thermogravimetric analysis
DTG	differential thermogravimetric
PVA	polyvinyl alcohol
UF	ultrafiltration
Cr	chromium
IEP	isoelectric point
PZC	point of zero charge
TEA	triethanolamine
JCPD	joint committee on powder diffraction standards
ICDD	international centre for diffraction data
MF	microfiltration
RO	reverse osmosis
PV	pervaporation

Nomenclature

J	permeate flux through the membrane ($m^3m^{-2}s^{-1}$)
L_h	permeability of the membrane ($m^3m^{-2}s^{-1}$ kPa)
ΔP	applied pressure across the membrane (kPa)
ε	porosity of the membrane
M_w	weight after the support membrane with pores filled with water (g)
M_A	Archimedes weight of the support membrane (g)
M_D	dry weight of the support membrane (g)
l	pore length (µm)
µ	viscosity of water(kPa S)
τ	tortuosity factor
D_{avg}	average pore diameter (µm)
di	diameter of pore
C_p	concentration of permeate solution (ppm)
C_f	concentration of feed solution (ppm)
ΔT	sampling time (s)
R	rejection (%)
Δx	thickness of the membrane or membrane support (µm or mm)
J_w	water flux through the membrane ($m^3m^{-2}s^{-1}$)
Q	volume of water permeated (m^3)
r_m	mean pore radius (µm)
V	volume of permeate sample (m^3)

Greek letters

ε	porosity of the membrane (dimensionless)
τ	tortuosity factor (dimensionless)
μ	viscosity (cP or kPa.s)
λ	CuKα radiation wavelength (A°)
θ	diffraction angle (deg.)
ρ	density of water (Kgm^{-3})

Chapter 1

Introduction and Literature Review

Introduction and Literature Review

This chapter presents a brief background on the fundamentals, terminologies, application involved in membrane separation processes and summary of state-of-the art in ceramic as well as zeolite-ceramic composite membranes and their applications. Selection of low cost circular shaped ceramic support and zeolite composite membranes in terms of raw materials, pore size, porosity, method of fabrication and sintering temperature are discussed. The performance and superiority of ceramic support and zeolite-ceramic composite membrane are elaborated with reference to cost and industrial applications. The possible applications of zeolite composite membranes for the separation of metal ions from aqueous solutions are presented.

1.1 Background

Wastewater coming from various sources of industrial streams is alarming problems and treatment processes are challenging task. The removal of metal ions from wastewater is important owing to high toxicity, non-biodegradability and their tendency to accumulate in living organism. The metal ions contaminations along with wastewater are produced from electroplating, textile industry, metal finishing, dyeing, printing, galvanization and leather tanning industry. These need to be treated before disposal into inland and surface water due to environmental legislations. Among the various conventional methods available for the treatment of wastewater, membrane separation processes are promising techniques for the removal of metal ions from aqueous solution. Recently, there has been greater interest in the preparation and application of ceramic membrane technologies for the diverse field of application. Ceramic membrane has advantageous features compared to polymeric membranes, such as better combination of chemical and thermal stability, mechanical

strength, and capability to withstand at high temperature, better cleaning property and longer life span (Monash and Pugazhenthi 2011a). However, inorganic membranes are being the higher cost. Hence, the research focuses on investigating and exploring a new kind of ceramic materials and adopting facile fabrication technique that could play a key role to achieve feasibility for industrial use with good performance characteristics.

Membranes are functional semi-permeable active or passive barriers that permit the preferential passage of one or more selected species of components (molecules, particles or polymers) of gaseous or liquid mixtures (Heieh 1996). A membrane can be defined as 'phase that acts as a barrier to prevent mass movement but allows restricted and/or regulated passage of one or more species through it' (Lakshminarayanaiah 1984). In the separation, the primary species that are rejected and retained are termed as retentate solutes and the species that pass through the membrane are termed as permeate solutes. In general, the driving force to achieve the desired separation is brought forward by the application of pressure or concentration or potential difference across the membrane.

Membrane separation processes have been found to be advantageous and promising separation technology compared to other separation technologies such as adsorption, distillation, extraction and crystallization processes. In reference to this, lower capital cost, higher separation factors, compact design and the elimination of secondary separation units are regarded as the primary advantages of the membrane technology.

In membrane based separation technology, the performance of the membrane depends on various factors such as porosity, pore diameter, and particle size distribution amongst the solutes that are processed in addition to the solubility/diffusivity of the permeating molecules. Because of these factors, membrane technology needs to be studied thoroughly in order to ensure its feasibility for industrial applications.

1.2 Classification of membranes

According to the occurring in nature, membrane can be classified into two types, namely biological and synthetic membrane (Cheryan 1998; Mulder 1991; Nunes 2001). Biological membranes refer to those that are present in living cells and aid in cellular functional separations. Synthetic membranes are those that are prepared using various materials such as solids and liquids.

A broad classification of the synthetic membranes based on morphology is presented in Fig. 1.1 (Mulder 1991). Synthetic membranes are generally classified into two types, namely solid and liquid membranes. Solid membranes are further classified into dense, porous and electrically charged membranes. Porous membranes possess highly void structures with random distribution of inter connected pores in a mechanically rigid morphology. For porous membrane, the separation occurs due to the size difference of the particles and membrane pores. The dense membranes consist of a dominating non-porous structure and hence separation occurs due to diffusion and activation phenomena. Electrically charged membranes are porous or dense membranes, where these a carry fixed positive or negative charge that aid in the separation of solutions with ions. Based on structure, a further classification of various membranes indicates symmetric and asymmetric membranes. Symmetric membranes are those which have only one layer with homogeneous porous structure, whereas asymmetric membranes possess heterogeneous membrane structure that is accomplished using two or more porous structures or layers. Asymmetric membranes consist of a thin permeable layer with narrow pores on the top of a porous structure (support). The support in the asymmetric membrane provides higher mechanical strength to the membrane with minimum resistance to permeation while the thin film provides higher separation and permeation characteristics of the membrane. Therefore, asymmetric membranes are always

regarded to be advantageous in comparison to symmetric membranes. Symmetric membranes are to be either isotropic or anisotropic, which is classified based on the pore size distribution. In isotropic membranes, uniform pore sizes are present through the membranes and varied pore sizes are present in anisotropic membranes. Solid phase symmetric and asymmetric membranes are primarily used for pressure driven membrane separation processes.

Depending upon the type of material used, the membranes are classified as polymeric and ceramic symmetric membranes and polymer-polymer, polymer-ceramic, ceramic-ceramic asymmetric membranes. Typical symmetric membranes are fabricated using single functional materials. Asymmetric multilayered membranes are typically fabricated by depositing a thin film of polymeric, inorganic or any other suitable materials over a porous support.

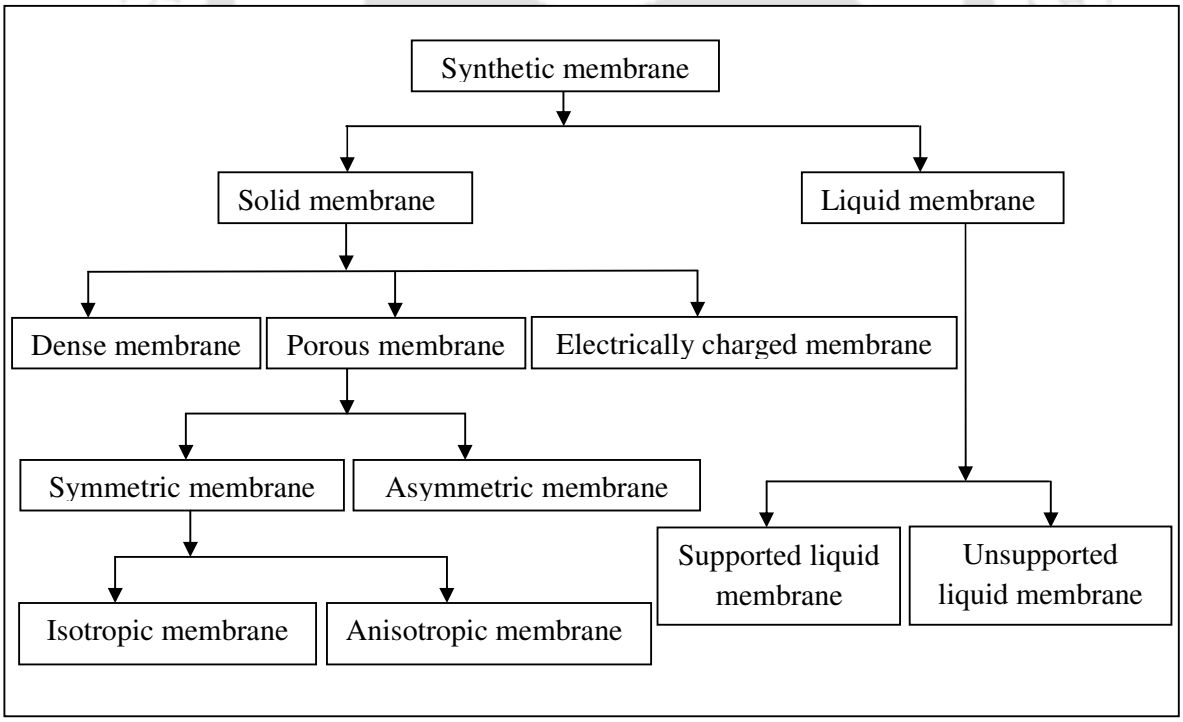

Fig. 1.1 Morphological classification of synthetic membranes (Mulder 1991)

1.2.1 Classification of membrane processes based on driving force

Classification of various membrane processes is described below and presented in Table1.1 (Heieh 1996; Baker 2004):

Microfiltration: Pressure-driven membrane-based separation process in which particles and dissolved macromolecules larger than 0.1 µm are rejected.

Ultrafiltration: Pressure-driven membrane-based separation process in which particles and dissolved macromolecules smaller than 0.1 µm and larger than about 2 nm are rejected.

Nanofiltration: Pressure-driven membrane-based separation process in which particles and dissolved molecules smaller than about 2 nm are rejected.

Reverse osmosis: Liquid-phase pressure-driven separation process in which applied transmembrane pressure causes selective movement of solvent against its osmotic pressure difference.

Osmosis: Transport of solvent through a semipermeable membrane from dilute solution to concentrate solution side of the membrane is called osmosis and this process is driven by chemical potential difference between water on either side of the membrane.

Dialysis: Membrane process in which the transport is driven primarily by concentration differences, rather than pressure or electrical-potential differences, across the thickness of a membrane.

Electrodialysis: Membrane-based separation process in which ions are driven through an ion-selective membrane under the influence of an electric field or voltage.

Pervaporation: Membrane based separation process where the feed and retentate streams are liquid phases while the permeate at the downstream side of the membrane is a vapor.

Table 1.1: Characteristics of membranes process (Cheryan 1998; Pabby *et al*., 2008)

Process	Driving Force	Retentate	Permeate
Osmosis	Chemical potential	Solutes, water	Water
Dialysis	Concentration difference	Large molecules, water	Small molecules, water
Microfiltration (MF)	Pressure difference	Suspended particles, water	Dissolved solutes, water
Ultrafiltration (UF)	Pressure difference	Large molecules, water	Small molecules, water
Nanofiltration (NF)	Pressure difference	Small molecules, divalent salts, dissociated acids, water	Monovalent ions, undissociated acids, water
Reverse osmosis (RO)	Pressure difference	All solutes, water	Water
Electrodialysis (ED)	Voltage	Non-ionic solutes, water	Ionized solutes, water
Pervaporation (PV)	Pressure difference	Non-volatile molecules, water	Volatile small molecules, water

1.2.2 Classification of membrane process based on modes of operation

Membrane flow pattern can be classified into either dead end or cross flow. It is based on the relative direction of the feed stream to the membrane orientation (Heieh 1996; Koros *et al*., 1996). The different flow patterns are depicted in Fig. 1.2. In dead end flow pattern, both feed and permeate flow are perpendicular to membrane surface and it is a batch process. In cross flow pattern, both permeate and feed flow parallel to the surface of the membrane. Cross flow can be operated in co current or counter current mode using a sweep stream. In counter current flow, the upstream and downstream move parallel to the membrane surface in opposite direction. However, in co current flow, the two streams flow in the same direction.

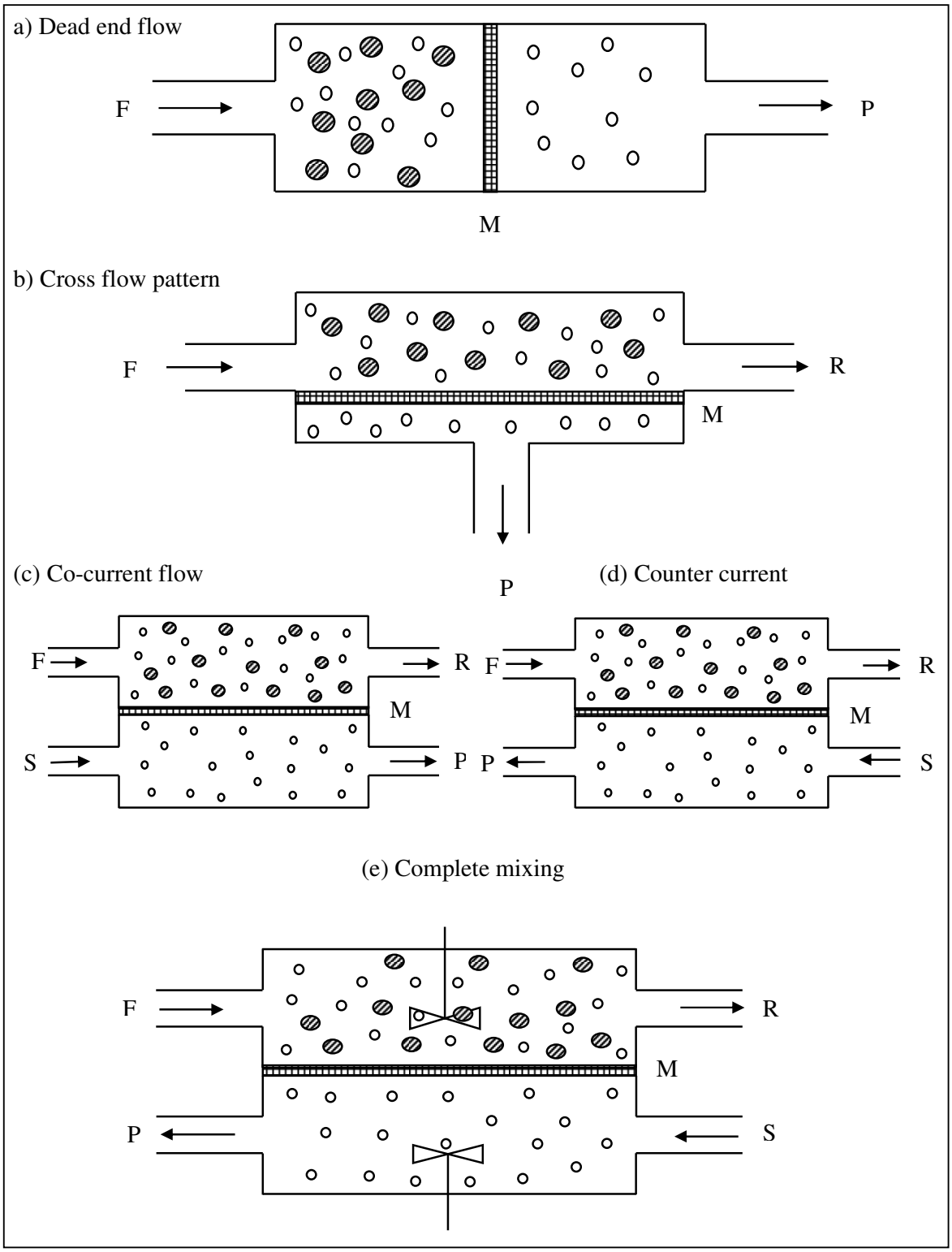

Fig. 1.2 Schematic representation of different modes of operation in membrane processes (F-feed stream, P-permeate stream, M-membrane, R-retentate stream and S-sweep stream.

1.2.3 Industrial application of membranes

Several industrial applications of synthetic solid symmetric and asymmetric membranes exist for MF and UF, which are summarized below: (Cheryan 1998; Porter 1989)

a) Treatment of industrial waste streams such as oily wastewater, pulp and paper wastewater, leather wastewater, removal of Cr (VI) and Cr (III), trivalent metal ions, dyes from its aqueous solution, removal of various suspended solids in the wastewater streams.
b) Biotechnological applications such as protein recovery, milk concentration and separation of fat from milk.
c) Production of drinking water from different sources to remove various particles as well as bacteria.
d) Production of clarified fruit juices, which possess long term storage characteristics and thereby enable the reduction of transportation costs of food products.

The industrial applications of other membrane separation processes such as NF, RO, pervaporation, dialysis, and gas separation are presented below:

1. **NF and RO**: Desalination of sea water to generate drinking water, treatment of various industrial wastewaters, removal of nitrates, fluorides, heavy metals, etc.
2. **Pervaporation**: Separation of organic and azeotropic mixtures (such as ethanol-water) which are difficult to separate using conventional methods, such as distillation.
3. **Dialysis**: Removal of different harmful components from human blood during kidney failure (Baker 2004).
4. **Gas permeation**: For the production of oxygen enriched air, nitrogen enriched air and hydrogen recovery using porous as well as dense membranes. In addition, dense membranes are used to accomplish carrier facilitated separations.

1.3 Ceramic membranes

Ceramic membranes are made of various inorganic materials such as α-alumina, γ-alumina, zirconia, silica, titania, kaolin, etc. In comparison with polymeric membranes, ceramic membranes possess superior chemical, thermal and mechanical stability. It can also be used in harsh environment in chemical process industry. The thickness of ceramic membrane is in the range of 2-5 mm and it may be higher depending on the specific applications. Asymmetric membranes constitute thin film in the range of 10-100 μm ceramic coating over a thick symmetric support.

Some advantages of ceramic membranes (Mulder 1991)**:**

a) High corrosion resistance; in very few chemicals, such as hydrofluoric acid and phosphoric acid, ceramic membranes don't have high corrosion resistance. One of the most useful features of the ceramic membranes is that their ability to tolerate strong doses of chlorine (up to 2000 mg/L in certain cases).
b) Applicable to wide range of pH (0.5-14).
c) Applicable to broad temperatures (350-500 °C). As a result, it can be used in industrial scale separations without any feed pre-conditioning steps.
d) Longer life span (5-10 years). In practical, there are many ceramic systems in industry, which are operating after 10-14 years of installation.
e) Less fouling tendency.
f) Inertness to common chemicals and solvents.
g) Higher mechanical strength.

Few drawbacks of ceramic membranes:

a) Ceramic membranes are comparatively higher cost. For instance, in 1996 cost indices of polymeric spiral wound modules and ceramic systems were 50-100 $/m^2 and 500-3000 $/m^2, respectively. Along with these cost including controls, pumps and fittings were estimated to be 225-350 $/m^2 and 2200-3600 $/m^2 for polymeric and ceramic membranes (Mulder 1991). This indicates that a tenfold higher cost of ceramic membranes when compared to polymeric membranes. In due course of time, though the price of ceramic membranes may have reduced, these costs have not been very competitive with polymeric membranes. Because of that, it is expected that the cost of ceramic membranes will be still higher to that extent of 2-3 orders of magnitude.
b) Ceramic membranes are brittle in nature. It may be broken or damaged if it drops.

1.3.1 General methods used for the preparation of ceramic membrane

Inorganic membranes have permselectivity's that are five to ten times higher than the conventional polymeric materials. Furthermore, they are more stable in aggressive feeds. The majority of ceramic glass, carbon and zeolitic membranes cost between one and three orders of magnitude more per unit of membrane area when compared to polymeric membranes. Moreover, they are complicated to fabricate into large and defect-free areas. The polymeric materials have an advantage that they can be processed into hollow fibers, which offer high separation output due to the inherently high surface area to volume ratio. Inorganic membranes classified into two major categories based on its structure: porous inorganic membrane and dense (non-porous) inorganic membranes. A few fabrication techniques of inorganic membranes are given in Fig. 1.3. Typically, the porous inorganic membranes have the structures of asymmetric and symmetric framework. The porous inorganic membrane with pores more than 0.3 nm usually work as a sieve for large molecules and particles. The

commercially utilized porous inorganic membranes are glass, metal, alumina, zirconia, zeolite and carbon. Other inorganic materials such as cordierite, silicon carbide, silicon nitride, titania, mullite, tin oxide and mica are used to produce inorganic membranes. These membranes vary significantly in pore size, support material and configuration. On the other hand, dense membranes made of palladium and its alloys, silver, nickel and stabilized zirconia are used for the fabrication of inorganic membranes.

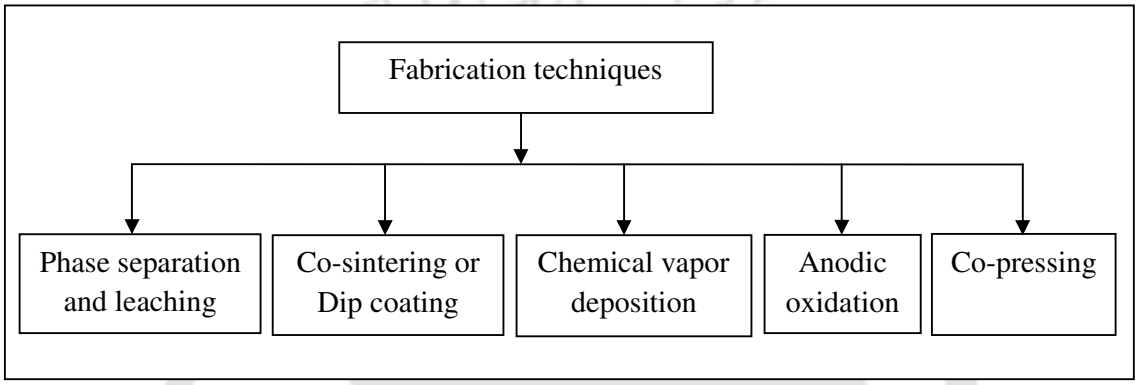

Fig. 1.3 Fabrication techniques of inorganic membranes

Mesoporous materials can be synthesized by different methods of preparation. In all these methods, common ingredients are (1) Silica source, (2) Templating agent i.e. structure directing agent, (3) Solvent and (4) Mineralising agent (NaOH, NH_3, HCl).

1.3.2 Solvent evaporation techniques

The solvent evaporation techniques involve formation of a liquid film containing the solvent, surfactant and silica precursor followed by evaporation of the solvent. It is divided into two methods.

1.3.2.1 Dip coating

The dip coating technique is widely used in the preparation of composite membrane. In this method, substrates are taken out from a homogeneous precursor solution and the dip-coated

solution is allowed to drain to a particular thickness. The thickness of the film is mainly determined by the rate of evaporation of the solvent and the viscosity of the solution. Fig. 1.4 displays the dip coating process.

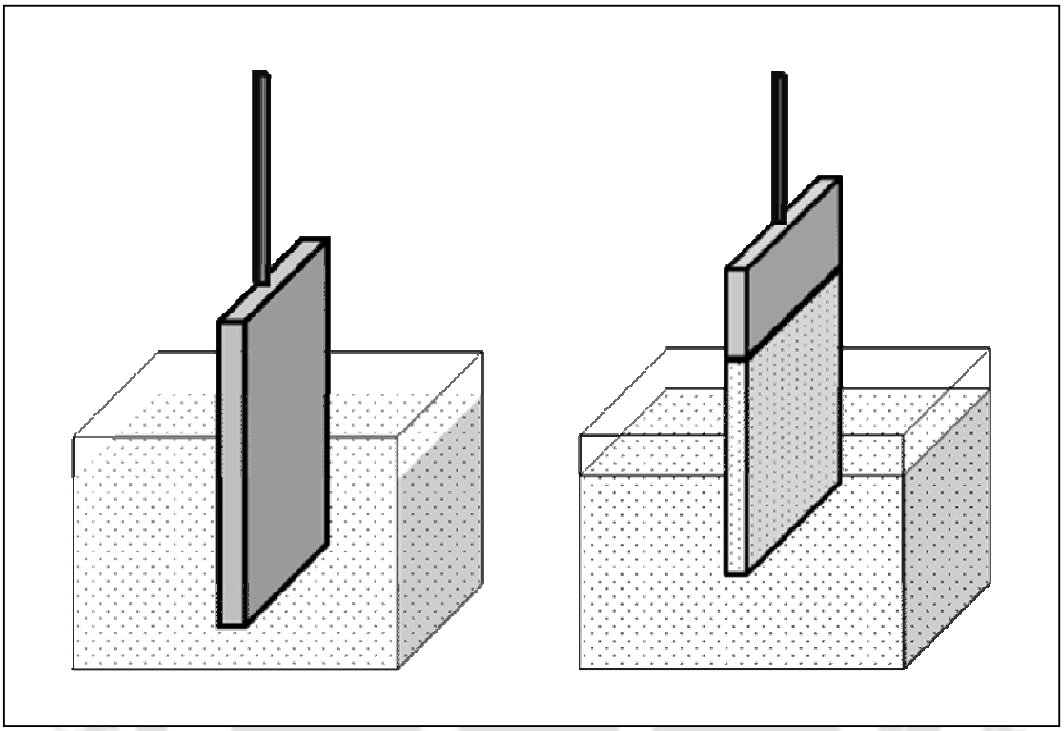

Fig. 1.4 (a) Dip coating, (b) After coating

1.3.2.2 Spin coating

Spin coating is a technique that utilizes centrifugal forces produced by a spinning substrate to spread a coating solution over a surface. This type of coating technique is faster and efficient. It can be controlled by a few parameters to yield a well defined coating coverage. The liquid solution is placed in the center of the sample and the sample spins at a given speed and time, where the centrifugal force will cause the liquid to spread evenly across the sample. Four stages (see Fig. 1.5) of spin-coating are: deposition of the surfactant/inorganic solution, spin-up, spin-off and evaporation. Initially, an excess of liquid is deposited on the surface of the substrate during the first stage. In the spin-up stage, liquid flows radially outwards by

centrifugal force. In the spin-off stage, excess of liquid flows to the outwards and leaves in a form of droplets. In the final stage, evaporation takes place leading to the formation of uniform thin films.

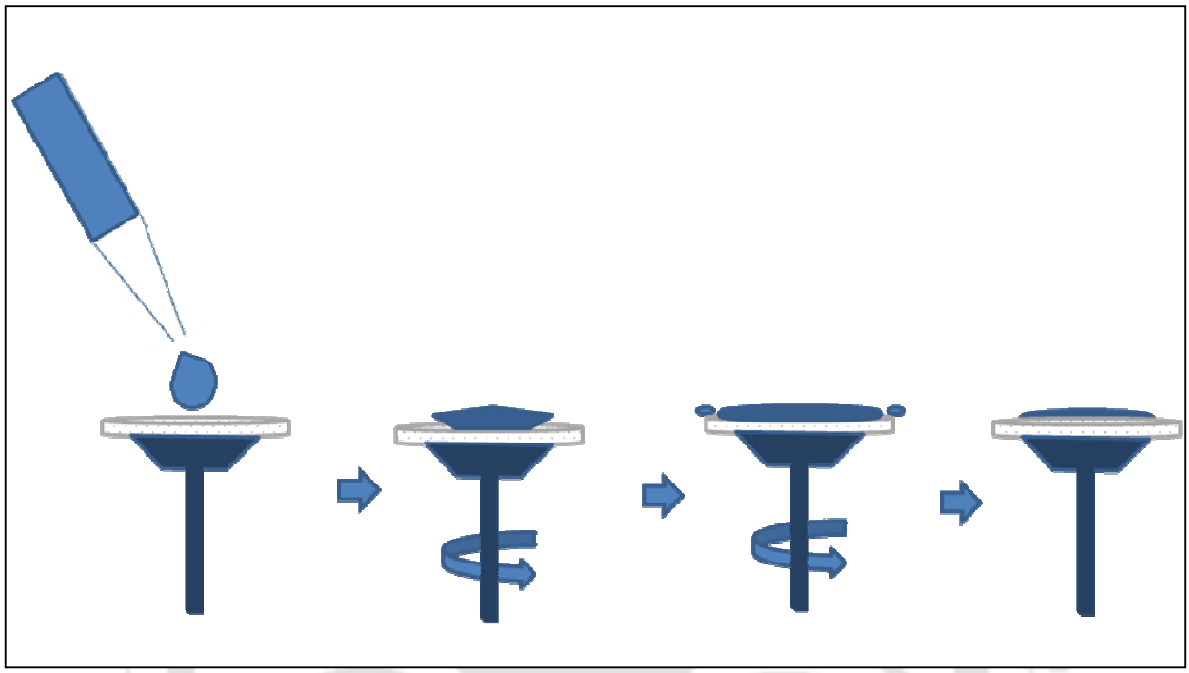

Fig. 1.5 Spin coating steps

1.3.3 Growth from solution

The basic principle for the synthesis of ordered mesoporous films by growth from solution is to bring the synthesis solution (including solvent, surfactant and inorganic precursor) in contact with a second phase, e.g. solid (ceramic), gas (air) or another liquid (oil). The two-phase system is kept under specific conditions and the ordered film is formed at the interface. Hydrothermal deposition technique comes under this process.

1.3.4 Sol-gel method

The sol-gel process is one of the most suitable techniques to acquire a functional active top layer on a membrane support. It has several advantages; it produces tremendously active

products with high surface area, controllable and facile amalgamation of other compounds such as promoters or stabilizers, alteration of fine pore structure and direct casting of the selective layer over the membrane support (Agrafiotis and Tsetsekou 2002). Further, it generates high purity products with narrow pore size distribution and needs low sintering temperature. Being the less energy, it is widely used due to its facile method and does not require sophisticated instrumentation. A sol is a stable dispersion of colloidal very fine particles or polymer in a liquid. The particles may be amorphous or crystalline. A gel consists of three dimensional continuous networks, which enclosed a liquid phase where the network is built from agglomeration of colloidal particles. For the fabrication of composite membrane, two sol-gel routes are used. The first one corresponds to colloidal route that explores colloidal chemistry in aqueous media and the other corresponds to the polymeric route, which searches the chemistry of metal organic precursors with organic solvents. Fig. 1.6 demonstrates the sol-gel method for both colloidal and polymeric routes. In the sol-gel process, the first stage refers to the preparation of a sol using molecular precursors either with metal salts or metal organics. The condensation reactions occurred at the sol stage for both cases with the formation of colloids or clusters that coalesce finally to form gel. For the fabrication of active layer, the coating must be carried out with the sol whose rheological behavior is adaptable for the porous membrane support or substrate. Drying and sintering steps subsequently followed, which determine the chemical characteristics of the membrane. In the drying process of coated sol, gelation takes place and cross linking of the gel particles are formed to produce desired product due to the thermal treatment. Usually, thin and crack free membrane layers are obtained with this technique.

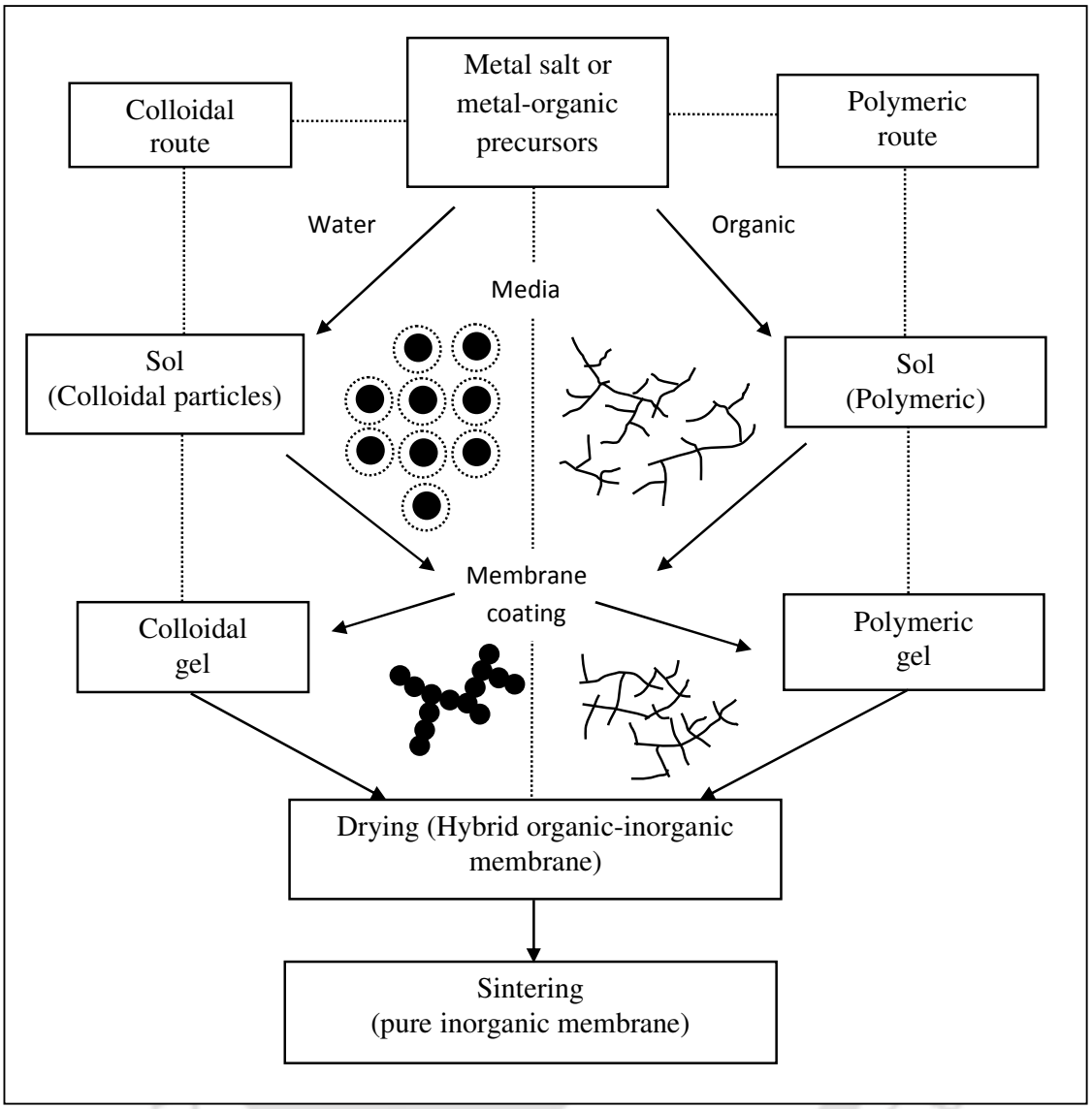

Fig. 1.6 Pictorial representation of inorganic membrane preparation by sol-gel method

1.4 Zeolite

Zeolites are three dimensional crystalline hydrated microporous aluminosilicate materials having minute's pores and a well defined structure (Georgiev *et al*., 2009). Zeolites occurred naturally many parts of the world and also can be made commercially in industrial applications as cation exchanger and molecular sieves. Zeolites can be readily dehydrated and rehydrated. Most of the zeolites consist of tetrahedral silicon and oxygen in coordinated form.

The oxygen atoms are at the corner of the tetrahedral with other atoms in the centre. Silicon tetrahedral is electrically neutral, while aluminum tetrahedral has an overall negative charge, which must be balanced by another atom. These tetrahedral forms channels and leads to an overall crystalline pore structures. The general characteristics of different types of zeolites are silicon to aluminum ratio and its pore size/shape. An increase in Si/Al ratio strongly affects the physical properties of the zeolites.

1.5 Composite membrane

Composite membrane is defined as multi-layered asymmetric membrane in which a thin layer (separating layer) is deposited as the top layer on the surface of the support as shown in Fig. 1.7 Generally mesoporous silica materials and zeolites have a well-defined pore geometry, high surface area, pore volume and uniform pore channel. Among different areas of potential applications, industrial application of these materials for separation process is not directly feasible. Therefore, a combination of mesoporous material and conventional support (ceramic) may make it more feasible for industrial application. Conventional ceramic supports have good mechanical, thermal and chemical stability, but wide distribution of their pore size. It is unfavorable for the separation process, which involves separation of small objects such as heavy metal ions, organic pollutants, dyes, etc. Hence, it is necessary to deposit/coat a mesoporous silica or zeolite materials on the ceramic supports to make composite membranes for liquid phase separation applications.

In general, the separation performance of the membrane such as selectivity and permeability, which depend upon the surface functionality, pore size distribution and pore volume fraction, can be achieved by mesoporous silica material as a thin film at the surface of support and producing high performance membrane. Thus, the membrane support does not impose any mass transfer limitations but offers only thermal, chemical and mechanical strength to the

membrane. Hence, the advantage of composite membrane is that each layer can be optimized independently to obtain optimal membrane performance with respect to selectivity, permeation rate, thermal and chemical stability. Synthesis of composite membrane consists of three steps, which includes preparation of support, preparation of precursor for selective layer (thin layer), and fabrication of composite membrane.

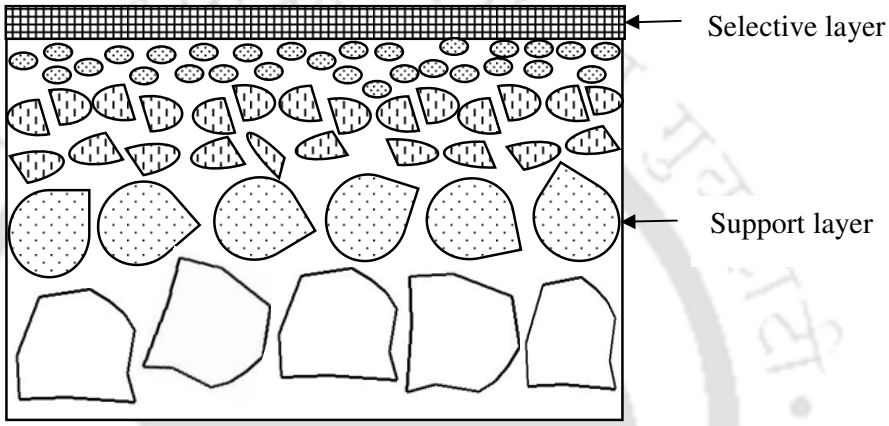

Fig. 1.7 Schematic of composite membrane

1.5.1 Fabrication of ceramic support

A ceramic support is prepared by shaping powder and then consolidation of green body by sintering. Fabrication process consists of four steps sequentially as follows (Burggraaf and Cot 1996):

a) Selection of appropriate inorganic raw materials or precursors.

b) Preparation of ceramic powder/paste.

c) Support fabrication or shaping.

d) Heat treatment (sintering/firing).

Symmetric ceramic membrane supports are fabricated by uniaxial pressing and paste methods (Burggraaf and cot 1996; Judd and Jefferson 2003). Both these methods involve the preparation of an inorganic mixture using suitable pore forming organic and inorganic materials along with binder materials. The uniaxial pressing method involves casting an inorganic mixture in a suitable disk or tubular shape and kept under very high pressure (30-50 MPa). Subsequently, the disk or tubular type mould is sintered to prepare the membrane.

The paste method involves the preparation of a paste using inorganic mixture with suitable solvent, which is eventually casted into suitable shape and sintered at high temperature. The properties of the ceramic support are largely influenced by the composition of the raw materials, sintering temperature and the process including the schedule of heating, sintering and cooling.

Colloidal processing method offers the potential to produce ceramic films and bulk forms through careful control of initial suspension "structure" and its evolution during fabrication. This technique involves five basic steps: powder synthesis, suspension preparation, consolidation into the desired component shape, removal of the solvent phase, and densification to produce the final microstructure required for optimal performance.

Different type of fabrication techniques have been practiced by researchers for their specific use in particular research area. Although it is difficult to classify the basis for the fabrication of ceramic support methods, many of the fabricated supports (commercial and home-made ceramic supports) come under any one of the methods presented in the Fig. 1.8.

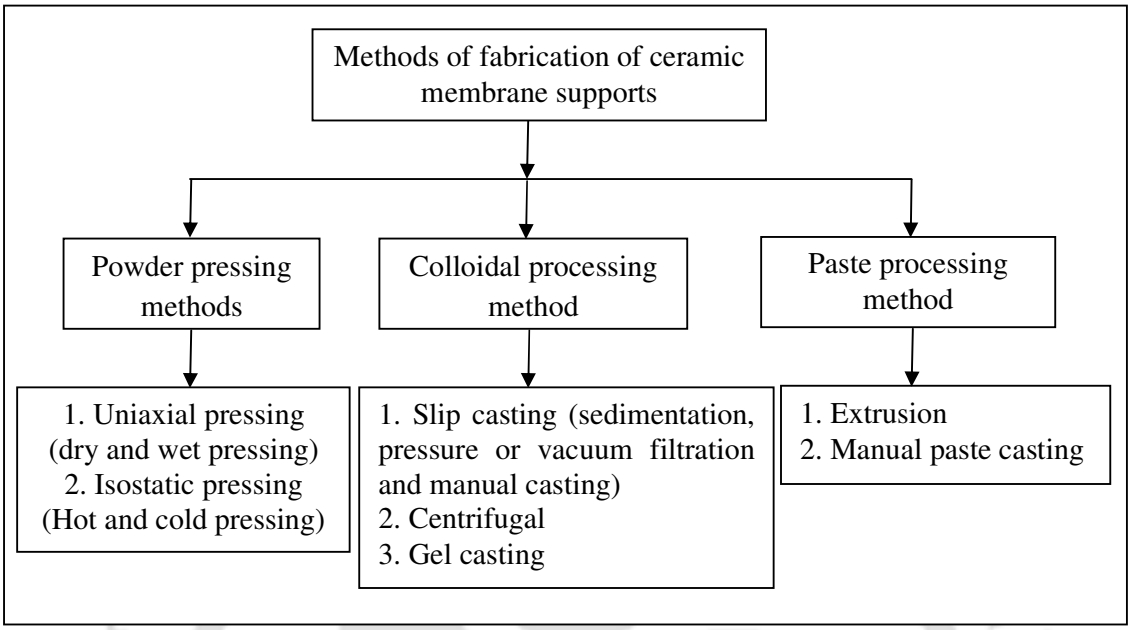

Fig. 1.8 Various methods used for the preparation of ceramic supports

1.6 State of the art

With the summary of the contemporary research, this section outlines the research outcome of different literatures. The main focus of this review is to identify the objective of the thesis and address the few promising areas. The state of the art can be presented in three sub-sections, like (a) preparation of ceramic membrane support, (b) preparation of ceramic-zeolite composite membranes, (c) application of composite membranes for the removal of chromium and trivalent metal ions from waste stream.

1.6.1 Preparation of ceramic membrane supports

Ceramic membranes possess several desirable chemical and mechanical properties such as resistance to corrosive environments, high thermal stability, mechanical strength and relative

inertness (Burggaraaf and Cot 1996; Workneh and Shukla 2008; Vasanth *et al*., 2011; Monash and Pugazhenthi 2011a). Membrane based separation processes have drawn much important in comparison with other existing technologies like distillation, adsorption, absorption and extraction. This is due to the likelihood of recovering important products from the effluent, operation at ambient condition and reducing environmental hazard. Inorganic ceramic membranes can tolerate at higher temperatures than polymeric membranes, which create them potential candidates for large scale of industrial applications. However, the cost of ceramic membrane is higher than the polymeric membrane due to higher cost of precursors for ceramic raw materials. In addition to that, ceramic membrane required higher sintering temperature (more than 1100 °C), which furthermore contributes to the manufacturing cost. Due to this fact, at early stage of research in the field of ceramic membrane was limited. In the last few decades, microporous inorganic membranes have been applied in different fields of applications based on their advantages including ability to withstand at high temperature and pressure, good chemical stability and defouling properties, long durability and high mechanical strength (Mulder 1991). The most often used materials for synthesis of inorganic membranes are α- and γ-alumina, TiO_2, ZiO_2, zeolites and microporous glass (Anderson *et al*. 1988). Several literatures reported on the preparation of ceramic support using expensive raw materials such as α-alumina (Okubo *et al*., 1991; Takagi *et al*., 2000; McCool *et al*., 2003; Chowdhury *et al*., 2003; Kumar *et al*., 2006; Bissett *et al*., 2008; Alem *et al*., 2009; Qi *et al*., 2010), zirconia (Falamaki *et al*., 2004) and titania (Patterson *et al*., 2006; Wang *et al*., 2006).

Okubo *et al*., (1991) synthesized tubular supports using α-Al_2O_3 as raw material by **e**xtrusion method and the support were sintered at different temperatures (1427-1927 ^oC). The pore size and porosity of the support were 0.17 µm, 0.3%, respectively. Takagi *et al*., (2000) prepared the disk shape α-Al_2O_3 support by pressing Al_2O_3 powder using water as a binder and sintered at 1245 ^oC for 2 h. The fabricated membrane possessed porosity and average pore

diameter of 54.09%, and 0.16 µm, respectively. McCool *et al*., (2003) prepared the disk shaped α-alumina support by dry pressing method and sintered at 1200 °C. The average pore diameter and porosity of the α-alumina support was 0.1µm, and 35 %, respectively. Chowdhury *et al*., (2003) fabricated the disk shaped α-alumina ceramic support by colloidal filtration technique followed by sintering at 1100 °C. The membrane possessed an average pore size of 80-120 nm and the porosity of 30%. Kumar *et al*., (2006) synthesized two types of α-alumina supports, A15 and A16 by compression method and sintered at 1500 °C for 30 h. The mean pore size of A15 and A16 membrane was found to be 0.3 and 0.2 µm, respectively. Bissett *et al*., (2008) manufactured and optimized the tubular α-alumina ceramic membrane supports derived from three different powder sizes (0.25, 0.31 and 0.61 µm) with different sintering temperature ranging between 1050 and 1400 °C. With the sintering temperature of 1150 °C, 37.2 % and 35.8 % porosity of the support were obtained for powder size of 0.25 and 0.31 µm, respectively. The support sintered at the lowest sintering temperatures had the highest porosity, water permeability and the largest pore sizes, while tensile strength was the lowest for all particle sizes used. Also the pore diameter of the supports produced by 0.31 and 0.61 µm powders were decreased, whereas powder size of 0.25 µm used remained constant with increasing sintering temperature. Alem *et al*., (2009) prepared α-alumina ceramic support using uniaxial pressing method at a sintering temperature of 1350 °C. The obtained porosity of the ceramic support was 38%. Qi *et al*., (2010) fabricated tubular support with α-Al_2O_3 and TiO_2 powders as raw materials. The ceramic support was prepared using extrusion method and sintered at 1400 °C. The membrane has average pore size and porosity of 6.8 µm and 41.4%, respectively. Ghaderi *et al*., (2013) prepared porous α-alumina supports using vibration and pressing compaction method. The author investigated the effect of sintering temperature (1325-1625 °C) as well as silica addition on ceramic support properties such as porosity, thermal conductivity,

compressive and flexural strength. It was found that compaction routes strongly affected the sintering temperature and properties of the ceramic support. Using the press and vibrational technique on alumina sample with and without silica addition, a transition was observed within the temperature range of 1475-1550 °C from initial to intermediate stage of sintering.

Falamaki *et al*., (2004) studied the initial sintering stage pore growth mechanism applied for the manufacturing of alumina and zirconia ceramic supports by uniaxial compaction. An alumina moulding powder with an average granule size of 160 µm was used without adding binder. For zirconia powder, zircosil 5 having particle size of 1.78 µm was used along with 4 wt % PVA. The investigation of the effect of sintering temperature (1200-1500 °C) on density, porosity, surface area, permeability, mean flow path pore size, mesoporous mean radius and tortuosity were reported. The samples, alumina and zirconia had a flexural strength higher than 20 MPa at the end of transition zone. It showed that porosity decreased with increasing sintering temperature for both Al_2O_3 and $ZrSiO_4$ supports. Patterson *et al*., (2006) fabricated tubular membrane support with α-Al_2O_3 as a raw material by centrifugal casting method and finally sintered at 1200 °C. The mean pore size of the tubular support was 0.16 µm. Wang *et al*., (2006) prepared the disk shaped support using Al_2O_3, TiO_2 (rutile), corn starch solution, methyl cellulose solutions and water as raw materials. The ceramic support was fabricated using uniaxial compression method and sintered at 1400 °C. The membrane possessed pore size and porosity of 1.6 µm and 40%, respectively.

The observation of the above literatures survey pointed out that the prepared membranes are expensive due to higher sintering temperature (more than 1000 °C) and higher cost of the raw materials. In order to overcome such disadvantages, the researchers need to focus on exploring a new kind of low cost raw materials and facile fabrication techniques. Furthermore, lower sintering temperature (less than 1000 °C) would be beneficial for industrial applications. Recently, large number of research studies illustrated the

manufacturing of ceramic membranes utilizing cheaper and naturally available raw materials such as clays (Saffaj *et al*., 2004; Bouzerara *et al*., 2006; Khemakhem *et al*., 2007; Masmoudi *et al*., 2007; Dong *et al*., 2007).

Saffaj *et al*., (2004) fabricated a tubular support using Cordierite, Amidon, Methocel, Polyethylene glycol and water as raw materials. The support was prepared using extrusion method and sintered at 1275 °C. The membrane possessed the average pore size and porosity of 7 µm and 40%, respectively. Bouzerara *et al*., (2006) prepared the ceramic support from kaolin and kaolin-dolama mixtures. Four different processing routes were investigated with two different configurations (tubular and flat). The tubular support was prepared by extrusion technique, whereas flat support prepared by both dry pressing and roll pressing. The results demonstrated that the mechanical strength, porosity, average pore size and pore size distribution were influenced by sintering temperature and processing route. Using extrusion method, Dong *et al*., (2007) manufactured a tubular support with low cost industrial grade cordierite powder and studied the effect of sintering temperature on the properties of tubular support. With increasing sintering temperature, the mechanical strength of the support increased and at the optimum sintering temperature of 1380 °C, the membrane possessed mean pore diameter of 8.66 µm and porosity of 36.20 %. Masmoudi *et al*., (2007) developed low cost tubular membrane support from natural apatite by extrusion method and sintered at various temperatures. The obtained result revealed that the pore diameter and mechanical strength increased with increasing sintering temperature and porosity of the support decreased with increasing temperature. The prepared ceramic support had a mean pore diameter of about 6 µm with an average porosity of 47 % at the sintering temperature of 1160 °C. The preparation of tubular support (10 mm diameter and 1.5 mm thickness) from Tunisian clay by extrusion process was reported by Khemakhem *et al*., (2007). The support

was sintered at 1090 °C. The mean pore diameter and porosity of the support was found to be 6.3 µm, 48 %, respectively.

Recently, few researchers have used mixture of precursors instead of using single raw materials to obtain proper combination of better membrane characteristic such as good mechanical and chemical resistance with lower average pore size. The following literatures summarize such attempt to fabricate ceramic membranes using mixed raw materials (Almandoz *et al*., 2004; Nandi *et al*., 2008; Workneh *et al*., 2008; Vasanth *et al*., 2011). Almandoz *et al*., (2004) used low cost ceramic materials such as ball clay, kaolin, alumina, quartz and calcium carbonate for the fabrication of membrane by paste method. The support was sintered at various temperatures ranging between 1100 and 1400 °C. The results indicated that an increase in sintering temperature led to a higher density, mechanical resistance and the smaller pore volume of the membrane. The authors found that optimum sintering temperature was in the range of 1200-1300 °C and the mean pore size of the membrane was between 0.1 and 1.0 µm. Nandi *et al*., (2006) prepared circular shaped ceramic membrane using low cost clay materials (kaolin, quartz, calcium carbonate, sodium carbonate, boric acid and sodium metasilicate) by casting method. The authors studied the effect of sintering temperature on the membrane properties such as porosity, average pore size, mechanical stability and chemical resistances. As the sintering temperature increased, the average pore size (550 nm-810 nm), mechanical strength (3-8 MPa) and chemical stability increased, while porosity (44 % to 33 %) of the support decreased. The optimum sintering temperature was found to be 900 ^{o}C for the chosen raw materials. The average pore diameter, porosity and mechanical strength was found to be 0.70 µm, 40 % and 6 MPa, respectively. Workneh *et al*., (2008) fabricated disk shaped ceramic support with mixture of clays (kaolin, ball clay, cristoballite, pyrophyllite, feldspar, calcium carbonate, sodium metasilicate, boric acid and quarts) by paste method and sintered at 950 °C. The

obtained mean pore diameter and porosity of ceramic support was 0.2 µm, and 51%, respectively. Vasanth *et al*., (2011) prepared the low cost ceramic microfiltration membrane from inexpensive raw materials such as kaolin, quartz, calcium carbonate, using uniaxial dry compaction method. They investigated the effect of sintering temperature on the membrane properties such as porosity, flexural strength, chemical stability and pure water permeability in the temperature range of 900 and 1000 °C. It was observed that the membrane sintered at 900 °C was optimum for microfiltration application that has porosity, flexural strength and average pore size of 30 %, 34 MPa and 1.30 µm, respectively.

Dry compaction and uniaxial methods were successfully employed for the fabrication of ceramic membrane. In addition, recent studies on membrane manufacturing demonstrated the minimal macro-defects and homogeneous compact structure. Tables 1.2-1.5 summarize the literature review on ceramic supports based on various factors.

Table 1.2 Various raw materials used for fabrication of ceramic supports/membranes

Author	Raw Material	Support	Method	Sintering Temp. (^oC)	Pore size (µm)	Porosity (%)
McCool *et al*., (2003)	α-Al_2O_3	Disk	Dry pressing	1200	0.1	35
Alem *et al*., (2009)	α-Al_2O_3	Disk	Uniaxial pressing	1350	1.0	38
Kumar *et al*., (2006)	α-Al_2O_3 (A15, A16)	Disk	Compressing	1500	A15=0.3 A16=0.2	40
Chowdhury *et al*., (2003)	α-Al_2O_3	Disk	Colloidal filtration	1100	0.08-0.12	~30
Bissett *et al*., (2008)	α-Al_2O_3	Tubular	Casting	1050-1400	0.25-0.31	37.2-35.8
Patterson *et al*., (2006)	α-Al_2O_3	Tubular	Centrifugal casting	1200	0.16	--
Wang et al., (2006)	Alumina, TiO_2 (rutile), corn starch and methyl cellulose water	Disk	Uniaxial	1400	1.6	>40
Okubo *et al*., (1991)	α-Al_2O_3	Tubular	Extrusion	1427-1927	0.2-6.0	0.3
Ghaderi *et al*., (2013)	α-Al_2O_3	Flat	Vibration and uniaxial pressing	1325-1625	6.8-8.1	30-50
Qi *et al*., (2010)	α-Al_2O_3 & TiO_2	Tubular	Extrusion	1400	6.8	41.4
Takagi *et al*., (2000)	Al_2O_3 & water	Disk	Pressing	1245	0.16	54.09
Falamaki *et al*., (2004)	α-Al_2O_3 & $ZrSiO_4$ with PVA	Disk	Uniaxial pressing	1425,1500	Both < 0.075	30
Vasanth *et al*., (2011)	Kaolin, quartz and calcium carbonate	Disk	Uniaxial dry compaction	900	1.30	30

Author	Raw Material	Support	Method	Sintering Temp. (^{o}C)	Pore size (µm)	Porosity (%)
Almandoz *et al*., (2004)	Ball clay, kaolin, alumina, quartz and calcium carbonate	Tubular	Paste method	1200-1300	0.1-1	35-46
Dong *et al*., (2007)	Cordierite powder	Tubular	Extrusion	1380	8.66	36.20
Workneh *et al*., (2008)	Kaolin, ball clay, cristoballite, pyrophyllite, feldspar, calcium carbonate, sodium metasilicate, boric acid and quartz	Disk	Paste method	950	0.2	51
Nandi *et al*., (2008)	Kaolin, quartz, sodium carbonate, boric acid sodium metasilicate and calcium carbonate	Disk	Casting method	900	0.285	23.6
Bouzerara *et al*., (2006)	Kaolin and kaolin-dolama mixtures	Tubular and flat	Extrusion and pressing	1250	22-28	43-51
Masmoudi *et al*., (2007)	Apatite powder	Tubular	Extrusion	1160	6	47
Khemakhem *et al*., (2007)	Tunician clay	Tubular	Extrusion	1090	6.3	48

Table 1.3 Various fabrication techniques involved in the preparation of ceramic supports/membranes

Author	Raw Material	Support	Method	Sintering Temp.(^oC)	Pore size (µm)	Porosity (%)
McCool *et al*., (2003)	α-Al_2O_3	Disk	Dry pressing	1200	0.1	35
Alem *et al*., (2009)	α-Al_2O_3	Disk	Uniaxial pressing	1350	1.0	38
Kumar *et al*., (2006)	α-Al_2O_3 (A15, A16)	Disk	Compressing	1500	A15=0.3 A16=0.2	40
Chowdhury *et al*., (2003)	α-Al_2O_3	Disk	Colloidal filtration	1100	0.08-0.12	~30
Vasanth *et al*., (2011)	Kaolin, quartz, CO_3	Disk	Uniaxial dry compaction	900	1.30	30
Falamaki *et al*., (2004)	α-Al_2O_3 and $ZrSiO_4$ with PVA	Disk	Uniaxial pressing	1425,1500	Both < 0.075	30
Takagi *et al*., (2000)	Al_2O_3 and water	Disk	Pressing	1245	0.16	54.09
Nandi *et al*., (2008)	Kaolin, quartz, sodium carbonate, boric acid, sodium metasilicate and calcium carbonate	Disk	Casting method	900	0.285	23.6
Workneh *et al*., (2008)	Kaolin, ball clay, cristoballite, pyrophyllite, feldspar, calcium carbonate sodium metasilicate, boric acid and quartz	Disk	Paste method	950	0.2	51
Wang *et al*., (2006)	Alumina, TiO_2 (rutile), corn starch and Methyl Cellulose water	Disk	Uniaxial	1400	1.6	> 40

Author	Raw Material	Support	Method	Sintering Temp. (^oC)	Pore size (µm)	Porosity (%)
Masmoudi *et al*., (2007)	Apatite powder	Tubular	Extrusion	1160	6	47
Dong *et al*., (2007)	Cordierite powder	Tubular	Extrusion	1380	8.66	36.20
Khemakhem *et al*., (2007)	Tunician clay	Tubular	Extrusion	1090	6.3	48
Bissett *et al*., (2008)	α-Al_2O_3	Tubular	Casting	1050-1400	0.25 0.31	37.2 35.8
Almandoz *et al*., (2004)	Ball clay, kaolin, alumina, quartz and calcium carbonate	Tubular	Paste method	1200-1300	0.1-1	35-46
Qi *et al*., (2010)	α-Al_2O_3 and TiO_2	Tubular	Extrusion	1400	6.8	41.4
Patterson *et al.*, (2006)	α-Al_2O_3	Tubular	Centrifugal casting	1200	0.16	--
Okubo *et al*., (1991)	α-Al_2O_3	Tubular	Extrusion	1427-1927	0.2-6.0	0.3
Bouzerara *et al*., (2006)	Kaolin and kaolin-dolama mixtures	Tubular and flat	Extrusion and dry pressing	1250	22-28	43-51
Ghaderi *et al*., (2013)	α-Al_2O_3	Flat	Vibration and uniaxial pressing	1325-1625	6.8-8.1	30-50

Table 1.4 Classification of literature based on sintering temperature

Author	Raw Material	Support	Method	Sintering Temp.(^oC)	Pore size (µm)	Porosity (%)
Okubo *et al*., (1991)	α-Al_2O_3	Tubular	Extrusion	1427-1927	0.2-6.0	0.3
Ghaderi *et al*., (2013)	α- Al_2O_3	Flat	Vibration and uniaxial pressing	1325-1625	6.8-8.1	30-50
Kumar *et al*., (2006)	α-Al_2O_3 (A15, A16)	Disk	Compressing	1500	A15=0.3 A16=0.2	40
Falamaki *et al*., (2004)	α-Al_2O_3 and $ZrSiO_4$ with PVA	Disk	Uniaxial pressing	1425 1500	Both < 0.075	30
Qi *et al*., (2010)	α-Al_2O_3 and TiO_2	Tubular	Extrusion	1400	6.8	41.4
Bissett *et al*., (2008)	α-Al_2O_3	Tubular	Casting	1050-1400	0.25 0.31	37.2 35.8
Dong *et al*., (2007)	Cordierite powder	Tubular	Extrusion	1380	8.66	36.20
Alem *et al*., (2009)	α-Al_2O_3	Disk	Uniaxial pressing	1350	1.0	38
Almandoz *et al*., (2004)	Ball clay, kaolin, alumina, quartz and calcium carbonate	Tubular	Paste method	1200-1300	0.1-1	35-46
Takagi *et al*., (2000)	Al_2O_3 and water	Disk	Pressing	1245	0.16	54.09

Author	Raw Material	Support	Method	Sintering Temp.(°C)	Pore size (µm)	Porosity (%)
Bouzerara *et al*., (2006)	Kaolin and kaolin-dolama mixtures	Tubular and flat	Extrusion and dry pressing	1250	22-28	43-51
Patterson *et al.*, (2006)	α-Al_2O_3	Tubular	Centrifugal casting	1200	0.16	--
McCool *et al*., (2003)	α-Al_2O_3	Disk	Dry pressing	1200	0.1	35
Wang et al., (2006)	Alumina, TiO_2 (rutile), corn starch and Methyl Cellulose water	Disk	Uniaxial	1400	1.6	40
Masmoudi *et al.*, (2007)	Apatite powder	Tubular	Extrusion	1160	6	47
Chowdhury *et al*. (2003)	α-Al_2O_3	Disk	Colloidal filtration	1100	0.08-0.12	~30
Khemakhem *et al*., (2007)	Tunician clay	Tubular	Extrusion	1090	6.3	48
Workneh *et al*., (2008)	Kaolin, ball clay, cristoballite, pyrophyllite, feldspar, sodium metasilicate, boric acid, quarts and calcium carbonate	Disk	Paste method	950	0.2	51
Nandi *et al*., (2008)	kaolin, quartz, sodium Carbonate, boric acid, sodium metasilicate and calcium carbonate	Disk	Casting method	900	0.285	23.6
Vasanth *et al.,* (2011)	Kaolin, quartz and calcium carbonate	Disk	Uniaxial dry compaction	900	1.30	30

Table 1.5 Classification of literature based on pore size of the ceramic support/membranes

Author	Raw Material	Support	Method	Sintering Temp. (^{o}C)	Pore size (µm)	Porosity (%)
Falamaki *et al*., (2004)	α-Al_2O_3 and $ZrSiO_4$ with PVA	Disk	Uniaxial pressing	1425 1500	Both < 0.075	30
Chowdhury *et al*., (2003)	α-Al_2O_3	Disk	Colloidal filtration	1100	0.08-0.12	~30
McCool *et al*., (2003)	α-Al_2O_3	Disk	Dry pressing	1200	0.1	35
Almandoz *et al*., (2004)	Ball clay, kaolin, alumina, quartz and calcium carbonate	Tubular	Paste	1200-1300	0.1-1	35-46
Takagi *et al*., (2000)	Al_2O_3 and water	Disk	Pressing	1245	0.16	54.09
Patterson *et al*., (2006)	α-Al_2O_3	Tubular	Centrifugal casting	1200	0.16	--
Okubo *et al*., (1991)	α-Al_2O_3	Tubular	Extrusion	1427-1927	0.2-6.0	0.3
Workneh *et al*., (2008)	Kaolin, ball clay, cristoballite, pyrophyllite, feldspar,sodium metasilicate, boric acid, quartz and calcium carbonate	Disk	Paste method	950	0.2	51
Kumar *et al*., (2006)	α-Al_2O_3 (A15 and A16)	Disk	Compressing	1500	A15=0.3 A16=0.2	40
Bissett *et al*., (2008)	α-Al_2O_3	Tubular	Casting	1050-1400	0.25 0.31	37.2 35.8

Author	Raw Material	Support	Method	Sintering Temp. (^oC)	Pore size (µm)	Porosity (%)
Nandi *et al.,* (2008)	Kaolin, quartz, sodium carbonate, boric acid, sodium metasilicate and calcium carbonate	Disk	Casting method	900	0.285	23.6
Vasanth *et al.,* (2011)	Kaolin, quartz, calcium carbonate	Disk	Uniaxial dry compaction	900	1.30	30
Masmoudi *et al.,* (2007)	Apatite powder	Tubular	Extrusion	1160	6	47
Khemakhem *et al*., (2007)	Tunician clay	Tubular	Extrusion	1090	6.3	48
Qi *et al*., (2010)	α-Al_2O_3 and TiO_2	Tubular	Extrusion	1400	6.8	41.4
Dong *et al.,* (2007)	Cordierite powder	Tubular	Extrusion	1380	8.66	36.20
Bouzerara *et al*., (2006)	Kaolin and kaolin-doloma mixtures	Tubular and flat	Extrusion and dry pressing	1250	22-28	43-51
Wang et al., (2006)	Alumina, TiO_2 (rutile), corn starch and Methyl Cellulose water	Disk	Uniaxial	1400	1.6	> 40
Ghaderi *et al*., (2013)	α-Al_2O_3	Flat	Vibration and uniaxial pressing	1325-1625	6.8-8.1	30-50
Alem *et al*., (2009)	α-Al_2O_3	Disk	Uniaxial pressing	1350	1.0	38

1.6.2 Fabrication of zeolite-ceramic composite membranes

Recently, various types of composite membranes were synthesized by several groups of researchers. These included different type of materials combination such as ceramic-polymeric, polymeric-polymeric and ceramic-ceramic composite membranes. There are growing interest in the development of ceramic-ceramic composite membrane due to fact that it has higher corrosive resistance, solvent resistance and wider pH range of applicability instead of other composite membranes. Usually, composite membranes are asymmetric membranes that constitute a dense layer on a macroporous support. The ceramic-ceramic composite membranes hold superior combination of structural property, fouling resistance, flux and selectivity as compared to symmetric ceramic composite membrane. The resources generally used for the development of ceramic-ceramic composite membranes are α-alumina, γ-alumina, titania, zirconia, zeolites, and microporous glasses. Generally, inorganic membranes are prepared by dip coating (Pan *et al*., 2003; *Hao et al*., 2004; Majhi *et al*., 2009), spin coating (Wang *et al*., 2011), chemical vapor deposition (CVD) (Amanipour *et al*., 2012), hydrothermal synthesis (Jia *et al*., 1993; Nishiyama *et al*., 2001; Weh *et al*., 2002; Liu *et al*., 2007; Cui *et al*., 2008) and microwave assisted hydrothermal synthesis (Zhu *et al*., 2008; Li *et al*., 2006). In the hydrothermal synthesis, the solution is kept under the influence of temperature and generates autogenic pressure. For this technique, the precursor sols are prepared by reactions in an aqueous or organo-aqueous solution in the presence of an alkali or acid under the influence of heat and pressure. The reaction mixture has pseudo-catalytic effect at this condition. There are significant advantages of coating under the hydrothermal conditions over other techniques (Kaya *et al*., 2002). Firstly, the particle size and the morphology can be controlled easily by varying synthetic conditions. Secondly, the required crystalline phase can be synthesized directly at lower temperature.

Pan *et al*., (2003) prepared asymmetric hollow fiber γ-Al_2O_3 and Pd-γ-Al_2O_3 on Al_2O_3 support using vacuum assisted dip-coating process. The synthesized membrane was sintered at 500 °C and used for gas permeation study. The membrane possessed average pore size and porosity of 0.2 μm, and 20%, respectively. Hao *et al*., (2004) synthesized ZrO_2-Al_2O_3 composite membranes by sol-gel method using aluminum iso-propoxide $Al(C_3H_7O)_8$ and zirconyl chloride ($ZrOCl_2.8H_2O$) as starting raw materials. To prepare composite sol, bochmite sol and zirconia sol were mixed together at molar ratio of 1:1 of Al:Zr. Polyvinyl alcohol with an average molecular weight of 72000 (3 g/100 ml of H_2O) added to the composite sol at room temperature to prevent cracking of membrane during drying. Using dip-coating technique, composite membrane was fabricated on the inner surface of alumina tube. The composite membranes existed only tetragonal ZrO_2 when the sintering temperatures varied between 700 and 1100 °C. The average pore diameter of composite membranes was found to be 4.3 nm.

Amanipour *et al*., (2012) manufactured hydrogen-selective nano-composite ceramic membrane adopting a co-current CVD technique by depositing dense SiO_2 and Al_2O_3 layer on alumina ceramic support. The thickness of the prepared membrane has been evaluated and it is found to be 80-100 nm. Wang *et al*., (2011) prepared polymeric membrane by spin coating using mixture of poly(vinylidene fluoride) (18% wt.), poly(vinylpyrrolidone) (2% wt.) and dimethylacetamide (DMAc, 80% wt.) with vigorously stirring for 10 h under 60 °C. The spin coating was carried out with spin coater at different spinning conditions. After coating, the membrane was immediately immersed into distilled water. After 3 days, the membrane was taken out and subjected to permeability and rejection test. Jia *et al*., (1993) prepared zeolite (silicate-1) membrane on a ceramic disk support having diameter of 50 mm and thickness of 3 mm with Teflon autoclave reactor at 180 °C for 3-72 h. To remove the organic surfactant, the fabricated membrane was calcined at 450 °C for 8 h. The prepared composite membrane

was used for permeation study at room temperature and true selectivity of the membrane was found to be 2.81 for He over N_2 and 47.7 for N_2 over n-butane. Nishiyama *et al*., (2001) synthesized mesoporous silica MCM-48 composite membrane on alumina support (having pore size of 0.1 µm) by hydrothermal synthesis method at 90 °C for 96 h. The prepared MCM-48 membrane was investigated for the permeation of H_2, He, CH_4, O_2, N_2 and CO_2 gases at various applied pressures (100-270 kPa). The permeation of H_2 was independent of the feed pressure and no contribution of viscous flow to the total permeation.

It is noted that the mesoporous inorganic membranes synthesized from inorganic precursors and surfactant template have gained sincere interest due to the highly ordered meso-structure and numerous prospective applications in separation, catalysis, sensors, and opto-electric devices (Sakamoto *et al*., 2000; Wirnsberger *et al*., 2001; Nishiyama *et al*., 1998; Aksay *et al.*, 1996). The highly ordered mesoporous molecular sieves designated as M41S was discovered in 1992 (Kresge *et al*., 1992; Beck *et al*., 1992). The surfactant liquid crystal structure has got the most advantageous templating strategy, where it can adjust the pore size between 2 to 10 nm by using surfactants with dissimilar chain lengths. Generally, mesoporous materials consist of three types of structures: MCM-41 having hexagonal two dimensional pore structure, laminar crystal structure for MCM-50 and the cubical form of MCM-48. MCM-41 (belongs to M41S family) acquires a larger specific surface area and two dimensional regular hexagonal arrays of cylindrical pores. This is mostly utilized in shape selective catalysis, selective adsorption and separation processes, chemical sensors, and also in nanotechnology (Qin *et al*., 2009). MCM-41 has narrow pore-size distribution, large pore volume and high surface area. It also contains a negative charge density owing to the existence of Si-O and Si-OH groups. MCM-48 is the most potential upcoming material due to the existence of three-dimensional pore structure and the narrow pore size distribution.

Several research groups studied the fabrication of zeolite composite membrane for the applications in pervaporation and gas phase separation due to their promising features such as uniform molecular sized pores, good adsorption properties, thermal stability, mechanical and chemical stability. Further, among all types of composites organic and inorganic membranes, zeolite composite membrane has the potential to attain both high flux and selectivity due to the presence of well-defined crystals microspores in the zeolite framework. Amongst these, zeolite as a separating layer provides numerous benefits, for instance; pore size of the membrane can be regulated by using appropriate zeolite type. It can separate the component of gaseous or liquid mixtures based on molecular size due to its molecular sieve function. Moreover, its hydrophilic/hydrophobic character can be changed by the introduction of various functional groups on the zeolite framework. Numerous experimental techniques were addressed to prepare the selective layer of polymer, ceramic and zeolite composite membranes. Unlike the polymeric membrane, zeolite composite membrane did not swell. Due to the swelling nature of polymeric membrane, it has higher permeability and lower selectively (Praptowidodo 2005). A series of literature reported that various zeolite membranes, such as MCM-48 (Nishiyama *et al*., 2003; Kumar *et al*., 2008; Pedernera *et al*. 2009; Seshadri *et al*., 2011), MFI (Çulfaz *et al*., 2006; Zhang *et al*., 2012), FAU (Faujasite) (Jeong *et al*., 2003; Sato *et al*., 2007; Zhu *et al*., 2008; Covarrubias *et al*., 2008; Huang *et al*., 2012), LTA (Linde Type A) (Li *et al*., 2006; Huang *et al*., 2014), Silicate-1 (Jia *et al*., 1994; Wirawan *et al*., 2011), Analcime (Potdar *et al*., 2002, Kumar *et al*., 2006), ZSM-5 (zeolite socony mobil-5) (Yan *et al*., 1997, Oonkhanond and Mullins 2001), NaA (Ling *et al*., 2011; Jafari *et al*., 2013), CHA (Chabazite) (Maghsoudi and Soltanieh 2014; Hasegawa *et al*., 2010), were fabricated on porous and non-porous support.

In comparison with other composite membranes, mesoporous membranes are typically found several applications in many fields of charged mechanism separation processes due to the

presence of Si-O and Si-OH groups. FAU zeolite (NaX with Si/Al of 1.0-1.5) membranes have a three dimensional pore structure and 12-membered oxygen ring pores (0.74 nm) are suitable for separation of large molecules, in which LTA membrane (Jeong *et al*., 2002) cannot handled properly. Generally at low Si/Al ratio, FAU zeolite membrane is hydrophilic and it can be used for the dehydration of organic solvents by pervaporation or steam permeation (Zhu *et al*., 2009; Kita *et al*., 1997).

Nishiyama *et al*., (2003) developed zirconium-containing mesoporous silica (Zr-MCM-48) on a porous alumina support with an average pore diameter of 0.1 µm. The reaction was carried out in a vessel without stirring at 150 °C for 24 h. The product was rinsed with deionized water and calcined in air at 500 °C for 5 h. Titanium containing MCM-48 (Ti-MCM-48) powder was also prepared by the same method and Zr-MCM-48 showed more stability in alkaline solutions. The pore size of the composite Zr-MCM-48 was 2.5 nm. Gas permeation and permporometry test suggested that there is no large pinhole or cracks in the calcined Zr-MCM-48 composite membrane. Liu *et al*., (2007) synthesized the mesoporous silica MCM-48 on α-alumina tubular support having an average pore size of 3-5 µm and porosity of 30-40% by adopting pore pre-filling before putting in to stainless steel autoclave at 100 °C for 72 h. The average pore size of the MCM-48 membrane was 2.7 nm. The permeation of the single gas through the MCM-48 membrane was independent of pressure drop indicating no large pinholes and cracks in the membrane, which agrees with SEM observation. Wu *et al*., (2008) prepared MCM-48 membrane on α-alumina tube support using hydrothermal treatment for 72 h at 100 °C and calcined at 550 °C for 6 h. The vacuum coated alumina tube support possessed (11.5 mm in outer diameter, 8 mm in inner diameter) the average pore diameter of 1.0 µm and porosity 38 %. First, the tube was soaked in 30 % H_2O_2 solution for 8 h to activate the surface, washed with deionized water and dried at 100 °C for 12 h and pretreated support was coated with MCM-48. The separation factor of the

membrane was 3.33 for H_2/N_2 and the total flux for N_2 permeation was 97.8 %. Iglesia *et al*., (2006) developed MCM-48 on α-alumina tubular support using hydrothermal method at 90 °C for 48 h. The powder product and the membrane were washed with distilled water and calcined at 540 °C for 6 h to remove surfactants. The prepared membrane was investigated for the separation of gas phase mixture and the selectivity of cyclohexane/O_2 greater than 270 was obtained. The pore size of the support showed significant influence on the quality of the membranes and the best membranes in terms of performance were prepared on the tubular support with pore size of 60 nm or lower. Kim *et al*., (2013) fabricated MCM-48 composite membrane on α-alumina disk support by seeded growth technique and utilized for the separation of organic and water. The template was removed by calcination at 550 °C for 6 h. The prepared membranes were modified to achieve better surface properties by silylation with hexamethydisilane. The silylated MCM-48 membrane was investigated for the separation of ethanol, methyl ethyl ketone and ethyl acetate and the separation factor was in the range of 5-35 and the flux was 0.03-0.22 kg m^{-2} h^{-1} at 30 °C.

Hamad *et al*., (2008) prepared MCM-41 ceramic membrane on alumina and zirconia tubular support by hydrothermal synthesis technique at 120 °C for 20 h. The fabricated membranes were used for single gas permeation experiments for hydrogen, helium, nitrogen and argon. The authors reported that the gas permeation of N_2 and Ar is 30% higher than that of other gases. Gao *et al*., (2014) synthesized MCM-41 on ceramic support (alumious oxide) using hydrothermal synthesis technique at 120 °C for 48 h. The prepared MCM-41 ceramic membrane was impregnated with p-toluenesulfonic acid with different concentration. The fabricated membrane was utilized as a catalyst in trans-esterification of palm oil with methanol for production of biodiesel.

Weh *et al*., (2002) fabricated FAU-type composite membrane on a porous α-Al_2O_3 support by hydrothermal method in two steps. First, a seed layer of Na-Y nanocrystals was deposited

externally on the surface of ceramic support. Crystallization was kept under the reflux at 100 °C for 240 h. Secondly, the seeded support was again synthesized hydrothermally in Teflon autoclave at 90 °C for 12 h and it was treated with microwave oven at 100 °C for 2 h. The dense FAU layer was intergrown with Si/Al ratio of 1.3-1.8 and thickness in the range of 0.8-6 µm depending on synthesis condition. The observed result revealed that permeation of the single gas was in the order of $H_2 > CH_4 > N_2 > O_2 > CO_2 > nC_4H_{10} > SF_6$. Jeong *et al*., (2003) prepared FAU-type zeolite membrane on a porous α-Al_2O_3 support tube by treating hydrothermally at 90 °C for 24 h. The catalyst, 1.0 wt % Pt/Al_2O_3 was deposited on the membrane by an impregnation method in the temperature range of 150-250 °C. The fabricated membrane was utilized for the selective separation of benzene and hydrogen from cyclohexane. They indicated that the conversion of cyclohexane increased with increasing flow rate and the decrease in the feed rate of cyclohexane led to a higher cyclohexane conversion upto 72.1% at 200 °C. Zhu *et al*., (2008) fabricated FAU-type zeolite membrane by microwave assisted in situ crystallization on porous α-Al_2O_3 tubes. The synthesis solution was prepared by dissolving aluminum foil into sodium hydroxide solution, and then adding silica sol into the solution. The synthesis solution was transferred in a Teflon autoclave for 8 h at 60 °C and microwave heating was done at 90 °C for 20 min with 1400 W power. The authors reported the single gas permeation of H_2, N_2, n-C_4H_{10} and i-C_4H_{10} through the fabricated membrane and H_2 a showed higher permeation. Guillou *et al*., (2009) synthesized FAU-type zeolite membrane on α-alumina tube using hydrothermal method at 85 °C for 24 h. The membrane was utilized for the separation of CO_2/N_2. The obtained results demonstrated the CO_2 permeance of 3.5×10^{-7} mol $s^{-1}m^{-2}Pa^{-1}$ and selectivity of 12 for the separation of equimolar CO_2/N_2 gas mixtures at 50 °C. Huang *et al*., (2012) prepared FAU zeolite membranes using 3-aminopropyltriethoxysilane (APTES) as covalent linker between the FAU layer and the alumina support by in-situ crystallization (about pH 7) at 75 °C for 24 h.

The developed membrane was tested for the separation of gas from the mixture of gases. The separation factors for H_2/CO_2, H_2/N_2, H_2/CH_4 and H_2/C_2H_8 were found to be 6.5, 6.0, 4.0, and 11.1, respectively.

Potdar *et al*., (2002) prepared modified Analcime zeolite composite membrane by hydrothermal crystallization on the clay disc support at 180 °C for 2-5 days. For modification, the membrane was nitrated using NOx and then aminated by reacting membrane with hydrazine hydrate. The unmodified (Z_1), nitrated (Z_2) and aminated (Z_3) zeolite membranes were used for the separation of surfactant (Cetyl Pyridinium Chloride, CPC) by ultrafiltration. The modified membrane displayed the improved surfactant retention of 300% and also showed a considerable enhancement in the permeate flux. Liu *et al*., (2005) fabricated analcime zeolite membrane on α-alumina plate support (15 × 15 × 2 mm) by hydrothermal synthesis method at 180 °C for 72 h. The product obtained was dried at 180 °C for overnight and calcined at 500 °C for 6 h for the removal of template. The structural and thermal stability of the prepared membrane were confirmed by means of XRD, FTIR and DTA analysis.

Cui *et al*., (2008) fabricated NaA zeolite composite membrane on α-alumina tube by hydrothermal synthesis method at 100 °C with various durations (i.e. 2, 4, 10 and 18 h). The support pore size was between 1 µm to 3 µm and porosity between 30 and 40%. The prepared composite membranes with pore sizes of 1.2 µm and 0.4 µm were used to treat oil-in-water emulsion containing 100 mg/ L oil and 99% oil rejection was reported. Sato *et al*., (2008) synthesized NaY zeolite membrane on a porous tubular shaped alumina support and used for the pervaporation of ethanol in industrial scale. The prepared zeolite membrane showed high performance for dehydration of the hydrous ethanol mixture at 75 °C. Jia *et al*., (1994) prepared ceramic-zeolite composite membrane on the inner surface of γ-alumina tube by in-situ hydrothermal synthesis at 180 °C for 12 h. SEM images showed that individual silicalite

crystals were grown together continuous as silicalite-1 layer. The membrane displayed high permeance for gases and shape-selectivity was found with the n-C_4H_{10}/i-C_4H_{10} permeance ratio of 3:1. Maghsoudi and Soltanieh (2014) prepared the CHA-type zeolite membrane on the disk shaped α-alumina support by in-situ crystallization method for the separation of H_2S and CO_2 gases from methane. The separation results specified that both gases can be removed from methane with selectivity of 3.14 for H_2S/CH_4.

In summary, numerous synthetic techniques have been employed for the preparation of zeolite membrane such as in-situ (without seeding) hydrothermal synthesis (Noble and Falconer 1995), secondary (seeded) growth (Lassinantti *et al*., 2000), vapor phase transport (Matsufuji *et al*., 2000) and post-treatments of zeolite membranes (Yan *et al*., 1997). Mesoporous silica, FAU and Analcime zeolite membranes have been prepared by hydrothermal synthesis method onto a porous support in one or multiple cycles involving either in-situ or with a preliminary seeding step. Hydrothermal synthesis method is easy to implement in operation point of view as compared to other preparation techniques. Table 1.6 represents summary of various literatures for the fabrication of zeolite-ceramic composite membranes.

1.6.3 Application of composite membranes

Till date, ceramic membranes have been found to be appropriate in various fields of separation applications such as desalination, food processing, nanotechnology, industrial effluent treatment and for treatment of potable water. In this work, an attempt has been made for the preparation of various types of zeolite membranes on low cost circular shaped ceramic support and to check the compatibility in liquid phase separation applications. The separation of metal ions (Cr, Fe, Al) from aqueous solution was considered. This is due to the fact that

these refer to the standard applications for the probable of ceramic membranes in industrial possessing scenario.

Table 1.6 State of the art in zeolite-ceramic composite membranes

Authors	Support materials	Skin layer material	Method of preparation
Pan *et al*., (2003)	Al_2O_3	γ-Al_2O_3	Dip-coating
Amanipour *et al*., (2012)	Alumina	Al_2O_3 and SiO_2	Chemical vapor deposition
Jia *et al*., 1993	Alumina	Silicate-1	In-situ hydrothermal
Nishiyama *et al*., (2001)	Alumina	MCM-48	Hydrothermal treatment
Weh *et al*., (2002)	Alumina	FAU zeolite	Hydrothermal synthesis
Wu *et al*., (2008)	α-alumina tube	MCM-48	Hydrothermal treatment
Huang *et al*., (2012)	Alumina	FAU zeolite	In-situ crystallization method
Cui *et al*., (2008)	α-alumina tube	NaA zeolite	Hydrothermal synthesis
Yan *et al*., (1997)	α-Al_2O_3	ZSM-5	In-situ crystallization method
Kim *et al*., (2013)	α-Alumina	MCM-48	Seeded growth technique
Guillou *et al*., (2009)	α-alumina tube	FAU zeolite	Hydrothermal synthesis
Jafari *et al*., (2013)	γ-alumina	NaA zeolite	Secondary growth method
Liu *et al*., (2005)	α-alumina	Analcime zeolite	Hydrothermal synthesis
Huang *et al*., (2014)	α -alumina tube	LTA zeolite	Hydrothermal synthesis
Çulfaz *et al*., (2006)	α -alumina tube	MFI	Dip-coating (seeding)
Zhang *et al*., (2012)	α-Al_2O_3	MFI	Hydrothermal crystallization
Maghsoudi and Soltanieh (2014)	α-Al_2O_3	CHA zeolite	Crystallization method
Wirawan *et al*., (2011)	α-alumina	Silicate-1	Hydrothermal synthesis
Covarrubias *et al*., (2008)	α-alumina disk and tubular	FAU zeolite	Seed growth and hydrothermal synthesis

1.6.3.1 Separation of chromium from aqueous solution

Chromium is a toxic chemical species involved in severe environmental pollution problem. It is mostly available in hexavalent (Cr (VI)) and trivalent states (Cr (III)), where Cr (VI) is more toxic in comparison to Cr (III) (Muthukrishnan and Guha 2008). Cr (VI) may exist in various forms such as $HCrO_4^-$, CrO_4^{2-}, and $Cr_2O_7^{2-}$ and stability of all chromate ions depends on pH of the system (Gzara and Dhabhi 2001; Cassano *et al*., 1996; Fabiani *et al*., 1996). The main human toxicities are lung cancer, kidney damage, liver and gastric problem (Kimbrough *et al*., 1999). Besides, chromium affects plants and animals. According to World Health Organization (WHO), the discharge limit of Cr (VI) into water bodies is 0.05 mg/L (Kozlowski and Walkowiak 2002). The Ministry of Environment and Forest, Government of India, has fixed the minimal national standards (MINAS) as 0.1 mg/L containing Cr (VI) for the safe disposal of effluent in surface water.

Chromium species are particularly present in the wastewater from various manufacturing units including, metal plating, paintings and pigments, galvanization, printing inks, textile and dye industries and leather tanning (Religa *et al*., 2011; Lakshmipathiraj *et al*., 2008; Sacmaci *et al*., 2012; Nataraj *et al*., 2007). Therefore, it is essential to recover chromium from waste disposal for the environmental eco-friendly system. Different technologies have been established for the removal of Cr (VI) such as adsorption (Garg *et al*., 2004; Namasivayam and Yamuna 1995; Sarma *et al*., 2005; Salgado-Gomez *et al*., 2014), precipitation (Golder *et al*., 2011), photocatalytic (Das *et al*., 2006; Mohapatra *et al*., 2005), ion-exchange (Galan *et al*., 2005), extraction using solvent (Alonso *et al*., 1994), bio-reduction (Han *et al*., 2007; Sahinkaya *et al*., 2012) and membrane based separation process (Neelakandan *et al*., 2003; Sanchez *et al*., 2011). The separation of inorganic pollutants with membrane processes has several advantages such as, no requirement or addition of chemicals, simple alteration of modular membrane area as per the effluent load, lower energy

requirement, maximum recovery and higher yield of purified water. According to the membrane separation techniques cited in the literature, microfiltration (MF) (Sondhi *et al.*, 2000), ultrafiltration (Kishore *et al.*, 2003; Shukla and Kumar 2004; Pugazhenthi *et al.*, 2005), nanofiltration (Hafiane *et al.*, 2000), reverse osmosis (Hafez and El-Manharawy 2004) and electrodialysis (ED) (Frenzel *et al.*, 2005) have been frequently used for the removal of chromium from aqueous solution.

Neelakandan *et al.*, (2003) studied the removal of Cr (VI) using modified and unmodified poly (methyl methacrylate-ethylene glycol dimethacrylate) copolymer ultrafiltration membrane. The rejection of unmodified and modified membrane was found to be 68 %, and 67 %, respectively. The hydrophilicity and the solute flux of the membrane were increased after modification with NOx. In another work, the unmodified carbon membrane displayed a maximum Cr (VI) rejection of 96% whereas nitrated and aminated carbon membrane demonstrated around 84%, and, 88%, Cr (VI) rejection, respectively (Pugazhenthi *et al.*, 2005). Shukla and Kumar (2007) investigated the removal of Cr (VI) using modified zeolite composite ultrafiltration membranes. The membranes were modified using NO_x (Z_2) and further by hydrazine hydride (Z_3). The results showed that the observed rejection of the modified membranes increased from ~20 % (unmodified) to 40 % (Z_2) and ~50 % (Z_3). Also, the observed rejection displayed anomalous trend with variations in pressure while the intrinsic rejection increased with increasing pressure, which is typical for the separation of electrolyte by charge membrane. Arthanareeswaran *et al.*, (2007) investigated the removal of Cr (VI) with ultrafiltration process using cellulose acetate and sulfonated poly (ether ether ketone) ultrafiltration membrane from aqueous solution. The role of various factors such as concentration of solute, pH, concentration of PVA, applied pressure and composition of blending membranes on the rejection and permeate flux was examined. The authors reported a maximum rejection of 93% at a feed concentration of 200 ppm. Sachdeva and Kumar

(2008) prepared styrene acrylonitrile composite membrane on a ceramic support by coating a prepolymer solution obtained using a dual initiator system. The prepared membrane was chemically modified by gas phase nitration followed by amination reaction to make charged. The modified composite membrane is employed for the separation of chromic acid at different pressures, feed concentrations and pH. The mean pore size of the unmodified, modified with NOx and aminated membrane were 6.26, 8.32 and 11.2 nm, respectively. The rejection was found to be 90% with modified membranes for the concentration of 1000 ppm at pH 3. Ren *et al*., (2010) fabricated asymmetric poly (m-phenylene isophthalamide) nanofiltration membrane by phase inversion method for the removal of Cr (VI) from wastewater. The highest retention of 98% was achieved at pH 8 among the studied parameters (applied pressure, feed concentration and pH). Sanchez and Rivas (2011) fabricated cationic hydrophilic polymers coupled to the ultrafiltration membrane for the retention of Cr (VI). They reported that the highest rejection capacity of all the membranes was obtained at operating pH of 9. Hafiane *et al*., (2000) employed the removal of hexavalent chromium by nanofiltration and the process was studied as function of pH as well as ionic force. The authors reported the rejection of 80% at a feed concentration of 1 mM and nanofiltration is a promising candidate with the charged for the removal of hexavalent chromium. Aroua *et al*., (2007) investigated the removal of Cr (III) and Cr (VI) from aqueous solution by polymer-enhanced ultrafiltration using polysulfone membranes. The complete removal of chromium was achieved for the feed concentration of 10 ppm. Vasanth *et al*., (2012) prepared ceramic microfiltration membrane by uni-axial dry compaction method from low cost clays and tested for the separation of Cr (VI) using baker's yeast biomass. They reported that the rejection increased with increasing concentration of biomass and the highest rejection was obtained at pH = 1. The Table 1.7 represents the summery of literatures on various membranes for the removal of Cr (VI).

Table 1.7 Performance characteristics of various membranes for the removal of Cr (VI) from aqueous solution

Membrane	Method of filtration	Concentration (ppm)	Rejection (%)	Reference
PMMA-EDGM	Dead-end UF	1000	68	Neelakandan *et al*., (2003)
Cellulose acetate	Dead-end UF	200	93	Arthanareeswaran *et al*., (2007)
Carbon	Dead-end UF	1000	96	Pugazhenthi *et al*., (2005)
Ceramic membrane	Cross flow filtration	1000	99	Sondhi *et al*., (2000)
Zeolite-clay	Dead-end filtration	1000	66	Shukla and Kumar (2007)
Styrene acrylonitrile	Dead-end UF	1000	90	Sachdeva and Kumar (2008)
Composite polyamide	NF	1000	99	Muthukrishna and Guha (2008)
Poly (m-phenylene isophthalamide)	NF	5	98	Ren *et al*., (2010)

1.6.3.2 Separation of trivalent metal ions from aqueous solution

$FeCl_3$ and $AlCl_3$ salts are major useful and hazardous compounds having a large field of application in chemical industries, such as dyeing, printing, industrial and sanitary wastewater treatment, paper and pulp wastes, oily wastes, chlorinating agent in metallurgical manufacturing and organic synthesis, catalyst and electronic print. The effluent produced from these industries contains heavy metal compounds. It was reported that the oily wastewater discharged from industries possesses $FeCl_3$ with concentration of 4820 ppm (Mohammed *et al*., 2007) while the dye industry produces an effluent containing 1000-6000 ppm of $FeCl_3$ with pH ~2 (Likhar and Shivramwar 2013). Pharmaceutical wastewater

containing chloride disposed concentration of 2030 ppm (Parmar and Upadhyay 2013). An inhalation of this hazard may damage liver and kidney, irritate nose, Parkinson, Alzheimer disease, blood cells, throat and eye problem (Lima *et al*., 2007). In general, such contaminated metals occurring in wastewater are acknowledged as inorganic micropollutants, which are non biodegradable in the environment. Moreover, these pollutants need to be reduced to standard level of disposal norms controlled by legislation before being thrown into the inland and surface water.

Inorganic micropollutants are normally toxic, non biodegradable and harmful to all living being in the environment. To minimize all these pollutants upto the standard level, there are few traditional practices, for instance, the reduction process or lime precipitation and adsorption method (Gzara and Dhabi 2001, Choksi and Joshi 2007). On the other hand, these methods are unable to reduce the concentration up to the required norms provided by legislation. Hence, various other separation techniques, such as ion-exchange (Frenzel *et al*., 2005; Nataraj *et al*. 2007, Kim *et al*., 2015) and reverse osmosis (Oh *et al*., 2014; Cassano *et al*., 1996, Ochando and Pulido 2015), have been employed for reaching the concentration level of pollutants to an acceptable limit. However, these are expensive processes. Therefore, an alternative feasible technique needs to be searched, which should be less expensive. Generally, majority of inorganic micropollutants contain metal ions accompanying charge and in this fact, charged membranes can be utilized for the separation of metal ions (Kumar *et al*., 2015). Shukla and Kumar (2005) utilized the modified zeolite-clay composite membrane for the removal of trivalent salts ($FeCl_3$ and $AlCl_3$) from aqueous solution. They reported that the observed rejection for $FeCl_3$ was higher than that of $AlCl_3$ and the rejection was dependent on the interaction between the membrane and the salt. Majhi *et al*., (2009) fabricated γ-Al_2O_3 composite membrane on a circular shaped ceramic support by dip coating method. The prepared membrane was utilized for the separation of $MgCl_2$ and $AlCl_3$. The

authors reported the maximum rejection of 72%, for $MgCl_2$ and 88% for $AlCl_3$ for the salt concentration of 3000 ppm. The rejection and flux behavior were strongly dependent on electrostatic interaction between the charged molecules and the composite membrane. Cifci and Kaya (2010) investigated the removal of metals (Fe (III), Cu (II)) from aqueous solution with PVA/cellulose composite membranes. Experiments were carried out batch stirred ultrafiltration. The membrane showed a maximum rejection of 82% for Fe (III) at an applied pressure of 414 kPa with pH 3 and for Cu (II), rejection was 44% for the same applied pressure with pH 7.

1.7 Outcome of literature review

From the above literature review, the following points are drawn:

- The raw materials (α-Al_2O_3, γ-Al_2O_3, zirconia, titania) used for the membrane support fabrication were expensive. Therefore, there is a need to explore alternative cheaper raw materials that should provide ceramic membranes with better characteristics.
- The methodology available in the literature for the fabrication of ceramic membrane support was complex practice. Therefore, the fabrication of ceramic support by a facile technique needs to be indentified for the minimization of cost.
- The sintering temperature used for the fabrication of support was greater than 1200 ^{o}C. Hence, the reduction of sintering temperature below 1000 °C would be beneficial for the additional reduction of cost of the membrane.
- Selective layer precursors of MCM family and Faujasite (FAU) zeolite were mostly prepared on α-Al_2O_3 support and exclusively used for gas phase separation applications. Very few studies were reported for liquid phase separation application.

- None of the literature reported the formation of selective layer of MCM-41, MCM-48, FAU zeolite and Analcime-C on low cost ceramic support derived from clays for liquid phase separation applications.
- Synthesis of coating (separating) layer under hydrothermal conditions has some significant advantages over any other chemical synthesis techniques, which includes easy controlling of particle size and morphology by varying the synthesis conditions.

1.7.1 Objectives of the thesis

Based on the literatures review, the following major objectives are indentified and addressed in the thesis:

1. Fabrication and characterization of low cost circular shaped ceramic support by uni-axial compaction method.
2. Preparation and characterization of MCM-41, MCM-48, Faujasite (FAU) and Analcime-C zeolite-ceramic composite membranes by hydrothermal synthesis method.
3. Performance evaluation of the prepared zeolite-ceramic composite membranes by the separation of chromium and trivalent metal ions from aqueous solution in a dead-end batch filtration set-up.
4. Cross flow ultrafiltration of chromium and trivalent metal ions from aqueous solution using zeolite composite membranes.

1.8 Organization of the thesis

Chapter 1 elaborates introduction and literature review

Chapter 2 addresses the fabrication and characterization of MCM-41 composite membrane on a porous circular shaped support by hydrothermal synthesis method. The properties of MCM-41-ceramic composite membrane and MCM-41 powder were evaluated by X-ray diffraction (XRD), porosity, thermogravimetric analysis (TGA), nitrogen adsorption-desorption isotherm (BET), Fourier transform infrared spectroscopy (FTIR), field emission scanning electron microscopy (FESEM), pure water permeation test and zeta potential measurement. The fabricated MCM-41-ceramic composite membrane was subjected to investigate its potential for the separation of metal ions from aqueous solution.

Chapter 3 presents the preparation of ordered mesoporous MCM-48 ceramic composite membrane on a macroporous ceramic support using tetraethyl orthosilicate (TEOS) and cetyltrimethyl ammonium bromide (CTAB) as source materials by hydrothermal crystallization technique. The performance of MCM-48 ceramic composite membrane was evaluated by one separation of metal ions from aqueous solution.

Chapter 4 deals with the development of Faujasite (FAU) zeolite composite membrane via hydrothermal treatment method on a circular shaped ceramic support. The potential of the synthesized FAU zeolite composite membrane was tested for the separation of metal ions with different operating parameters such as applied pressure, initial feed concentration and pH.

Chapter 5 describes the removal of metal ions from aqueous solution in cross flow mode using MCM-41, MCM-48 and FAU zeolite composite membranes.

Chapter 6 elaborates the synthesis of analcime-C zeolite membrane on a ceramic support by hydrothermal crystallization technique. The separation performance of the membrane was evaluated by removal of Cr (VI) from aqueous solution using dead-end ultrafiltration (UF) set up at various operating conditions.

Chapter 7 presents the summary of the inference drawn from the present research work and provides some suggestion towards future direction of research.

Chapter 2

Fabrication, Characterization of MCM-41-Ceramic Composite Membrane and Its Application in the Separation of Metal Ions from Aqueous Solution

Fabrication, Characterization of MCM-41-Ceramic Composite Membrane and Its Application in the Separation of Metal Ions from Aqueous Solution

This chapter addresses the selection of low cost raw materials and its composition, fabrication techniques used for low cost circular shaped ceramic support, which can yield symmetric membrane support with nominal pore size of ~1.00 µm. The ceramic support was sintered at 950 °C and characterized with various techniques that would be an alternative for high cost commercial α-alumina, zirconia and titania membrane supports. The fabrication of MCM-41 membranes on ceramic support by in-situ hydrothermal method and the characterization of prepared membranes are presented. The synthesized membrane is investigated for the separation performance of chromium and trivalent metal ions from aqueous solution with homemade dead-end filtration set up.

2.1 Experimental

2.1.1 Materials

The precursors utilized for the fabrication of ceramic support were kaolin [$Al_2Si_2O_5(OH)_4$], ball clay ($3SiO_2Al_2O_3$), feldspar (Na, Ca)($AlSiO_8$), pyrophyllite [$Al_2(Si_2O_5)_2(OH)_2$], and quartz (SiO_2). These materials were collected from Kanpur, India. Tetraethyl orthosilicate [$Si(OC_2H_5)_4$], calcium carbonate ($CaCO_3$), hydrochloric acid, chromium (VI) oxide and polyvinyl alcohol (PVA, M.W. 72000) were purchased from Merck (I) Ltd, Mumbai. Ferric chloride, aluminium chloride (hexahydrate) and sodium hydroxide were procured from Loba Chemie (Laboratory Reagents & Fine Chemicals), Mumbai, India. Cetyltrimethyl ammonium

bromide (CTAB) was obtained from SRL, Mumbai, India. Water used in this work was taken from Millipore water system (ELIX-3).

2.1.2 Preparation of ceramic membrane support

For the preparation of circular shaped ceramic support, the composition of the clay powders along with its significance is given in Table 2.1. The precursors were mixed in a ball mill with the addition of 4 ml of 2 wt% aqueous polyvinyl alcohol (Monash and Pugazhenthi 2011a). After that, an appropriate amount of the mixture was compacted by uniaxial pressing at an applied pressure of 50 MPa. The prepared supports were first dried at 100 °C for 24 h, 200 °C for 24 h in a hot air oven (make: Reico, India; model: ROV/DG) and sintered at 950 °C for 6 h with a heating rate of 2 °C/min in a muffle furnace (make: Lab Tech, Korea; model: LEF-115P-2). Then the supports were allowed to reach room temperature by natural cooling. To obtain smooth surface of supports, both sides of the prepared supports were polished using silicon carbide abrasive paper (No. C-220). The ceramic supports were cleaned with Millipore water in an ultrasonic bath [make: Elma (Germany); model: T460] for 15 min to remove the loose particles created during polishing. Fig. 2.1 displays the procedure used for the fabrication of ceramic support. The uniaxial hydraulic press and the mould used for the preparation of ceramic support at different stages are illustrated in Fig. 2.2.

Table 2.1 Composition of clay powders used for the fabrication of ceramic support

Raw Material	Composition (wt %)	Significance
Kaolin ($Al_2(Si_2O_5)(OH)_4$)	14.45	Low plasticity and high refractory property
Ball Clay ($3SiO_2Al_2O_3$)	17.58	Provides plasticity and strength to the green support.
Feldspar ((Na.Ca) ($AlSi_3O_8$))	5.60	Acts as a flux to form glassy phase at low temperature
Quartz (SiO_2)	26.59	Increases mechanical and thermal stability
Calcium carbonate ($CaCO_3$)	17.14	Pore forming agent
Pyrophyllite ($Al_2(Si_2O_5)_2(OH)_2$)	14.73	To reduce crazing

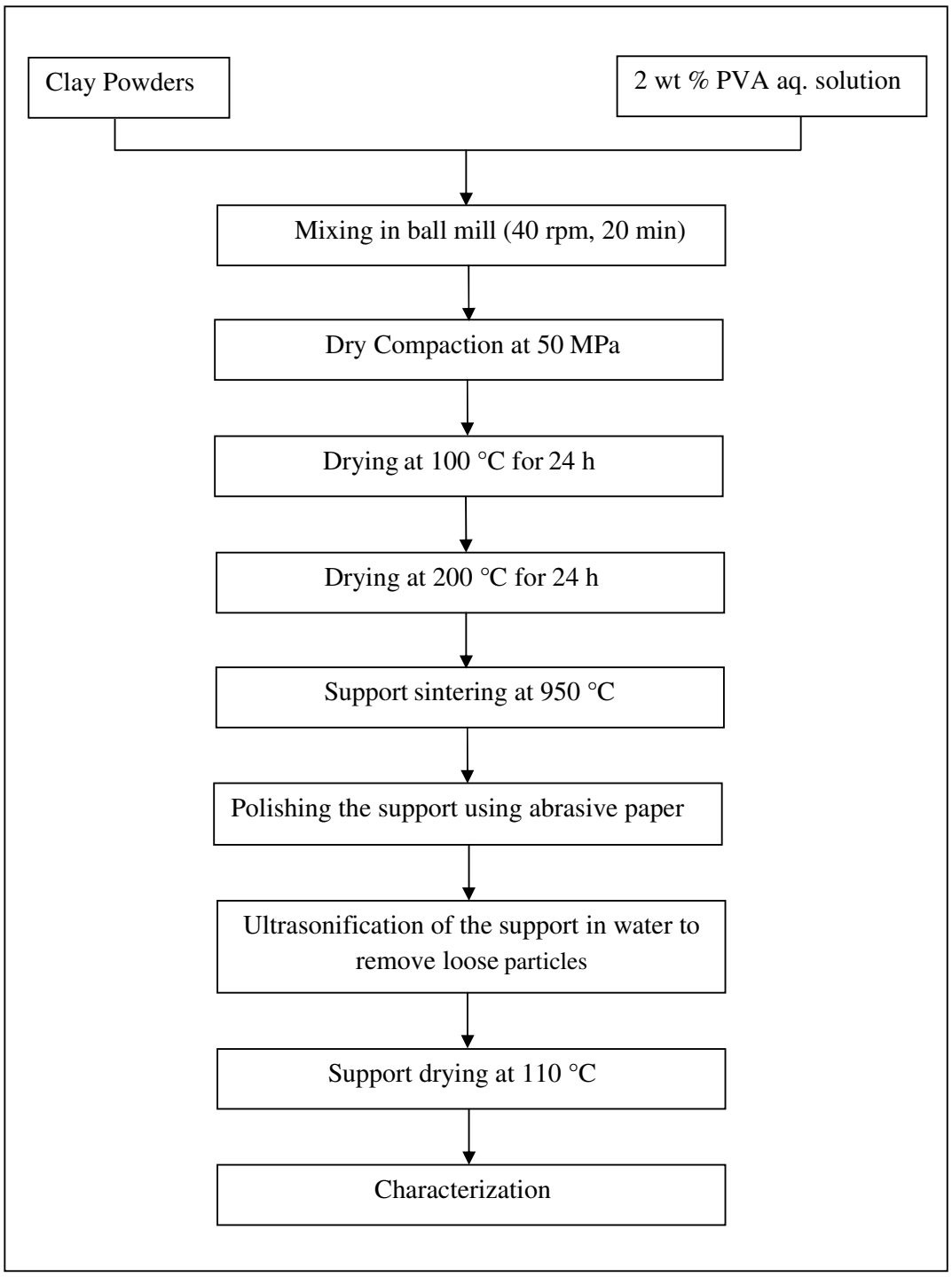

Fig. 2.1 Schematic representation for the fabrication of circular shaped ceramic support

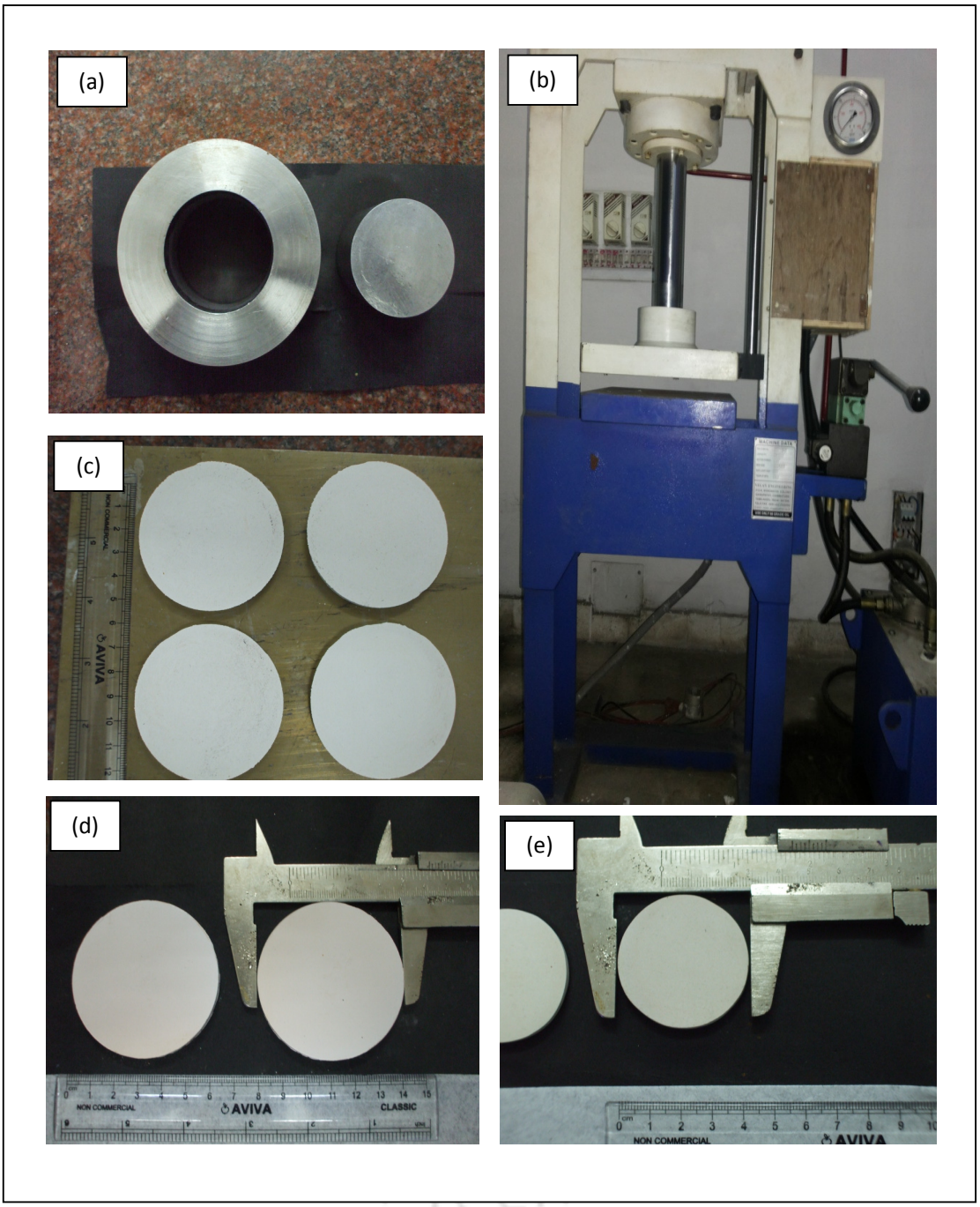

Fig. 2.2 Photographs of various stages of circular shaped ceramic support (a) Stainless steel mould, (b) Hydraulic Uniaxial Press, (c) green membrane supports, (d) sintered membrane support and (e) shaped membrane support.

2.1.3 Preparation of MCM-41-ceramic composite membrane

A solution was firstly prepared by dissolving 4.65 g of CTAB in 110 ml of Millipore water and an another separate solution was also made in 27 ml of Millipore water with 1.53 g of NaOH. Both solutions were mixed together and stirred continuously for 4-5 h at room temperature to get a homogeneous solution. Then the dried ceramic support (42 mm in diameter and 4 mm thickness) was placed in the beaker and 26.59 g of TEOS was added in the beaker. Finally, the above prepared solution mixture was also added in the beaker and stirred using a laboratory stirrer at 200-300 rpm till a gel like suspension formation was obtained. The resulting gel mixture was then crystallized under the static hydrothermal condition at 110 °C in a Teflon coated autoclave reactor placing a ceramic support at the bottom for 96 h. The molar composition of the gel was 1TEOS:0.1CTAB:0.3NaOH:60H_2O. Solid products were obtained by filtration and washed with Millipore water. Then as-synthesized material was dried in a hot air oven at 100 °C for 24 h and calcined at 550 °C for 5 h at the heating rate of 1 °C/min in a muffle furnace. Fig. 2.3 illustrates the synthesis of the MCM-41-ceramic composite membrane. To enhance the amount of MCM-41 deposition on ceramic support, MCM-41-ceramic composite membrane was fabricated by repeated cycle of deposition with synthesized sol followed by crystallization reactions. The gain in the mass of ceramic membrane was estimated after every cycle of synthesis. No significant weight increment was observed after third coating. Therefore, further coating with MCM-41 on the support was stopped and the prepared MCM-41-ceramic composite membrane (three cycle of coating) was used for the separation applications.

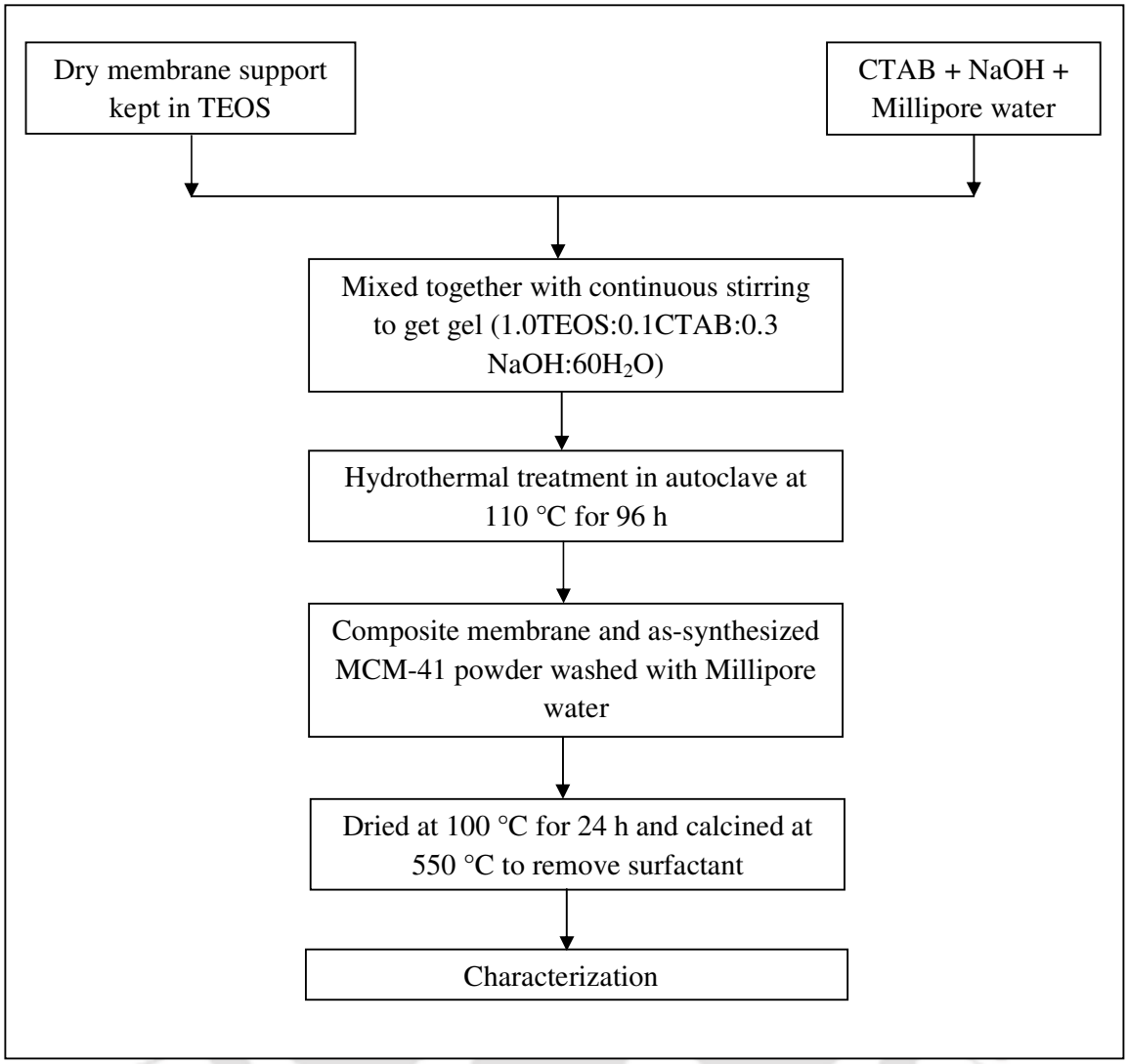

Fig. 2.3 Flowchart for fabrication of MCM-41-ceramic composite membrane

2.2 Characterization

X-ray diffraction (XRD) analysis of ceramic support and MCM-41 powder was carried out at room temperature under air atmosphere on a Bruker A8 advance instrument operating at 40 kV and 40 mA using CuKα (λ=1.5406 A˚) radiation. The diffraction data were recorded in the 2θ range of 1-10° for MCM-41 powder and 2θ range of 5-75° for supports at a scanning rate of 0.01 °s^{-1} and a step size of 1 s. Thermogravimetric analysis (TGA) of raw materials used for the fabrication of ceramic support and as-synthesized MCM-41 powder was

performed on a Netzsch TG 209F1 Libra at an air atmosphere. The particle size distribution analysis was performed in a particle sizing machine Malvern Mastersizer 2000 (APA 50005 ® model) for clay materials in wet dispersion mode by circulating the feed at fixed flow rate (pump speed = 2700 rpm) with an ultrasound to avoid the agglomeration of the clay powder during experiments. FTIR spectra for MCM-41 powders were recorded in the 4000-450 cm^{-1} region employing KBr powder with a Shimadzu IR Affinity-1 model spectrometer. Nitrogen adsorption/desorption isotherm of MCM-41 powder samples was carried out using a Quantachrome ® Asiqwin ^{TM}-Automated Gas Sorption (Version 3.0). First, samples were degassed at 150 ^{o}C for 3 h prior to measurement. The specific surface area was computed from the BET (Brunauer-Emmett-Teller) model. According to the BJH (Barrett-Joyer-Halenda) approach, the pore size distribution and the total pore volume were determined at a relative pressure (P/P_0) of 0.99, assuming that full surface saturation has been accomplished with nitrogen. Zeta potential measurement of MCM-41 powder was carried out with Beckman Coulter model Delsa Nano at various pH values.

Porosity of ceramic support and the MCM-41-ceramic composite membrane was calculated using Archimedes' principle (Monash and Pugazhenthi 2011b). Firstly, the dry mass (M_D) of the membrane was determined after drying the membrane in a hot air oven (make: Reico, India; model: ROV/DG) at 110 °C for 6 h. Then, the mass of the wet membrane (M_W) was measured when all pores are filled with water under vacuum. After that, the mass of water saturated membrane (M_A) was measured when the membrane is immersed in water (A refers to Archimedes). The porosity (ε) of the membrane was computed using the following relation,

$$\varepsilon = \frac{M_W - M_D}{M_W - M_A} \tag{2.1}$$

The surface morphology of support and the MCM-41-ceramic composite membrane was monitored by field-emission scanning electron microscope (FESEM) using a Zeiss Sigma instrument at 3-KeV acceleration voltage. The membrane sample was coated with gold to a thickness of approximately 150 A°, before being analyzed the FESEM images of both top surface of support and elaborated layer.

2.2.1 Pure water flux and hydraulic permeability

Pure water permeation experiments through the support and composite membrane were conducted in a dead-end flow filtration set-up made up of stainless steel 316 as shown in Fig. 2.4. Prior to water flux measurement, Millipore water was allowed to pass through the membranes at high pressure (483 kPa) to remove the loose particle (if any) present in the membrane. Then the pure water flux was measured at various applied pressure. For every experiment at different pressure, 150 ml of pure water was filled in the top compartment, the initial 50 ml of permeate was discarded and the time required for second 50 ml of water was noted down for the calculation of pure water flux and the permeability. From that data, the permeability (L_h) and the average pore size of the membranes are determined assuming cylindrical pores using Hagen-Poiseuille equation (Almandoz *et al.*, 2004; Bowen *et al.*, 1997),

$$J_w = \frac{\varepsilon r^2 \Delta P}{8\mu\tau l} = L_h \Delta P \qquad (2.2)$$

where J_w is the water flux through the membrane, ΔP is the applied pressure across the membrane, L_h is the water permeability of the membrane, r is the mean pore radius, μ is the viscosity of water, τ is the tortuosity factor, l is pore length, and ε is the porosity of the membrane.

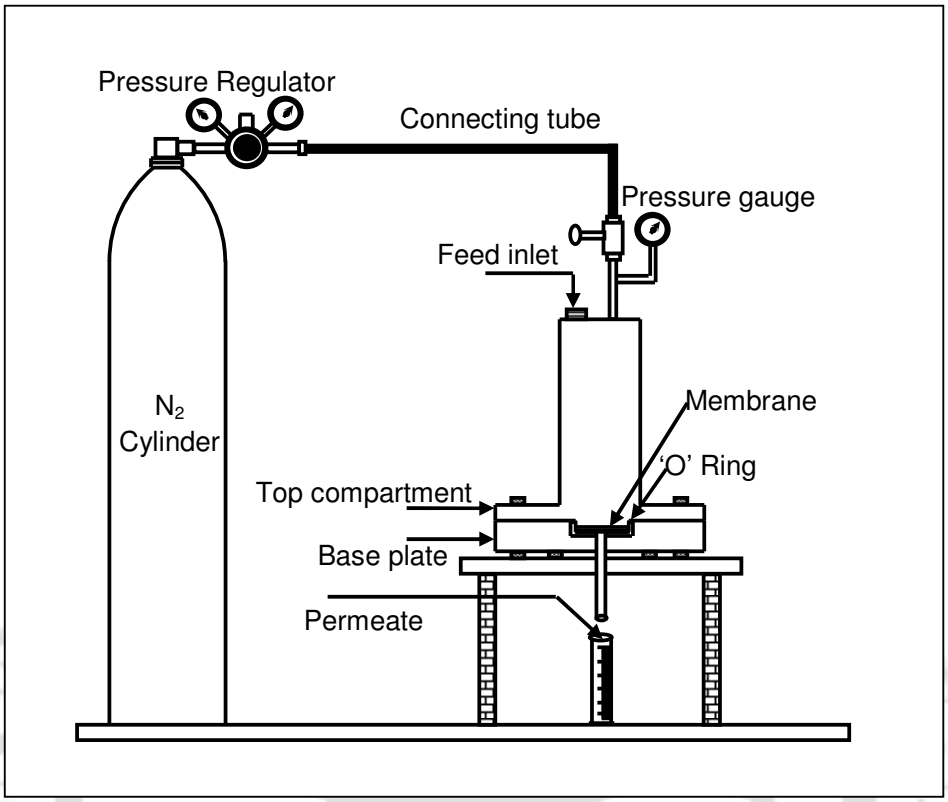

Fig. 2.4 Experimental set up for permeation test

2.2.2 Solvent permeation test

In order to check the stability of the composite membrane in various solvents, solvent permeation experiments through the MCM-41-ceramic composite membrane were conducted in a dead-end flow filtration set-up (see Fig. 2.4) using polar and non polar solvents. The solvent flux was measured at various applied pressures ranging from 69 to 345 kPa. For each applied pressure, the experiment was conducted by filling the cell with 150 ml of solvent in the top compartment. Then, the first 50 ml of permeate was discarded and the time required for second 50 ml of solvent permeation was noted down to calculate the solvent flux and the permeability of the MCM-41-ceramic composite membrane. All the solvents employed in

this study were of analytical grade purchased from Loba Chemie (Laboratory Reagents & Fine Chemicals), Mumbai, India.

2.2.3 Separation of chromium and trivalent metal ions

The separation capability of the MCM-41-ceramic composite membrane was evaluated by performing filtration experiments of Cr (VI) and trivalent metal salts ($AlCl_3$ and $FeCl_3$) from aqueous solution. Experiments were carried out at room temperature (25 °C). The required concentration of Cr (VI), $AlCl_3$ and $FeCl_3$ solution was prepared using Millipore water and its concentration was determined using conductivity meter (Eutech Instruments, Model: CON 2700).

For each experiment, the permeation cell was filled with 100 ml of chromium solution (1000 ppm) and then first 10 ml of permeate passed through the membrane was discarded. The next 10 ml of permeate was collected and time required was noted to estimate the permeate flux. At the end of each experiment, the membrane was properly washed with Millipore water followed by flushing with Millipore water at higher pressure to regain the original pure water flux. The permeate flux and the rejection of chromium solution were investigated as a function of operating parameters such as applied pressure, pH and concentration of the feed solution. In order to study the inference of applied pressure, the experiments were performed at five different pressures (69-345 kPa) for a fixed concentration of chromium solution (1000 ppm) with natural pH of the solution (~ 2.35). The effect of concentration on the permeate flux and rejection was conducted by changing five different concentrations (250-3000 ppm) at an applied pressure of 207 kPa. The influence of pH in the range of 2-9 was also examined at a fixed feed concentration (1000 ppm) and an applied pressure of 207 kPa, where the pH of the chromium solution was adjusted by adding dilute NaOH and HCl solution.

Similarly for trivalent metal slats, the permeate flux and rejection of $AlCl_3$ and $FeCl_3$ were examined as a function of operating parameters such as effect of applied pressure, salt concentration and pH of the solution. In order to study the effect of applied pressure, the concentration of the feed was fixed as 3000 ppm without alteration of its pH. While studying the effect of concentration (250-3000 ppm) on the performance characteristics of the fabricated membranes, the applied pressure was fixed at 276 kPa with natural pH of the feed solution. Further, the effect of pH was examined ranging between 2 and 5 at an applied pressure of 276 kPa and a feed concentration of 250 ppm. It is worth to mention that above pH 5, $AlCl_3$, and $FeCl_3$ salts start forming precipitation.

The percentage rejection (R) for the separation of chromium and trivalent metal ions was calculated as,

$$R(\%) = \left[1 - \frac{C_p}{C_f}\right] \times 100 \tag{2.3}$$

where C_f, C_p are the concentration of chromium or trivalent metals in feed, and permeate, respectively.

2.3 Results and discussion

2.3.1 Characterization of clay powders

Size of clay particles determines the pore size and sintering temperature of the ceramic support. Pore growth is a function of particle size and compaction pressure. Finer particles need relatively low temperature for sintering, however they have large transport resistance due to small effective pore size. On the other hand, coarser particles require higher sintering temperature, less transport resistance and less mechanical strength. Particle size distribution of clay powders is shown in Fig. 2.5.

The diameter of clay particle is calculated using volume weighted mean formula, which is in the range of 5 to 10 µm. Surface area of raw materials are in sequence of feldspar < pyrophylite < ballclay <quartz < calcium carbonate < kaolin, which is also considered while choosing the composition of the raw materials for support preparation. This gives a rough idea about the use of raw materials for the fabrication of supports.

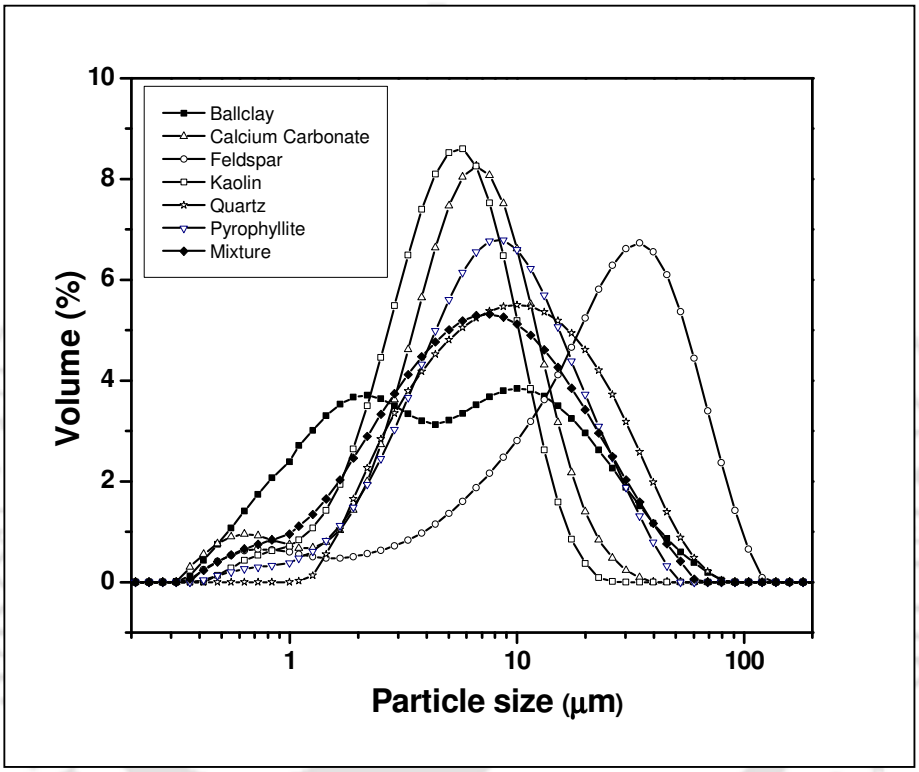

Fig. 2.5 Particle size distribution of raw materials used for the preparation of support

Sintering temperature is an important parameter for controlling the porosity, mechanical stability and pore size of the membrane supports. Thermogravimetric analysis was performed to indentify the minimum sintering temperature required to fabricate the membrane supports with sufficient strength and the corresponding results are illustrated in Fig. 2.6. The weight loss at less than 150 °C is due to removal of physisorbed water. The weight loss between 500-800 °C, corresponds to the hydroxylation of surface hydroxyl group or removal of structural water. For $CaCO_3$, the major weight loss takes place between 540 and 760 °C,

which is due to thermal decomposition of $CaCO_3$ to CaO and CO_2. The porosity of support is mainly dependent upon the path taken by CO_2 gas. Owing to the release of more OH group attached to the Al and Si and the conversion of kaolin to metakaolin, ball clay displays relatively higher weight loss (14.15%) than that of kaolin (5.58%) and pyrophyllite (4.46%). Quartz and feldspar show no significant weight loss.

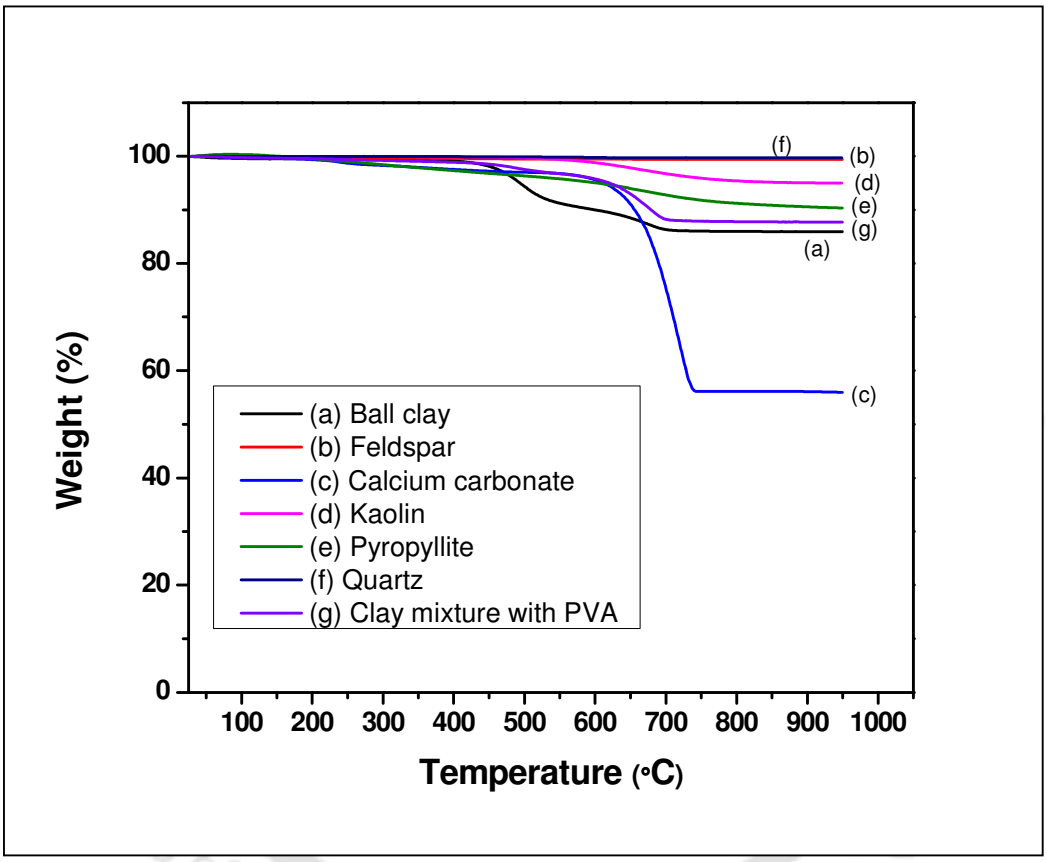

Fig. 2.6 Thermogravimetric analysis (TGA) of the clay powders

It is apparent from Fig. 2.6 that after 820 °C, the weight loss is negligible indicating that the support needs to be sintered at > 850 °C. Therefore, the chosen sintering temperature of 950 °C is justified. Furthermore, the binder burnout mechanism has also been studied for the given composition of clays (with binder). The binder initially spreads on the clays and burn out while sintering. The degradation of the organic binder takes place in two steps, side-groups elimination between 200 and 350 °C, and main chain decomposition of binder

between 450 and 650 °C. The binder, PVA is completely removed at 720 °C (Monash and Pugazhenthi 2011a). The PVA chain enhances the thermal stability of the ceramic support.

2.3.2 Characterization of MCM-41 powder

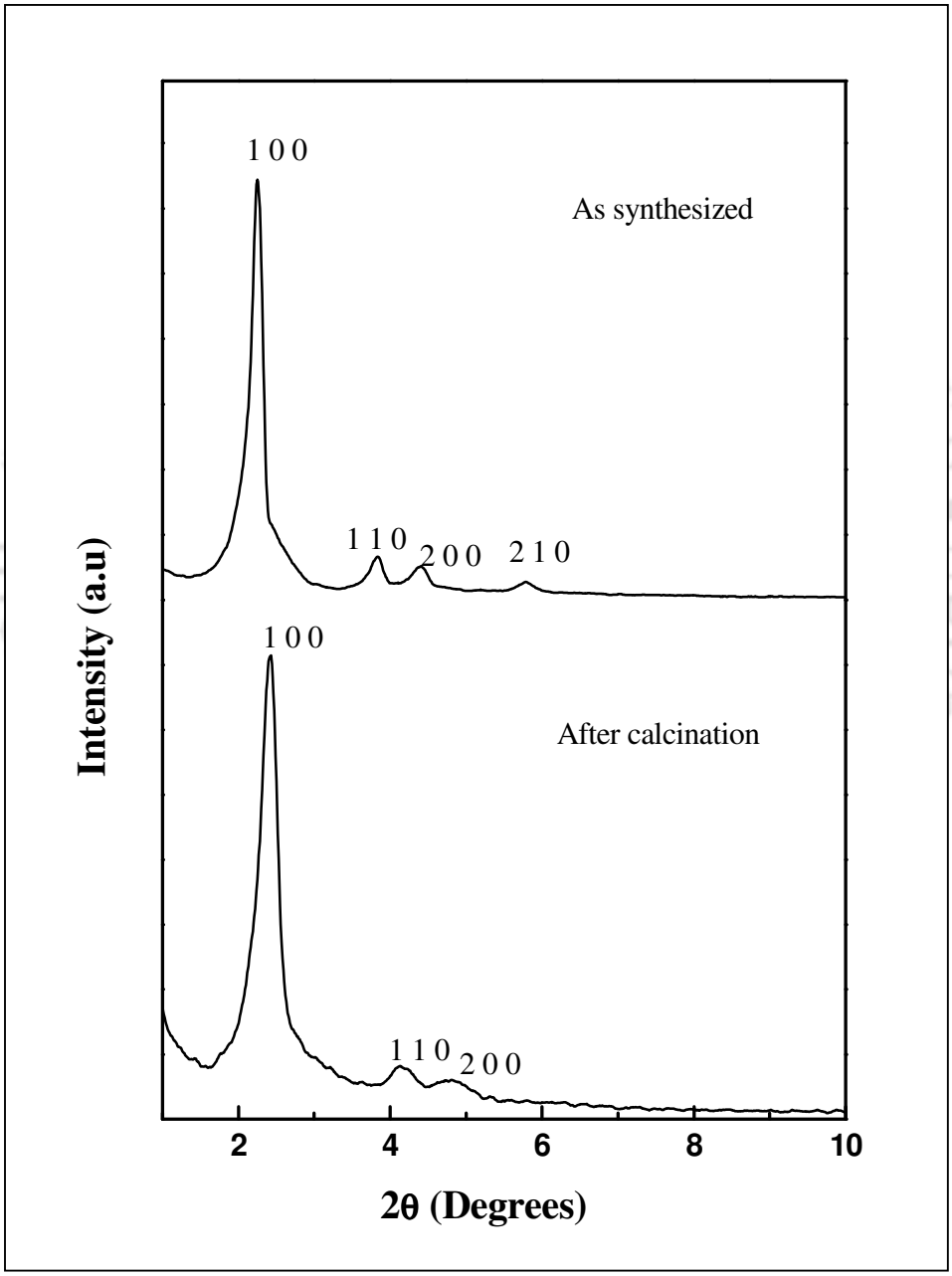

Fig. 2.7 XRD pattern of MCM-41 powder samples (as-synthesized and after calcination)

The XRD pattern of MCM-41 is depicted in the Fig. 2.7. The XRD profiles of as-synthesized MCM-41 (before calcination) demonstrate a strong (1 0 0) peak and three higher order reflections such as (1 1 0), (2 0 0) and (2 1 0) at $2\theta<10°$. The presence of (1 0 0), (1 1 0) and (2 0 0) diffraction peaks in the MCM-41 (after calcination) is a confirmation of good crystallinity of the prepared powder that specifies the existing of well-resolved hexagonally assembled pore geometry as well as high structural order of MCM-41. XRD patterns of MCM-41 (after calcinations) match closely with JCPDS file no. 00-049-1711 and before calcination sample with file no. 00-049-1712. Similar observations were also reported by Liou (2011) and Udaykumar *et al*., (2005) for MCM-41. The 2θ position of the calcined sample shifts slightly to a higher value due to the elimination of the template and succeeding condensation of silanol groups (Hui and Chao 2006). The calcined MCM-41 powder possesses a well defined pore structure owing to the condensation of Si-OH groups and hence, the peak (2 1 0) is removed.

Fig. 2.8 displays the FTIR spectra of as-synthesized and calcined MCM-41 powder samples. The as-synthesized sample shows two different sharp intense bands at 2924 and 2851 cm^{-1} (Monash and Pugazhenthi 2010). These represent the presence of C-H stretching in the hydrocarbon chain of surfactant molecules. Subsequently, the bending vibrational mode is noticed at 1475 cm^{-1}. The hydroxyl band emerged at 3208 cm^{-1} is ascribed to adsorbed water molecules and surface silanols. The adsorption band appeared at 1650 cm^{-1} corresponds to bending vibration of adsorbed water molecules. The absorption bands noticed at 1055 and 1224 cm^{-1} are due to the asymmetric stretching vibrations of Si-O-Si (Loganathan *et al*., 2013). The band at 958 cm^{-1} is attributed to Si-OH vibrations. The absorption peaks in the range of 460-795 cm^{-1} are due to bending vibration of Si-O-Si bond and bands at 795 cm^{-1} corresponds to free silica (Monash and Pugazhenthi 2010). The spectrum of the calcined MCM-41 sample also illustrates similar bands and the bond stretching properties

(Loganathan *et al.*, 2013). All the bands corresponding to the organic groups are disappeared for the sample calcined at 550 ^{o}C. This proves that the surfactant is removed from the sample calcined at 550 ^{o}C. Table 2.2 demonstrates the summary of FTIR spectra of MCM-41 powder samples.

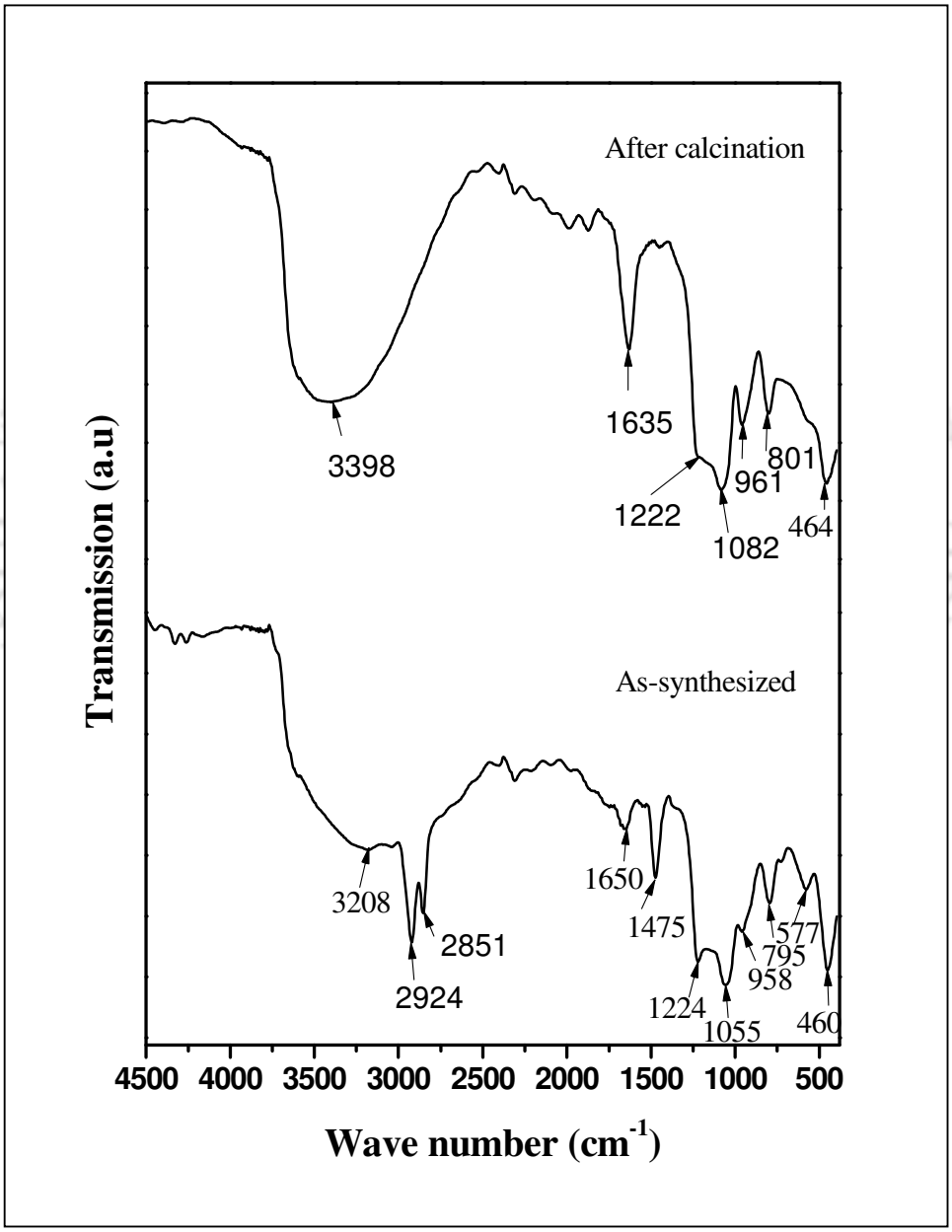

Fig. 2.8 FTIR spectra of MCM-41 powder samples (as-synthesized and after calcination)

Table 2.2 Summary of FTIR spectra of MCM-41 samples

Wave Number, cm^{-1}	Band stretching
2924, 2851	C-H stretching of hydrocarbon chain of surfactant
3208	Surface silanols and adsorbed water
1650	Bending vibration of adsorbed water
1475	C-H vibrational stretching
1224, 1055	Si-O-Si asymmetric stretching
958	Si-OH vibration
795, 577, 460	Si-O-Si bending vibration
795	Band corresponds to free silica

Thermogravimetric analysis (TGA) and differential thermogravimetric (DTG) analysis of the as-synthesized MCM-41 powder are depicted in Fig. 2.9. The as-synthesized MCM-41 powder sample displays the weight loss in three separate regions (Monash and Pugazhenthi 2010). In the first region, the removal of physisorbed water molecules from the external surface of the material causes the weight loss of 4-5% between the temperature of 50 and 150 °C. The second region of weight loss (36%) between 150 to 320 °C is due to the decomposition of the surfactant. Further, the weight loss (6%) between 320 to 550 °C is attributed to the combustion of the surfactant and loss of water, which is created from the condensation of adjacent silanol groups. The weight loss at >550 °C is only 2% that is probably due to the degradation of germinal and vicinal silanol groups remained in the sample (Loganathan *et al*., 2013). This elucidates that surfactant is completely removed at 550 °C. DTG curve also illustrates three stage of decomposition during heating of as-synthesized powder. According to the DTG curve, an endothermic peak at 48 °C is due to the removal of moisture and peak at 239 °C is caused by the removal of the trimethylamine group, via Hofmann degradation (Liu *et al*., 2007) that leads to the formation of the alkenes

and removal of water molecules. The last peak in the DTG curves at 341 °C is the oxidation of remaining organic compounds to carbon dioxide, water and the most likely carbonaceous species.

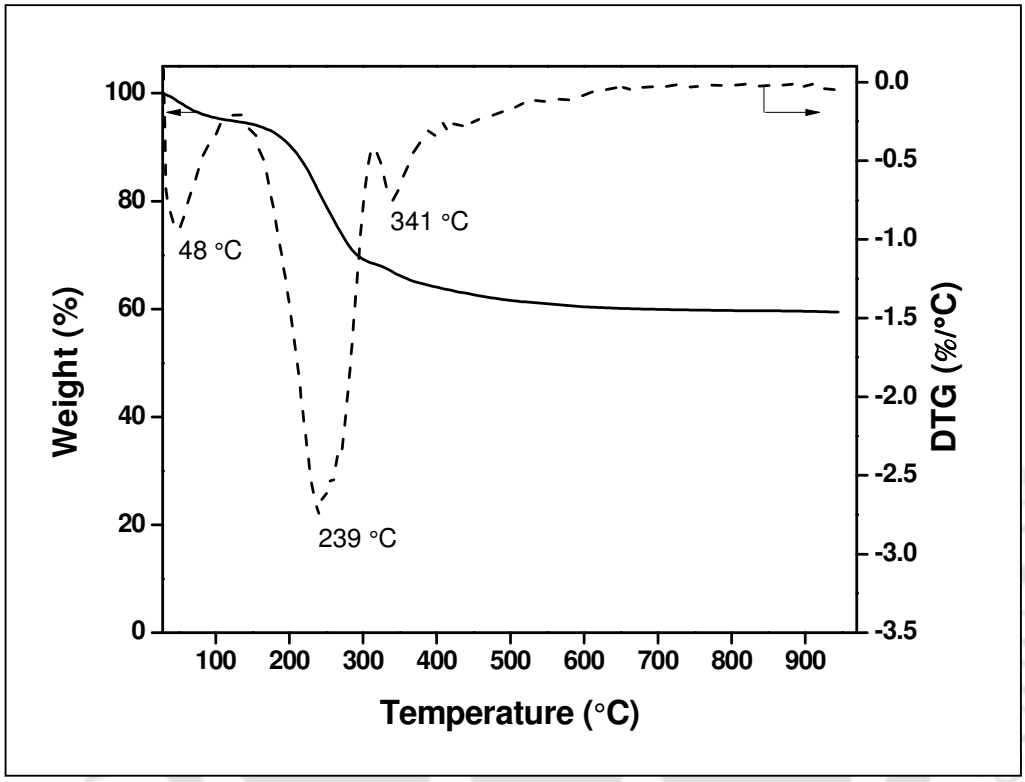

Fig. 2.9 TGA and DTG curve of as-synthesized MCM-41 sample

The nitrogen adsorption/desorption isotherm and BJH pore size distribution of the calcined MCM-41 powder are depicted in Fig. 2.10 (a) and (b). The isotherm observed for the MCM-41 powder shows a typical type IV adsorption-desorption isotherm and exhibits capillary condensation steps, indicating the characteristic of the mesoporous material. The pore size distribution is determined from desorption isotherm by the BJH method as shown in Fig. 2.10 (b). This plot clearly indicates that the synthesized MCM-41 powder contains only mesopores not micropores. The average pore size of the MCM-41 powder is 3.35 nm, which is computed by BJH approach method from the desorption curves. The BET surface area and total pore

volume are found to be 1305 m^2g^{-1}, 0.7472 cm^3g^{-1}, respectively, which are derived from the amount of N_2 adsorbed at relative pressure (P_s/P_o) of 0.99.

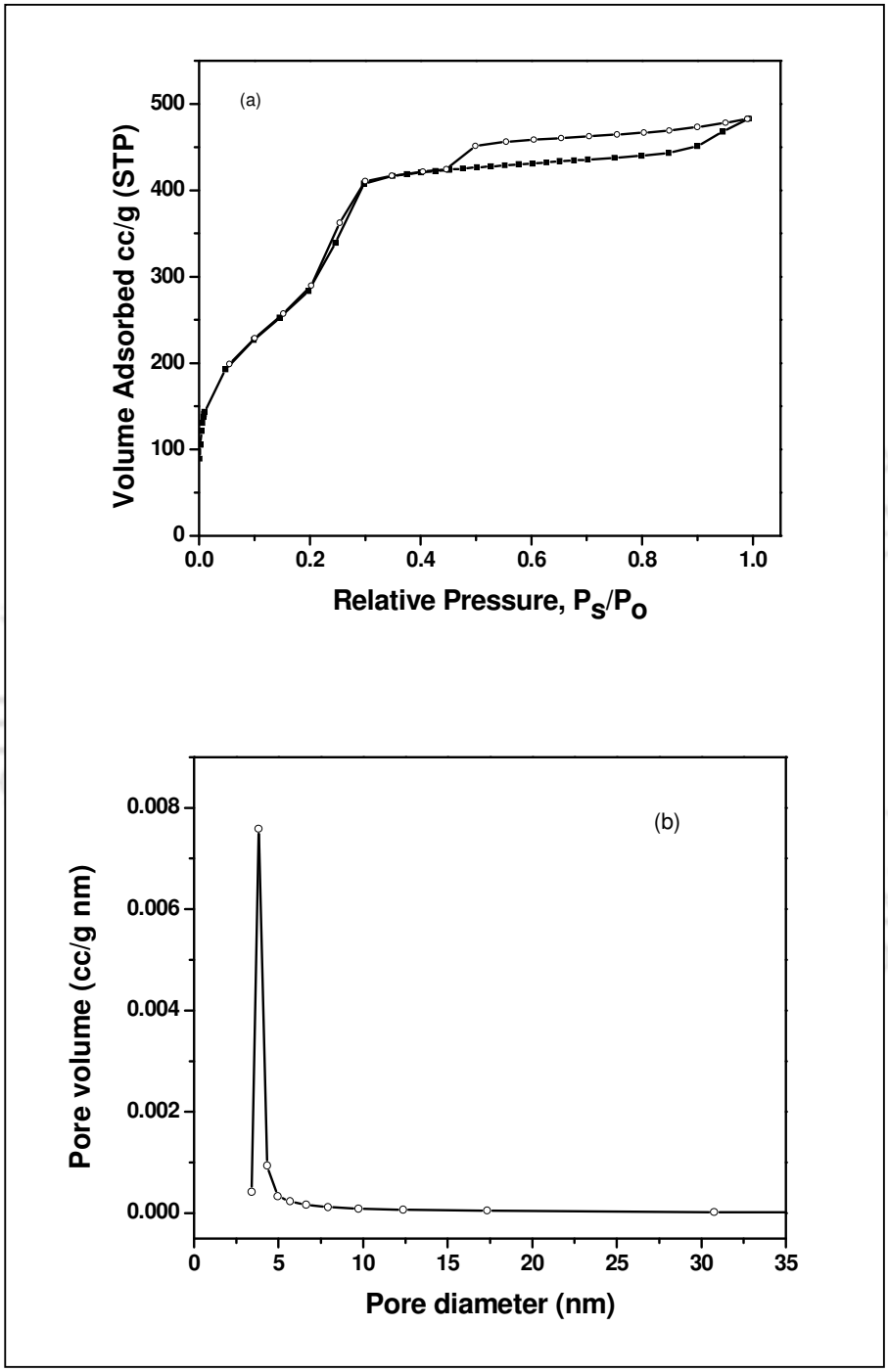

Fig. 2.10 (a) Nitrogen adsorption-desorption isotherm and (b) BJH pore size distribution of MCM-41 powder (after calcination)

The variation of zeta potential with function of pH is illustrated in Fig. 2.11. The surface charge of the membrane pores depends on the pH of the contact solution, and it can be either positive or negative. In order to find out the surface charge of the MCM-41 membrane, zeta potential of the calcined MCM-41 particles were measured using an electrophoretic light scattering method in Delsa Nano C (Beckman coulter) by keeping the powders in water suspension at different pH. The surface charge of the MCM-41 powder is altered by adding HCl in water suspension solution to make lower pH, and for higher pH, NaOH is added. At lower pH, the surface charge of MCM-41 powder becomes positive due to larger quantity of H^+ ions as seen in Fig. 2.11. Higher pH values are adjusted by adding more quantity of NaOH solution, where negative hydroxyl (OH^-) ions become more. Hence, the surface charge of the MCM-41 gets more negative at higher pH. At acidic pH (pH=2), zeta potential value is around +19 mV while at pH 12, it is approximately -36 mV (Fig. 2.11). Thus, electrostatic interactions play a major role in the surface activity of MCM-41. In this study, the iso-electric point (IEP) of the MCM-41 powder is found to be 3.9. It has been reported in the literature that the isoelectric point (IEP) of MCM-41 nanoparticles was 3.6±0.18 (Benhamou *et al*., 2013). The IEP of MCM-41 powder synthesized using the gel composition of $1SiO_2$: 0.45CTAB:0.32 TMAOH (tetramethylammonium hydroxide):$67H_2O$ was reported to be 5.2 (Deere *et al*., 2002) whereas the IEP of γ-Al_2O_3 was 8 (Parks 1965). The comparison study clearly reveals that the obtained IEP of MCM-41 in this work is well accordance with the literature.

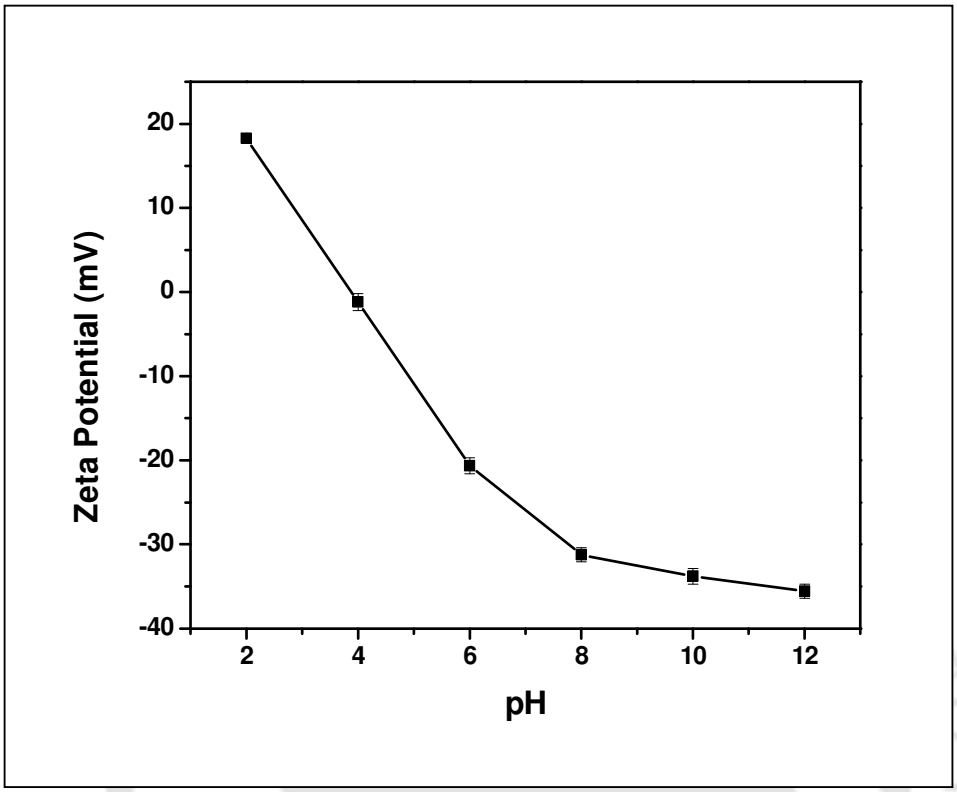

Fig. 2.11 Zeta potential of MCM-41 powder at various pH

2.3.3 Characterization of the MCM-41-ceramic composite membrane

The phase transformation behavior of ceramic support before and after sintering was identified by XRD analysis as displayed in Fig. 2.12. The phase transformation occurs during the sintering process, resulting in formation of new phases that are identified by shifting of XRD peak positions. The complete crystalline phase is observed for the support sintered at 950 °C. The main absorbed phases are quartz (SiO_2), mullite ($3Al_2O_3.2SiO_2$), anorthite ($CaO.Al_2O_3.2SiO_2$) and wollastonite ($CaSiO_3$). The major phase transformation of kaolin to mullite via metakaolinite takes place during sintering temperature, which is confirmed by XRD analysis (Reed 1989).

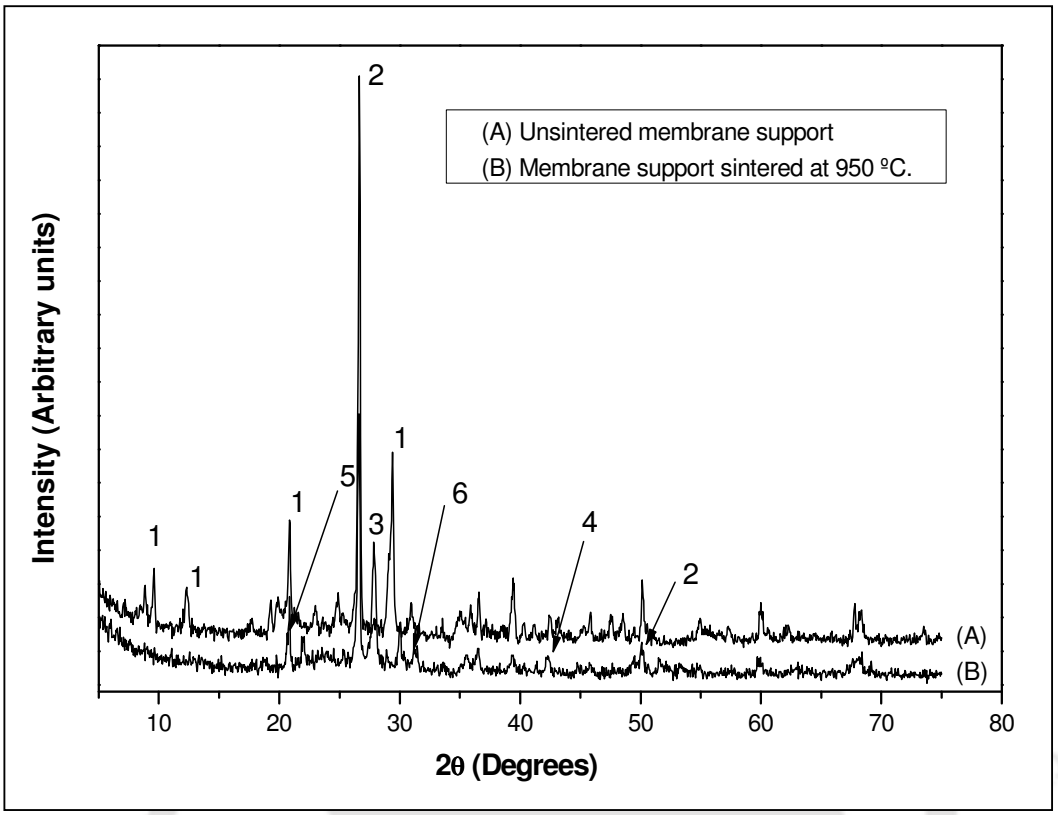

Fig. 2.12 XRD profile of unsintered and sintered ceramic support at 950 °C (1-Kaolin, 2-Quartz, 3-Anorthite, 4-Calcium oxide, 5- Mullite, 6-Wollastonite)

The porosity of ceramic support was determined by Archimedes principle and it is found to be 47% as shown in Fig. 2.13. The porosity of the MCM-41-ceramic composite membranes is estimated to be 34%, 29% and 23% for 1st, 2nd, and 3rd coating membranes, respectively (see Fig. 2.13). It clearly demonstrates that the porosity of the composite membrane decreases with increasing number of coatings due to increase in the mass of MCM-41 deposition on the support as seen in Table 2.3.

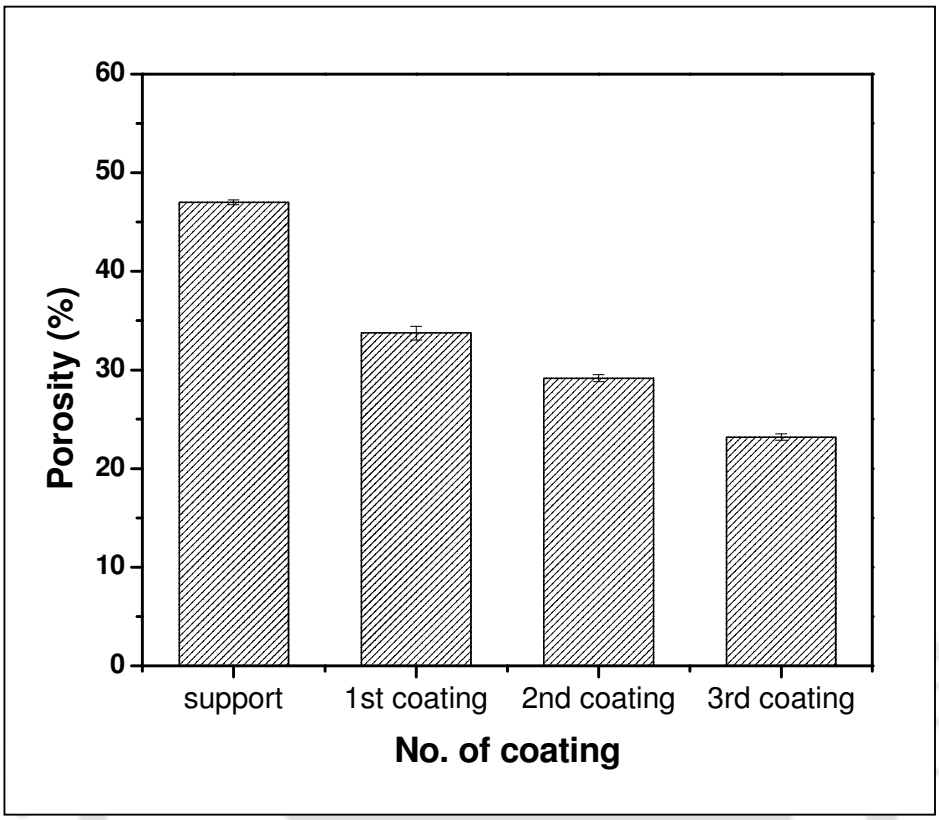

Fig. 2.13 Porosity of the support and MCM-41-ceramic composite membrane

Table 2.3 Characterization results of MCM-41-ceramic composite membranes.

Membranes	**Porosity (%)**	**Average pore size (µm) calculated from water flux data**	**Permeability ($m^3m^{-2}s^{-1}.kPa^{-1}$)**	**Cumulative weight increment (g)**
Support	47	1.00	3.63×10^{-6}	-
1st coating	34	0.692	1.26×10^{-6}	0.45
2nd coating	29	0.481	5.90×10^{-7}	0.68
3rd coating	23	0.173	6.05×10^{-8}	0.89

The surface morphology of ceramic support and composite membranes was analyzed by field-emission scanning electron microscopy (FESEM). To confirm the formation of MCM-41 layers on the membrane, FESEM imaging technique was employed to visualize the layers on ceramic support. Fig. 2.14 (a-d) illustrates the surface images of support and composite membranes prepared with repeated cycle of MCM-41 coatings (1-3). It is observed that after

first coating, MCM-41 deposits unevenly on the surface of ceramic support. The rough morphology resembles that there is no crack as well as pinholes on the surface of the membrane. The presence of MCM-41 on ceramic support is clearly visible in the FESEM images. With the same magnification scale, images are shown for support, and 1-3 cycles of coatings. It is noticed that more quantity of MCM-41 deposits on ceramic support as the number of coating increases. Also, the pore size of the membrane reduces when the number of repeated cycle of coating increases.

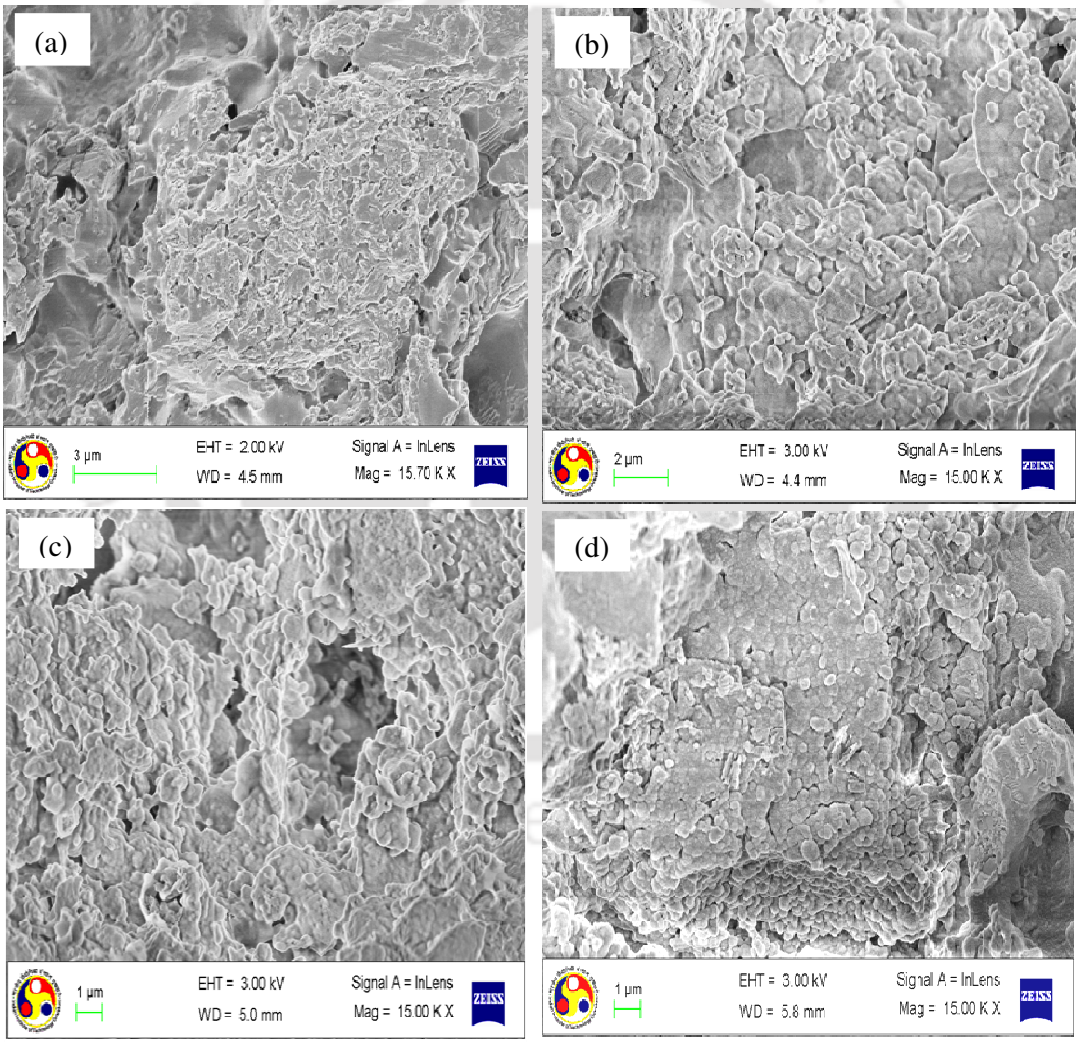

Fig. 2.14 FESEM images of a) support and composite membranes with repeated cycle of coatings (b) 1st coating, (c) 2nd coating, (d) 3rd coating.

2.3.4 Pure water permeation experiment

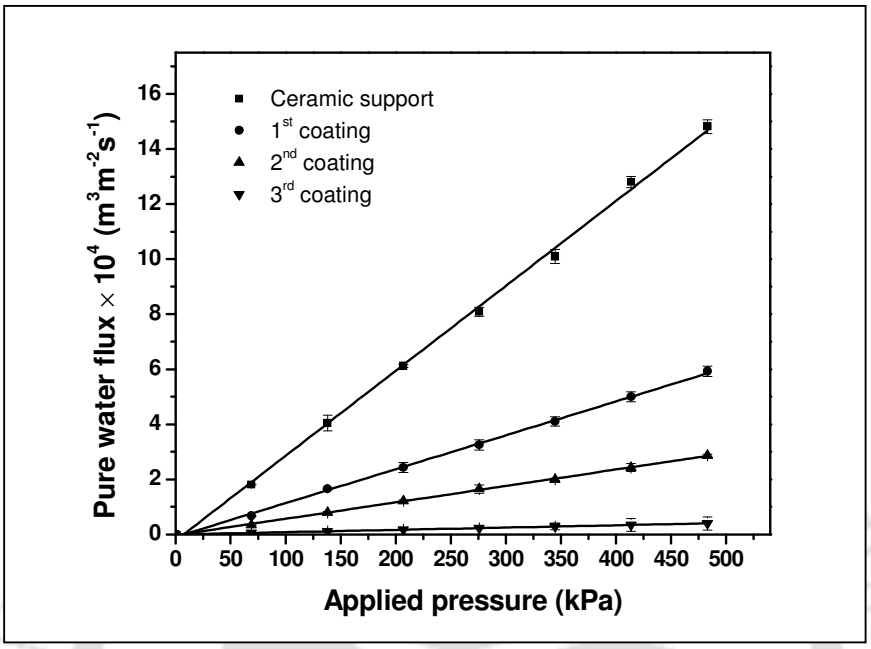

Fig. 2.15 Variation of pure water flux with applied pressure for support and composite membranes

Fig. 2.15 depicts the pure water flux of support and MCM-41-ceramic composite membrane (1st, 2nd and 3rd coating). The results clearly indicate that with increasing pressure, the water flux increases linearly and follow Darcy's law for all the membranes. The pure water flux of the MCM-41 ceramic composite membrane is much lower than that of ceramic support. The hydraulic permeability of ceramic support is estimated to be 3.63×10^{-6} $m^3m^{-2}s^{-1}.kPa^{-1}$ (see Table 2.3). Table 2.4 displays the comparison of pure water permeability of synthesized membrane with other membranes.

Table 2.4. Comparison of pure water permeability (Lp) value of synthesized membrane with other membranes reported in literature

Membrane	Pure water permeability (L_p) ($m^3m^{-2}s^{-1}kPa^{-1}$)	Reference
Unmodified analcime zeolite membrane	7.946×10^{-8}	Shukla and Kumar, 2005
Unmodified SAN membrane	4.54×10^{-8}	Sachdeva and Kumar, 2008
γ-Al_2O_3-clay composite membrane	2.357×10^{-7}	Majhi *et al*, 2009
MCM-41 membrane	6.05×10^{-8}	Present work

2.3.5 Solvent permeation through MCM-41-ceramic composite membrane

In order to study the surface interaction of MCM-41-ceramic composite membrane with solvents as well as the resistance of the membrane, polar (alcohol) and non polar (alkanes) aliphatic solvents have been chosen for solvent permeation experiments. In Table 2.5, the physical properties of the solvents used for permeation experiment are listed. The permeation experiments were conducted in the following sequence: methanol, ethanol, propanol, butanol, toluene, pentane, hexane and heptane. When changing the experiments from one solvent to other, the permeation cell was loaded and flushed with 100 ml of the next solvent. The flux of pure solvents through the MCM-41-ceramic composite membrane is depicted in Fig. 2.16. It is clearly seen that a linear relation between the flux and applied pressure exists. It also represents that applied pressure is the only driving force for the solvent permeation test. For all the studied solvents, R^2 value of linear fit for the flux versus applied pressure plot is higher than 0.99. This represents that the transport mechanism follows the viscous flow model given by Darcy. It is also observed that non-polar solvents demonstrate higher permeability than the polar solvents (see Fig. 2.17). If the viscosity is the main controlling factor for solvent permeation through the membrane, the flux of methanol and toluene would be similar because of the same viscosity. From Fig. 2.17, one can conclude that despite viscosity of solvent, other factors influence the permeability of solvents.

In addition to viscosity, membrane-solvent interactions have an impact on solvent permeability through the MCM-41-ceramic composite membrane (Bhanushali *et al.*, 2001; Chen *et al.*, 2010). The permeability of water and alcohols seems to be affected by solvent-pore interactions on the molecular scale. Besides these solvent interactions, other solvent properties such as surface tension, di-electric constant and molecular size, play a role on the

permeability (Mchado *et al*., 1999; Machado *et al*., 2000; Chowdhury *et al*., 2003). Amongst these, polarity plays a major role as it is directly related to the surface tension (Machado *et*

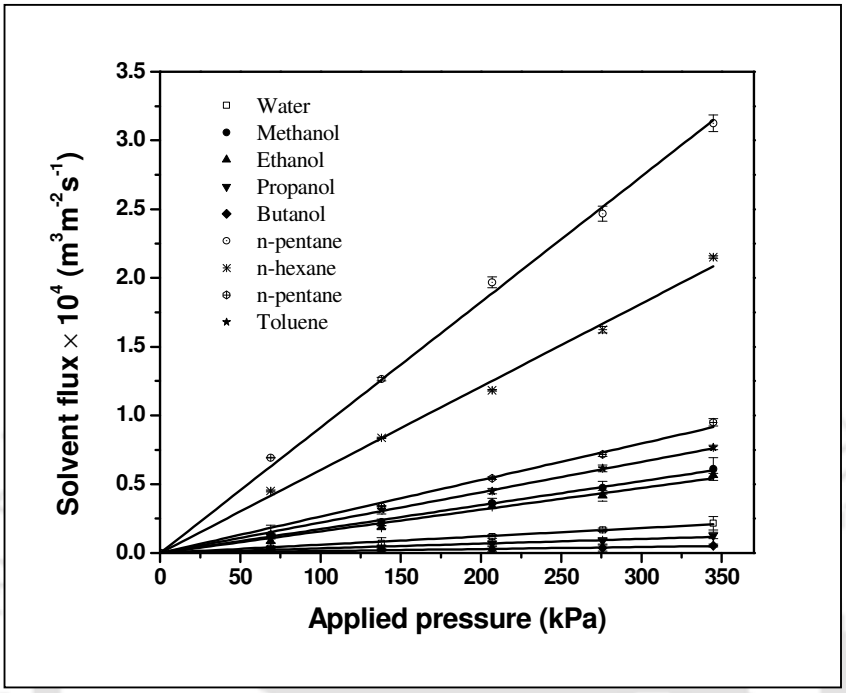

Fig. 2.16 Solvent permeation test through MCM-41-ceramic composite membrane

Table 2.5 Physical properties of the solvents used in the permeation test

Solvent	Molar volume (cm^3mol^{-1})	Viscosity (cP)	Density (gcm^{-3})	Dielectric constant	Surface energy (mNm^{-1})	Kinetic diameter (nm)	Molar volume /Viscosity (cm^3mol^{-1} cP^{-1})
Methanol	40.7	0.59	0.7917	32.6	22.6	0.38	69.0
Ethanol	58.5	1.20	0.7893	24.3	22.3	0.44	48.8
Propanol	76.9	2.25	0.7854	20.1	23.8	0.48	34.3
Butanol	91.5	2.95	0.810	17.8	24.6	0.50	31.0
Water	18.0	1.02	0.998	80.3	72.0	0.27	17.7
Toluene	25.4	0.56	0.8669	2.38	28.0	0.59	184.4
Pentane	116.2	0.234	0.626	1.80	16.0	0.43	496.0
Hexane	131.6	0.32	0.659	1.90	17.9	0.45	411.3
Heptane	146.2	0.40	0.684	1.93	19.7	0.47	366.0

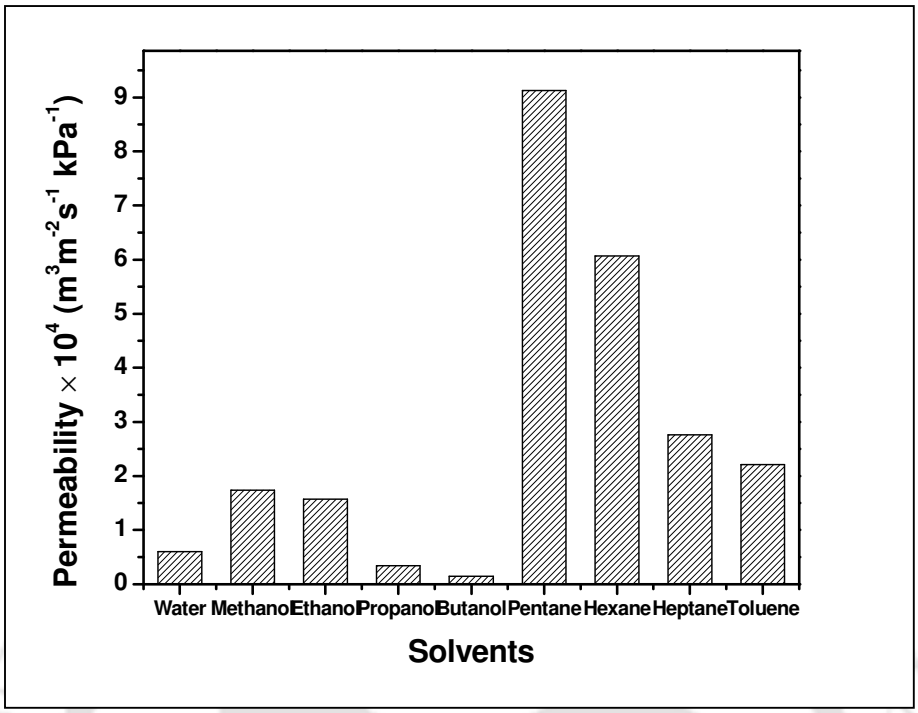

Fig. 2.17 Solvent permeability value of MCM-41-ceramic composite membrane

al., 2000). Fig. 2.16 and 2.18 display directly measured and viscosity corrected fluxes of various solvents through the MCM-41-ceramic composite membrane. In the plot of solvent permeability (Fig. 2.17), the permeabilities of methanol and ethanol are higher than water, while propanol and butanol have lower permeabilities than water. If viscosity is the only controlling factor, then the data points in Fig. 2.18 should lie on single line, but these do not happen, hence surface tension affects the permeation in addition to viscosity. However, for water and methanol; ethanol and hexane; the plots of viscosity corrected flux almost lie on the same line (see in Fig. 2.18). This suggests that it roughly governs the viscous flow model. Although water has lower viscosity than ethanol, it has higher surface tension than ethanol, which makes water to penetrate gradually through the composite membrane. Likewise, pentane has higher flux due to its lower surface tension. In the homologous series of linear alcohols, the flux increases with decreasing molar volume and increasing dielectric constant.

The specific interactions with solvent molecules and the MCM-41 surface become more significant as the pore size of the membrane is small. The disparity between various solvents is due to differences in interactions between the pore walls and the solvents or alkoxylation of surface Si-OH groups. Alkoxylation yields Si-OR surface groups that are bulkier than Si-OH groups (Chowdhury *et al*., 2003). Therefore, this may decrease the effective pore radius resulting in an effective smaller cross-sectional pore area and the permeability of alcohol groups go on decreasing to higher alcohols.

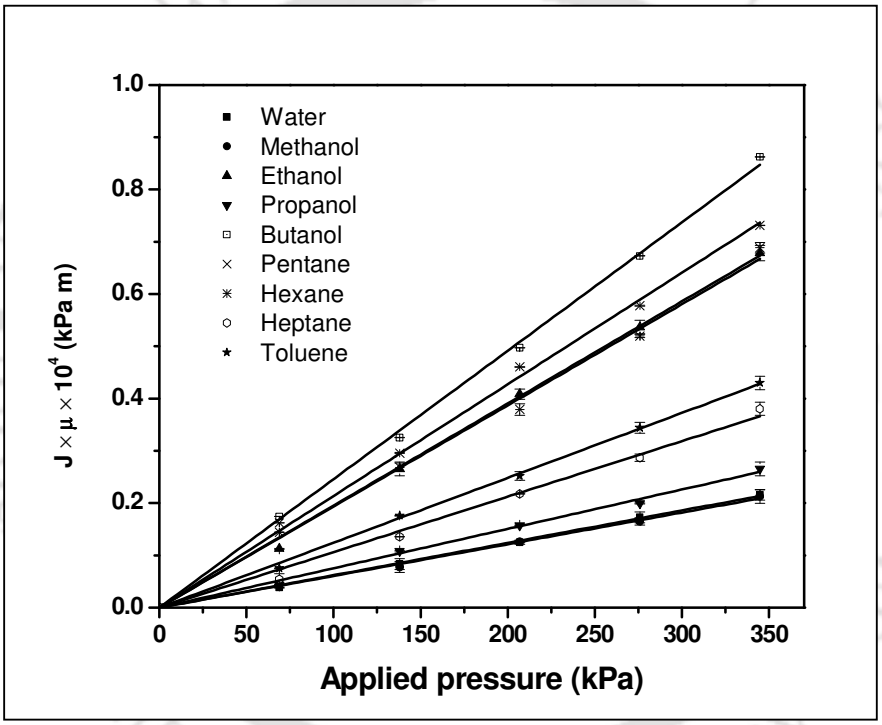

Fig. 2.18 Viscosity corrected solvents permeation of MCM-41-ceramic composite membrane

2.3.6 Separation of Chromium (VI) from aqueous solution

2.3.6.1 Effect of applied pressure

The most common forms of chromium dissolved in natural water within the environmental normal range of pH are CrO_4^{2-}, $HCrO_4^-$ and CrO_7^{2-} ions (Deere *et al*., 2002). The

concentration and pH of the chromium solution used in this study are 1000 ppm and ~2.35, respectively. In our experimental conditions (pH~2.35), the chromium exists in the form of acid chromate ions ($HCrO_4^-$) and not as chromate ions (CrO_4^{2-}) (Deere *et al.*, 2002). The influence of applied pressure on the permeate flux and rejection of Cr (VI) was studied in the range of 69-345 kPa as depicted in Fig. 2.19. It is observed that with increasing applied pressure, the permeate flux enhances for the composite membrane; however, the permeability of Cr (VI) solution is lesser than the pure water permeability. This implies that the chromate ions generate an extra resistance (concentration polarization) to the flow of solvent. With increasing applied pressure, the observed rejection slightly increases, which may be due to the reduction of the pore size of the membrane surface because of chromium accumulation over time (Hafez and Maharawy 2004). The permeate flux increases linearly with increasing applied pressure up to 275 kPa and follows Darcy's law. After that, the flux declines slowly with an increase in the applied pressure. From this analysis, it may be concluded that Cr (VI) rejection would be endangered and concentration polarization would be increased when the applied pressure is more than 275 kPa. As there is an extra amount of solute particle accumulation on the membrane surface at higher pressure (>275 kPa) that causes extreme concentration polarization and enhances permeate concentration because of convective flux. In addition to the applied pressure, solute concentration and other parameters also play a role in determining the rejection of Cr (VI). Those are charge density present in the membrane and interaction of the constant membrane charge sites with ionic solutes indicating that the concentration polarization effect leads to considerable loss. Therefore, the MCM-41-ceramic composite membrane is cleaned after each experiment until the original water flux was obtained.

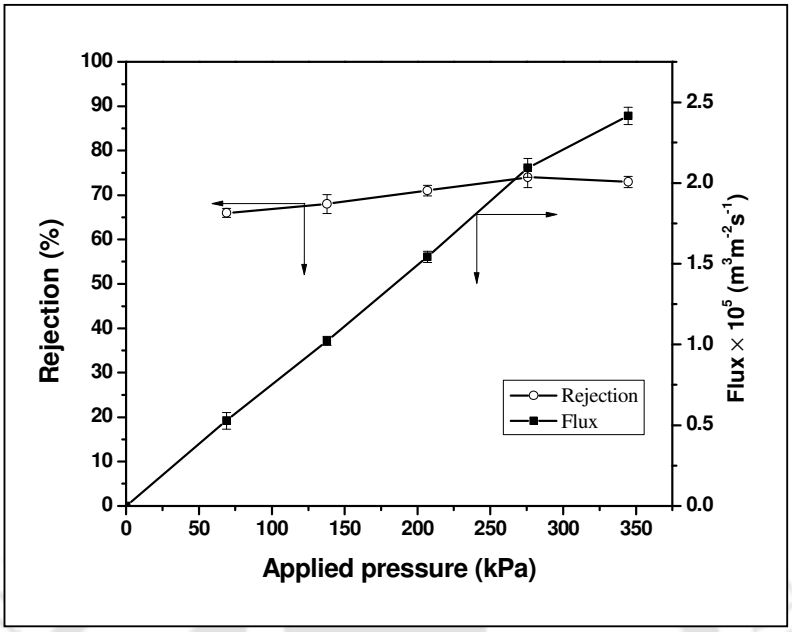

Fig. 2.19 Effect of applied pressure on the permeate flux and rejection for the composite membrane

2.3.6.2 Effect of feed concentration

The influence of feed concentration of Cr (VI) on the permeate flux and rejection was examined and the obtained results are depicted in Fig. 2.20. The experiments were performed at constant pressure of 207 kPa with various concentrations (250-3000 ppm) at natural pH ~ 2.35 (Shukla and Kumar 2007). Fig. 2.20 clearly demonstrates that the rejection of Cr (VI) increases as the feed solution concentration increases from 250 to 2000 ppm and it is almost constant after 2000 ppm. The best rejection is observed with a feed concentration of 2000 ppm.

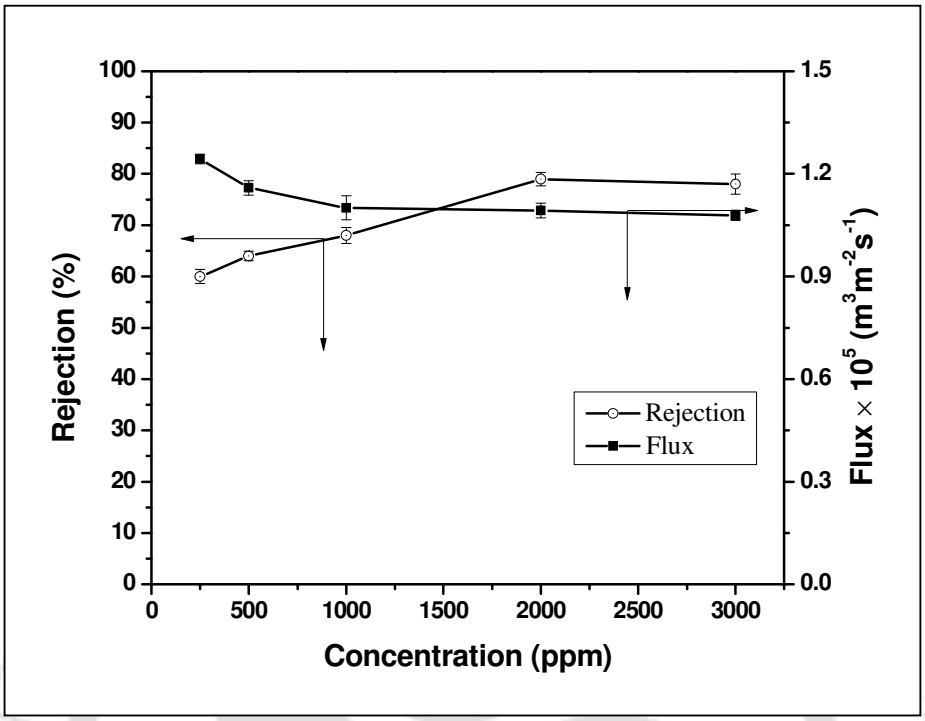

Fig. 2.20 Effect of feed concentration on the permeate flux and rejection for the composite membrane

2.3.6.3 Effect of pH on Cr (VI) separation

Chromium generally presents in two oxidation states, Cr (VI) and Cr (III). The species of Cr (VI) are assumed to be present in aqueous solution as the following way (Deere *et al*., 2002):

$$H_2CrO_4 + H_2O \rightleftharpoons HCrO_4^- + H_3O^+ \qquad PK_1 = -0.5$$

$$H_2CrO_4^- + H_2O \rightleftharpoons CrO_4^{2-} + H_3O^+ \qquad PK_2 = 5.8$$

$$2H_2CrO_4^- \rightleftharpoons Cr_2O_7^{2-} + H_2O \qquad PK_3 = 2.2$$

$HCrO_4^-$ dominates in the pH range of 0-5.8 except that above a certain Cr (VI) concentration (~10^{-3} M) it coexist with $Cr_2O_7^{2-}$; at pH > 8, Cr (VI) exists only as CrO_4^{2-}.

The surface charge of the MCM-41-ceramic composite membrane depends on the pH of the solution, and the membrane is positively charged for pH value lower than the isoelectric point (IEP) while negatively charged for pH greater than IEP. Hence, the pH is an important parameter in determining the efficiency of a membrane separation process, particularly when removing ionic species. In this regard, the rejection is measured over the range of pH from 2 to 9 for a fixed feed concentration (1000 ppm) and an applied pressure of 207 kPa. Fig. 2.21 shows the observed rejection as the function of pH. The result elucidates that the rejection strongly depends on the working pH value and the highest rejection (80%) is obtained at pH=2. Since the IEP of the composite membrane is 3.9 (see Fig. 2.11), the membrane is electrically positive at pH < 3.9 and negative at pH > 3.9. When the charged membrane is in contact with chromic acid solution, the concentration of ions with the same charge as the membrane will be lower at near the surface of the membrane than that in the solution, and the other ions, which have the opposite charge, have a higher concentration in the membrane than in the solution. On account of this concentration difference, a potential difference is generated at the interface between the membrane and the solution to maintain electrochemical equilibrium between solution and membrane. With this potential, the membrane repels the ions with same charge as the membrane (Chung *et al.*, 2005). While the pH of the solution increases from 2 to 3.9, the magnitude of membrane charges (positive) decreases since the IEP of the membrane is 3.9. Thus, the repulsion between positively charged membrane and positive species (H_3O^+) decreases and the rejection declines from 80 %. As the cation and anion cannot act independently, hence, $HCrO_4^-$ is also rejected to maintain electroneutrality. With increasing the pH of the solution from 3.9 to 9 by adding NaOH, OH^- ions get accumulated on the membrane surface. As a result, the membrane would acquire more negative charge while putting in contact with the feed. It is noteworthy to mention that when the pH increases, CrO_4^{2-} concentration also increases in comparison with $HCrO_4^-$. As the pH

is raised from 3.9 to 9, the magnitude of membranes charge (negative) increases as evidenced from Fig. 2.11 and hence, the higher surface charge (negative) leads to increase the intensity of the electrostatic repulsion between ions present in the solution (CrO_4^{2-}, $Cr_2O_7^{2-}$) and the membrane surface. This justifies an increase of rejection with increasing pH from 3.9 to 9.

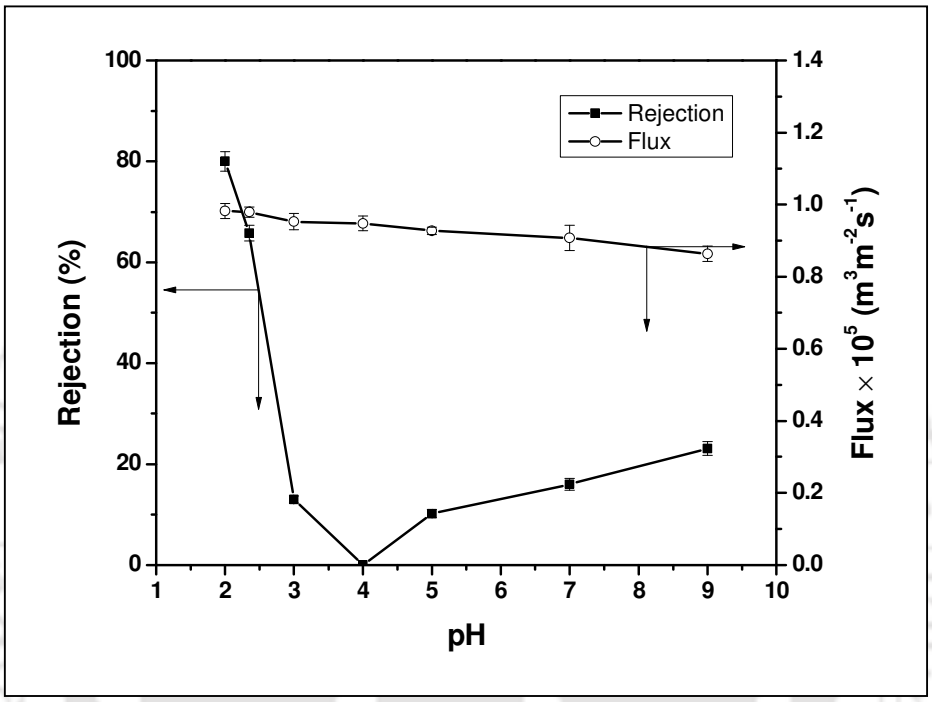

Fig. 2.21 Effect of pH on the permeate flux and rejection for the composite membrane

Table 2.6 presents the comparison of the results obtained in this work with other membranes for the rejection of Cr (VI) from aqueous solution. The rejection (80%) of Cr (VI) reported in this study at pH 2 with an applied pressure of 207 kPa for the feed concentration of 1000 ppm is comparable or even better than the value reported in the literature (Neelakandan *et al.*, 2003; Pugazhenthi *et al.*, 2005; Sachdeva and Kumar 2008; Muthukrihna and Guha 2008; Shukla and Kumar 2007). Neelakandan *et al.*, (2003) have obtained the Cr (VI) rejection of 68% with permeates flux of 5.96×10^{-10} ms^{-1} at an applied pressure of 275 kPa for the feed concentration of 1000 ppm. In the work reported by Pugazhenthi *et al.*, (2005), the modified carbon membranes showed 96% rejection for Cr (VI) and permeate flux of 1.464×10^{-8} ms^{-1}

at a higher applied pressure of 483 kPa with the feed concentration of 1000 ppm. It is important to mention that most of the researchers have used higher applied pressure for the separation of Cr (VI) in comparison to this study (207 kPa). Moreover, the permeate flux (1.1007×10^{-5} ms^{-1}) obtained in this work is three to five order higher even at lower applied pressure due to bigger pore size of the MCM-41 membrane in comparison to other membranes presented in Table 2.6. In order to adopt the membrane technology for industrial applications, the membrane should provide better rejection and permeate flux. Keeping this in view, it can be concluded that the membrane cited in this work is better than other membranes reported in the literature for similar purpose.

Table 2.6 Comparison of separation performance of the MCM-41-ceramic membrane with other membranes

Membrane material	Pore size (nm)	Feed conc. (ppm)	Solute flux (ms^{-1})	Rejection (%)	Applied pressure (kPa)	Reference
Zeolite-clay membrane	30	1000	2.733×10^{-6}	66	483	Shukla and Kumar, 2007
Styrene acrylonitrile membrane	55	1000	2.38×10^{-6}	90	275	Sachdeva and Kumar, 2008
PMMA-EGDM membrane	1.35	1000	5.96×10^{-10}	68	275	Neelakandan *et al*., 2003
Composite polyamide membrane	---	1000	1.489×10^{-6}	99	500	Muthukrishna and Guha, 2008
Clay-carbon membrane	2	1000	1.464×10^{-8}	96	483	Pugazhenthi *et al*., 2005
MCM-41-ceramic composite membrane	**173**	**1000**	**1.10×10^{-5}**	**80**	**207**	**Present work**

2.3.7 Separation of trivalent metal ions

The fabricated MCM-41-ceramic composite membrane was used for the separation of $AlCl_3$ and $FeCl_3$ from its aqueous solution, based on interaction between the metal ions and the

charged MCM-41 membrane. The effect of applied pressure, salt concentration in the feed and pH of the feed on the performance characteristics of the membrane was examined separately.

2.3.7.1 Variation of applied pressure

In order to examine the influence of applied pressure on permeate flux and rejection of salts, the concentration and pH of $AlCl_3$ salt solution were fixed as 3000 ppm, and 1.5, respectively. Fig. 2.22 clearly displays that the flux enhances with increasing applied pressure. The permeate flux and rejection of $FeCl_3$ are also plotted against the applied pressure for a fixed salt concentration of 3000 ppm, as illustrated in Fig. 2.23. It is noticed that the permeability of both $AlCl_3$ and $FeCl_3$ solution is lesser than the pure water permeability. This indicates that the presence of Al^{3+} and Fe^{3+} generates an additional resistance to the flow of the membrane. The permeate flux increases with an increase in the applied pressure, which can be explained by considering the solute flux through the membrane, as a sum of convective (due to applied pressure gradient across the membrane) and diffusive (due to concentration difference) flux. At lower applied pressure, diffusion contributes towards the flux, whereas convection dominates the overall process at higher applied pressure. In addition to this, the permeate flux of the salt solution is influenced by the electrostatic interaction between electrolyte and the membrane surface, thereby providing an additional resistance in the flow through the composite membrane.

The observed rejection (both $AlCl_3$ and $FeCl_3$) exhibits a decreasing trend with increasing applied pressure (see Figs. 2.22 and 2.23) due to severe concentration polarization caused by the enhanced accumulation of solute particles on the membrane surface at elevated pressure. As a result, the permeate concentration increases owing to increase in convective flux. In addition to the applied pressure, few other parameters such as charge density of the

membrane and the interaction of the membrane charge sites with the ionic solute, also play a key role in altering the rejection of Al^{3+} and Fe^{3+} ions. The obtained rejection of $AlCl_3$ is 69% at an applied pressure of 69 kPa for a feed concentration of 3000 ppm with pH = 1.5 whereas the maximum rejection of $FeCl_3$ is found to be 64% for MCM-41-ceramic composite membrane at an applied pressure of 207 kPa (natural pH = 2.45) and the feed concentration of 3000 ppm.

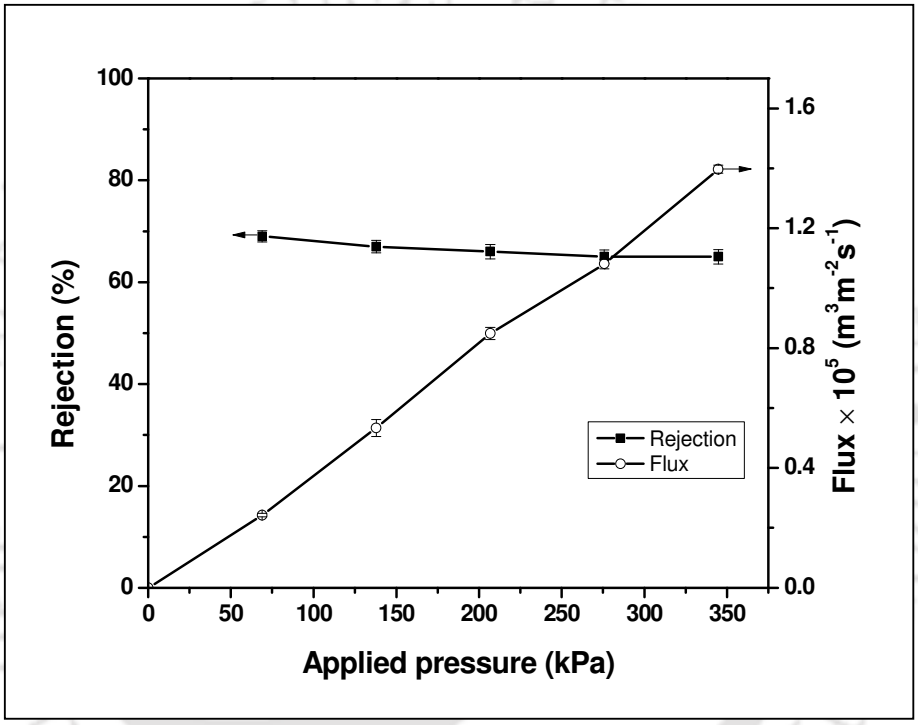

Fig. 2.22 Variation of rejection and permeate flux of $AlCl_3$ with applied pressure on MCM-41-ceramic composite membrane (feed concentration = 3000 ppm; pH of the solution = 1.5)

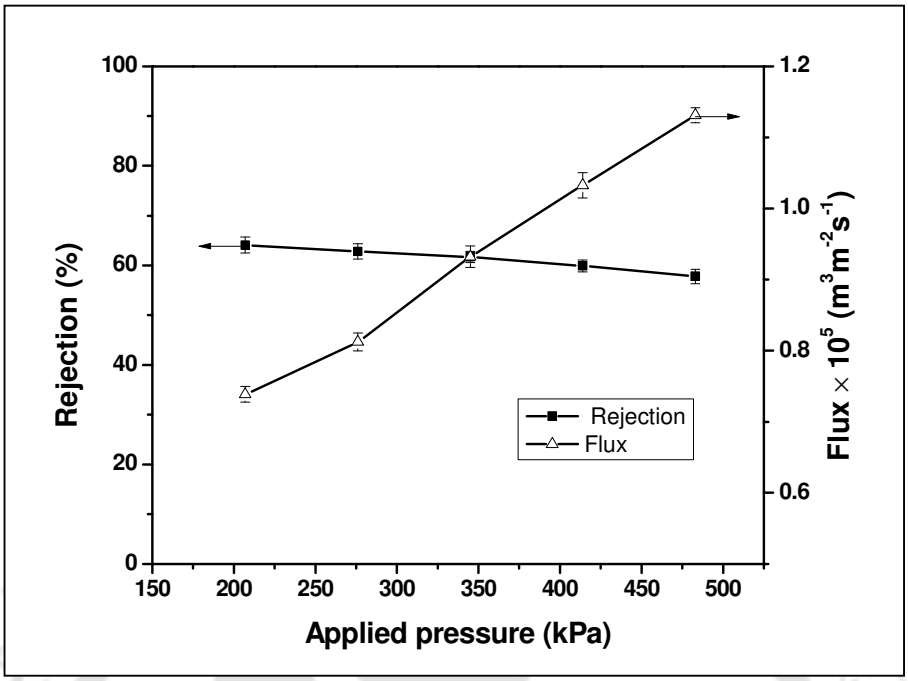

Fig. 2.23 Variation of rejection and permeate flux of $FeCl_3$ with applied pressure on MCM-41-ceramic composite membrane (conc. = 3000 ppm, natural pH = 2.45)

2.3.7.2 Variation of feed concentration

The influence of feed concentration of $AlCl_3$ and $FeCl_3$ was also examined on the permeate flux and removal efficiency as shown in Figs. 2.24 and 2.25, respectively. The permeate flux displays the decreasing trend with increasing salt concentration. This is due to the partial plugging of the pores of the membrane and concentration polarization. At a lower feed concentration (250 ppm), the highest rejection of 82% is observed for $AlCl_3$. The membrane charge will be shielded to a larger degree at higher salt concentration. As a result, effective charge is less and consequently decreasing trend for rejection is observed. The rejection of 82% outlined in this work at an applied pressure of 276 kPa with the salt concentration of 250 ppm is comparable or even better than those cited (Majhi *et al.*, 2009) in the literature. For $FeCl_3$ separation, the best rejection of 71% is obtained for a feed concentration of 250 ppm at an applied pressure of 276 kPa.

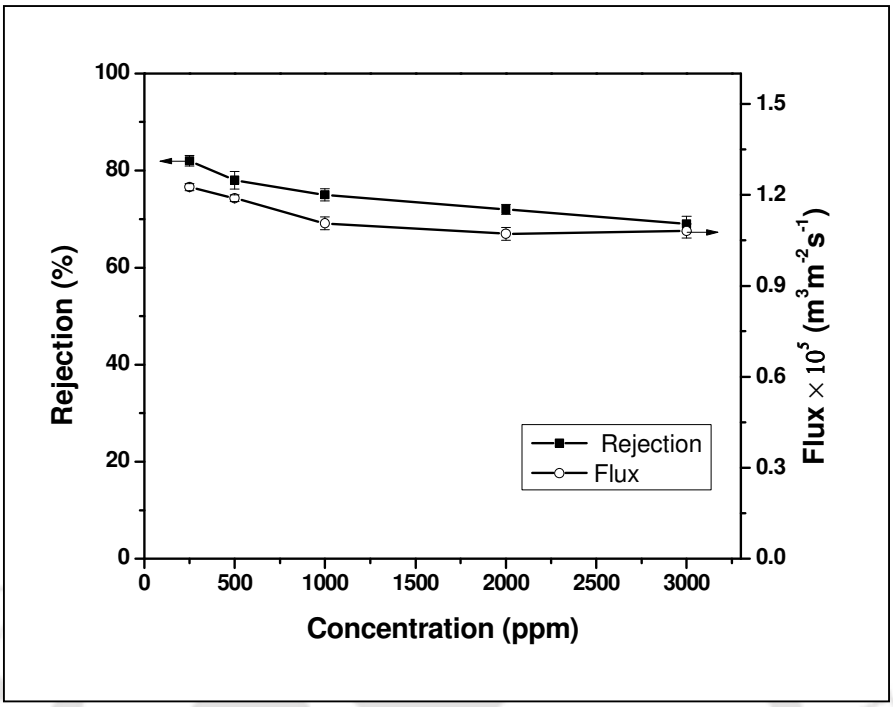

Fig. 2.24 Rejection and permeate flux of $AlCl_3$ as a function of feed concentration for MCM-41-ceramic composite membrane (applied pressure = 276 kPa; pH of the solution = 1.5)

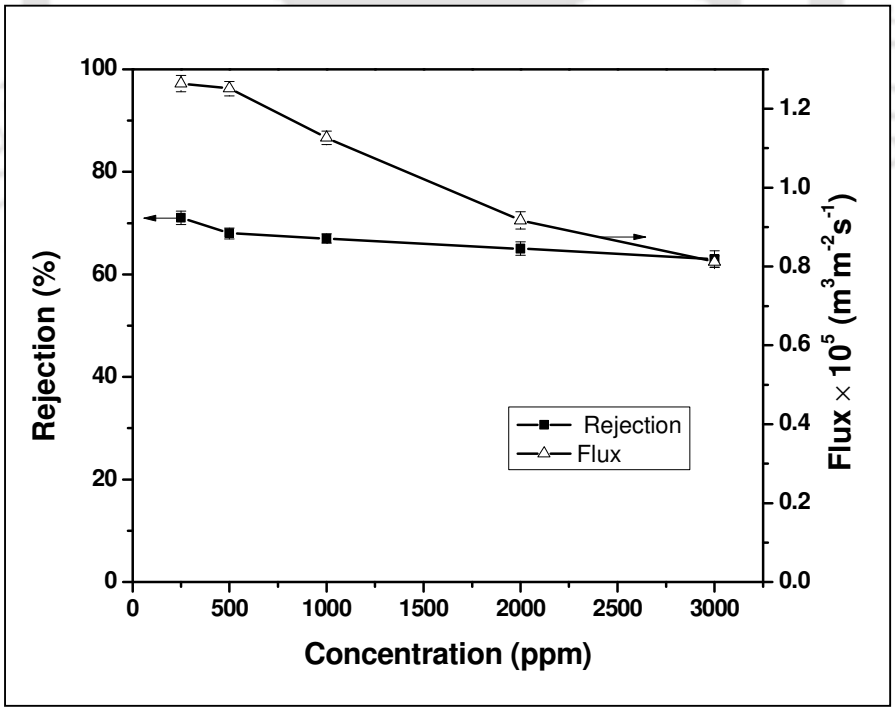

Fig. 2.25 Rejection and permeate flux of $FeCl_3$ as function of feed concentration for MCM-41-ceramic composite membrane (applied pressure = 276 kPa, natural pH = 2.45)

2.3.7.3 Variation of pH

The surface charge of the material is a useful parameter that determines the separation efficiency of the membrane and also it changes with pH of the solution. Keeping this in mind, experiments were conducted over the pH ranging between 1.5 and 5.0 for a fixed feed concentration (250 ppm) with an applied pressure of 276 kPa and the results are depicted in Figs. 2.26 and 2.27. It is apparent that at lower pH, the maximum rejection of 82% and 85% is obtained for $AlCl_3$ and $FeCl_3$, respectively. The rejection of $FeCl_3$ and $AlCl_3$ through the membrane is strongly influenced by the operating pH of the feed solution. The rejection phenomena can be explained with the help of Fig. 2.28. Since the isoelectric point (IEP) of MCM-41 is about 3.9, the membrane is positively charged at pH < 3.9 and negatively charged at pH > 3.9. As the pH increases from 1.5 to 4, the removal of $AlCl_3$ and $FeCl_3$ is lowered due to decrease of magnitude of positive charge (surface potential) of the membrane. Thus, the repulsion between the positively charged membrane and cation (Al^{3+} and Fe^{3+}) decreases and accordingly, the rejection of Al^{3+} and Fe^{3+} reduces. It is also noticed that the rejection enhances slightly with increasing pH beyond IEP of the membrane. This is due to the fact that membrane is negatively charged at pH > IEP and the surface charge (negative) of the membrane at pH 5.0 is higher than that of pH 4.0. The permeate flux increases with decreasing the magnitude of the surface potential due to the decreased electroviscous effect as observed in Figs. 2.26 and 2.27. A higher surface charge (negative) leads to increase in the intensity of electrostatic repulsion between the Cl^- ions present in the solution and the membrane surface, thereby resulting in increased rejection while increasing the pH of the solution from 4.0 to 5.0.

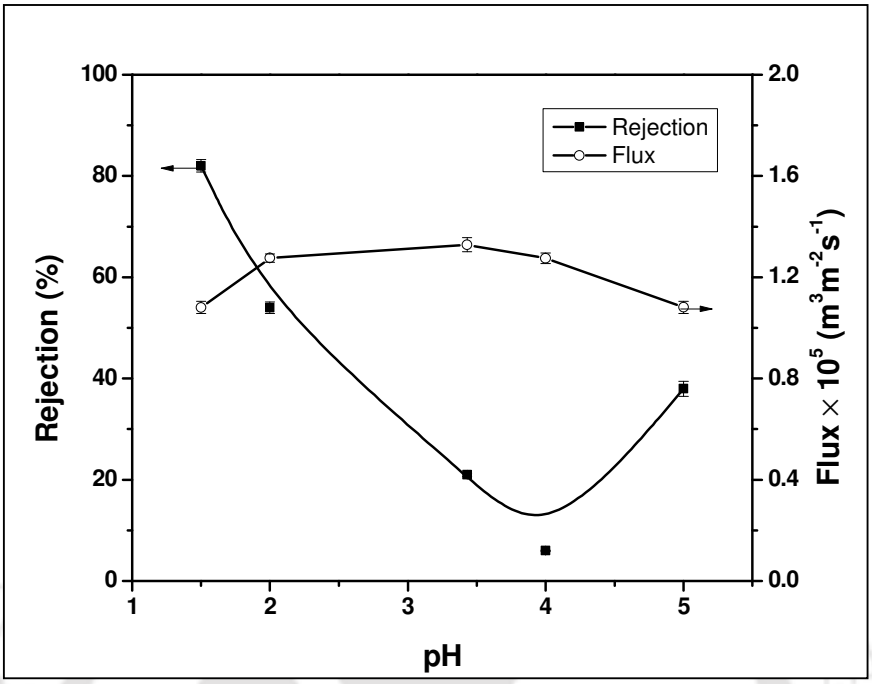

Fig. 2.26 Permeate flux and rejection of $AlCl_3$ as a function of pH for MCM-41-ceramic composite membrane (applied pressure = 276 kPa; feed concentration = 250 ppm)

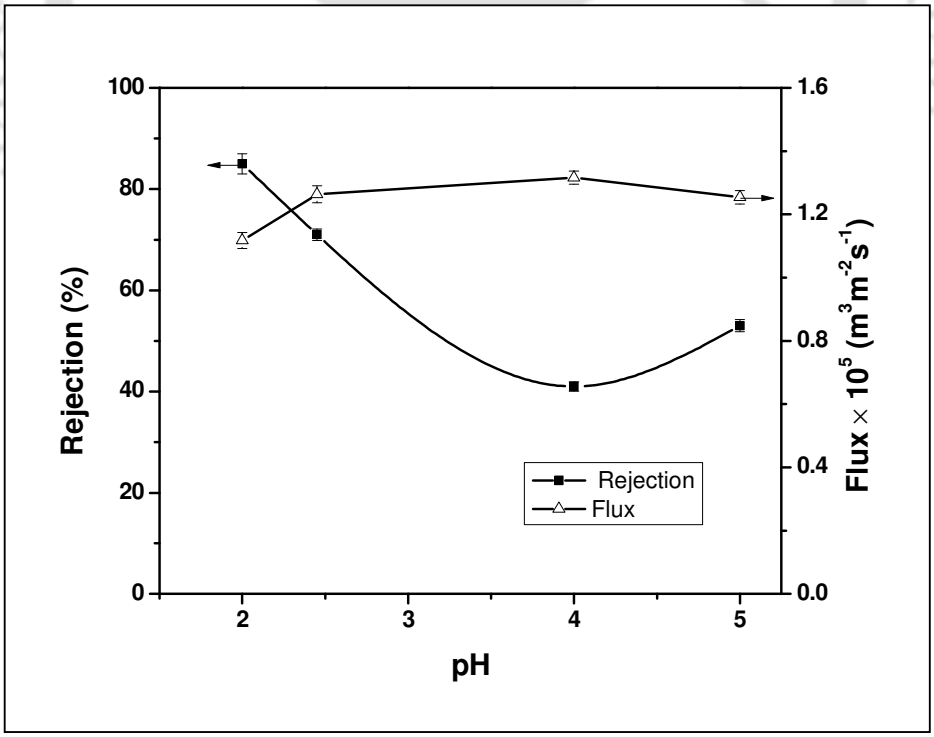

Fig. 2.27 Permeate flux and rejection of $FeCl_3$ as a function of pH for MCM-41-ceramic composite membrane (concentration = 250 ppm, applied pressure = 276 kPa)

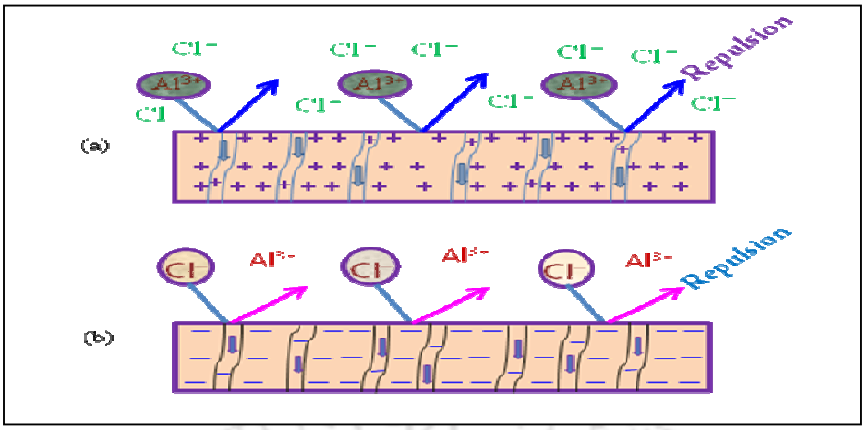

Fig. 2.28 Schematic illustration of $AlCl_3$ repulsion on variation of pH (a) when pH < IEP and (b) pH > IEP.

2.4 Summary

MCM-41-ceramic composite membranes have been successfully fabricated on ceramic support by hydrothermal synthesis method. The porosity and pore size of the ceramic support reduce from 47% to 23% and 1.0 to 0.173 µm, respectively by multiple deposition of MCM-41 on the support. Solvent permeation experiments confirm that the permeation of solvents through the MCM-41-ceramic composite membrane is influenced by chemical nature of the solvents. Separation characteristic of the prepared composite membrane is checked by performing filtration studies of chromium and trivalent metal salts from aqueous solution individually as a function of applied pressure, feed concentration and pH of the feed solution. The experimental results confirm that the rejection of metal ions strongly depends on the operating pH. The highest Cr (VI) rejection of 80% is obtained at pH 2 with an applied pressure of 207 kPa for the feed concentration of 1000 ppm. The maximum rejection of $AlCl_3$ and $FeCl_3$ is found to be 82%, and 85%, respectively for the salt concentration of 250 ppm with lower pH of the solution. The obtained results point out that the MCM-41 membrane could be utilized as a potential candidate for the removal of metal ions from aqueous solution.

Chapter 3

Preparation, Characterization and Application of MCM-48-Ceramic Composite Membrane for the Removal of Metal Ions from Aqueous Solution

Preparation, Characterization and Application of MCM-48-Ceramic Composite Membrane for the Removal of Metal Ions from Aqueous Solution

MCM-41-ceramic composite membrane reported in the previous chapter was prepared with the synthesis time of 96 h and possessed the porosity and mean pore size of 23% and 0.173 µm, respectively. The lesser hydrothermal reaction time can minimize the fabrication cost of the membrane. Therfore, it is important to identify lower synthesis time for the preparation of zeolite composite membrane. This chapter presents the preparation of ordered mesoporous MCM-48-ceramic composite membrane on a low cost circular shaped ceramic support using tetraethyl orthosilicate (TEOS) and cetyltrimethyl ammonium bromide (CTAB) as source materials by in-situ hydrothermal crystallization technique. The repeated multiple coating of MCM-48 on ceramic support reduces the pore size and porosity of the membrane. Various solvent permeation tests through MCM-48-ceramic composite membrane were conducted to identify the solvent resistance of the fabricated composite membrane. Further, the performance of MCM-48-ceramic composite membrane is evaluated in a dead-end batch filtration set-up by the separation of chromium and trivalent metal ions from aqueous solution independently at various operating pressures, feed concentrations and pH of the feed solution.

3.1 Experimental

3.1.1 Materials

Tetraethyl orthosilicate (TEOS), chromium (VI) oxide, and hydrochloric acid were purchased from Merck (I) Ltd., Mumbai. Ferric chloride, aluminium chloride (hexahydrate) and sodium

hydroxide were procured from Loba Chemie (Laboratory Reagents & Fine Chemicals), Mumbai, India. Cetyltrimethyl ammonium bromide (CTAB) was obtained from SRL, Mumbai, India. For this work, water was taken from Millipore system (ELIX-3).

3.1.2 Preparation of MCM-48-ceramic composite membrane

The procedure used for the fabrication of ceramic support was explained in detail in chapter 2 (section 2.1.2). MCM-48 ceramic composite membrane was prepared on ceramic support by hydrothermal technique. Firstly, 21.22 g of CTAB was disslolved in 80 mL of Millipore water and another solution was also prepared by dissolving 1.8 g of NaOH in 20 mL of water. Afterthat, both solutions were mixed and continuously stirred at room temperature for 5-6 h to get a homogeneous solution (called as solution A). The above prepared solution was poured into a beaker containing tetraethyl orthosilicate (TEOS) solution (called as solution B) with ceramic support (diameter: 42 mm and thickness: 4 mm) and continuously stirred to a gel-like suspension. The molar composition of the gel was $1TEOS:0.25Na_2O:0.65CTAB:0.62H_2O$. This gel along with ceramic support was placed in an autoclave reactor and subjected to hydrothermal treatment at 110 °C for 72 h. After completion of reaction, the membrane and MCM-48 powder (as-synthesized) were recovered from the reactor, washed with Millipore water and dried at 100 °C for 24 h. Finally, MCM-48 powder and the fabricated membrane were calcined at 550 °C for 6 h with a heating rate of 1 °C/min in an air atmosphere. Fig. 3.1 illustrates the complete fabrication technique of MCM-48 ceramic composite membrane. To increase the amount of MCM-48 deposition on ceramic support, the membrane was synthesized with a repeated cycle (3 times) of coating using the same molar composition of gel followed by crystallization reaction and calcination. After each cycle of synthesis, the weight gain of the ceramic membrane in comparison to the dry weight of the support was estimated. After the third coating cycle, no significant weight

increment was observed in the fabricated membrane and hence, the composite membrane prepared with three coating cycles was applied for the assessment of liquid phase separation efficiency.

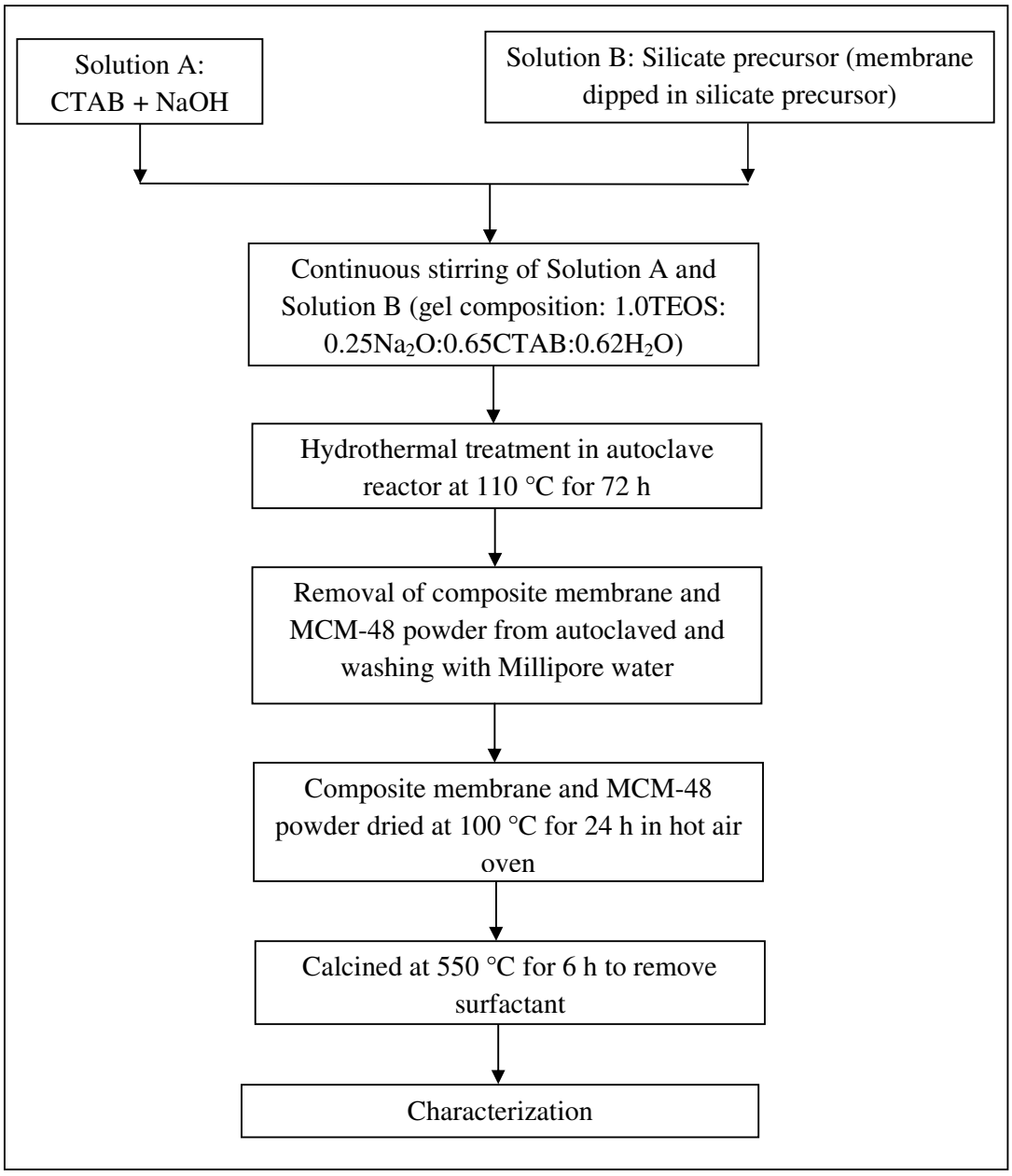

Fig. 3.1 Flow chart for the fabrication of MCM-48 ceramic composite membrane

3.2 Characterization

3.2.1 MCM-48 powder sample

The X-ray diffraction (XRD) measurement of MCM-48 powder was taken at room temperature under air atmosphere on a Bruker A8 advance instrument with CuKα (λ=1.5406 A˚) radiation. The operating conditions were 40 kV and 40 mA. The diffractograms were recorded in the 2θ range of 1-10° with a step size of 0.05 $°s^{-1}$. FTIR spectra of MCM-48 powder samples (as-synthesized and after calcination) were performed in the range of 4000-450 cm^{-1} using KBr powder with a Shimadzu IR Affinity spectrometer. TGA analysis of MCM-48 powder (as-synthesized) was carried out to characterize the thermal stability of the prepared sample in a Netzsch TG 209F1 Libra with an air atmosphere. The sample was heated from 25 to 950 °C at the heating rate of 10 °C/min. N_2 adsorption/desorption isotherms of MCM-48 powder samples were carried out using a Quantachrome ® Asiqwin TM-Automated Gas Sorption (Version 3.0). Samples were degassed at 190 °C for 3 h before analysis. From the BET (Brunauer-Emmett-Teller) model, the specific surface area of the sample was computed. The BJH (Barrett-Joyer-Halenda) approach was used to calculate the pore size distribution and total pore volume was computed at P_s/P_o of 0.99 by assuming nitrogen was fully saturated. To know the surface charge of MCM-48 powder, zeta potential measurement was conducted with Beckman Coulter model Delsa Nano at various pH values.

3.2.2 Composite Membrane

The porosity of ceramic support and MCM-48 ceramic composite membrane was computed using Archimedes' principle. The detail procedure for the determination of porosity was elaborated in chapter 2 (section 2.2). FESEM analysis was employed to determine the surface morphology of ceramic support and MCM-48 ceramic composite membrane using a Zeiss

Sigma instrument at 3-KeV acceleration voltage. Prior to FESEM analysis, the sample was coated with thin layer of gold to a thickness of approximately 150 A° to minimize the charging effect. The images were taken at different magnifications.

Pure water permeation experiments through ceramic support and the fabricated MCM-48 composite membrane were performed in a dead-end filtration set up as shown in chapter 2 (section 2.2.1). By filling the permeation cell with 150 mL of water, experiments were carried out at different applied pressures. After discarding the first 50 mL of permeated water, the time needed for the second 50 mL of permeate collection was noted down for calculating the water flux. The water flux at different applied pressures ranging from 69 to 483 kPa was estimated from the following equation:

$$J_W = \frac{Q}{A\Delta T} \tag{3.1}$$

where, J_W is the water flux through the membrane ($m^3m^{-2}s^{-1}$), Q is the volume of water permeated (m^3), A is the effective membrane area (m^2), and ΔT is the sampling time (s).

The average pore diameter of the membrane is calculated using deduced form of Hagen-Poiseuille (H-P) equation (Almandoz *et al*., 2004; Bowen *et al*., 1997) given below:

$$J_w = \frac{\varepsilon r^2 \Delta P}{8\mu\tau l} = L_h \Delta P \tag{3.2}$$

where, r is the mean pore radius (μm), μ is the viscosity (kPa s), J_w is water flux through the membrane (μm/s), l is pore length (μm), τ is the tortuosity factor, ΔP is the applied pressure across the membrane (kPa), ε is the porosity of the membrane. The permeability of the membrane (L_h) was obtained from the slope of the linear relationship between the applied pressure and the pure water flux.

3.2.3 Solvent permeation study

Solvent flux measurements were performed using polar and non-polar solvents to study the surface interaction of the solvents through the membrane. For each run of the test, initially 100 mL of test solvent was flushed through the MCM-48 membrane. After that, the cell was filled with a fresh 150 mL of solvent. The permeation tests were conducted at various applied pressures ranging between 69 and 345 kPa. Various properties of solvents applied in the permeation experiments are reported in section 2.3.4 of chapter 2 (see Table 2.5).

3.2.4 Separation of chromium and trivalent metal ions from aqueous solution

The separation performance of MCM-48 ceramic composite membrane was investigated by conducting filtration experiments of chromium and trivalent metal salts from aqueous solution using dead-end filtration set up. All the experiments were performed at room temperature (25 °C). The concentration of feed and permeate solution was measured using a calibrated conductivity meter (Eutech Instruments, Model: CON 2700).

In a typical separation experiment, the permeation cell was filled with 100 mL of chromium solution and first 10 mL of permeate across the membrane was discarded. The next 10 mL of permeate through the membrane was collected and the time required for the collection of 10 mL was recorded. Using these data, permeate flux was calculated. After each experiment, the membrane was thoroughly washed and flushed with water at higher pressure in order to regain the initial pure water flux. The influence of operating parameters such as applied pressure, feed concentration and pH of the solution on the permeate flux and rejection of Cr (VI) was investigated. In order to study the influence of applied pressure, experiments were conducted at five different pressures (69-375 kPa) for a fixed chromium concentration (1000

ppm) at natural pH (~ 2.35) of the solution. The effect of feed concentration on the permeate flux and rejection was performed at different feed concentrations (250-3000 ppm) with a constant applied pressure (207 kPa) and natural pH of the solution. The pH study was carried out in the range of 2-9 at a fixed applied pressure of 207 kPa with the feed concentration of 1000 ppm where pH of the chromium solution was adjusted by adding NaOH or HCl solution.

In the same way, the permeate flux and rejection of $AlCl_3$ and $FeCl_3$ were also studied as a function of working parameters, such as the influence of applied pressure, feed concentration and pH of the solution. The rejection (R) percentage of chromium, $AlCl_3$ and $FeCl_3$ was calculated from the following expression:

$$R(\%) = \left[1 - \frac{C_p}{C_f}\right] \times 100 \tag{3.3}$$

where, C_f and C_p are the concentration of chromium or trivalent metal ions in the feed and permeate, respectively.

3.3 Results and discussion

3.3.1 Characterization of MCM-48 powder

XRD pattern of MCM-48 powder samples (as-synthesized and after calcination) is displayed in Fig. 3.2 The XRD profile of as-synthesized (before calcination) MCM-48 demonstrates two sharp diffraction peaks at 2θ value of 2.76 and 3.15 corresponding to the planes of (2 1 1) and (2 2 0), respectively. The mesoporous phase of the cubical structure is verified by the distinct (2 1 1) and (2 2 0) reflections. After calcination, the intensity of the XRD peaks increases as compared to the as-synthesized sample. With the removal of surfactant, the ordering degree of intensity is improved. Similar observations in XRD patterns were also

reported for MCM-48 (Kumar *et al*., 2001; Liu *et al*., 2007 and Wu *et al*., 2008). The shifted 2θ position of calcined sample indicates the contraction of structure attributed to elimination of the template and successive condensation of silanol groups (Si-OH) (Hui *et al*., 2006).

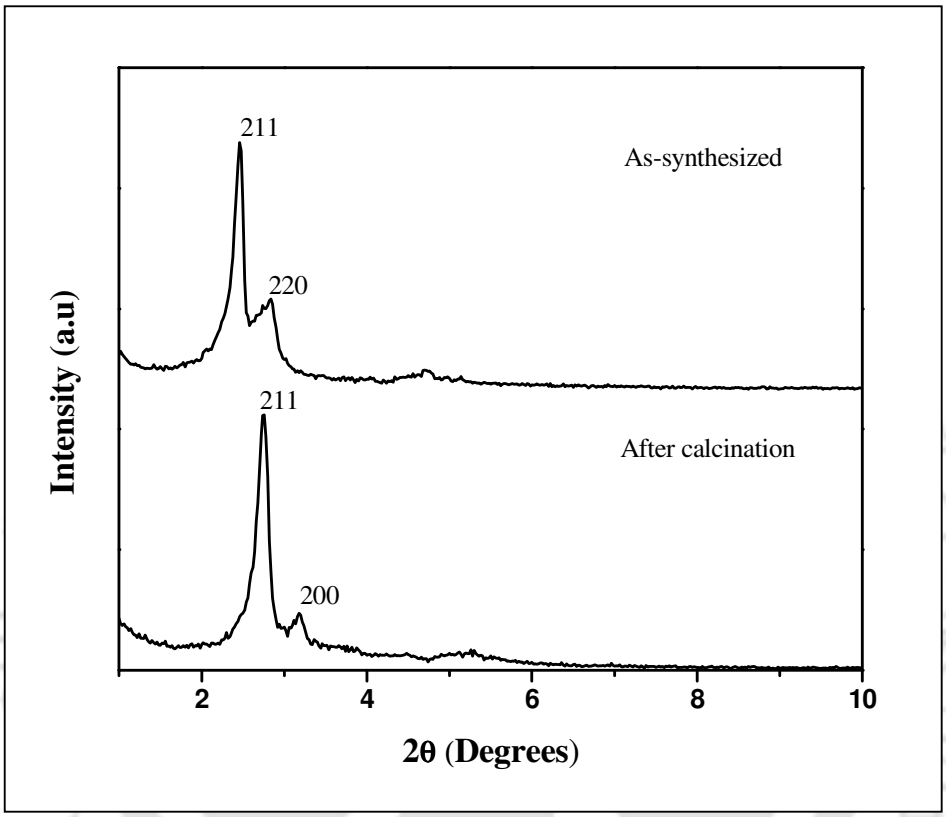

Fig. 3.2 XRD pattern of MCM-48 powder samples (as-synthesized and after calcination)

Fig. 3.3 illustrates the FTIR spectra of as-synthesized and calcined MCM-48 powders. For the as-synthesized sample, the sharp intense bands occurred at 2920 and 2853 cm^{-1} are owing to the presence of hydrocarbon chain of C-H stretching of the surfactant molecules (Monash and Pugazhenthi 2010). The analogous bending vibrational mode is noticed at 1478 cm^{-1}. A broad band appeared at around 3213 cm^{-1} in the hydroxyl region of 3600-3200 cm^{-1} is ascribed to surface silanols and adsorbed H_2O molecules. The peak observed at 1068 and 1221 cm^{-1} is due to the asymmetric stretching vibrations of Si-O-Si absorption bands (Loganathan *et al*., 2013). The band at 959 cm^{-1} corresponds to Si-OH vibration (Monash and

Pugazhenthi 2010). The calcined MCM-48 powder sample also displays similar band spectrum and the bond stretching properties. In the calcined sample, the disappearance of all bands belonging to the organic group reveals that the surfactant is completely removed at the calcination temperature (550 °C) (Loganathan *et al*., 2013).

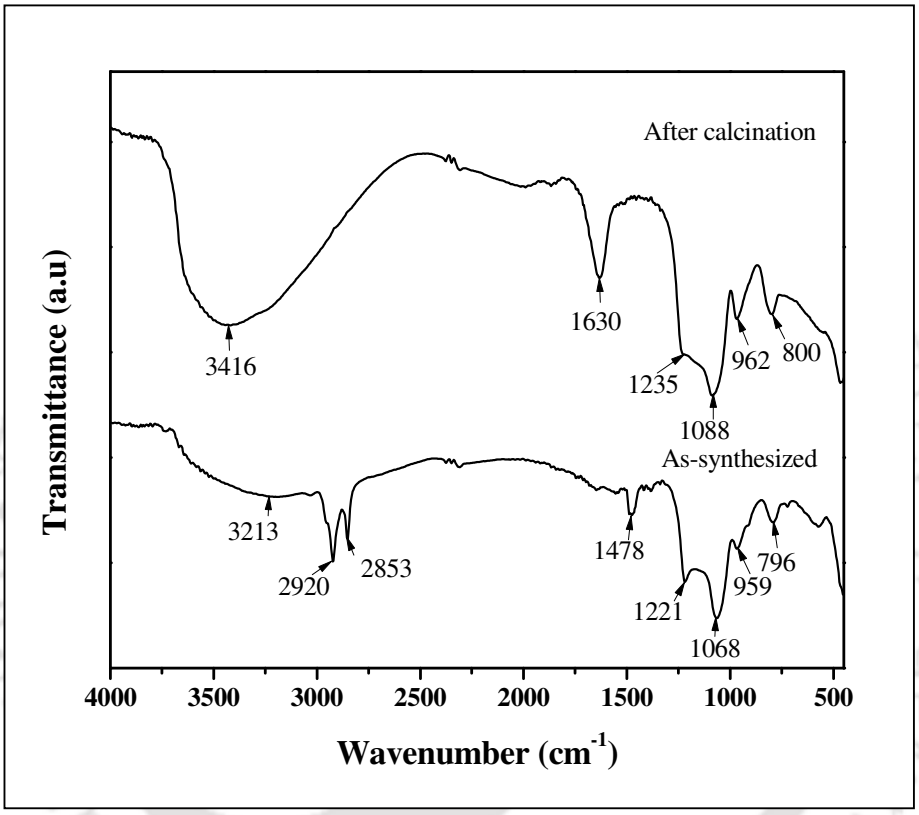

Fig. 3.3 FTIR spectra of as-synthesized and calcined MCM-48 powder

The removal of template from the membranes by calcination technique has great influence on the structure and selectivity of the prepared composite membrane. The thermogravimetric analysis (TGA) and differential thermogravimetric (DTG) analysis of the as-synthesized MCM-48 powder are depicted in Fig. 3.4. The TGA of as-synthesized MCM-48 powder sample shows three distinct regions of weight loss (Monash and Pugazhenthi 2010). In the first region, the weight loss noticed around 3% for the temperature less than 170 °C is attributed to the removal of physisorbed water molecules from the external surface of the

material. The weight loss of 42 % is observed between 170 to 340 °C, which is attributed to the decomposition of surfactant molecules. The weight loss (15%) of the third region in the temperature of 340 to 540 °C is because of the combustion of the surfactant and the loss of water produced from the condensation of adjacent silanol groups (Hui *et al*., 2006). At above 540 °C, the weight loss is about only 2%, which may possibly be attributed to the degradation of germinal and vicinal silanol groups contained in the sample (Loganathan *et al*., 2013). DTG curve also confirms three stages of decomposition during heating of as-synthesized MCM-48 powder. An endothermic peak observed at 51 °C in the DTG curve is due to removal of moisture. The second peak at 214 °C is caused by the removal of trimethylamine head group, via Hofmann degradation (Liu *et al*., 2007), which leads to the formation of alkenes and the removal of water molecules. The third peak in the DTG curve at 319 °C corresponds to the oxidation of remaining organic compounds to carbon dioxide, water and probably carbonaceous species (Liu *et al*., 2007).

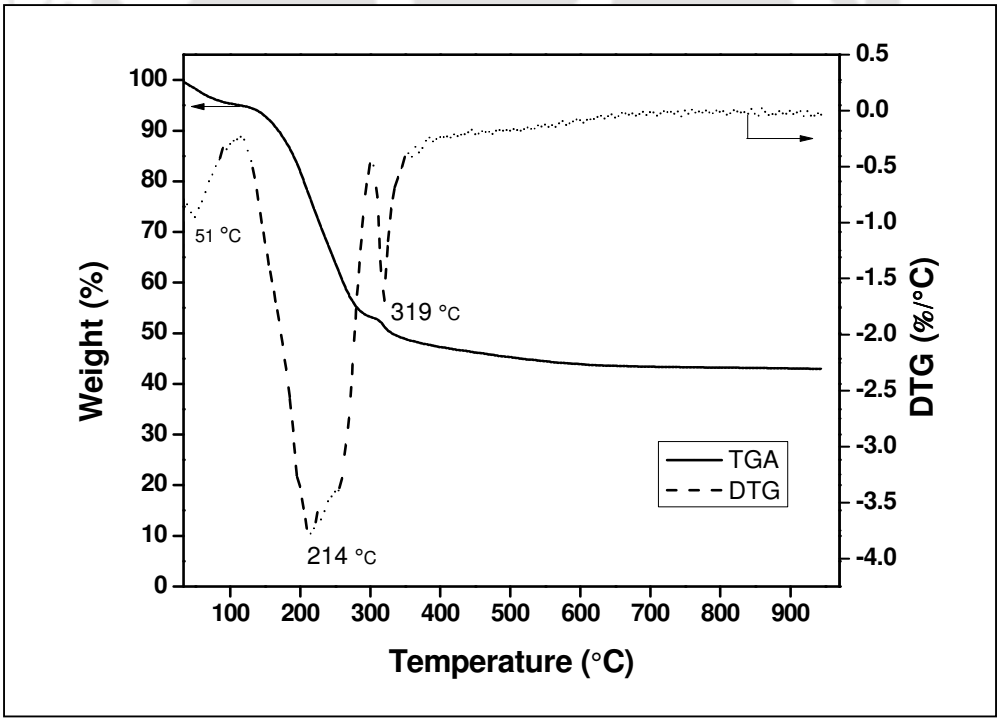

Fig. 3.4 TGA and DTG curve of as-synthesized MCM-48 powder with air atmosphere

The surface area of MCM-48 powder is measured using N_2 adsorption/desorption isotherm as illustrated in Fig. 3.5. According to IUPAC nomenclature (Schumacher *et al.*, 1999), the isotherm observed for MCM-48 powder can be classified as a type IV isotherm. The isotherm possesses capillary condensation and exhibits hysteresis loop, which is the typical feature of mesoporous materials**.** BET surface area and total pore volume are found to be 1175 m^2g^{-1}, and 0.6780 cm^3g^{-1}, respectively, that are determined from the amount of N_2 adsorbed at relative pressure (P_s/P_o) of 0.99. The pore size distribution computed by BJH method using desorption curve is also shown in Fig. 3.5 (inset) and the calculated average pore size of MCM-48 powder material is 3.3 nm.

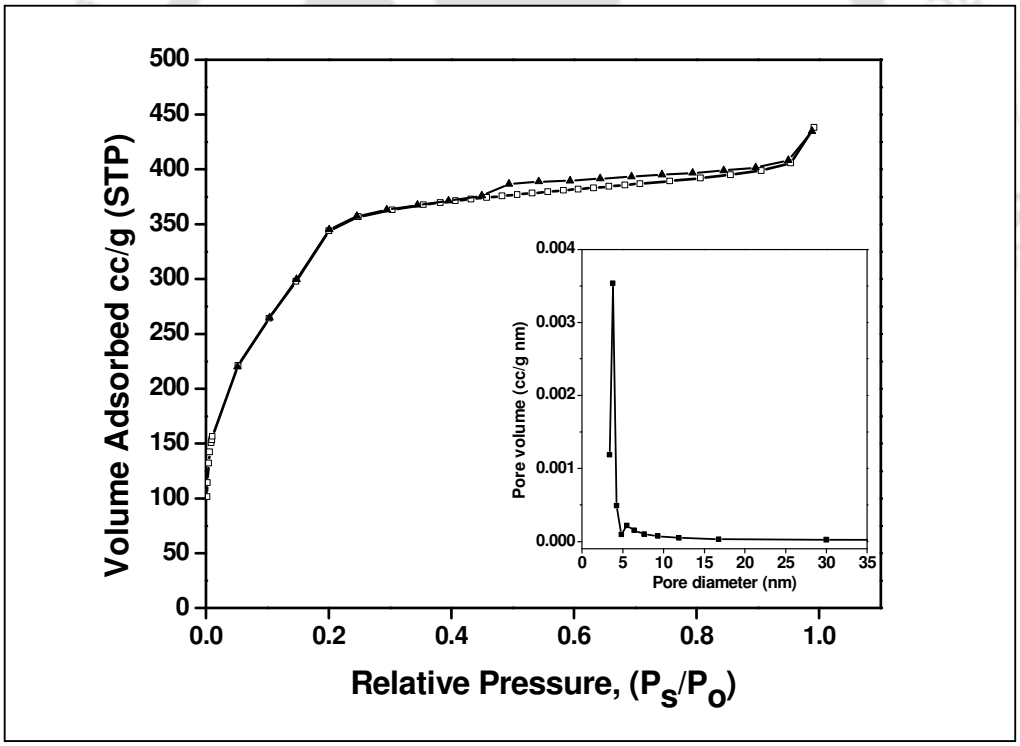

Fig. 3.5 N_2 adsorption-desorption isotherm of calcined MCM-48 powder. Inset shows the pore size distribution of the powder.

Fig. 3.6 demonstrates the variation of zeta potential as a function of pH. The surface charge of the MCM-48 ceramic composite membrane depends on the pH of the contact solution and

it can be either positive or negative. With the intention of finding the surface charge of MCM-48 ceramic composite membrane, zeta potential of the calcined MCM-48 powder particles were measured by keeping the powder in water suspension at different pH of 2-12 using electrostatic light scattering method in Delsa Nano C. To determine the speed of particles movement, the particles are irradiated with a laser light and the scattered light emitted from particles is detected. Since the frequency of scattered light is shifted from the incident light in proportion to the speed of particles movement, the electrophoretic mobility of particles could be measured from the frequency shift of the scattered light. The surface charge of the MCM-48 powder is altered by adding NaOH in water suspension for higher pH and HCl is added to lower the pH of the solution. At higher pH (pH = 12), zeta potential value is observed to be -40.1 mV and it is +3.96 mV at lower pH (pH = 2). The isoelectric point (IEP) of the MCM-48 powder is found to be 3.2.

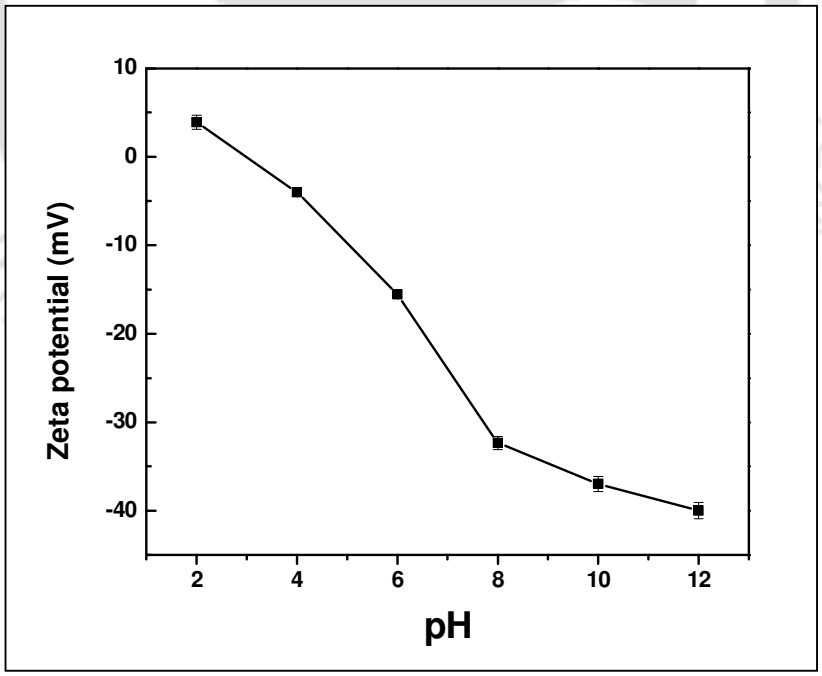

Fig. 3.6 Zeta potential measurement of MCM-48 powder at various pH

3.3.2 Characterization of MCM-48 ceramic composite membrane

The porosity of the MCM-48 composite membrane with number of coating cycles was estimated and the obtained results are presented in Table 3.1. It can be seen that porosity of the composite membrane decreases with increasing the number of coatings. This is because of an increase in the mass of MCM-48 deposition on the support with increasing cycle of coating. The porosity of the three cycle coated membrane is found to be 22%.

Table 3.1 Characterization results of MCM-48 ceramic composite membranes

Membrane	Porosity (%)	Average pore size calculated from water flux data (µm)	Water permeability ($m^3m^{-2}s^{-1}kPa^{-1}$)	Cumulative weight gain (g)
Support	47	1.00	3.63×10^{-6}	-
1st coating	33	0.506	6.20×10^{-7}	0.59
2nd coating	27	0.254	1.31×10^{-7}	0.98
3rd coating	22	0.142	4.18×10^{-8}	1.28

In order to check the formation of MCM-48 layers on the membrane, FESEM imaging technique was employed to visualize the surface of the composite membranes. Fig. 3.7(a-f) shows the surface images of support and MCM-48 composite membranes prepared with multiple coatings. It can be seen from Fig. 3.7(b) that after first cycle of deposition, MCM-48 particles are randomly deposited on the surface of ceramic support. Moreover, there is no crack on the surface of the membrane. FESEM images also clearly display the presence of cubic structure of MCM-48 on the ceramic support. With the same magnification scale, images are shown in Fig. 3.7(a-d) for ceramic support as well as composite membranes (1-3 coating). It is noticed that with increasing number of cycle of coatings, a greater quantity of MCM-48 is deposited on the ceramic support. Also, the pore size of the membrane is reduced

when the number of repeated cycle of coating increases. With higher magnification scale, a larger amount of MCM-48 deposition is clearly visible in three cycle coated membrane (Fig. 3. 7(e-f)).

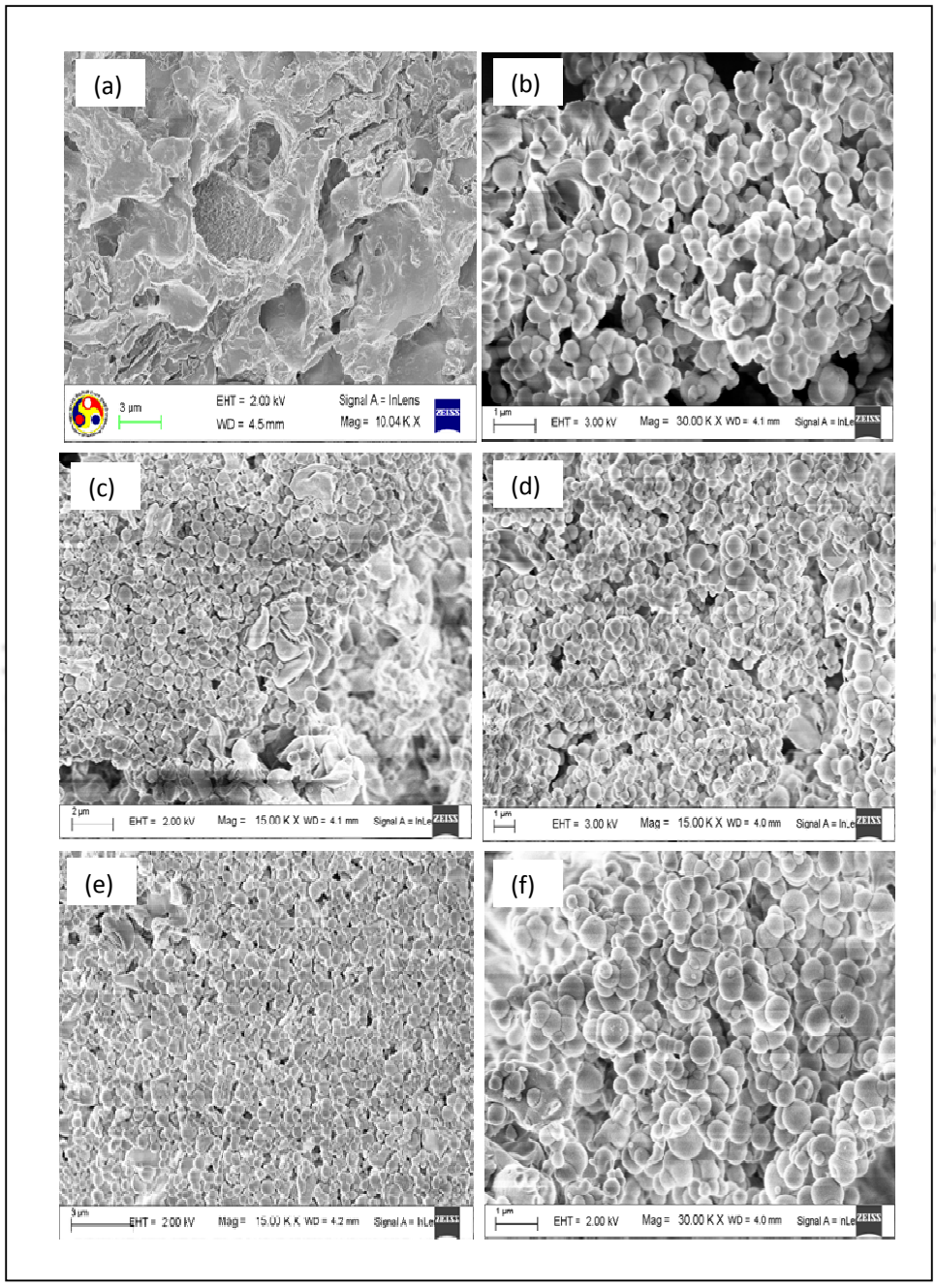

Fig. 3.7 (a-f) FESEM images (a) support, (b) MCM-48 particles, (c) 1st, (d) 2nd, (e) 3rd coating, and (f)3rd coating at higher magnification.

The pure water permeation experiments through ceramic support and MCM-48 ceramic composite membranes were conducted at various applied pressures and the obtained results are illustrated in Fig. 3.8. As expected, the pure water flux increases linearly with an increase in applied pressure and obeys Darcy's law. In comparison with ceramic support, the pure water flux of the MCM-48 composite membrane is lower, demonstrating that the composite membrane possesses lower pore size than that of the support. Table 3.1 presents the characteristic feature of MCM-48 ceramic composite membrane. According to Hagen-Poiseuille equation, calculated average pore size of the MCM-48 composite membrane (3 cycle coated) and ceramic support is found to be 142 nm and 1.0 μm, respectively.

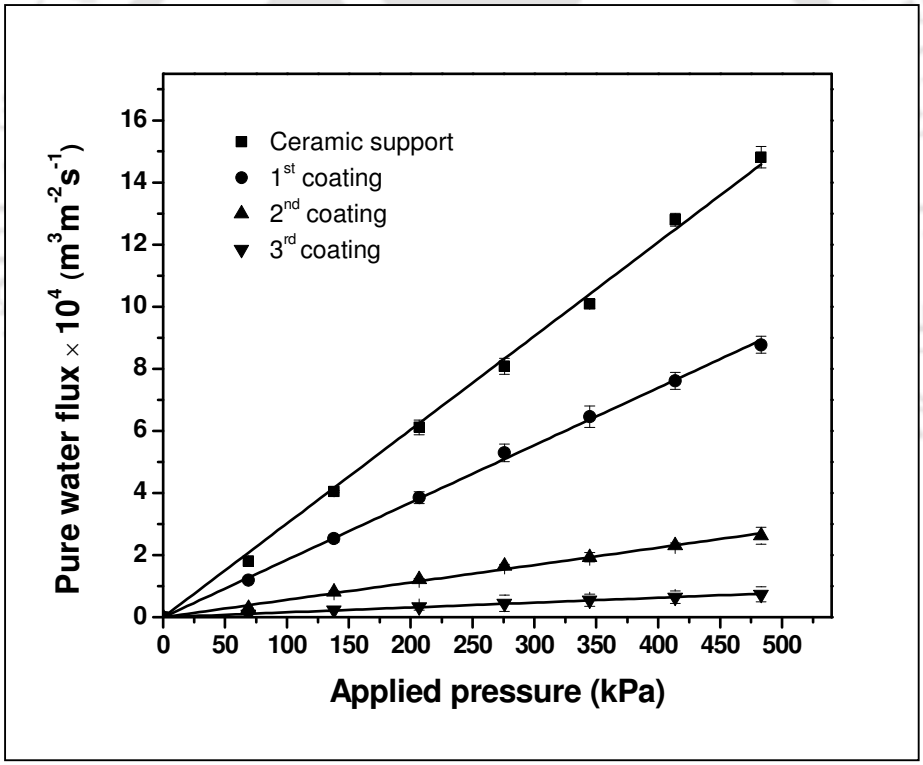

Fig. 3.8 Variation of pure water flux with applied pressure for the support and MCM-48 ceramic composite membrane

3.3.3 Solvent permeation study

To investigate the solvent resistance of the MCM-48 composite membrane and surface interaction of the membrane with solvents, polar and non polar solvents were selected for the permeation experiments. The experiments were performed with the following order: methanol, ethanol, propanol, butanol, toluene, hexane, pentane and heptane. Fig. 3.9 shows the flux of various solvents through the MCM-48 ceramic composite membranes. It is clearly observed that the flux increases linearly with an increase in the applied pressure for all the liquids. Hence, it demonstrates that the applied pressure is one of the driving forces for the solvent permeation test. The highest R^2 value (R^2 >0.99) for the flux versus applied pressure plot infers that solvent permeation via composite membrane follows the viscous flow pattern given by Darcy for the transport mechanism. It is also seen that non polar solvents provide higher permeability than the polar solvents as shown in Fig. 3.10. Although the viscosity of methanol and toluene is almost same, but both solvents show different flux. This clearly indicates that other than viscosity, some other factors control the flow of solvents through the membrane.

Besides viscosity, membrane-solvent interaction has an impact on the solvent permeability (Bhanushali *et al*., 2001; Chen *et al*., 2010). The solvent-pore interactions have effect on the scale of molecular level to the permeability of water and alcohols. In addition to this interaction, other parameters like surface tension, di-electric constant and molecular size of the solvent, play a vital role on the permeability of the solvents (Machado *et al*., 1999, 2000; Chowdhury *et al*., 2003). Polarity of the solvent also plays a major role as it is directly related to the surface tension (Machado *et al*., 2000). Figs. 3.9 and 3.11 illustrate directly measured and viscosity corrected fluxes of various solvents through the MCM-48 ceramic composite membrane. Considering the combined permeability of solvents, plot of water and alcohol

family groups (Fig. 3.10), the permeability of methanol and ethanol is higher than that of water, whereas propanol and butanol have lower permeability than water. If viscosity is the only controlling factor, then all data points in Fig. 3.11 should lie on a single line but it does not obey except for ethanol and toluene. Hence, the surface tension also affects the permeation through the membrane along with viscosity. Although water has low viscosity than ethanol, it has higher surface tension than ethanol, which makes water to penetrate gradually through the composite membrane. Similarly, pentane has higher flux because of its lower surface tension. In case of ethanol and toluene, it has different viscosity but multiplication of viscosity with permeability, it becomes almost same and both approximately lie on the same line. Therefore, viscosity is playing a dominant role here (Chowdhury *et al.*, 2003).

In alkane series, the viscosity and dielectric constant slightly increase from pentane to heptane and the permeability is higher in case of lower viscosity and dielectric constant liquid (pentane). In the homologous series of linear alcohols, it is observed that the flux increases with decreasing molar volume. In the composite membrane, the interaction of hydrogen bond with the polar liquid easily wets the internal surface of membrane. On the other hand, in case of non-polar liquids, the interaction of the liquid and the membrane surface creates resistance owing to hydrophobic in nature. Therefore, for such molecular use (alcohols), the membrane cross sectional area of pores for flow is less i.e., in such case, the effective pore size is smaller, which may be decreased the permeability of liquids. The specific interactions with the solvent molecules and the surface of MCM-48 ceramic composite membrane can be assigned to dissimilarity in hydrophobic-hydrophilic nature of interactions with the pore walls and the liquids, or to alkoxylation of surface Si-OH groups. This may yield Si-OR surface groups that are some extent bulkier than Si-OH groups (Chowdhury *et al.*, 2003).

Hence, alkoxylation is capable of reducing the effective pore radius resulting lower cross sectional pore area. Thus the membrane has a lower permeability for higher alcohols.

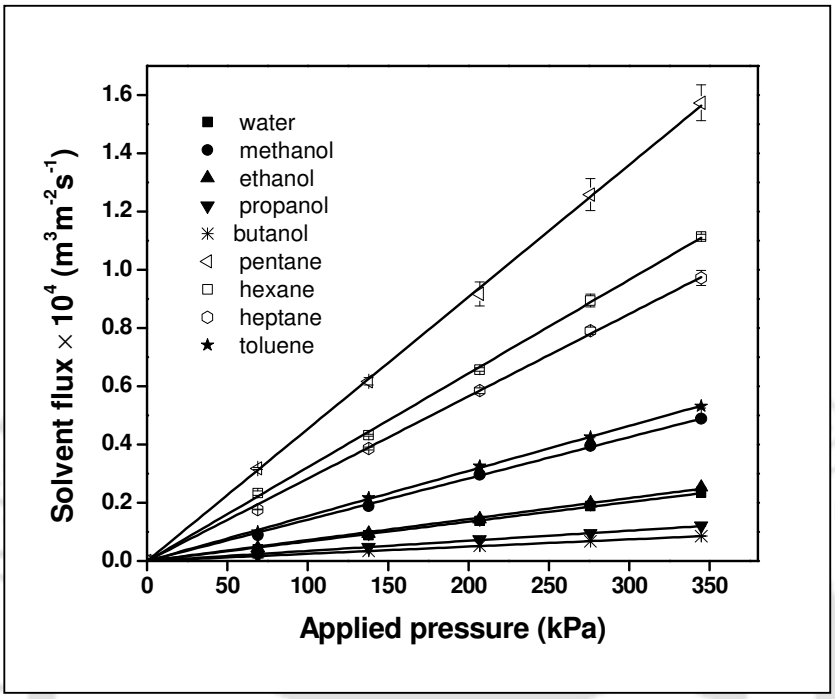

Fig. 3.9 Solvent permeation test through MCM-48 ceramic composite membrane

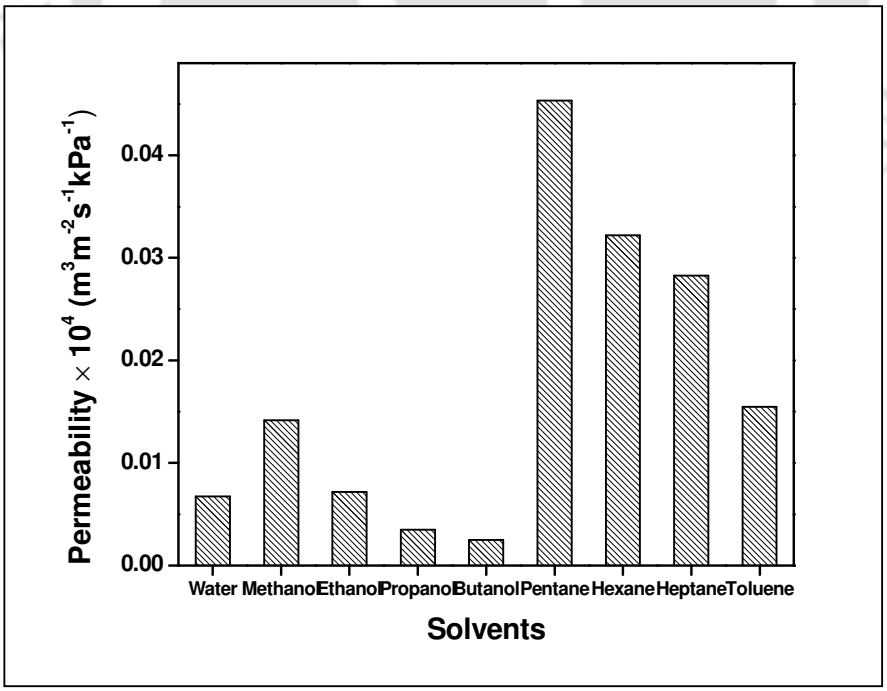

Fig. 3.10 Solvent permeability value of MCM-48 ceramic composite membrane

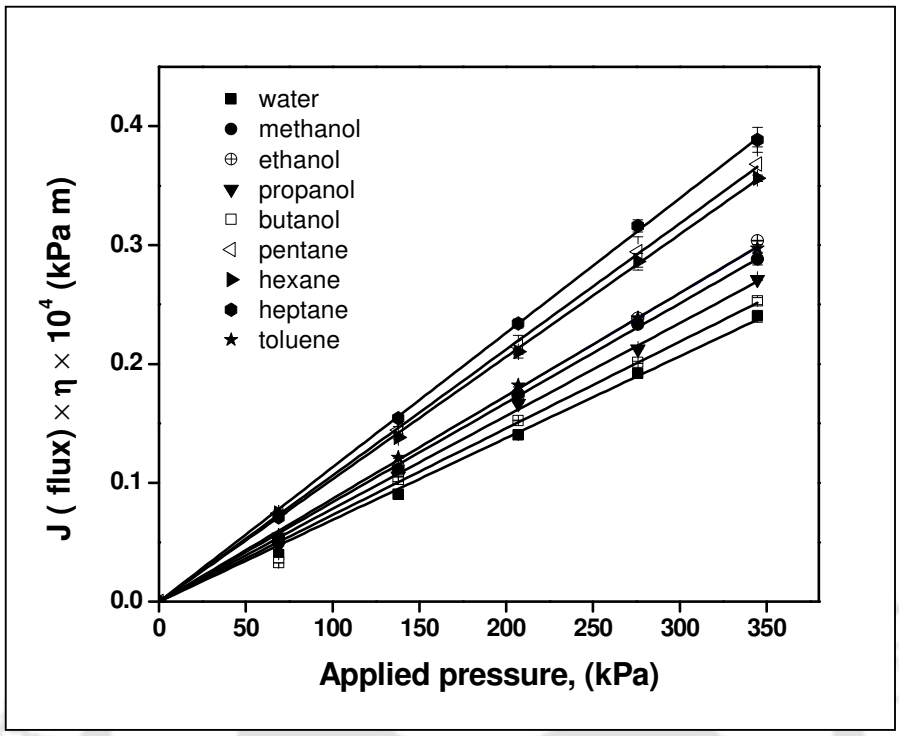

Fig. 3.11 Viscosity corrected solvents permeation of MCM-48 ceramic composite membrane

3.3.4 Separation of Cr (VI)

3.3.4.1 Effect of applied pressure

The performance of the MCM-48 ceramic composite membrane (3 cycle coated) in terms of permeate flux and rejection, was investigated by the separation of Cr (VI) from aqueous solution at various applied pressures (69-345) kPa and the results are shown in Fig. 3.12. As can be seen from this plot, the permeate flux increases linearly with increasing applied pressure and follows Darcy's law. However, it is found that the permeability of Cr (VI) solution is lower than that of pure water permeability. This reduced permeability is due to the combined effect of partial pore plugging, concentration polarization and electro-viscous effect (Shukla and Kumar 2007). When the applied pressure augments, the rejection of Cr (VI) increases gradually on account of decreased pore size of the membrane by accumulation of chromium on the surface of the membrane over time (Hafez and El-Manharawy 2004). No

significant increase in rejection is found after the applied pressure of 207 kPa. Thus the applied pressure of 207 kPa is fixed for effect of concentration study.

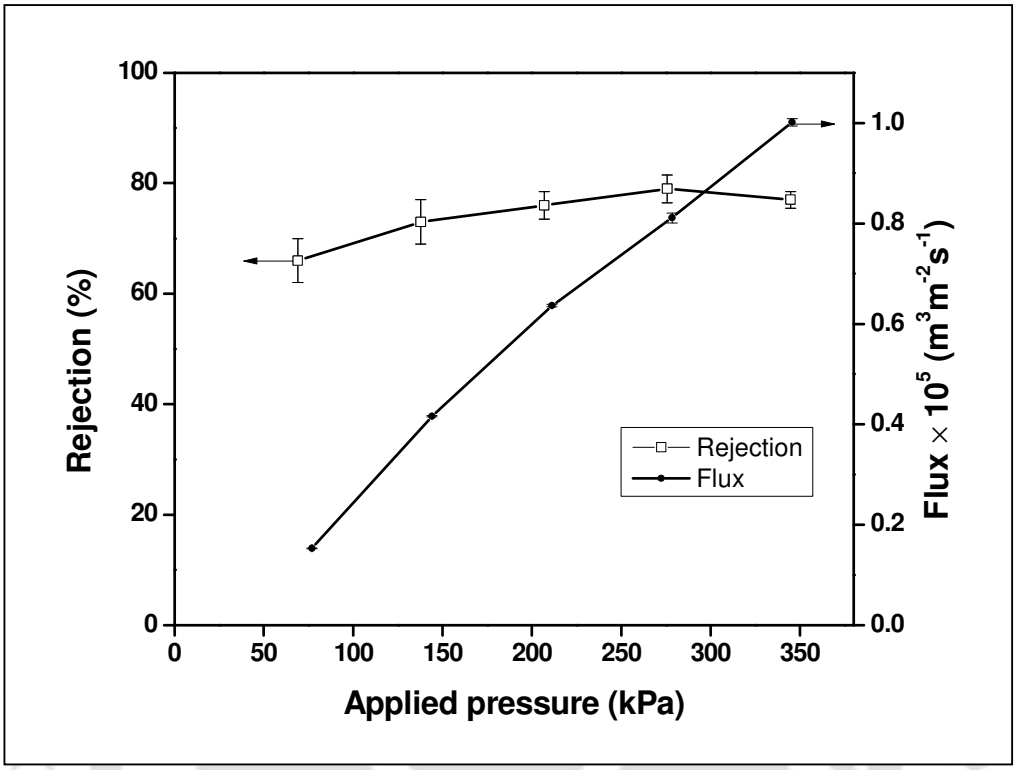

Fig. 3.12 Effect of applied pressure on the permeate flux and rejection for the composite membrane (concentration: 1000 ppm, pH = 2.35)

3.3.4.2 Effect of feed concentration

The effect of feed concentration on Cr (VI) rejection with MCM-48 ceramic composite membrane is illustrated in Fig. 3.13. The experiments were conducted at various concentrations (250-3000 ppm) with a constant applied pressure of 207 kPa and natural pH (~2.35). The plot clearly displays that the rejection of Cr (VI) increases with an increase in feed concentration from 250 to 500 ppm and the rejection becomes almost constant for feed concentration greater than 500 ppm. The maximum rejection of Cr (VI) is observed at 2000 ppm. This is mainly attributed to different factors such as: concentration polarization,

membrane fouling, osmotic pressure on the surface of the composite membrane (Shukla and Kumar 2007).

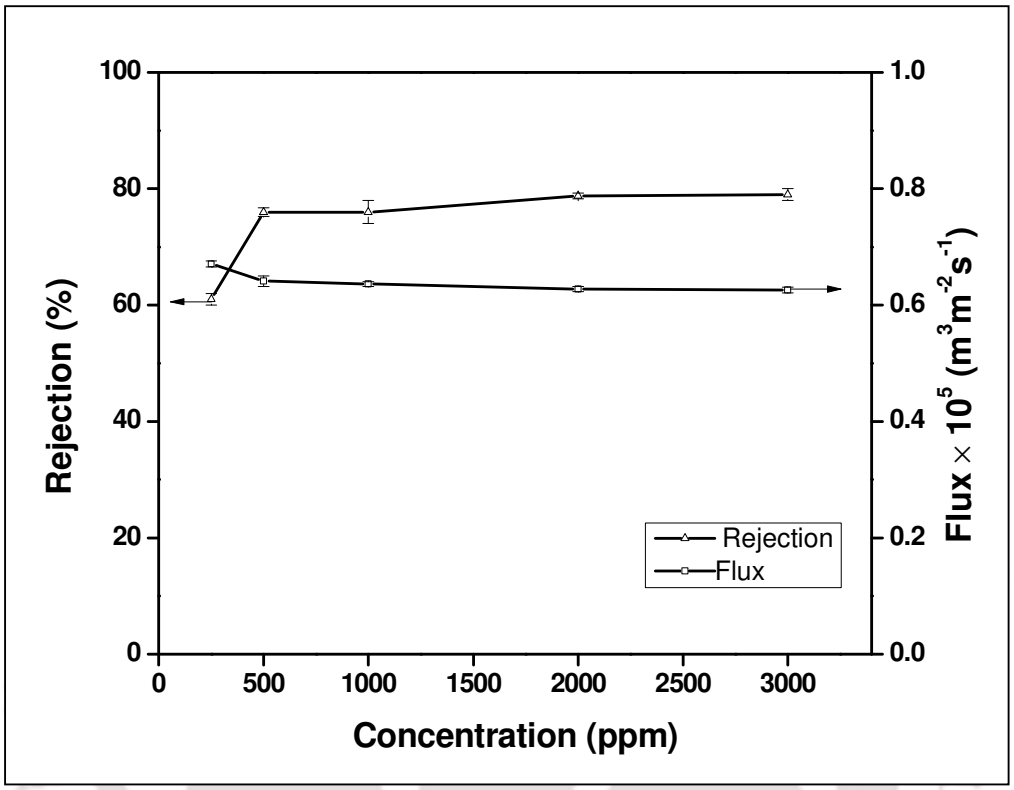

Fig. 3.13 Effect of concentration on the permeate flux and rejection for the composite membrane (applied pressure: 207 kPa, pH = 2.35)

3.3.4.3. Effect of pH

The rejection of Cr (VI) is measured in the pH range of 2-9 with the fixed applied pressure of 207 kPa and the feed concentration of 1000 ppm. The result elucidates that the rejection strongly depends on the working pH value and the highest rejection (81%) is obtained at pH=2 (Fig.14). The isoelectric point (IEP) of the fabricated MCM-48 ceramic composite membrane determined by zeta potential analysis (Delsa Nano) is found to be 3.2. It means that the membrane is positively charged at lower pH (< 3.2) and negatively charged at pH > 3.2. When the charged membrane makes contact with ionic solution, a potential difference is

generated at the interface between the membrane and the solution to maintain electrochemical equilibrium between solution and membrane. With this potential, the membrane repels the ions with same charge as the membrane (Chung *et al*. 2005).

In an aqueous solution, the species of Cr (VI) are assumed to be present as follows: $HCrO^{4-}$, $Cr_2O_7^{2-}$, and CrO_4^{2-} (Benhamou *et al*. 2013).

$$H_2CrO_4 + H_2O \rightleftharpoons HCrO_4^- + H_3O^+ \qquad PK_1 = -0.5$$

$$H_2CrO_4^- + H_2O \rightleftharpoons CrO_4^{2-} + H_3O^+ \qquad PK_2 = 5.8$$

$$2H_2CrO_4^- \rightleftharpoons Cr_2O_7^{2-} + H_2O \qquad PK_3 = 2.2$$

$HCrO^{4-}$ dominates in the pH range from 0 to 5.8 except that above a certain Cr (VI) concentration (~10^{-3} M) it coexists with $Cr_2O_7^{2-}$. When pH > 8, Cr (VI) exists only as CrO_4^{2-}. As the pH of the solution increases from 2 to 3.2, the magnitude of membrane charges (positive) decreases because the IEP of the membrane is 3.2. As a result, the repulsion between positively charged membrane and positive species (H_3O^+) decreases and the rejection diminishes from 81%. When increasing the pH of the solution by addition of NaOH, OH^- ions get accumulated on the membrane surface. Hence, the membrane would acquire more negative charge while put into contact with the feed. As the pH increases from 3.2 to 9, the magnitude of membrane's charge (negative) increases and hence, the higher surface charge (negative) amplifies the intensity of the electrostatic repulsion between ions present in the solution and the membrane surface, which justifies the increased rejection trend.

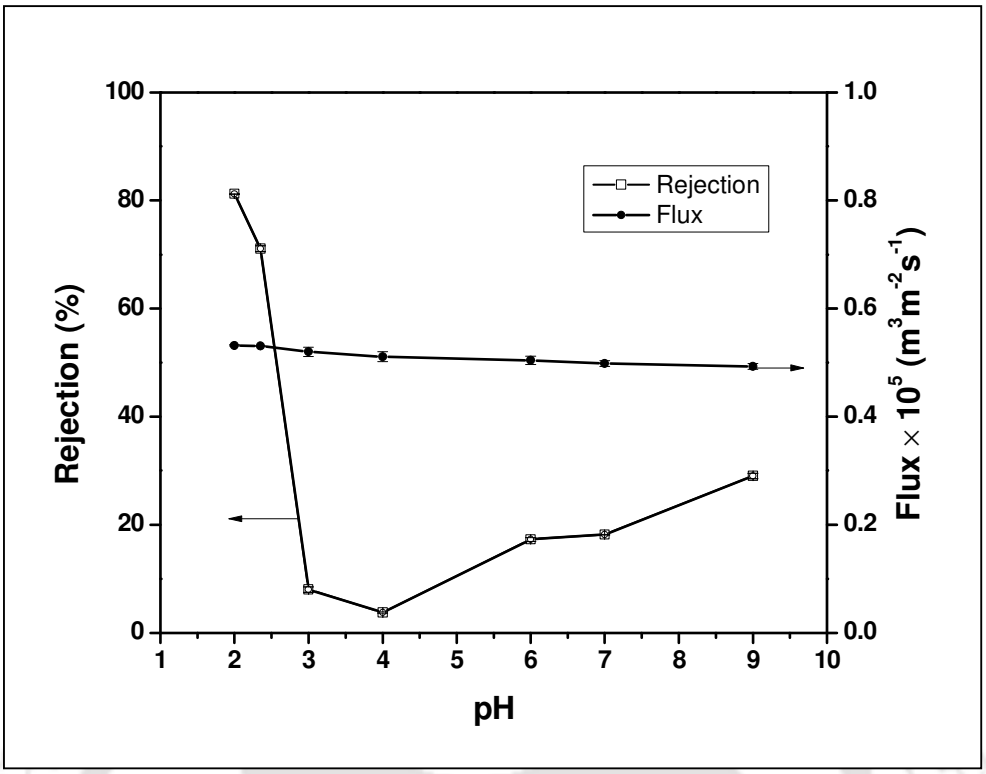

Fig. 3.14 Cr (VI) separation at different pH for MCM-48 ceramic composite membrane (applied pressure = 207 kPa, concentration = 1000 ppm)

Table 3.2 presents the comparison of results obtained in this investigation with other membranes for the separation of Cr (VI). This table clearly points out that the rejection (81%) of Cr (VI) reported in this study at an applied pressure of 207 kPa for feed concentration of 1000 ppm can be compared or even better than the value presented in the literature (Muthukrishnan and Guha 2008; Neelakandan *et al*., 2003; Pugazhenthi *et al*., 2005; Shukla and Kumar 2007; Sachdeva and Kumar 2008). Neelakandan *et al*., (2003) have found 68% of Cr (VI) rejection with permeates flux of 5.96×10^{-10} ms^{-1} for feed concentration of 1000 ppm at an applied pressure of 275 kPa. The modified carbon membranes displayed 96% rejection for Cr (VI) and permeate flux of 1.464×10^{-8} ms^{-1} at a higher applied pressure of 483 kPa with the feed concentration of 1000 ppm (Pugazhenthi *et al*., 2005). It is to be noted that most of the researchers have employed a higher applied pressure for the separation of Cr (VI) in comparison to the present study (207 kPa). However, the permeate flux (5.31×10^{-6} ms^{-1})

observed in this work is higher even at lower applied pressure. For industrial applications point of view, the membrane should provide better removal efficiency as well as good permeate flux.

Table 3.2 Comparison of the separation performance of MCM-48 ceramic composite membrane with other membranes

Membrane material	Pore size (nm)	Feed conc. (ppm)	Solute flux (ms^{-1})	Rejection (%)	Applied pressure (kPa)	Reference
PMMA-EDGM membrane	1.35	1000	5.96×10^{-10}	68	275	Neelakandan *et al*., 2003
Styrene acrylonitrile membrane	55	1000	2.38×10^{-6}	90	275	Sachdeva and Kumar, 2008
Zeolite-clay membrane	30	1000	2.733×10^{-6}	66	483	Shukla and Kumar, 2007
Clay-carbon membrane	2	1000	1.464×10^{-8}	96	483	Pugazgenthi *et al*., 2005
Composite polyamide membrane	--	1000	1.489×10^{-6}	99	500	Muthukrishnan and Guha, 2008
MCM-48-ceramic composite membrane	**142**	**1000**	**5.31×10^{-6}**	**81**	**207**	**Present work**

3.4.5 Separation of trivalent metal ions

3.4.5.1 Influence of applied pressure

The influence of applied pressure on the permeate flux and rejection of $AlCl_3$ and $FeCl_3$ was investigated with constant feed concentration (3000 ppm) and pH as shown in Figs. 3.15 and 3.16. It is apparent from both figures that the flux enhances when the applied pressure increases. The flux of $AlCl_3$ and $FeCl_3$ solution is lower than the pure water flux. This implies

that the presence of these ions (Al^{3+} and Fe^{+3}) creates an extra resistance for the flow through the membrane. The rejection of $AlCl_3$ and $FeCl_3$ decreases slightly with an increase in applied pressure due to the accumulation of these ions (Al^{3+} and Fe^{+3}) on surface of membrane. The convective transport of ions towards the membrane increases as the applied pressure increases, which build more numbers of ions over the surface of the membrane. A substantial augment in the surface concentration offers driving force for the solutes to pass through the composite membrane due to the elevated concentration gradient. As a result, the concentration of $AlCl_3$ and $FeCl_3$ in permeate amplifies and hence, the rejection declines slowly at a higher applied pressure. A similar result was also reported by Majhi et al. (2009) for the separation of $AlCl_3$ and $MgCl_2$ using γ-Al_2O_3 membrane.

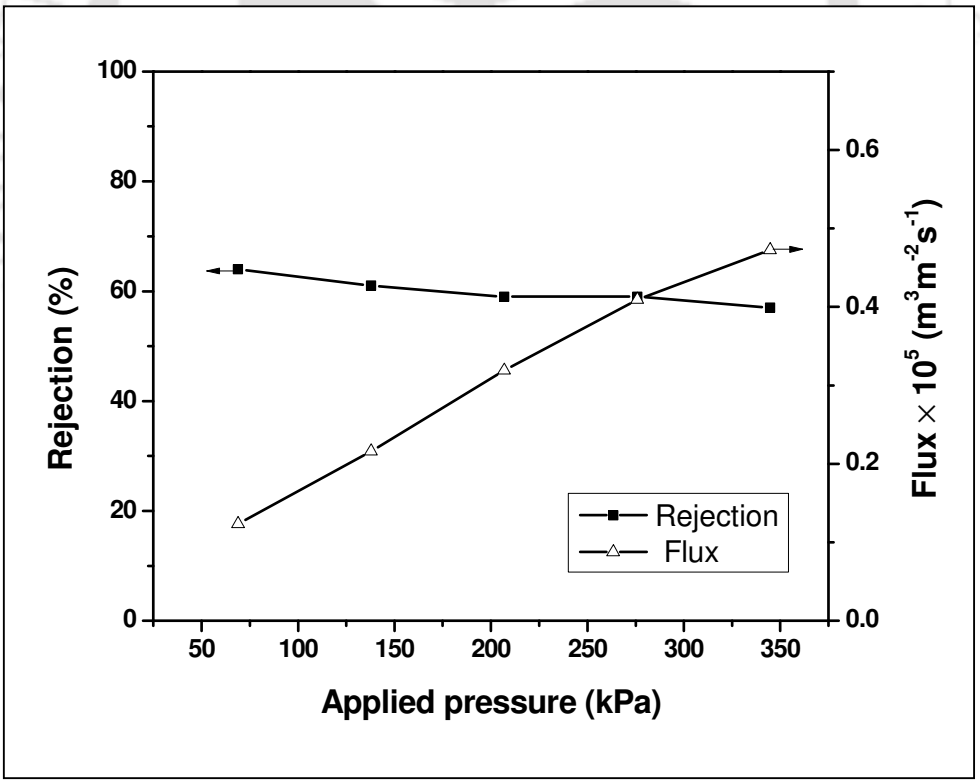

Fig. 3.15 Influence of applied pressure on permeate flux and rejection of $AlCl_3$ for MCM-48 composite membrane (feed concentration = 3000 ppm; pH of the solution = 1.5)

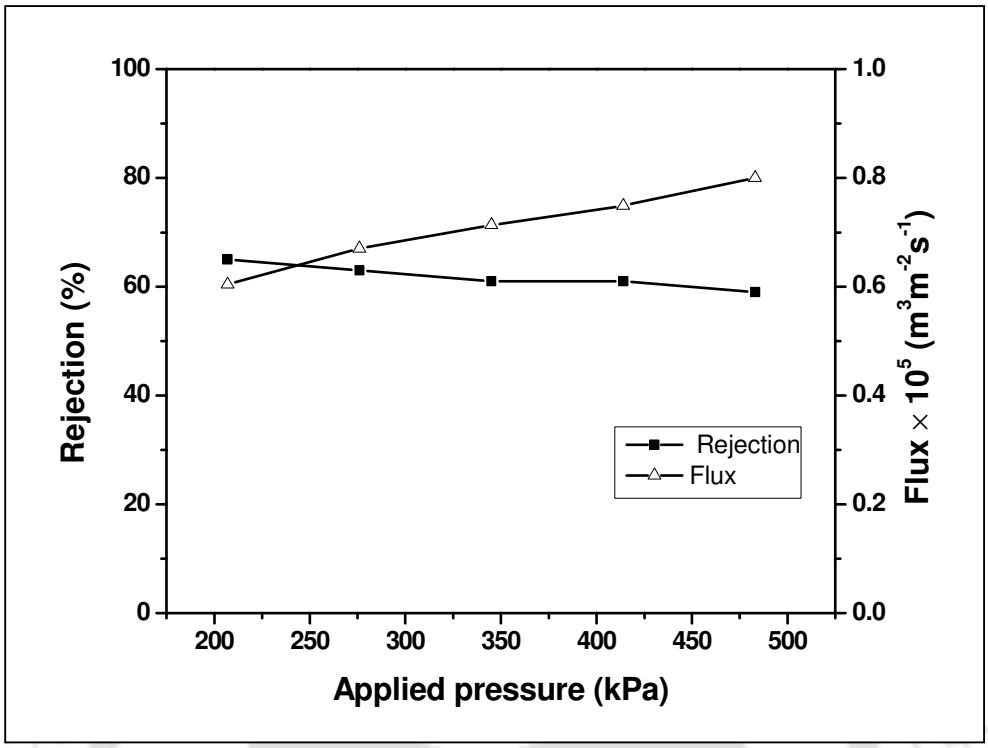

Fig. 3.16 Influence of applied pressure on permeate flux and rejection of $FeCl_3$ for MCM-48 composite membranes (feed concentration = 3000 ppm; initial pH of the solution = 2.45)

3.4.5.2 Influence of feed concentration

Figs. 3.17 and 3.18 depict the effect of feed concentration of $AlCl_3$ and $FeCl_3$ on the rejection and permeate flux. Experiments were carried out at a constant applied pressure (276 kPa) and pH (pH 1.5 for $AlCl_3$ and natural pH of 2.45 for $FeCl_3$). As expected, the permeate flux demonstrates a decreasing trend with increasing salt concentration from 250 to 3000 ppm. This is due to the partial plugging of the pores of the membrane and concentration polarization at higher feed concentration. The membrane charge will be shielded to a larger degree at higher salt concentration. Hence, the effective charge is less and consequently, a decreasing trend is observed for rejection. At a lower feed concentration (250 ppm), the highest rejection of 81% is obtained for $AlCl_3$, while 72% rejection is observed for $FeCl_3$.

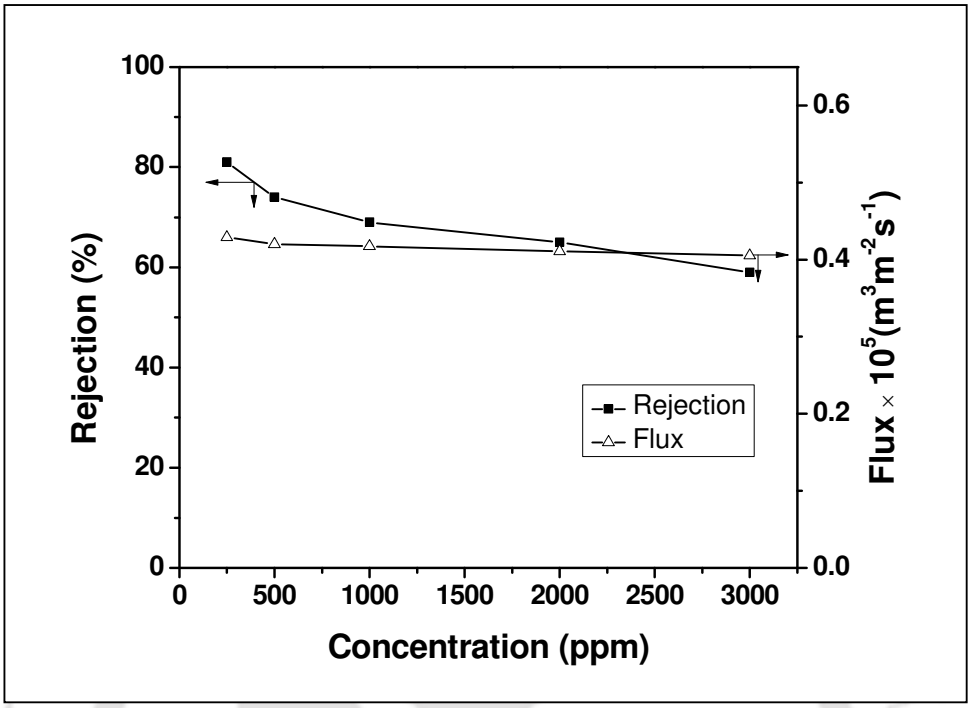

Fig. 3.17 Influence of feed concentration on permeate flux and rejection of $AlCl_3$ for MCM-48 composite membrane (applied pressure = 276 kPa; initial pH of the solution = 1.5)

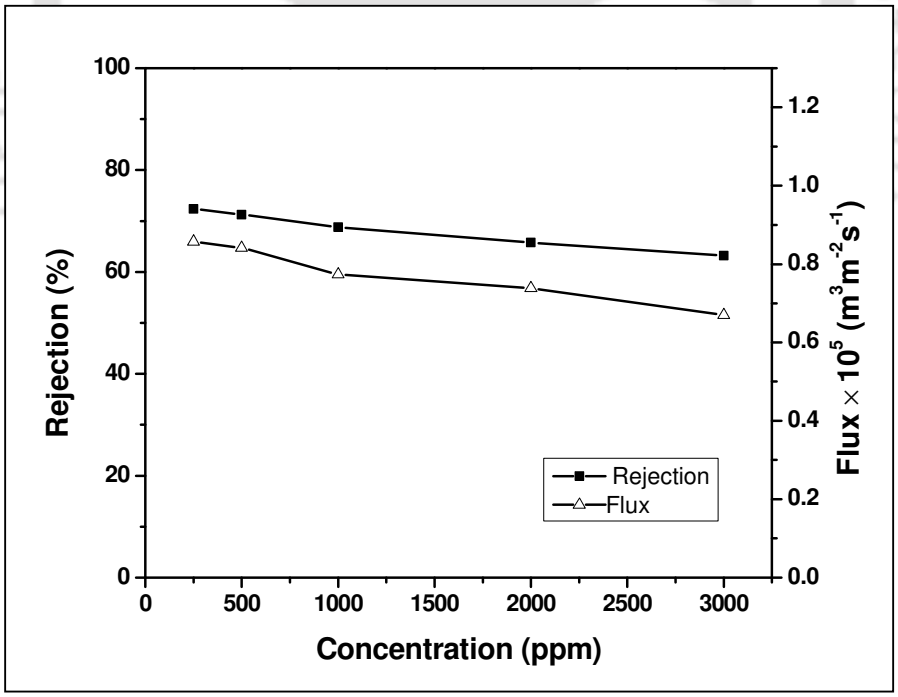

Fig. 3.18 Influence of feed concentration on permeate flux and rejection of $FeCl_3$ for MCM-48 composite membrane (applied pressure = 276 kPa; natural pH of the solution = 2.45)

3.4.5.3 Influence of pH

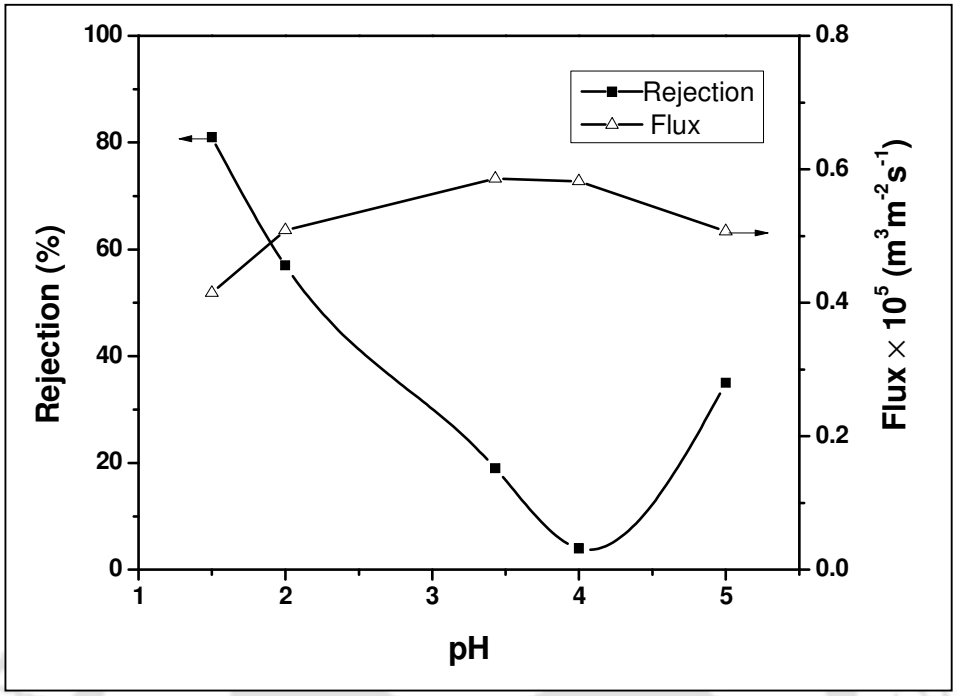

Fig. 3.19 Influence of pH on permeate flux and rejection of $AlCl_3$ for MCM-48 composite membranes (applied pressure = 276 kPa; concentration = 250 ppm)

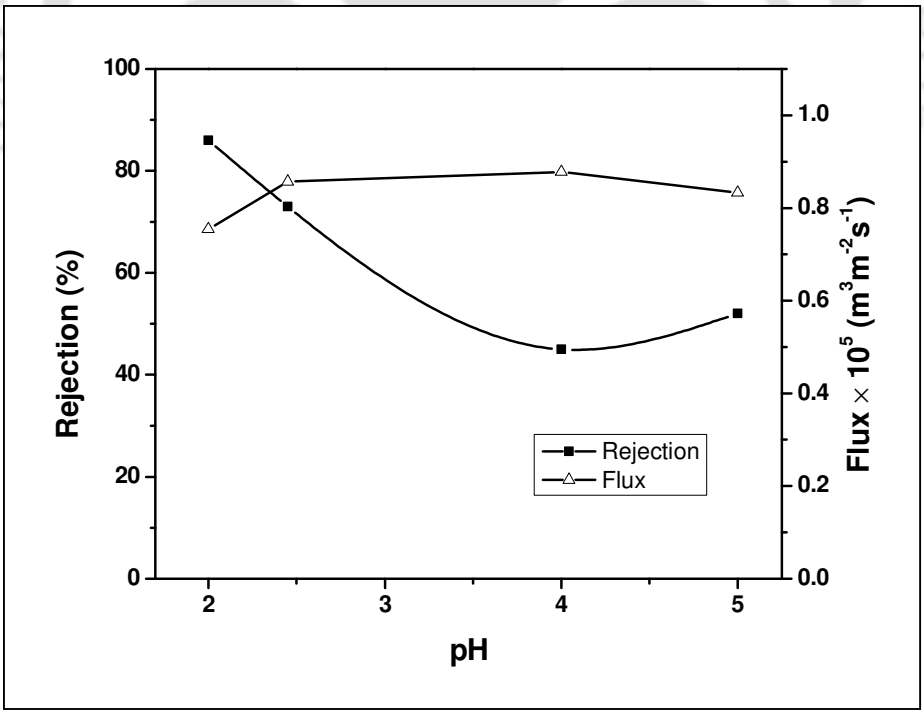

Fig. 3.20 Influence of pH on permeate flux and rejection of $FeCl_3$ for MCM-48 composite membranes (applied pressure = 276 kPa; concentration = 250 ppm)

The surface charge of the material is a valuable factor for determining the separation efficiency of the membrane and also it varies with the pH of the solution. To study the influence of pH on the rejection, the applied pressure and concentration of feed solution were fixed as 276 kPa, and 250 ppm, respectively. The pH of the solution was adjusted using NaOH and HCl. Figs. 3.19 and 3.20 demonstarte that for both salt separation, the maximum rejection (81% for $AlCl_3$ and 84% for $FeCl_3$) are achieved at lower pH. It is clearly noticed that the rejection of $AlCl_3$ and $FeCl_3$ is mainly influenced by the operating pH of the solution. Since the IEP of the membrane is 3.2, the membrane is positively charged at pH < 3.2 and negatively charged at pH > 3.2. When the pH increases from 1.5 to 4.0, the removal of salts ($AlCl_3$ and $FeCl_3$) is lowered due to decrease of magnitude of positive charge (surface potential) of the membrane. Thus, the repulsion between the positively charged membrane and cations (Al^{3+} and Fe^{3+}) decreases and accordingly, Al^{3+} and Fe^{3+} rejection declines. It is also noticed that the rejection enhances slightly with increasing the pH beyond IEP of the membrane. This is due to the fact that the membrane is negatively charged at pH > IEP and the surface charge (negative) of the membrane at pH 5.0 is higher than that of pH 4.0. Higher surface charge (negative) guides to increase the intensity of electrostatic repulsion between the Cl^- ions present in the solution and the membrane surface, thereby resulting in improved rejection while increasing pH from 4 to 5.0. This study clearly reveals that even though the pore size of the membrane is larger in comparison with the size of ions, the membrane displays good rejection of salts due to the electrostatic interaction between ions and the charged membrane surface and pores. As stated by several researchers (Pugazhenthi *et al*., 2005; Kishore *et al*., 2003; Shukla and Kumar 2004), in a charged UF membrane, the salt rejection is primarily due to the Donnan exclusion effect. The flux tends to enhance with an increase in pH of the solution due to decreased electro-viscous effect. Because the magnitude

of surface potential of the membrane decreases at a higher pH value closer to its corresponding IEP. Moreover, the permeate flux seems to decrease as the pH of the solution increases beyond the IEP of the membranes (Nazzal and Wiesner 1994).

3.4 Summary

MCM-48 ceramic composite membrane was synthesized on ceramic support by in situ hydrothermal treatment method and successfully characterized with various techniques such as XRD, FTIR, BET, FESEM, TGA, and porosity measurement. The porosity and pore size of the membrane are found to reduce with repeated cycle of coating of MCM-48. Solvent permeation test signifies that in addition to viscosity, the chemical nature of solvents also affects the permeation through the MCM-48 ceramic composite membrane. The composite membrane is examined for the separation of chromium and trivalent metal ions from aqueous solution at ambient temperature and the performance evaluation is checked by conducting filtration experiments individually as a function of applied pressure, feed concentration and pH of feed solution. The highest Cr (VI) rejection of 81% is found at an applied pressure of 207 kPa with the feed concentration of 1000 ppm. The maximum rejection of 81% and 84% is obtained for $AlCl_3$ and $FeCl_3$, respectively at an applied pressure of 276 kPa for a salt concentration of 250 ppm.

Chapter 4

Development, Characterization and Application of Faujasite Zeolite-Ceramic Composite Membrane for the Removal of Metal Ions from Aqueous Solution

Development, Characterization and Application of Faujasite Zeolite-Ceramic Composite Membrane for the Removal of Metal Ions from Aqueous Solution

As addressed in the previous chapters (2 and 3), the preparation of MCM-41 and MCM-48-ceramic composite membranes required longer synthesis time and calcination process was also involved. In order to minimize the fabrication cost further, Faujasite (FAU) zeolite is chosen to prepare a composite membrane due to shorter duration of hydrothermal reaction and no calcinations process is required. This chapter deals with the development of Faujasite (FAU) zeolite composite membrane via hydrothermal synthesis method on a circular shaped macroporous ceramic support. The FAU zeolite powder and the composite membrane were characterized by X-ray diffraction (XRD), Fourier transform infrared spectroscopy (FTIR), thermogravimetric analysis (TGA), zeta potential measurements, porosity, field emission scanning electron microscopy (FESEM), and pure water permeation test. The potential of the synthesized FAU zeolite composite membrane is studied for the separation of chromium, $AlCl_3$ and $FeCl_3$ from aqueous solution with different operating parameters such as applied pressure, initial feed concentration and pH of the feed solution in a dead-end batch filtration set-up.

4.1 Experimental

4.1.1 Materials

Alumium fine powder, hydrochloric acid and chromium (VI) oxide were purchased from Merck (I) Ltd, Mumbai. Ferric chloride, aluminium chloride (hexahydrate) and sodium hydroxide were procured from Loba Chemie (Laboratory Reagents & Fine Chemicals),

Mumbai, India. Fumed silica (Aerosil 200) was procured from CDH, Laboratory Reagents, Mumbai. Water used in this work was taken from the Millipore water system (ELIX-3).

4.1.2 Development of FAU zeolite composite membrane

The detailed protocol used for the fabrication of ceramic support was described in chapter 2 (section 2.1.2). FAU zeolite composite membrane was synthesized by hydrothermal method (Huang *et al.*, 2012). The hydrothermal reaction mixture was prepared by mixing of aluminate and silicate solution at room temperature. To prepare the aluminate solution, a requisite amount of sodium hydroxide was dissolved in Millipore water and subsequently aluminum powder was added in the solution. Then, a separate solution of silicate was made by adding an estimated quantity of fumed silica in Millipore water with mild heating. After that, both the aluminate and silicate solutions were mixed together and stirred overnight till to get homogenous solution. The molar ratio of the reaction mixture was $70Na_2O:Al_2O_3:20\ SiO_2:2000H_2O$. In order to synthesize FAU zeolite membrane, the prepared reaction mixture was poured into the Teflon coated stainless steel autoclave reactor along with a circular shaped ceramic support and the reactor was subjected to hydrothermal crystallization at 75 °C for 24 h. After completion of reaction, the membrane and synthesized FAU powder were removed from the reactor, washed with Millipore water and dried at 110 °C for 24 h. Fig. 4.1 illustrates the schematic diagram for the synthesis of FAU zeolite composite membrane.

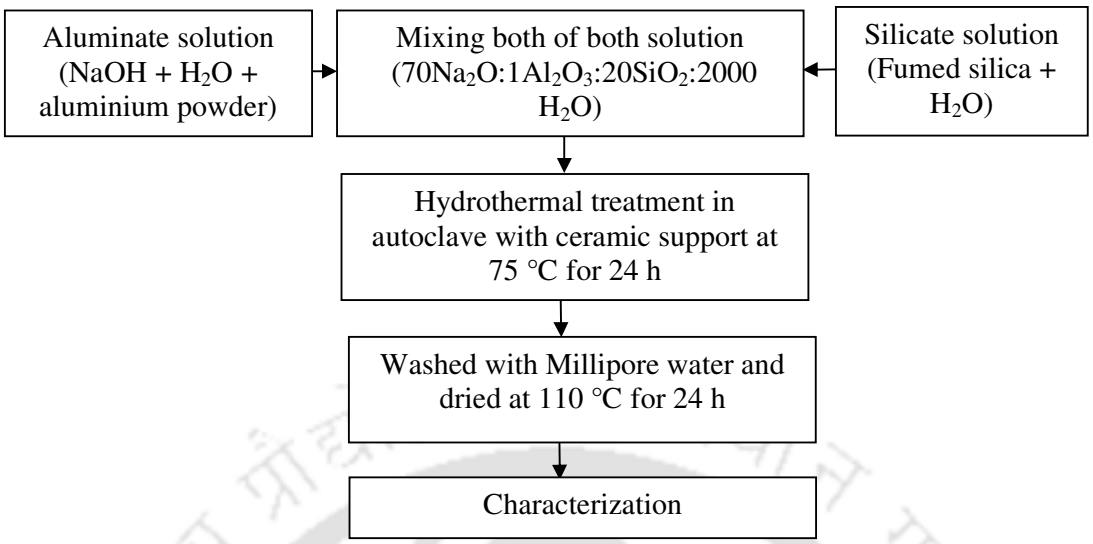

Fig. 4.1 Flow chart for synthesis of Faujasite zeolite-ceramic composite membrane

4.2 Characterization

The XRD patterns of FAU zeolite powder was analyzed on a Bruker A8 advance instrument. The patterns were taken in the 2θ range of 1-50° at a scanning speed of 0.02 °s^{-1}. The FTIR spectrum of FAU zeolite powder was measured in the range of 4000 to 450 cm^{-1} with KBr powder in a Shimadzu IR Affinity-1 model spectrometer. Thermogravimetric analysis (TGA) of FAU zeolite powder was conducted on a Netzsch TG 209F1 Libra with an air atmosphere. The sample was heated from 30 °C to 950 °C with heating rate of 10 °C/min. N_2 adsorption/desorption measurements were performed using a Quantachrome ® Asiqwin TM - Automated Gas Sorption (Version 3.0). Samples were out-gassed at 150 °C for 3 h prior to measurement. The specific surface areas were computed with the BET (Brunauer-Emmett-Teller) equation. The pore volumes and pore diameters were estimated by BJH method. Zeta potential measurement of FAU zeolite powder was carried out at various pH (2-9) using Beckman Coulter model Delsa Nano instruments. The surface images of the fabricated membrane and ceramic support were analyzed by FESEM using a Zeiss Sigma instrument.

Prior to analysis, the surface of samples was coated with gold to an approximate thickness of 150 A°. The porosity of ceramic support and the FAU zeolite composite membrane was measured using Archimedes' principle as described in chapter 2 (section 2.2).

4.2.1 Water flux measurement

In order to estimate the hydraulic permeability of the membrane, water permeation test was performed in a dead-end flow filtration set up made up of stainless steel 316 given in chapter 2 (section 2.2.1). Prior to assessment of water flux, the compaction of the membrane was carried out with Millipore water at high pressure to remove any loose particles present in the pores of the membrane. To measure the water flux at various applied pressures (69-483 kPa), the permeation cell was filled with 150 ml of pure water and required pressure was applied. First 50 ml of water passed across the membrane was removed and the time needed to get next 50 ml of water was noted down to compute water flux of the membrane using equations given in chapter 2 (section 2.2.1).

4.2.2 Filtration experiments for chromium and trivalent metal ions

The separation capability of the fabricated FAU zeolite composite membrane was investigated by conducting filtration experiments for chromium and trivalent metal ions removal. All the tests were performed at room temperature (25 °C). Chromium solution was made with Millipore water and its concentration was measured by means of conductivity meter (Eutech Instruments, Model: CON 2700). For each run of the experiment, the filtration cell was filled with 100 ml of chromium solution and then first 10 ml of permeate passed through the membrane was discarded. The time needed for the collection of second 10 ml permeate through the membrane was noted to measure the permeate flux and the concentration of permeate was determined to estimate the rejection of chromium. After every

experiment, the membrane was systematically cleaned and flushed with Millipore water at higher pressure to get back the original water flux of the membrane. The rejection of chromium solution was examined as a function of operating parameters, such as applied pressure, initial feed concentration and pH of the feed solution. To investigate the influence of operating pressure on the permeate flux and rejection, filtration experiments were carried out at various applied pressures for a fixed concentration of chromium solution (1000 ppm) with natural pH of the solution (~ 2.35). In order to inspect the effect of concentration, filtration was conducted at different concentrations (250-3000 ppm) with an applied pressure of 207 kPa and natural pH of the solution. The variation of pH on the performance of the membrane was studied in the range of 2 to 9 with a fixed feed concentration (1000 ppm) at an apllied pressure of 207 kPa. The pH of the chromium solution was adjusted by the addition of HCl or NaOH solutions.

Similary, the separation of trivalent metal salts ($FeCl_3$ and $AlCl_3$) were carried out to assess the potential of FAU zeolite membrane. The permeate flux and rejection of both $AlCl_3$ and $FeCl_3$ solutions were studied as a function of working parameters such as applied pressure, concentration and pH of the feed solution. The variation of operating pressure was conducted at five different pressures for fixed concentration (3000 ppm) with the natural pH. The effect of concentration on permeates flux and rejection was conducted at a fixed applied pressure (276 kPa) by varying concentration (250-3000 ppm) with natural pH of the solution. The influence of pH was studied in the range of 2-5 with a fixed feed concentration (3000 ppm) and an applied pressure of 276 kPa. The pH of the salt solutions was adjusted by the addition of HCl and NaOH.

The percentage rejection (R%) of chromium and trivalent metal ions was computed from the following relation:

$$R(\%) = \left[1 - \frac{C_p}{C_f}\right] \times 100 \quad (4.1)$$

where, C_p and C_f denote the concentration of chromium or trivalent metal ions in the permeate and feed solution, respectively. The concentration of trivalent salts was also measured using conductivitymeter.

4.3 Results and discussion

4.3.1 Characterization of FAU zeolite powder

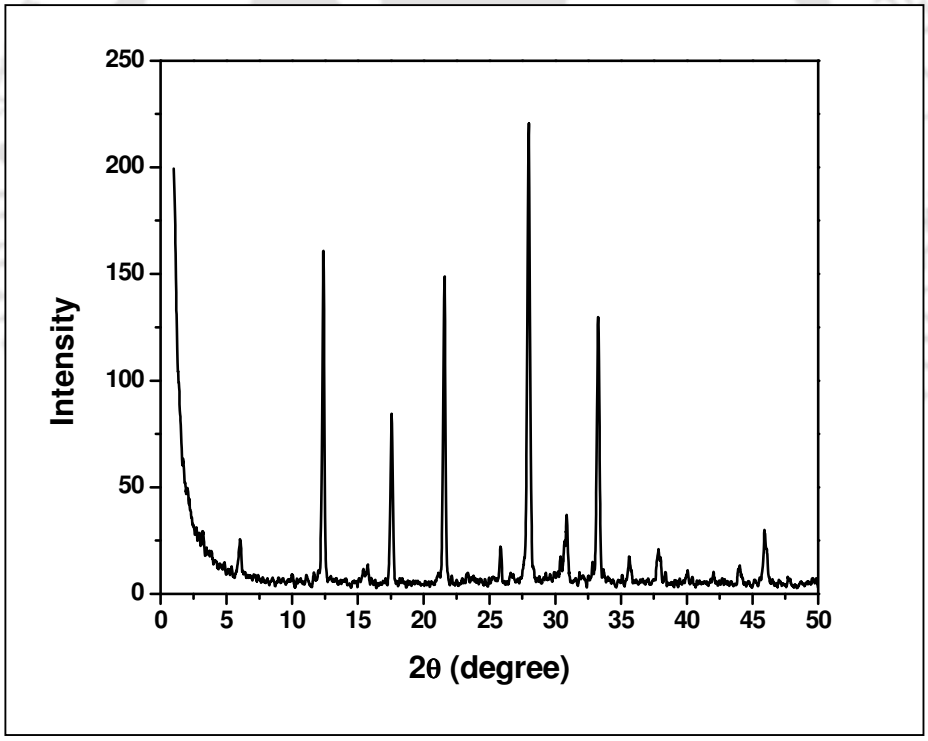

Fig. 4.2 XRD pattern of FAU zeolite powder

Figure 4.2 illustrates the XRD profile of the synthesized FAU zeolite powder, which closely matches with the standard XRD pattern of FAU zeolite reported elsewhere (Treacy and Higgins 2007). The pattern observed at 2θ value of 12.4 demonstrates the formation of a high

degree of crystallinity and the production of FAU zeolite. A similar observation was also reported by Haung *et al.,* (2012) for FAU zeolite, which was synthesized by seeding free method. Fig. 4.3 displays the FTIR spectrum of FAU zeolite powder. A broad sharp intense band appeared at 3500 cm^{-1} is due to OH stretching vibration of hydroxyl groups of alumina content (Su *et al*., 2010). The peak observed at 1610 cm^{-1} is owing to the H-O-H bending of water. The asymmetric stretching vibration of Si-O-Si is noticed at 1078 cm^{-1}. The band appeared at 970 cm^{-1} is attributed to O-H deformation linked to $2Al^{3-}$ (Huang *et al*., 2012).

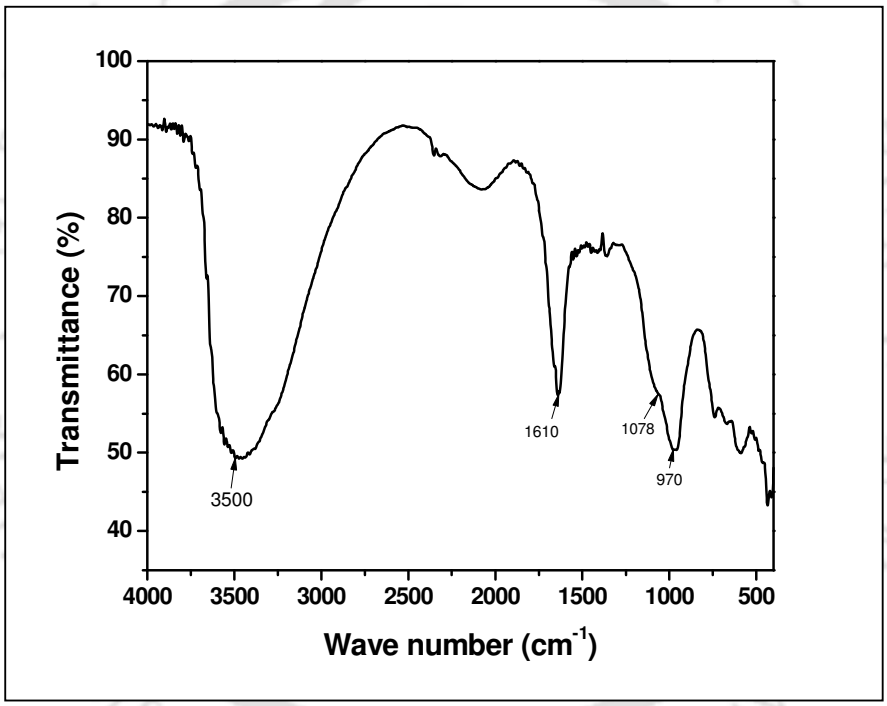

Fig. 4.3 FTIR spectrum of FAU zeolite powder

The thermogravimetric (TGA) analysis of FAU zeolite powder is depicted in Fig. 4.4. It can be observed from TGA profile of FAU zeolite powder that majority of weight loss occurrs at the temperature ranging between 84 to 330 ^{o}C and total weight loss is found to be 16%. The weight loss in the first region (50-150 °C) corresponds to the removal of physically adhered water molecule on external surface of the materials. The last stage of weight loss at 150 and

330 ^{o}C is due to the liberation of crystal water from the sample and no further significant weight loss is noticed after 330 °C. Fig. 4.5 displays the variation of zeta potential of FAU powder at various pH. The surface charge of the membrane will be positive or negative, depending upon the pH of the contact solution. In order to find out the surface charge of the FAU zeolite composite membrane, the zeta potential of FAU zeolite powder particles in solution is measured by electrostatic light scattering method. The surface potential of FAU zeolite powder is altered by the addition of NaOH to make higher pH and HCl solution is added to make lower pH. The surface charge of FAU zeolite becomes positive due to larger amount of H^+ ions at lower pH and at higher pH, negative hydroxyl (OH^-) ions become more. Therefore, the zeta potential value is 4 mV at pH 2 while it is approximately -45 mV at pH 12. Hence, electrostatic interactions play a major role in the surface activity of FAU zeolite. The iso-electric point (IEP) of FAU zeolite powder is obtained to be 3.8. When pH is < IEP, the zeolite membrane is positively charged and if pH > IEP, it is negatively charged. The N_2 adsorption/desorption isotherm and BJH pore size distribution of FAU powder are illustrated in Fig. 4.6 (a, b). The isotherm recognized for the FAU powder as a typical type II adsorption/desorption isotherm and exhibits capillary condensation step as depicted in Fig. 4.6(a). The pore size distribution is determined from desorption isotherm by the BJH method as shown in Fig. 4.6 (b). The average pore size of the FAU powder is 3.57 nm as computed by the BJH approach from desorption curves. The BET surface area of FAU-type zeolite powder is 9.843 m^2/g.

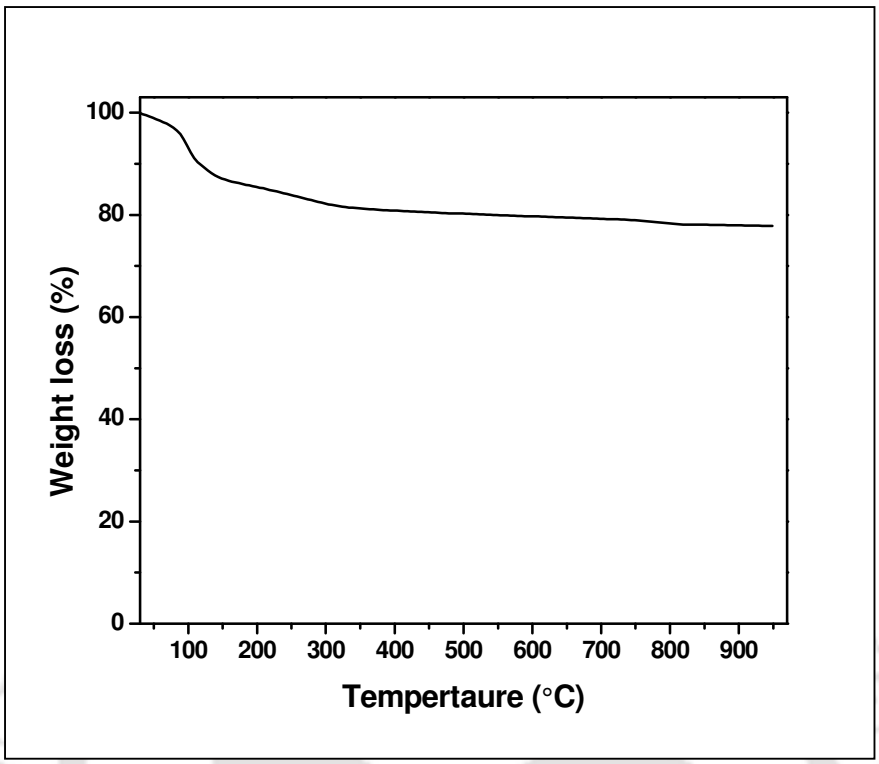

Fig. 4.4 TGA analysis of FAU zeolite powder with air atmosphere

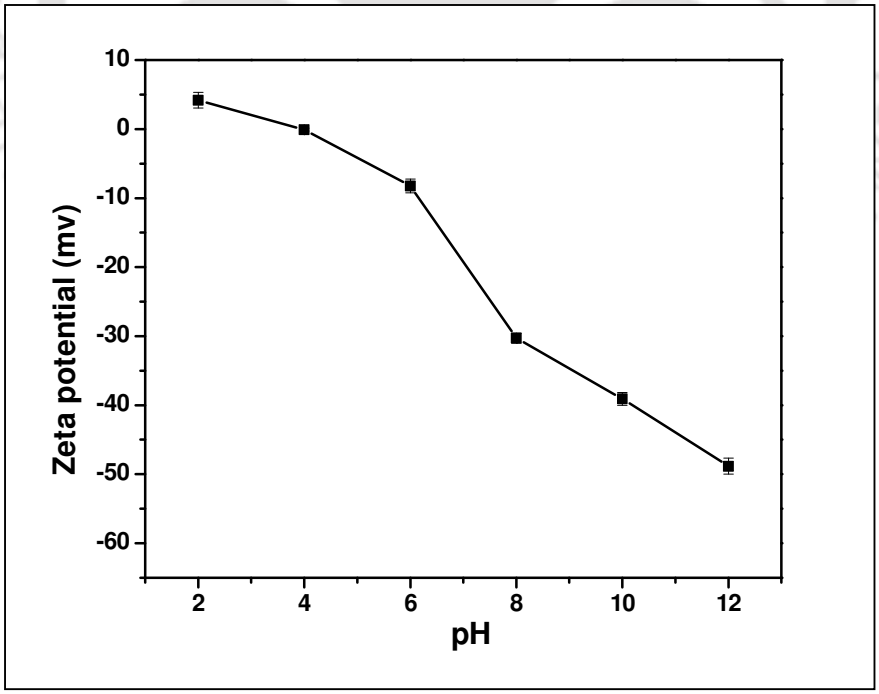

Fig. 4.5 Zeta potential measurement of FAU zeolite powder

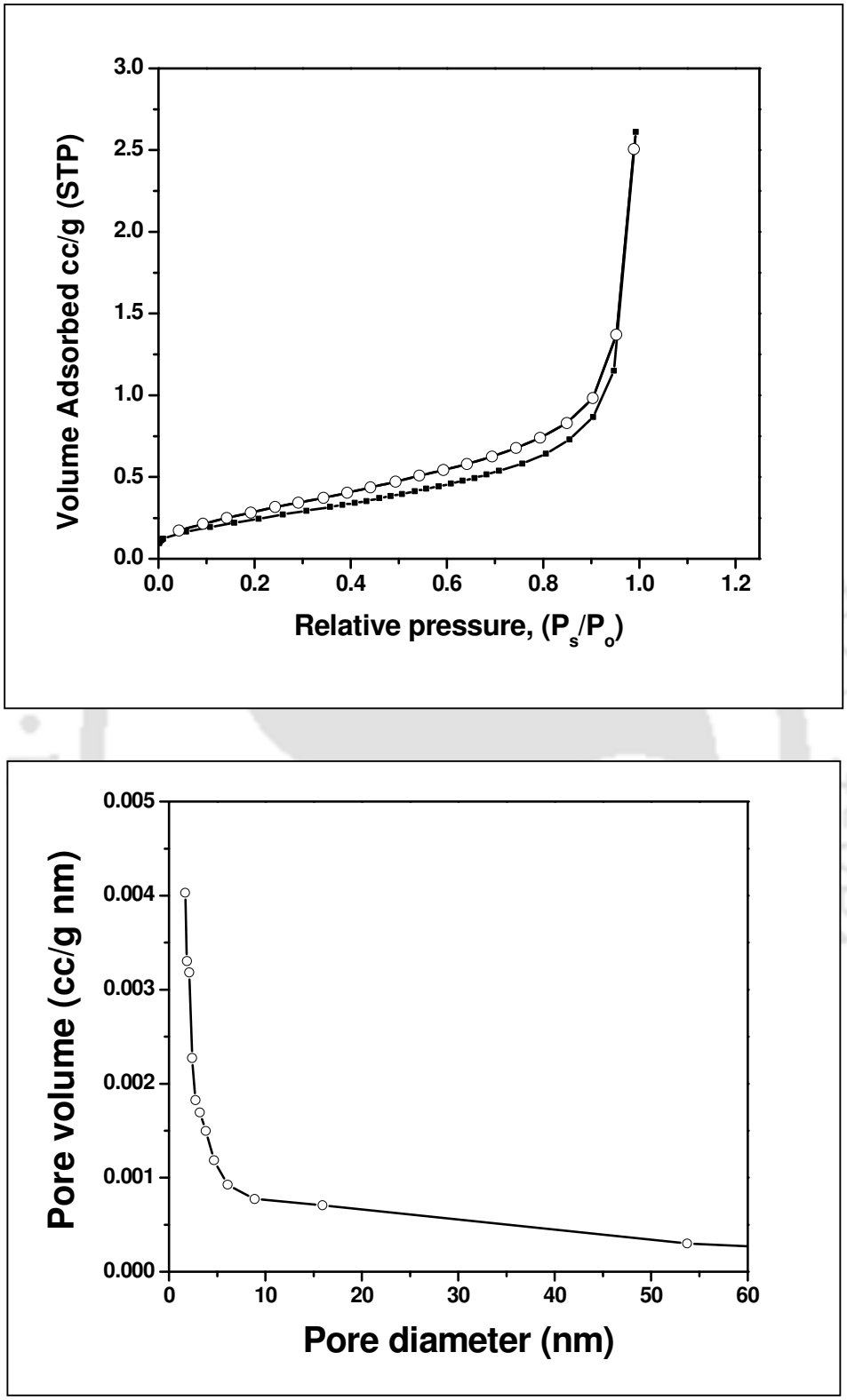

Fig. 4.6. (a) N_2 adsorption/desorption isotherm, and (b) BJH pore size distribution of FAU zeolite powder

4.3.2 Characterization of FAU zeolite membrane

The porosity of the ceramic support and FAU zeolite composite membrane is found to be 47% and 33%, respectively. With the deposition of FAU zeolite on the support, the porosity and pore size of the composite membrane are reduced. The FESEM imaging technique is employed to check the formation of FAU zeolite on the ceramic support. The surface images of support and FAU zeolite composite membranes are shown in Fig. 4.7. It is apparent that after hydrothermal treatment, the surface of the ceramic support is coated with FAU zeolite. The surface morphology resembles that there is no crack on the surface of the membrane. The cubical FAU zeolite is distinctly visible in higher magnification images.

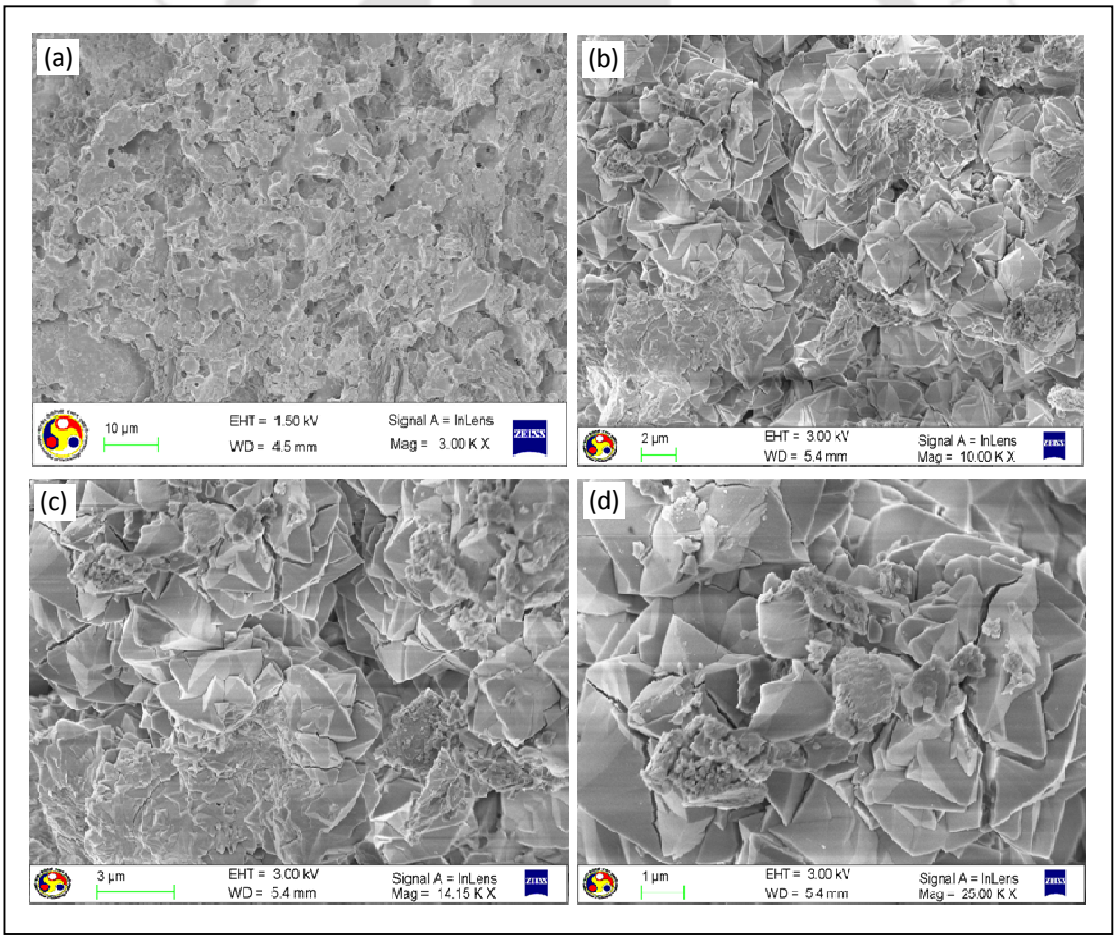

Fig. 4.7 FESEM images of support (a) and FAU membrane at various magnification (b-d).

The pure water permeation experiments on the ceramic support and FAU zeolite composite membranes were carried out at various applied pressures. With these data, the average pore size and hydraulic permeability (L_h) of the membranes are determined using the equation given in Chapter 2 (Equation 2.2.1). It is clearly seen from Fig. 4.8 that permeate flux enhances linearly with increasing applied pressure. The pure water permeability of zeolite composite membrane (6.09×10^{-8} $m^3m^{-2}s^{-1}$ kPa) is much lesser than that of the ceramic support demonstrating the lower pore size of the zeolite membrane as compared to support. The pore size of ceramic support and FAU composite membrane is found to be 1.0 and 0.153 µm, respectively.

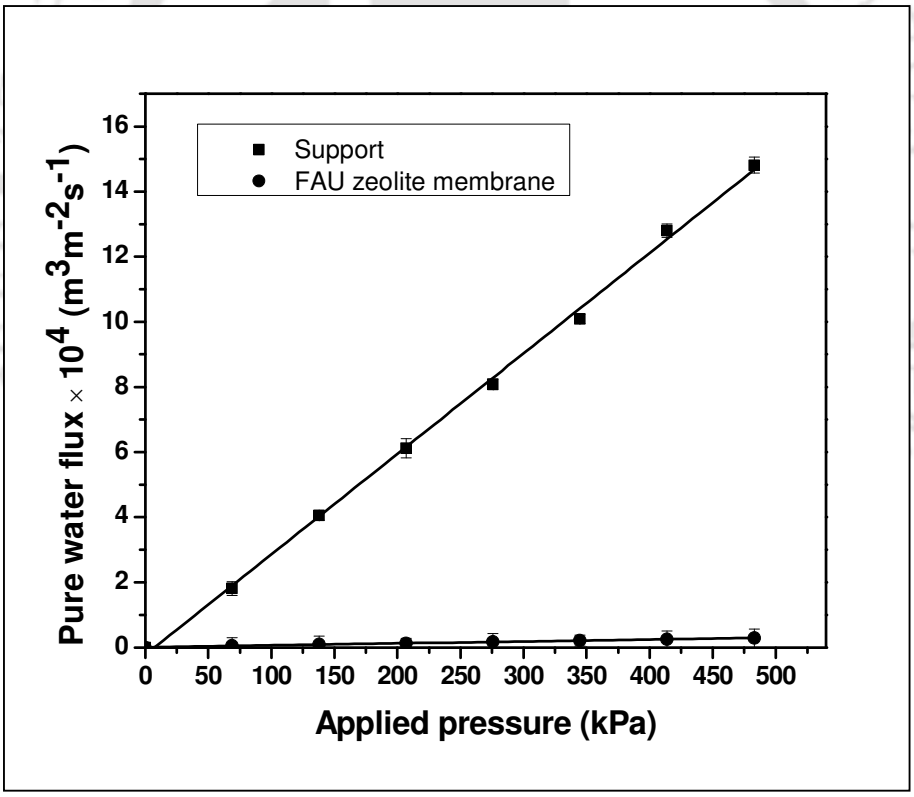

Fig. 4.8 Pure water flux for the support and FAU zeolite composite membrane

4.3.3 Separation of Cr (VI)

4.3.3.1 Influence of applied pressure

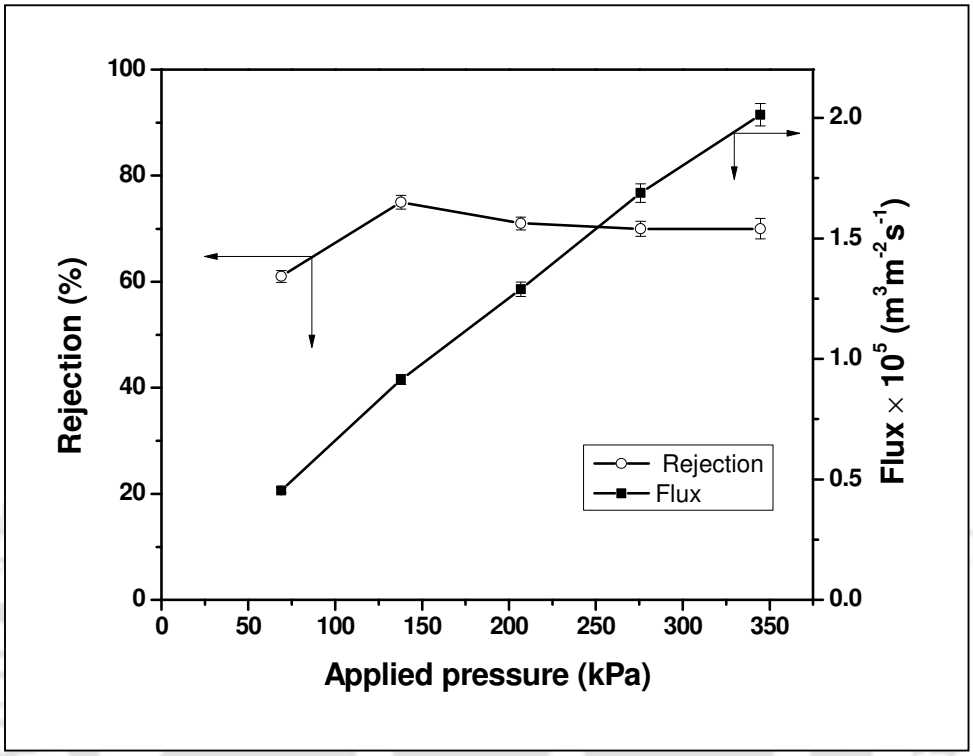

Fig. 4.9 Influence of applied pressure on the permeate flux and rejection (%) for FAU zeolite composite membrane (concentration = 1000 ppm, natural pH ~2.35)

To study the influence of operating pressure, concentration and pH of the chromium solution are kept constant as 1000 ppm and ~2.35, respectively. The variation of operating pressure on the permeate flux and rejection of Cr (VI) was investigated in the applied pressure range of 69-345 kPa and the obtained results are reported in Fig. 4.9. It is observed that when the applied pressure increases, the permeate flux also enhances linearly for the FAU composite membrane. With increasing applied pressure, the observed rejection augments up to the certain level (138 kPa) and then declines slightly. The possible reason is that more amount of solute particle accumulates on the membrane surface when the applied pressure increases (Hafez and Maharawy 2004). Besides applied pressure and solute concentration, other

parameter also play a role in determining the rejection of Cr (VI). Those are charge density present in the membrane and the interaction of membrane charge sites with ionic solutes. After each experiment, FAU zeolite composite membrane is washed and flushed with Millipore water at a higher pressure till the initial water flux is obtained.

4.3.3.2 Influence of feed concentration

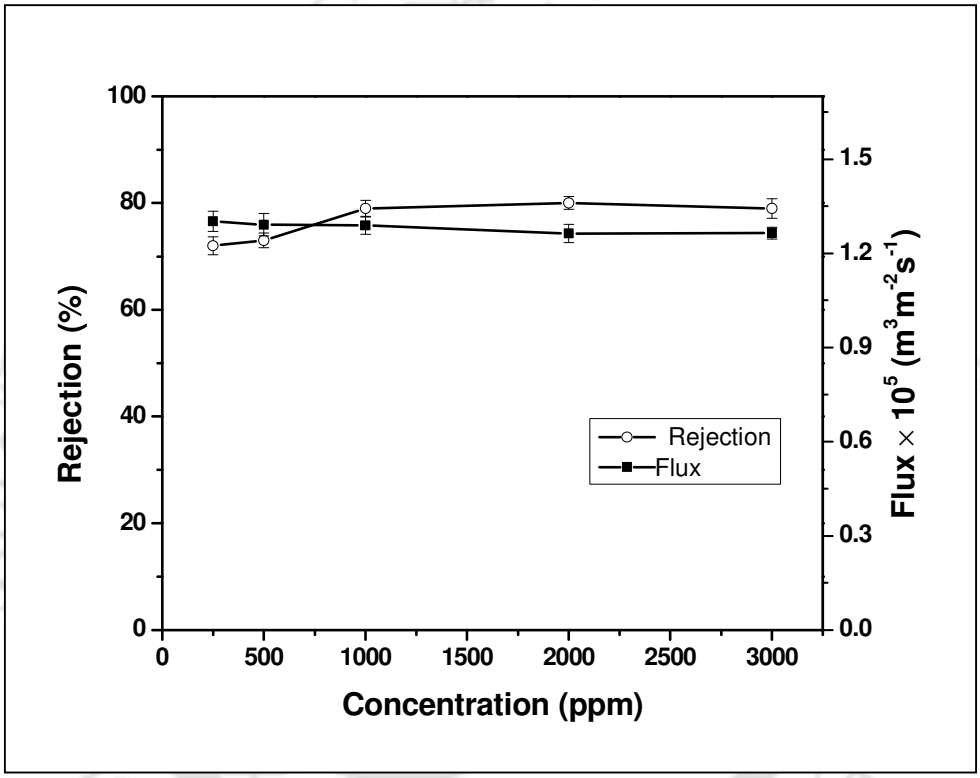

Fig. 4.10 Influence of feed concentration on the permeate flux and rejection (%) for FAU zeolite composite membrane (applied pressure = 207 kPa, natural pH ~2.35)

The variations of feed concentration on permeate flux and rejection by the zeolite membrane is displayed in Fig. 4.10. Experiments were conducted at a fixed applied pressure of 207 kPa, and various feed concentrations (250-3000 ppm) with natural pH (2.35) of the solution. Fig. 4.10 clearly indicates that the permeate flux decreases slightly with an increase in the feed concentration due to the enhanced metal ion concentration that creates an additional

resistance to the flow. The rejection of Cr (VI) increases with an increase in the feed concentration from 250 to 1000 ppm and it remains almost constant after 2000 ppm.

4.3.3.3 Influence of pH on Cr (VI)

The FAU zeolite composite membrane alters its surface charge depending upon the working pH of the solution as evidenced in Fig. 4.5. Therefore, the influence of pH on the separation effeciency of the membrane was investigated from the pH of 2 to 9 at a fixed applied pressure of 207 kPa and a feed concentration of 1000 ppm. Fig. 4.11 demonstrates the variation of observed rejection of Cr (VI) with pH. It signifies that the Cr (VI) rejection is mainly dependent on the operating pH and optimal removal (83%) is achieved at pH = 2. It is to be mentioned here that the isoelectric point (IEP) of FAU zeolite composite membrane is 3.8 (see Fig. 4.5). It means that the membrane is positively charged at pH < 3.8, and negatively charged at pH > 3.8. When the charged membrane is in contact with the Cr (VI) solution, the concentration of ions having the same charge as the membrane will be lesser at closer to the surface of membrane. On the other hand, the other ions containing the opposite charge have a higher concentration in the membrane than in the solution. A potential difference is created due to this concentration variation at the interface with the membrane and the solution in order to keep the electrochemical equilibrium between the solution and the membrane. With this potential, the membrane repels the ions with same charge as the membrane (Chung *et al.*, 2005). When the pH augments from 2 to 3.8 with the addition of NaOH solution, the surface charge of the membrane alters and the magnitude of the membrane charge (positive) diminishes as the IEP of FAU zeolite composite membrane is 3.8. Therefore, a decrease in the repulsion between positively charged membrane and positive charged species (H_3O^+) occurred and consequently, the rejection declines from 83%. Since cation and anion cannot act separately, hence $HCrO_4^-$ is also rejected for maintaining electroneutrality. On increasing pH from 3.8 to 5, the rejection increases to 2% as the repulsion or attraction phenomena play

a role with the ionic species present in the charged membrane and the solution. At higher pH (pH > 3.8), OH^- ions accumulate owing to the addition of NaOH and the membrane gets negative charge with contact in feed. Moreover, in comparison with $HCrO^-_4$, the concentration of CrO_4^{2-} increases with an increase in the pH. The magnitude of membrane charge (negative) enhanced from –15.66 mV to –34.88 mV with increasing pH from 5 to 9, which is evidenced in Fig. 4.5. This leads to improve the electrostatic repulsion between ions present in the membrane surface and solutions. Therefore, the rejection augments with increasing the pH from 3.8 to 9 as depicted in the Fig. 4.11.

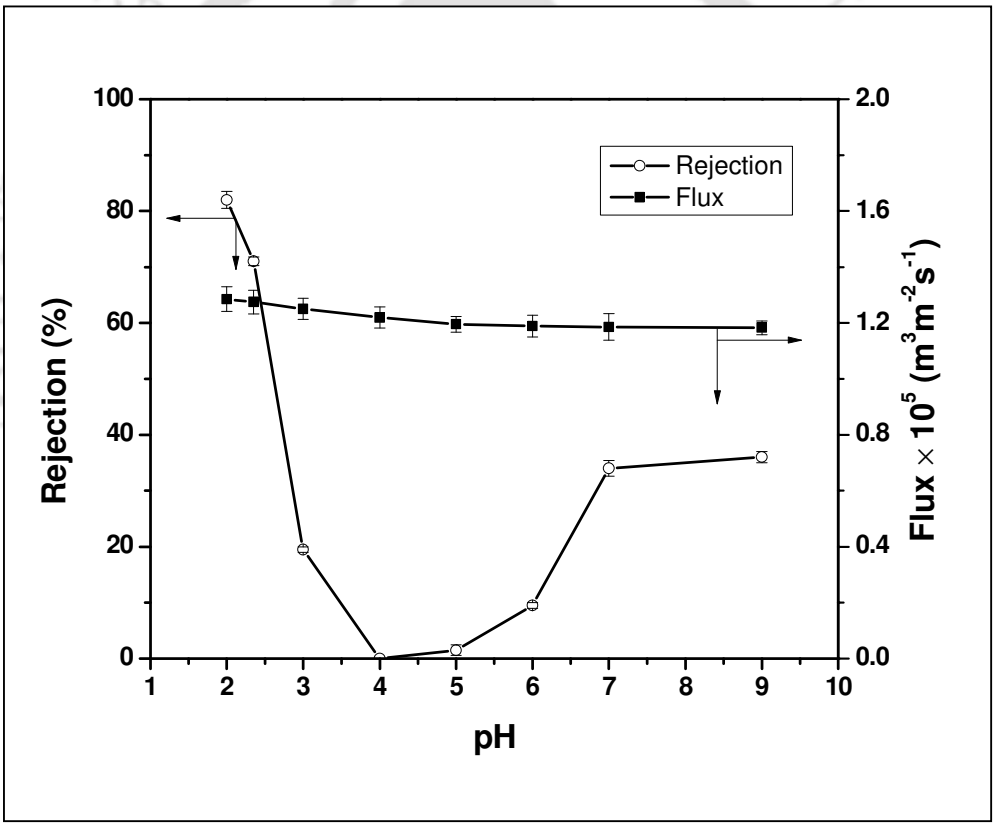

Fig. 4.11 Influence of pH on the permeate flux and rejection (%) for FAU zeolite composite membrane

The observed rejection reported (83%) in this work at the concentration of 1000 ppm and the applied pressure of 207 kPa can be comparable with other membranes reported in literature

(Table 4.1). Arthanareeswaran *et al.*, (2007) have obtained 82% rejection of chromium with solute flux of 3.3×10^{-7} ms^{-1} using cellulose acetate ultrafiltration membrane for the feed concentraton of 1000 ppm, and the applied pressure of 345 kPa. In an earlier work (Pugazhenthi *et al.*, 2005), carbon membrane displayed 96% rejection with solute flux of 1.464×10^{-8} ms^{-1} for the applied pressure of 483 kPa and the feed concentration of 1000 ppm. Comparing to the result reported in literature, the solute flux is 2-4 order higher in this work and the removal percentage is promising or even better, indicating that the prepared FAU zeolite composite membrane is capable for the separation Cr (VI) from aqueous solution.

Table 4.1 Comparison of Cr (VI) rejection with other membranes

Membrane material	Pore size (nm)	Feed conc. (ppm)	Rejection (%)	Solute flux (ms^{-1})	Applied pressure (kPa)	Reference
PMMA-EDGM membrane	1.35	1000	68	5.96×10^{-10}	275	Neelakandan *et al.*, 2003
Cellulose acetate	-	1000	82	3.3×10^{-7}	345	Arthanareeswaran *et al.*, 2007
Clay carbon membrane	2.0	1000	96	1.464×10^{-8}	483	Pugazhenthi *et al.*, 2005
Ceramic membrane	200	1000	99	3.4194×10^{-8}	172	Sondhi *et al.*, 2000
FAU zeolite composite membrane	**153**	**1000**	**83**	**1.29×10^{-5}**	**207**	**Present work**

4.3.4 Separation of trivalent metal ions

4.3.4.1 Variation of applied pressure

The variation of applied pressure on the rejection and permeate flux of $FeCl_3$ and $AlCl_3$ as examined for a fixed concentration of feed solution (3000 ppm) at natural pH and the results are shown in Fig. 4.12. It can be deduced that the presence of Fe^{3+} and Al^{3+} ions offer an extra

resistance to permeate due to which, the solution permeability of $FeCl_3$ and $AlCl_3$ are observed to be lesser than that of pure water. From the figure, it is clearly noticed that the permeate flux increases with an increase in the applied pressure due to the solute flux across the membrane, i.e., sum of convective (applied pressure gradient across the membrane) and diffusive (concentration difference) flux. At lower applied pressure, diffusion contributes to the flux, whereas convection controlled on the whole process at elevated applied pressure. In addition to this, the permeate flux of the salt solution depends on the electrostatic interaction between the electrolyte and surface of the membrane providing an extra resistance to the flow of the membrane. It is observed that the rejection exhibits a decreasing trend with increasing applied pressure due to severe concentration polarization caused by the enhanced accumulation of solute particles on the membrane surface at elevated pressure. As a result, the permeate concentration increases owing to enhancement in convective flux. For both salts, the declined rejection with increasing in the applied pressure was also reported in the literature (Shukla and Kumar 2005). In addition to the applied pressure, few other parameters, such as charge density of the membrane and the interaction of membrane charge sites with ionic solute, also play a key role in altering the rejection of Fe^{3+} and Al^{3+} ions. Both salts show higher rejection at an operating pressure of 207 kPa and then the rejection decreases as the applied pressure goes on increasing. In comparision with $AlCl_3$, rejection of $FeCl_3$ higher, which may be due to the fact that $AlCl_3$ accumulates more quantity in the boundary layer of the upstream side of the membrane (Shukla and Kumar 2005). Moreover, this study is conducted at natural pH of the feed solutions. It is worth to mention that the natural pH of $FeCl_3$ is 2.45, whereas it is 3.43 for $AlCl_3$. Hence, $FeCl_3$ shows higher rejection.

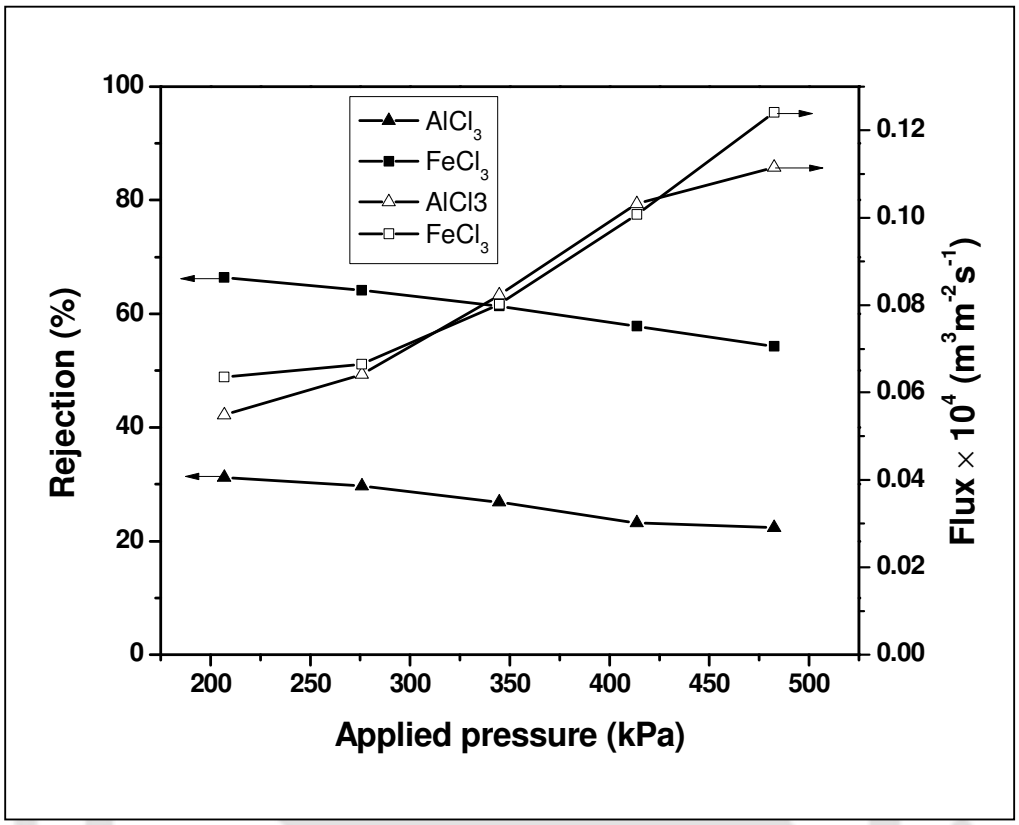

Fig. 4.12 Variation of applied pressure on the permeate flux (□) and rejection (■) for $FeCl_3$ and $AlCl_3$ (concentration = 3000 ppm)

4.3.4.2 Variation of feed concentration

The influence of feed concentration on the rejection and permeate flux is illustrated in Fig. 4.13. For both salts solution, the permeate flux displays decreasing trends with increasing salt concentration. This is due to the partial plugging of pores of the membrane and concentration polarization. At a lower feed concentration (250 ppm), higher rejection is observed for both the salts. The membrane charge will be shielded to a larger degree at higher salt concentration. Due to this, effective charge is less and consequently decreasing trends for rejection is noticed.

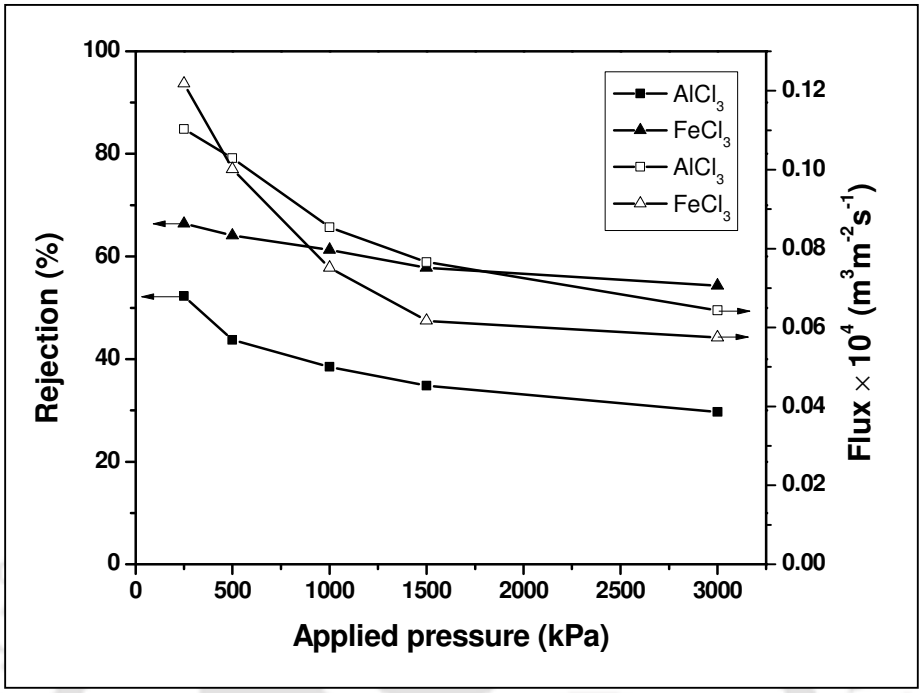

Fig. 4.13 Variation of feed concentration on the permeate flux (□) and rejection (■) for $FeCl_3$ and $AlCl_3$ (applied pressure = 276 kPa)

4.3.4.3 Variation of pH

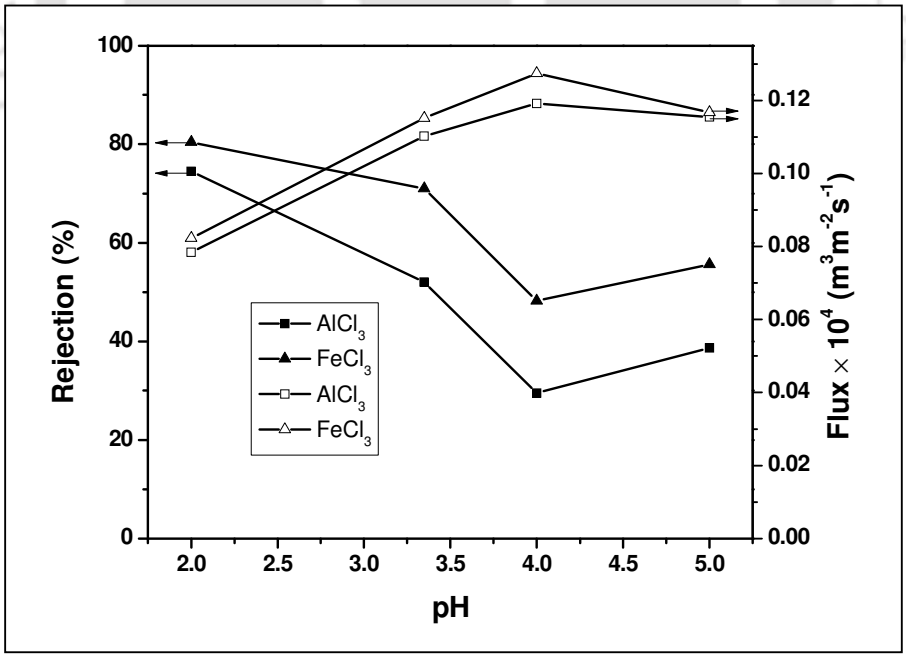

Fig. 4.14 Variation of pH on the permeate flux (□) and rejection (■) for $FeCl_3$ and $AlCl_3$ (concentration = 250 ppm, applied pressure = 276 kPa)

The surface charge of the material is a significant parameter incorporating the separation effectiveness of the membrane and it is dependent on the pH of the solution, especially when removing ionic species. Fig. 4.14 demonstrates that the observed rejection of $FeCl_3$ and $AlCl_3$ strongly depends on operating pH of the solution and a maximum rejection of 81%, and 75% was obtained at pH 2 for $FeCl_3$ and $AlCl_3$, respectively. It is important to mention that the isoelectric point (IEP) of FAU zeolite is 3.8 and hence, the membrane is positively charged at pH < 3.8 and negatively charged at pH > 3.8. When the pH of the solution raised from 2 to 4, the experimental rejection of $FeCl_3$ and $AlCl_3$ displays a decreasing trend due to decrease in the electro-potential of the membrane (Majhi *et al*., 2009). When the electrolyte solution is in contact with the charged membrane, the concentration of co-ions close to the membrane surface is lesser than that in the solution. Moreover, counter ions which is opposite in sign will have a larger concentration in the membrane than in the solution. Hence, the membrane and the solution will have concentration difference at the interface. To maintain electrochemical equilibrium, a potential variation is generated between the membrane and the solution. By this potential, known as Donnan potential, co-ions are repelled by the membrane, when pH < IEP as well as pH > IEP (Chung *et al*., 2005). Therefore, the repulsion between the charged membrane and metal ions (Fe^{3+} or Al^{3+}) decreases when the pH increases from 2 to 4 and accordingly rejection of Fe^{3+} and Al^{3+} declines. Subsequently, Cl^- ions are also rejected for maintaining electroneutrality since the cation and anion cannot act separately. Furthermore, it is noticed that the rejection enhances slightly when the pH increases beyond IEP of the membrane. This is due to the fact, that membrane is negatively charged at pH higher than IEP and the surface charge (negative) of the membrane at pH 5.0 is higher than that of pH 4.0. The higher surface charge (negative) guides to increase the intensity of the electrostatic repulsion between the Cl^- ions present in the solution and the membrane surface, resulting in improved rejection while increasing pH from 4 to 5. The

highest rejection observed in this finding at 276 kPa with the salt concentration of 250 ppm is 81% and 75% for $FeCl_3$ and $AlCl_3$, respectively.

4.4 Summary

The potential of FAU zeolite composite membrane was successfully demonstrated by evaluating Cr (VI) removal. The prepared composite membrane via hydrothermal synthesis technique was effectively characterized by XRD, FTIR, TGA, FESEM and porosity measurement. The pore size and porosity of the membrane decrease with the deposition of FAU zeolite on the support from 1.0 to 0.153 μm, and 47% to 33%, respectively. The end results illustrate that FAU zeolite composite membrane could be used for Cr (VI) removal from aqueous solution and a maximum rejection (83%) is obtained at an applied pressure of 207 kPa for the feed concentration of 1000 ppm. The outcome of this study indicates promising advantage of Faujasite (FAU) zeolite composite membrane for the separation of Cr (VI). Further, the rejection potential of the composite membrane was also evaluated by separating $FeCl_3$ and $AlCl_3$ salt solution as a function of applied pressure, salt concentration and pH. An optimum rejection is found to be 81%, and 75% for $FeCl_3$, and $AlCl_3$ respectively, at an applied pressure of 276 kPa for the salt concentration of 250 ppm.

Chapter 5

Cross Flow Ultrafiltration of Metal Ions from Aqueous Solution using MCM-41, MCM-48 and Faujasite Zeolite-Ceramic Composite Membrane

Cross Flow Ultrafiltration of Metal Ions from Aqueous Solution using MCM-41, MCM-48 and Faujasite Zeolite-Ceramic Composite Membrane

This chapter describes the removal of chromium, $AlCl_3$ and $FeCl_3$ from aqueous solution in cross flow mode using MCM-41, MCM-48 and FAU zeolite composite membranes prepared on circular shaped porous ceramic support. Ceramic support was manufactured using locally available clay materials via a facile uni-axial compaction method followed by sintering process. A hydrothermal technique was employed for the deposition of zeolites on the ceramic support. Cross flow ultrafiltration experiments of chromium were conducted at five different applied pressures (69 to 345 kPa) and three cross flow rates (1.11×10^{-7} - 2.22×10^{-7} m^3s^{-1}). The filtration studies infer that the performance of all the zeolite composite membranes is optimum at the maximum applied pressure (345 kPa) and the highest rejection is obtained with the lowest cross flow rate (1.11×10^{-7} m^3s^{-1}). For the separation of trivalent metal ions, the effect of applied pressure was studied in the range of 69 to 345 kPa at a fixed flow rate of 1.11×10^{-7} m^3s^{-1} with the three zeolite membranes.

5.1 Experimental

The main target of this work is to conduct the filtration experiment in cross flow mode for the removal of chromium, $AlCl_3$ and $FeCl_3$ from aqueous solution.

5.1.1 Materials

Tetraethyl orthosilicate (TEOS), triethanolamine (TEA), aluminum fine powder, hydrochloric acid and Cr (VI) oxide were bought from Merck (I) Ltd, Mumbai. Cetyltrimethyl ammonium

bromide (CTAB) was obtained from SRL (I) Ltd, Mumbai. Fumed silica (Aerosil 200) was procured from CDH, Laboratory Reagents, Mumbai. Ferric chloride, aluminum chloride (hexahydrate), and sodium hydroxide were bought from Loba Chemie (Laboratory Reagents & Fine Chemicals) Mumbai, India. All chemicals and reagents were utilized directly without further purification. Water was taken from Millipore water system (ELIX-3).

5.1.2 Fabrication of zeolite membranes

The technique involved for the manufacturing of circular shaped porous low cost ceramic support was elaborated in chapter 2 (section 2.1.2). The procedure for the fabrication of MCM-41, MCM-48 and FAU zeolite composite membranes were also explained details in chapter 2 (section 2.1.3), 3 (section 3.1.2) and 4 (section 4.1.2), respectively. For the synthesized of MCM-41 composite membrane, the gel mixture was prepared with the molar composition of 1TEOS:0.1CTAB:0.3NaOH:60H_2O and crystallized under the static hydrothermal condition at 110 °C with placing a ceramic support in a Teflon container autoclave reactor for 96 h. The MCM-48 ceramic composite membrane was fabricated with a gel composition of 1TEOS:0.25Na_2O:0.65CTAB:0.62H_2O. This suspension along with ceramic support was kept in autoclave reactor and subjected to hydrothermal treatment at 110 °C for 72 h. After completion of the reaction, the membrane and zeolite powders were recovered, washed and dried at 100 °C for 24 h. Finally, zeolite powders and membranes were calcined at 550 °C for 5 h for MCM-41 and 6 h for MCM-48 at the heating rate of 1 °C/min. To enhance the quantity deposition of MCM-41 and MCM-48 on ceramic support, the membrane was synthesized with repeated cycles (three times) of coating using the same molar composition of gel mixture followed by crystallization reactions and calcination. The weight increment in mass of the zeolite membrane in comparison with the dry weight of support was estimated following after cycle of synthesis. After third cycle of coating, no

significant weight increment was observed for both MCM-41 and MCM-48 membranes. In order to develop FAU zeolite-ceramic composite membrane, the reaction mixture was prepared with a molar composition of $70Na_2O:Al_2O_3:20SiO_2:2000H_2O$. The above prepared solution along with the ceramic support was subjected to hydrothermal treatment in a autoclave at 75 °C for 24 h. After hydrothermal treatment, the membrane and FAU powder were taken out from the autoclave reactor and dried for 24 h at 110 °C. All the composite membranes (MCM-41, MCM-48 and FAU) were applied for the assessment of liquid phase separation efficiency.

5.2 Characterization

The various characterization techniques involved for MCM-41, MCM-48 and FAU zeolite powder and composite membranes were presented in chapters 2, 3 and 4, respectively. The surface wettability of ceramic support and zeolite composite membranes (MCM-41, MCM-48 and FAU) was measured using contact angle Drop Shape Analyzer-DSA 25, Kruss, maintaining fixed water droplet size of 4 μL and a falling rate of 0.16 mL min^{-1}. Five measurements were carried out for each membrane at different locations and the average value was reported.

5.2.1 Water flux measurement

Fig. 1 illustrates the schematic representation of cross flow ultrafiltration setup. It consists of a feed tank, high pressure peristaltic pump, assembled membrane module, pressure gauge, rotameter (1-12 L/h) and a retentate valve (needle valve). The membrane was fixed in membrane module housing with a perforated casing. Experiments were conducted at room temperature (~ 25 °C). Using cross flow ultrafiltration set up, pure water flux of MCM-41,

MCM-48 and FAU zeolite composite membranes are measured at different applied pressures (69-345 kPa) at a fixed cross flow rate (1.667×10^{-7} m^3s^{-1}) for 1 h.

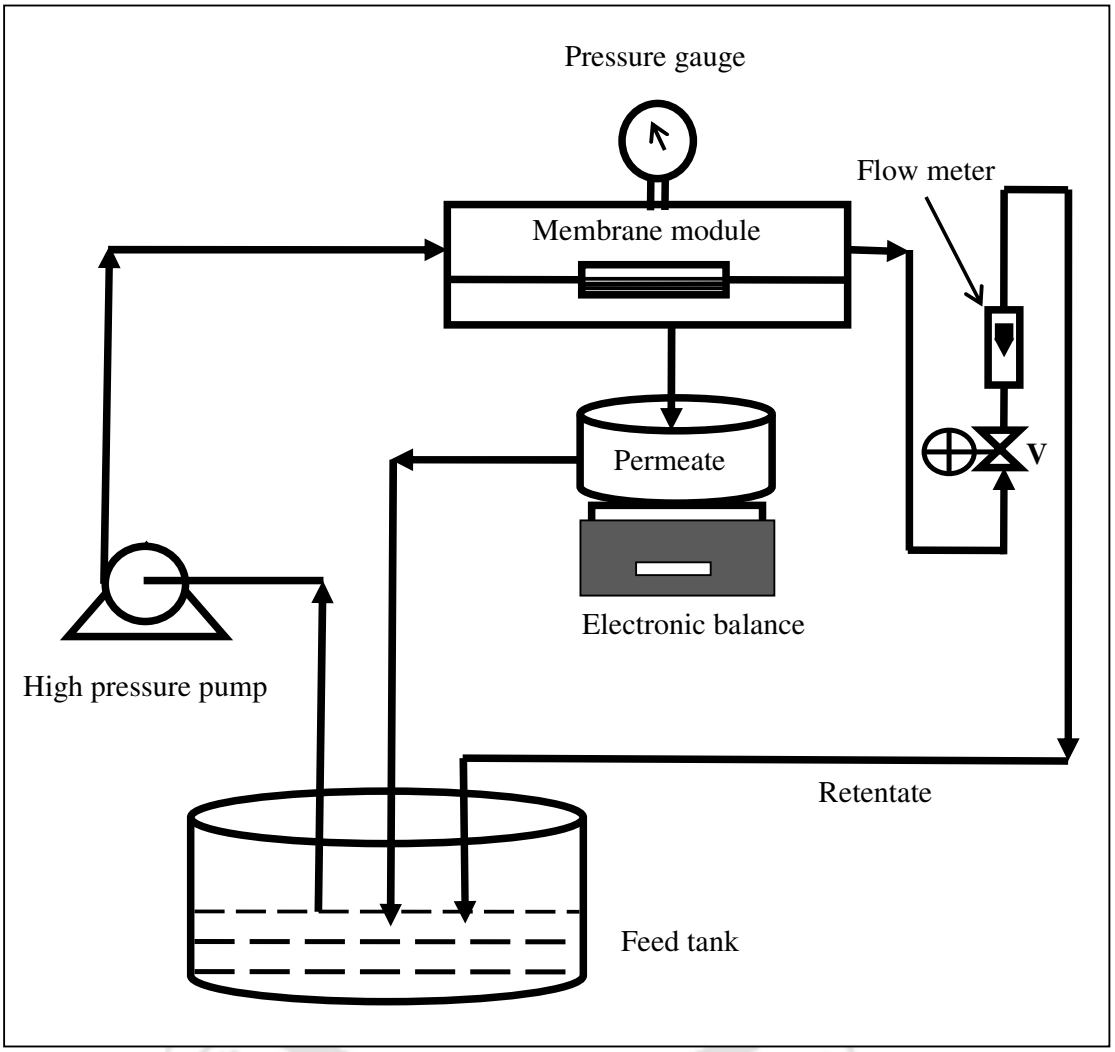

Fig. 5.1 Schematic of cross flow ultrafiltration setup (V-retentate valve)

5.2.2 Cross flow ultrafiltration experiments

For ultrafiltration experiments, Cr (VI) solution was prepared with the concentration of 1000 ppm in Millipore water at natural pH (~2.35). A typical cross flow ultrafiltration run involves the measurement of transmembrane flux at time intervals of 3 min for pure water flux and 5 min for the separation of Cr (VI) solution for total time period of 1 h. All experiments were

conducted at different applied pressures (69-345 kPa) with the fixed cross flow rate (1.667×10^{-7} m^3s^{-1}) to evaluate the effect of applied pressure on the separation characteristics of the zeolite composite membranes. The effect of cross flow rate (1.11×10^{-7} - 2.22×10^{-7} m^3s^{-1}) was also inspected with a fixed applied pressure of 207 kPa. For the removal of trivalent metal ions, $AlCl_3$ and $FeCl_3$ solutions were prepared with the concentration of 250 ppm in Millipore water at pH of 2 for cross flow ultrafiltration test. It is worth to mention that during investigation of batch filtration, the maxium rejection of trivalent salts was obtained at lower pH with a feed concentration of 250 ppm. Hence, the conditions were selected for the cross-flow filtration study. With the fixed cross flow rate (1.11×10^{-7} m^3s^{-1}), all experiments were conducted at different applied pressures (69-345 kPa) to evaluate the effect of applied pressure on the separation characteristics of zeolite composite membranes. In order to study the effect of applied pressure, the cross flow rate was maintained constant by controlling the retentate valve (V) and the applied pressure was varied by adjusting the speed of peristaltic pump. For the investigation of effect of cross flow rate, the applied pressure was fixed and the cross flow rate was changed by adjusting both retentate valve (V) as well as speed of high pressure peristaltic pump. Both the retentate and permeate were returned to the feed tank in order to maintain constant concentration in the feed tank throughout the experiments.

For each cross flow ultrafiltration experiments, the feed and permeate concentration were measured using conductivity meter (Eutech Instruments, Model: CON 2700). At the end of each experiment, the composite membrane was systematically cleaned with Millipore water followed by flushing with water at higher pressure to regain its initial water flux of the membrane. For all three composite membranes, the permeate flux (J), and percent rejection (R) of metals was calculated using the following expressions:

$$J = \frac{V}{A \times \Delta t} \tag{5.1}$$

$$R = \left[1 - \frac{C_p}{C_f}\right] \times 100 \tag{5.2}$$

where, A is the effective area of membrane (m^2), V is volume of permeate (m^3), Δt is the sampling time (s), C_f and C_p are the concentration of chromium, $AlCl_3$ and $FeCl_3$ in the feed and permeate (ppm), respectively.

5.3 Results and discussion

5.3.1 Characterization

Figure 5.2(a-d) illustrates the contact angle of ceramic support, MCM-41, MCM-48 and FAU zeolite composite membranes. The contact angle helps in understanding the surface interaction phenomena and wettability of the fabricated membrane with liquid phase. MCM-41, MCM-48 and FAU zeolite membranes show contact angle of 38°, 28.9° and 8.4°, respectively, demonstrating that FAU membrane is more hydrophilic. The contact angle of the ceramic support is 81.8°, which is far higher than that of the deposited zeolite composite membrane. This implies that ceramic support is hydrophobic in nature compared to zeolite membranes. The hydrophilicity of membrane varies in the following sequence: FAU > MCM-48 > MCM-41 > ceramic support. The advantage of highly hydrophilic membrane surface in the separation process is to reduce the fouling and concentration polarization that leads to enhance the permeability of solvent.

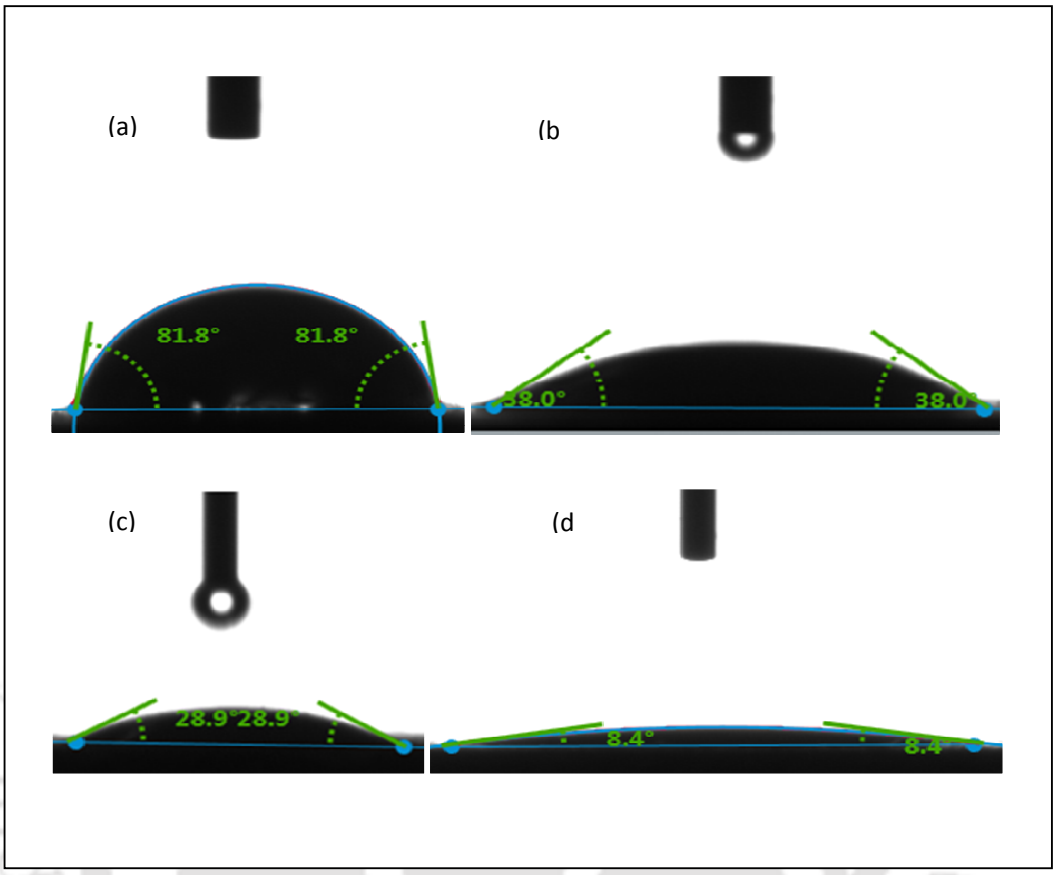

Fig. 5.2 Contact angles of (a) Ceramic support, (b) MCM-41, (c) MCM-48 and (d) FAU zeolite composite membranes

The porosity of membranes is evaluated to be 47, 23, 22 and 33% for ceramic support, MCM-41, MCM-48 and FAU zeolite membrane, respectively. The reduction in the porosity of the composite membranes clearly points out the deposition of zeolite materials on the ceramic support. With batch experimental setup, the water permeability and mean pore size of the membranes are calculated using Hagen Poiseuille equation cited in chapter 2 (section 2.2). The pore size of the fabricated membranes is found to be 1.00 µm, 0.173, 0.142, and 0.153 µm for ceramic support, MCM-41, MCM-48 and FAU zeolite membranes, respectively.

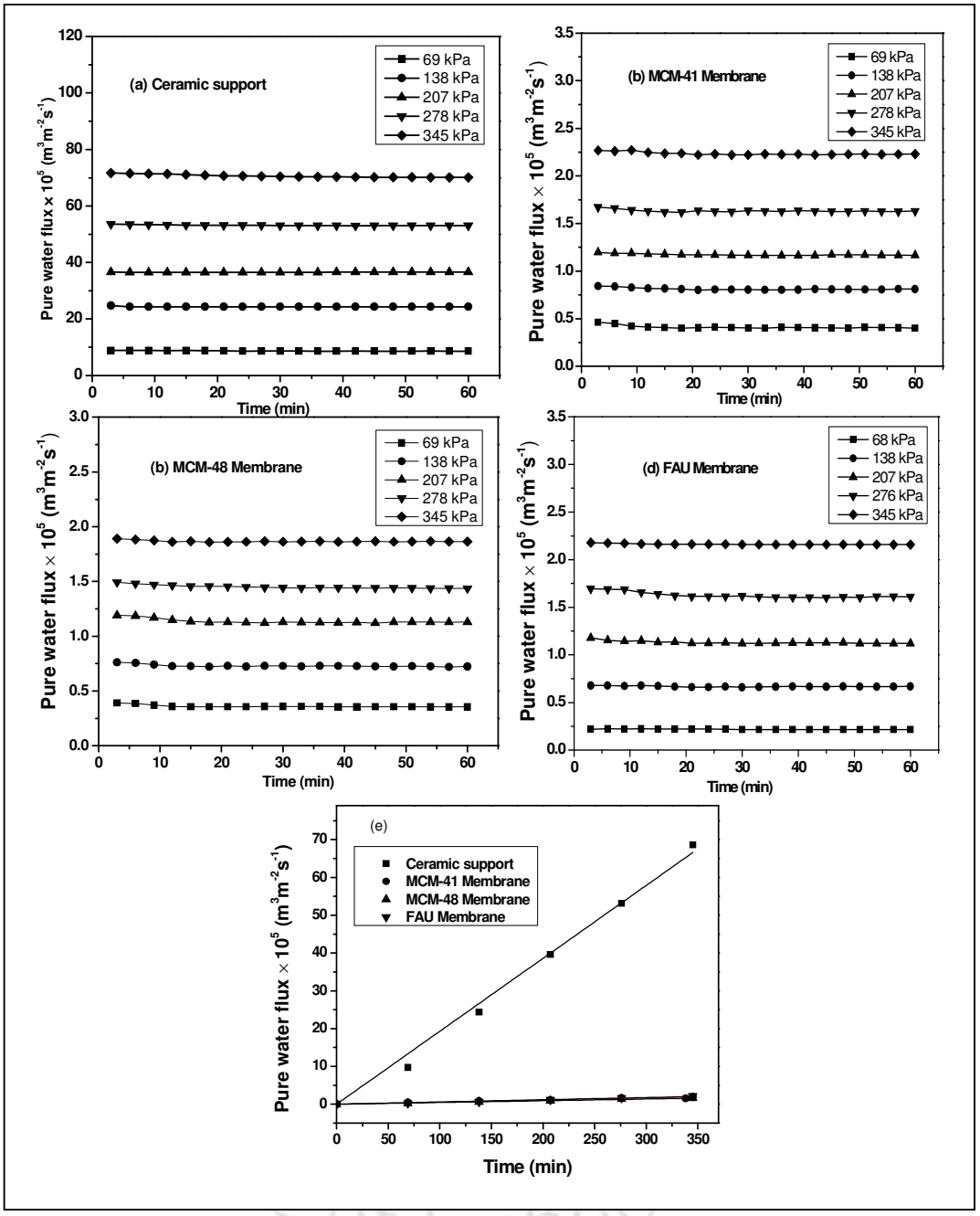

Fig. 5.3 Variation of pure water flux as a function of time for (a) ceramic support, (b) MCM-41, (c) MCM-48, (d) FAU membrane and (e) pure water flux as a function of applied pressure for support and composite membranes

The pure water flux obtained using cross flow filtration unit for MCM-41, MCM-48 and FAU zeolite composite membranes is depicted in Fig. 5.3(a-d). It is apparent that with increasing applied pressure, the pure water flux increases linearly and follows Darcy's law

for all zeolite composite membranes. Fig. 5.3(e) displays pure water flux as a function of applied pressure for all zeolite composite membranes. It is noticed that with the deposition of MCM-41, MCM-48 and FAU zeolite on the ceramic support, the pure water flux is drastically reduced for all zeolite composite membranes. It indicates that the pore size and water permeability of zeolite membranes are decreased, which justifies the pore size obtained from Hagen-Poiseuille equation.

5.3.2 Ultrafiltration of Cr (VI)

5.3.2.1 Influence of applied pressure on the performance of zeolite composite membranes

Figure 5.4 (a-c) presents the variation of permeate flux with time for MCM-41, MCM-48 and FAU zeolite composite membranes at various applied pressures (69-345 kPa) and a fixed cross flow rate (1.667×10^{-7} m^3s^{-1}). It is observed from this figure that the flux of zeolite composite membranes is augmented with an increase in the applied pressure owing to enhancement of driving force. It can also be noticed from Fig. 5.4(a) that the variation of permeate flux with time is almost negligible in 1 h operation and similar patterns are also observed with MCM-48 and FAU zeolite composite membranes (Fig. 5.4(b, c)). The permeate flux varies almost linearly with increasing applied pressure for all the zeolite composite membranes. This may be due to the fact that there is no significant contribution of an additional transport resistance from concentration polarization and adsorption. However, the permeate flux of the zeolite composite membrane is slightly lower than the pure water flux of the corresponding membrane. This may due to the osmotic pressure generated by the retained ions, which results in reducing the effective pressure across the membrane. Rashdi *et al*., (2015) also observed the improvement of permeate flux with enhancing applied pressure for the separation of heavy metal ions by cross flow nanofiltration with commercial NF270

membrane. Fig. 5.4(d) illustrates the permeate flux of zeolite membranes (MCM-41, MCM-48 and FAU) as a function of applied pressure. MCM-41 membrane displays marginally higher flux value, whereas MCM-48 offers less flux compared to other two membranes. This may be due to a slightly bigger pore size of MCM-41 when compared to other membranes. Among these membranes, MCM-48 composite membrane has the lowest pore size. The deposition of FAU zeolite on the ceramic support acquires promising permeate flux during the separation of Cr (VI). This may be due to better compatibility of liquid phase separation and hydrophilicity nature of FAU zeolite membrane. Even though FAU zeolite membrane has slightly smaller pore size than that of MCM-41 composite membrane, it displays almost similar permeate flux of MCM-41 composite membrane at a fixed flow rate.

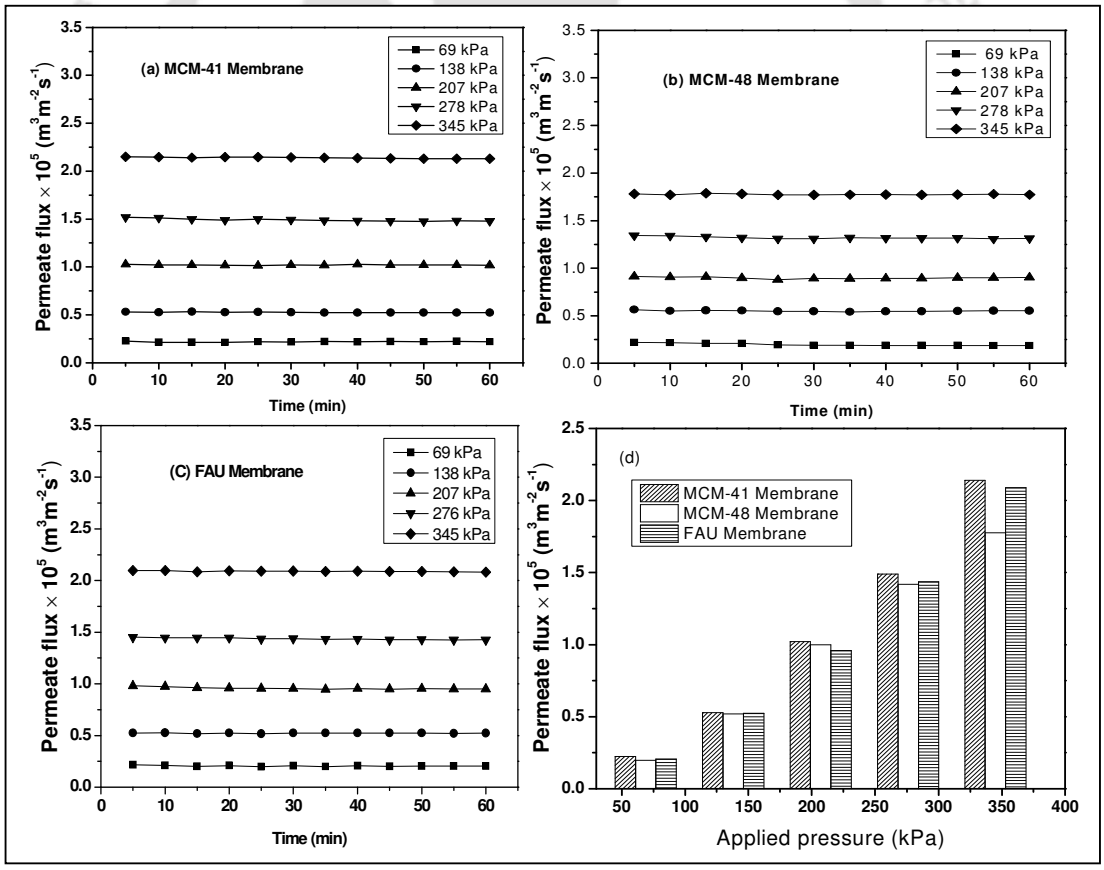

Fig. 5.4 Variation of permeate flux with time at different applied pressures for (a) MCM-41,(b) MCM-48, (c) FAU and (d) permeate flux as a function of applied pressure (feed concentration = 1000 ppm, natural pH~ 2.35)

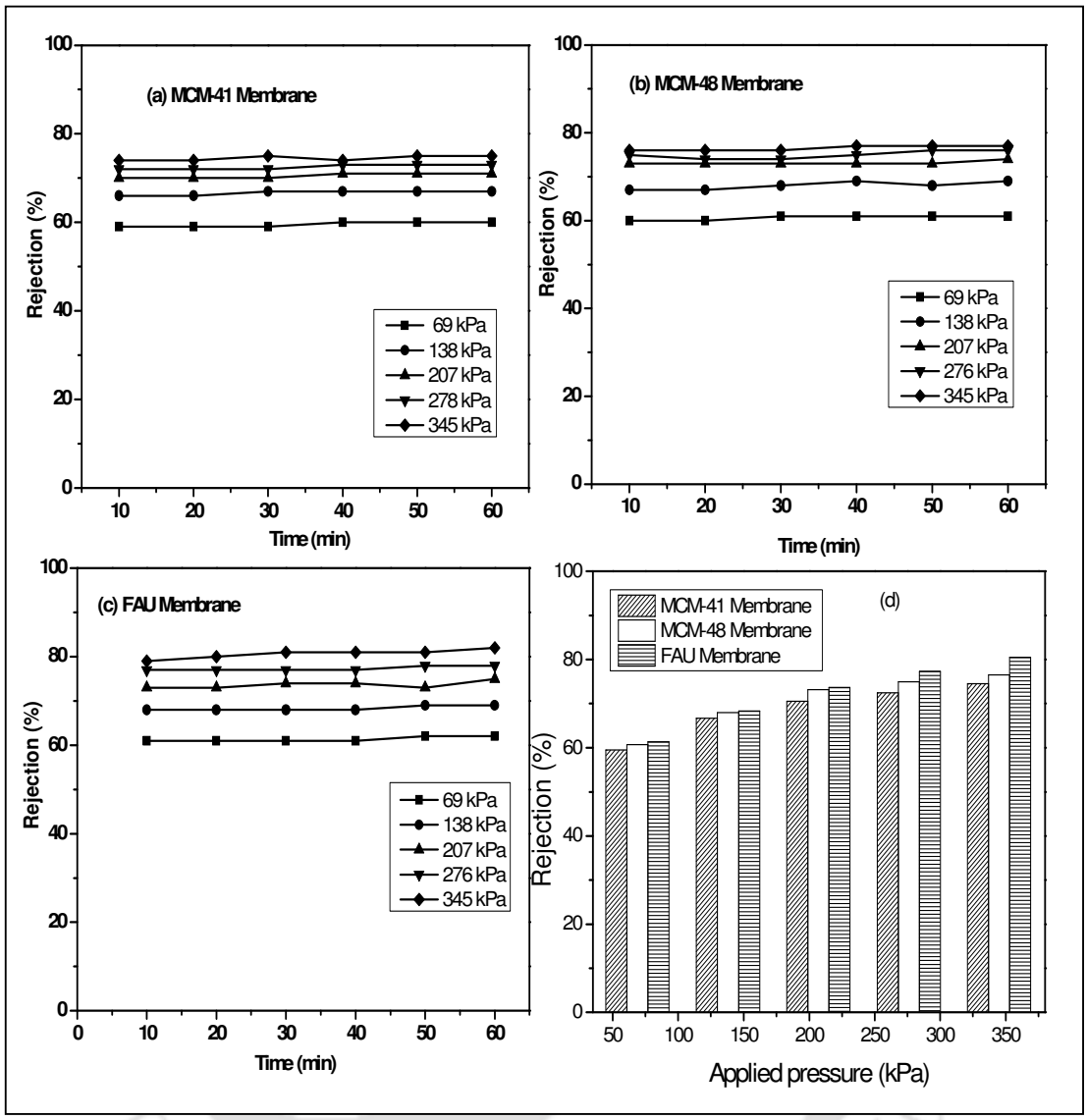

Fig. 5.5 Variation of rejection of Cr (VI) with time at different applied pressures for (a) MCM-41, (b) MCM-48, (c) FAU and (d)rejection as a function of applied pressure (feed concentration = 1000 ppm, natural pH~ 2.35)

The variation of percentage rejection of MCM-41, MCM-48 and FAU zeolite composite membranes with time at various applied pressures for a fixed cross flow rate of 1.667×10^{-7} m^3s^{-1} is presented in Fig. 5.5(a-c). For all the zeolite membranes, the rejection of Cr (VI) marginally increases with the duration of the process for all the studied pressure. This is possibly due to due to building up of the concentration polarization till steady state is reached

at the membrane surface (Danis and Keskinler 2009). The rejection also augments with increasing applied pressure for all the composite membranes. At the initial stage of process as well as at lower applied pressure, the formation of concentration polarization effect doesn't take place. However, with enhancing time, it starts forming due to retention of ions within the pore of the membrane. When the applied pressure increases, the convective transport becomes more important than the diffusive transport and hence the retention will increase. Therefore, Cr (VI) rejection increases with enhancing pressure due to the dilution effect, as the higher transport solvent flux would result in a dilution of permeate. As a result, higher rejection is observed at an elevated pressure (Gherasim and Mikulasek 2014).

In order to get comprehensive information on the influence of applied pressure on the removal of Cr (VI), the rejection against applied pressure is plotted. Fig. 5.5(d) illustrates the rejection of Cr (VI) as a function of applied pressure for zeolite composite membranes. It represents increasing rejection of Cr (VI) with an increase in the applied pressure (Mehiguene *et al*., 1999). A maximum rejection of 75, 77 and 82%, is achieved using MCM-41, MCM-48 and FAU zeolite composite membrane, respectively at a higher applied pressure (345 kPa). The surface charge is an important factor for determining the separation efficiency of the membrane with ionic solution and also it varies with the pH of the solution. The isoelectric point (IEP) of MCM-41, MCM-48 and FAU zeolite membrane is 3.9, 3.2 and 3.8, which are determined using zeta potential measurement. MCM-41, MCM-48 and FAU zeolite membrane have zeta potential value of +14.6, +2.486 and +2.95 mV, respectively, at natural pH (2.35) of chromium solution (1000 ppm). In addition to charge density, the removal of Cr (VI) is also influenced by the amount of zeolite materials deposited on the ceramic support. The quantity of FAU zeolite deposition (1.26 g) on ceramic support is more than that of MCM-41 (0.89 g), whereas zeta potential value of MCM-41 is higher than the FAU zeolite, and both membranes have almost similar IEP value. However, the rejection of FAU zeolite

composite membrane is found to be higher when compared to MCM-41 membrane and this may be due to more hydrophilic nature of FAU zeolite membrane. The removal of Cr (VI) for MCM-48 membrane is slightly higher compared to MCM-41 membrane due to a larger quantity of MCM-48 depsoition (1.28 g) on the ceramic support. Among the three zeolite membranes, the rejection of FAU membrane is higher as it has almost equal amount of deposition with MCM-48 and its hydrophilicity is also greater than that of other two composite membranes.

5.3.2.2 Influence of cross flow rate on the performance of zeolite composite membranes

In order to investigate the influence of cross flow rate on the performance zeolite composite membranes, three different feed flow rates were chosen ranging from 1.11×10^{-7} m^3s^{-1} to 2.22×10^{-7} m^3s^{-1}, at a fixed applied pressure of 207 kPa with the feed concentration of 1000 ppm. Fig. 5.6(a-c) displays permeate flux with time, which enhances with an increase in the cross flow rate for all the zeolite composite membranes. This is due to insignificant concentration polarization on the composite membranes at higher cross flow rate. With augmenting cross flow rate, it contributes to increase the shear stress on the membrane surface and minimize the chance of Cr (VI) adsorption on the surface of composite membrane. Cross flow rate plays a considerable role in reducing the concentration polarization by virtue of its sweeping action on the surface of the membrane. Consequently, the resistance and fouling occurring chances are less as seen in Fig. 5.6(a-c) for all the zeolite composite membranes. Minimization of concentration polarization boosts the convective force, which in turn improves the solvent flux due to upcoulping nature of the solvent and solute flux during filtration. Fig. 5.6(d) depicts the permeate flux of Cr (VI) against three cross flow rate of 1.11×10^{-7} m^3s^{-1}, 1.66×10^{-7} m^3s^{-1}, and 2.22×10^{-7} m^3s^{-1} for MCM-41, MCM-48 and FAU zeolite composite membranes. It is apparent that with increasing cross flow rate, the permeate flux of all zeolite composite membranes (MCM-41, MCM-48 and

FAU) increases almost linearly. The highest permeate flux is observed for FAU zeolite composite membrane with all three cross flow rates. This may be due to higher polarity behavior of FAU membrane than that of MCM-41 and MCM-48 composite membranes, which is also evidenced in the contact angle measurement.

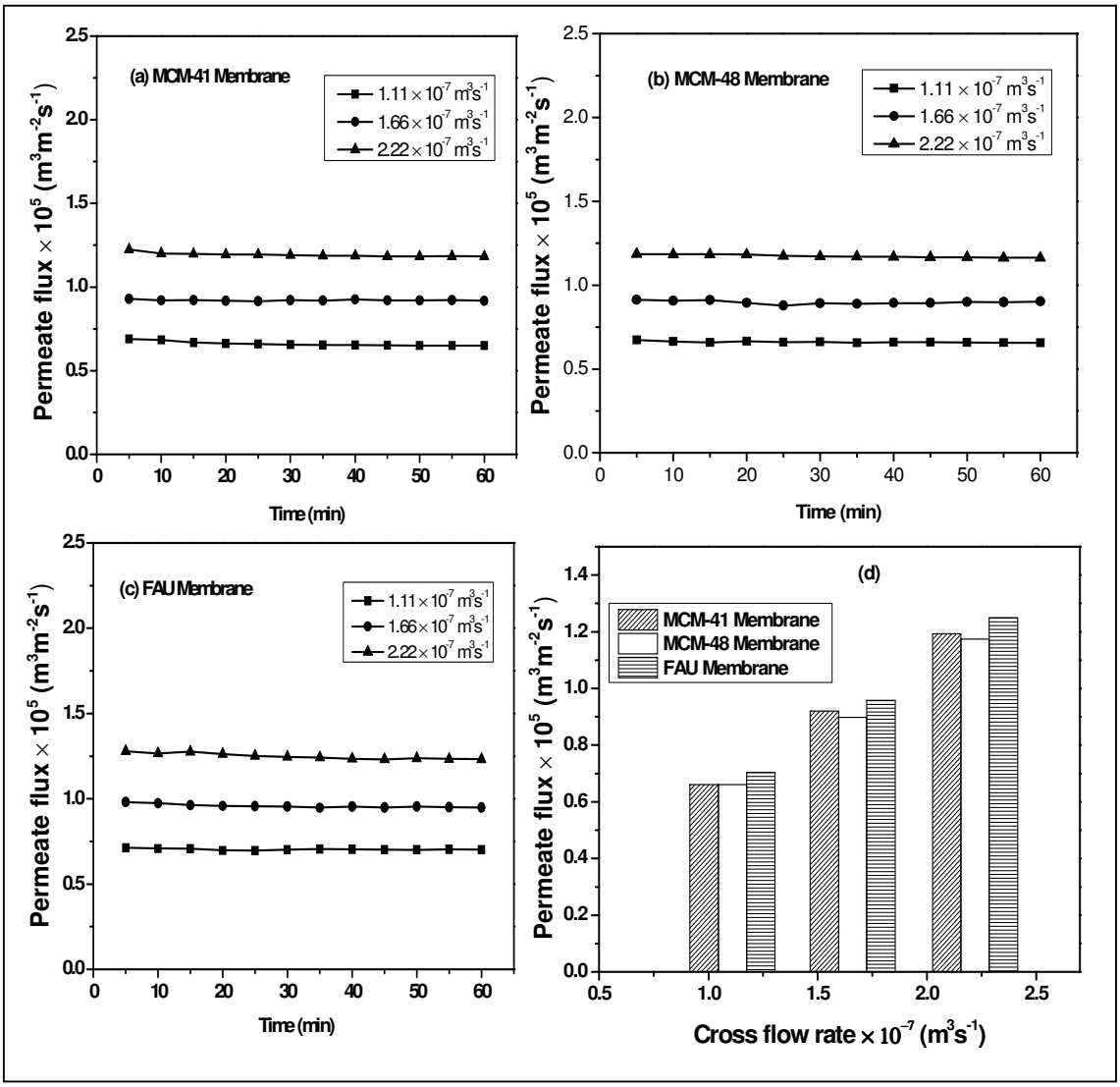

Fig. 5.6 Variation of permeate flux with time at different cross flow rates for (a) MCM-41, (b) MCM-48, (c) FAU and (d)permeate flux as a function of flow rate (feed concentration = 1000 ppm, natural pH~ 2.35)

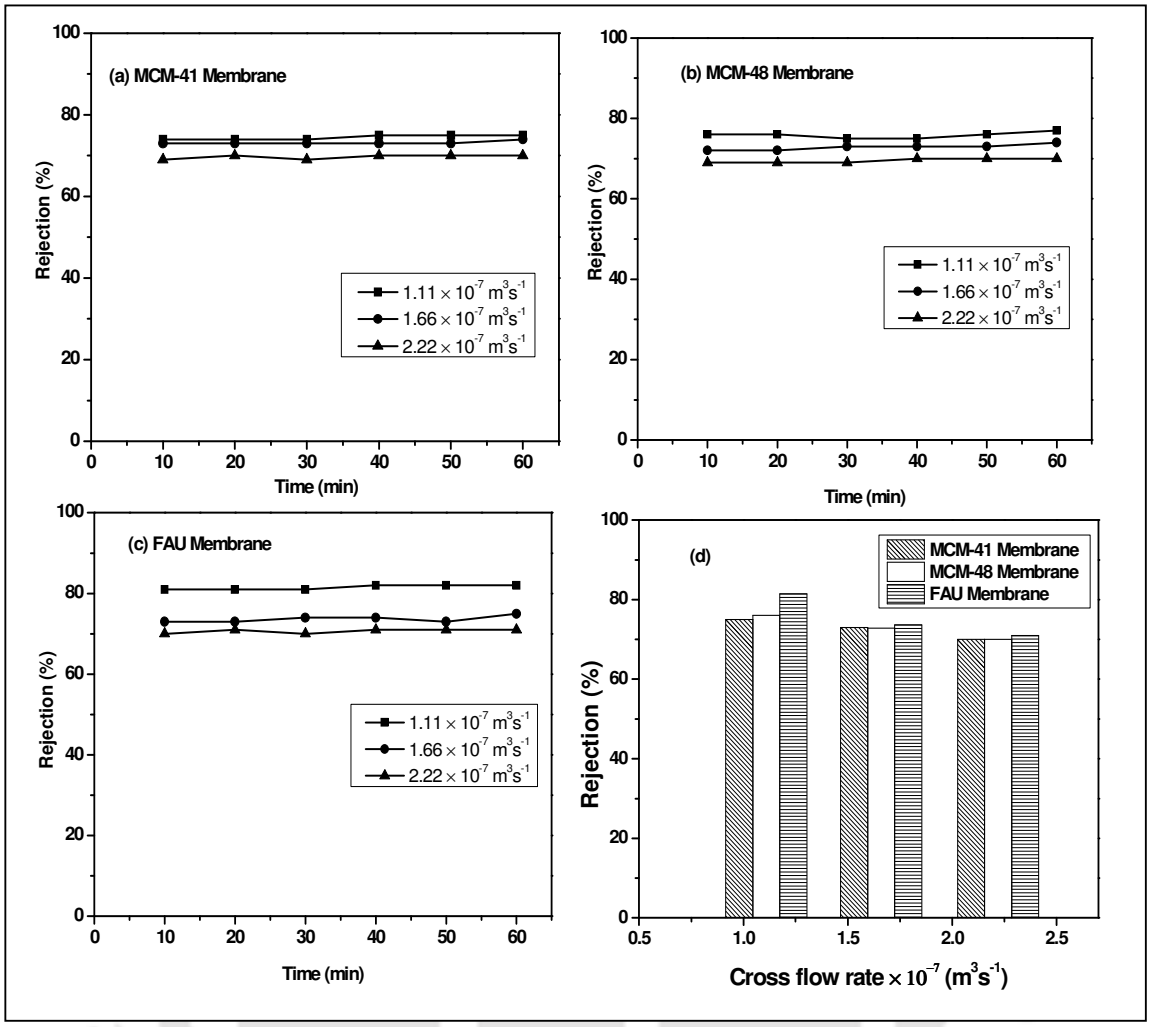

Fig. 5.7 Variation of rejection of Cr (VI) with time at different cross flow rates for (a) MCM-41, (b) MCM-48, (c) FAU and (d) rejection as a function of cross flow rate (feed concentration = 1000 ppm, natural pH~ 2.35)

The rejection of Cr (VI) on zeolite composite membranes decreases with an increase in the cross flow rate is illustrated in Fig. 5.7(a-c). At high cross flow rates, boundary layer is thinner. The balance between solute's diffusive transport from membrane surface to bulk and convective transport from bulk to membrane surface at steady state may result in higher concentration of solute at the membrane. Hence, chromium ions move to the permeate side through the pores of the membrane. As a result, rejection is less at higher cross flow rate. Similar trends are observed in all zeolite composite membranes (MCM-41, MCM-48 and FAU). MCM-41, MCM-48 and FAU zeolite composite membrane display a maximum

rejection of 76, 77, and 82%, respectively at lower cross flow rate of 1.11×10^{-7} m^3s^{-1} with a fixed applied pressure (207 kPa). Fig. 5.7(d) demonstrates the rejection with three flow rates for all zeolite composite membranes. A slight decrease in rejection is observed with increasing cross flow rate for all zeolite composite membranes due to sweeping action and no proper interaction of membrane surface charge with solute ions. The FAU zeolite composite membrane displays a maximum rejection at lower cross flow rate. The reason may be due to more quantity of FAU deposition as well as hydrophilicity nature of FAU zeolite composite membrane. In case of MCM-41 and MCM-48 composite membranes, much effect on rejection with changing the cross flow rate is not seen. A marginally higher rejection with MCM-48 membrane is observed at lower cross flow rate in comparison with MCM-41 membrane owing to higher deposition of MCM-48 on the ceramic support.

The rejection obtained for the separation of Cr (V) in a batch mode with MCM-41 composite membrane is 73% at natural pH (~2.35) of the feed solution and applied pressure of 345 kPa, and the decline trend of permeate flux is noticed (Chapter 2, section 2.3.6). Moreover, in cross flow mode with the same membrane, the rejection of 75% is observed at the same condition and no decline trend (i.e. no fouling of membrane) in the permeate flux is noticed. This implies that cross flow mode of filtration is better than the batch mode. In the batch mode operation, the achieved rejection is 76 and 70% for MCM-48 and FAU zeolite composite membrane, respectively with natural pH of the solution at an applied pressure of 345 kPa, whereas in the cross flow mode operation with the same membrane at natural pH, the rejection is 77 and 82 %, respectively. There is no declining trend in the permeate flux of MCM-41, MCM-48 and FAU zeolite composite membranes in the cross flow ultrafiltration of Cr (VI). Hence, it can be concluded that the separation of Cr (VI) in cross flow mode is more advantageous than the batch setup. With the constant flux trend, the prepared zeolite composite membranes (MCM-41, MCM-48 and FAU) can be effectively employed for the

separation of Cr (VI) from aqueous solution in a cross flow. Among the investigated composite membranes (MCM-41, MCM-48, and FAU), Faujasite zeolite membrane is better in terms of flux and removal efficiency. Besides, it requires less synthesize time (24 h), lower hydrothermal temperature (75 °C), and no calcination step involved in the fabrication, which leads to minimize the manufacturing cost of the membrane.

5.3.3 Separation of trivalent metal ions

5.3.3.1 Influence of applied pressure

To investigate the influence of applied pressure on cross flow ultrafiltration, the feed concentration and pH were maintained at 250 ppm and 2, respectively. The effect of permeate flux with time for MCM-41, MCM-48 and FAU zeolite composite membranes at different applied pressures ranging from 69-345 kPa and a fixed cross flow rate of 1.11×10^{-7} m^3s^{-1} is displayed in Fig. 5.8(a-c). It is clearly noticed from this figure that the flux of zeolite composite membranes enhances with an increase in the applied pressure due to increase in driving force. The variation of permeate flux with time is almost negligible for entire operation (1 h) as seen in Fig. 5.8 for the separation of $AlCl_3$ and $FeCl_3$. The permeate flux of all zeolite membranes varies almost linearly with increasing applied pressure. This may be explained that there is no adsorption and significant contribution of additional transport resistance from the concentration polarization. On the other hand, the permeate flux of all zeolite composite membranes is marginally lower than the pure water flux of the corresponding membrane. It is due to the osmotic pressure produced by the retained ions, which results in reducing the effective pressure across the membrane. The permeate flux of $AlCl_3$ and $FeCl_3$ demonstrates similar pattern with an increase in the applied pressure for all zeolite composite membranes (MCM-41, MCM-48 and FAU) (Rashdi *et al*., 2015). Fig. 5.9(a-c) represents the permeate flux as a function of applied pressure for $AlCl_3$ and $FeCl_3$.

The permeability of ions through the membrane is mainly influenced by the ionic size, shape, pore diameter and charge characteristic of the membranes (Tansel *et al*., 2006). In Fig. 5.9(c), the permeate flux of $AlCl_3$ is marginally higher than the $FeCl_3$ even though the hydrated radii of both ions are same. In $FeCl_3$, the complex salt formation (Fe^{3+} and Fe^{2+}) in hydrolysis, due to ion interference, prevents their transport rate, hence a slight reduction in permeate flux is obsvered (Kir *et al*., 2005). A similar pattern is also noticed for MCM-48 and FAU zeolite composite membranes

.

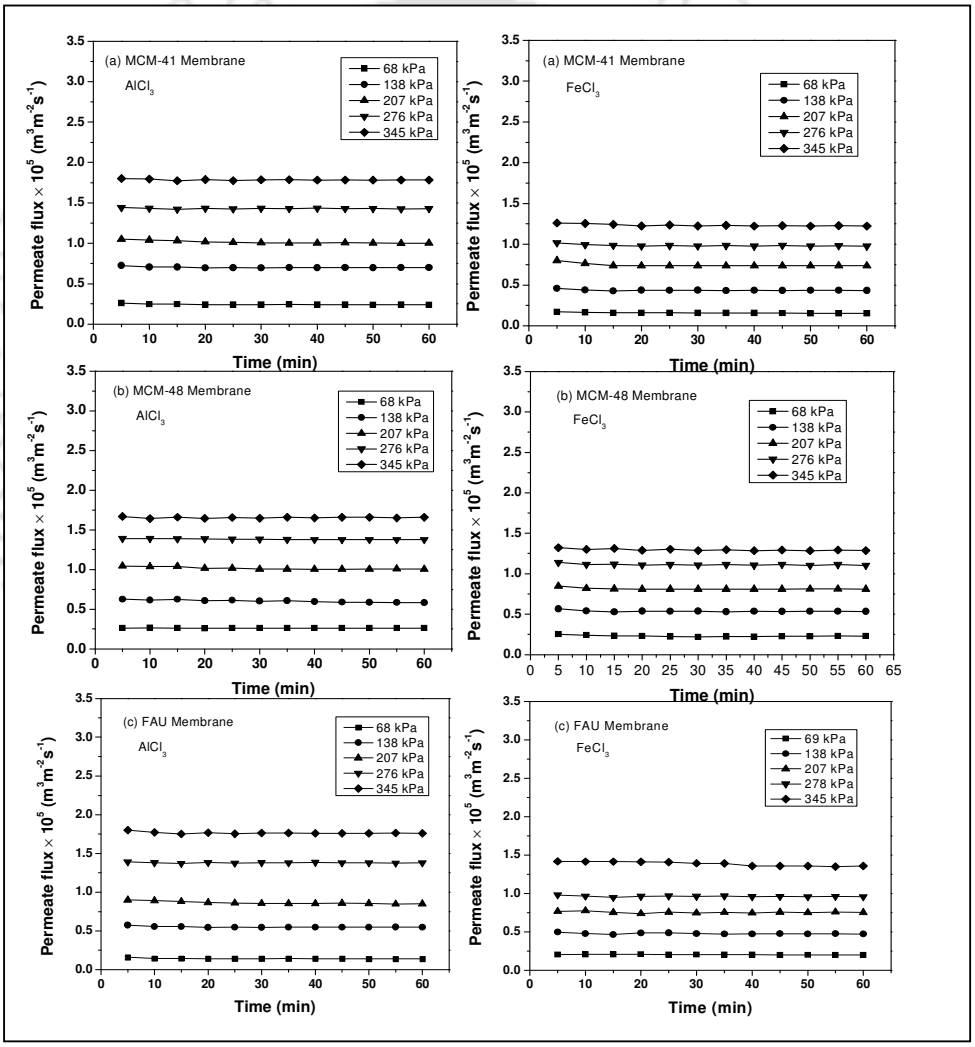

Fig. 5.8 Variation of permeate flux with time at different applied pressures for $AlCl_3$ and $FeCl_3$ using (a) MCM-41, (b) MCM-48 and (c) FAU membrane (feed concentration = 250 ppm, pH= 2.0)

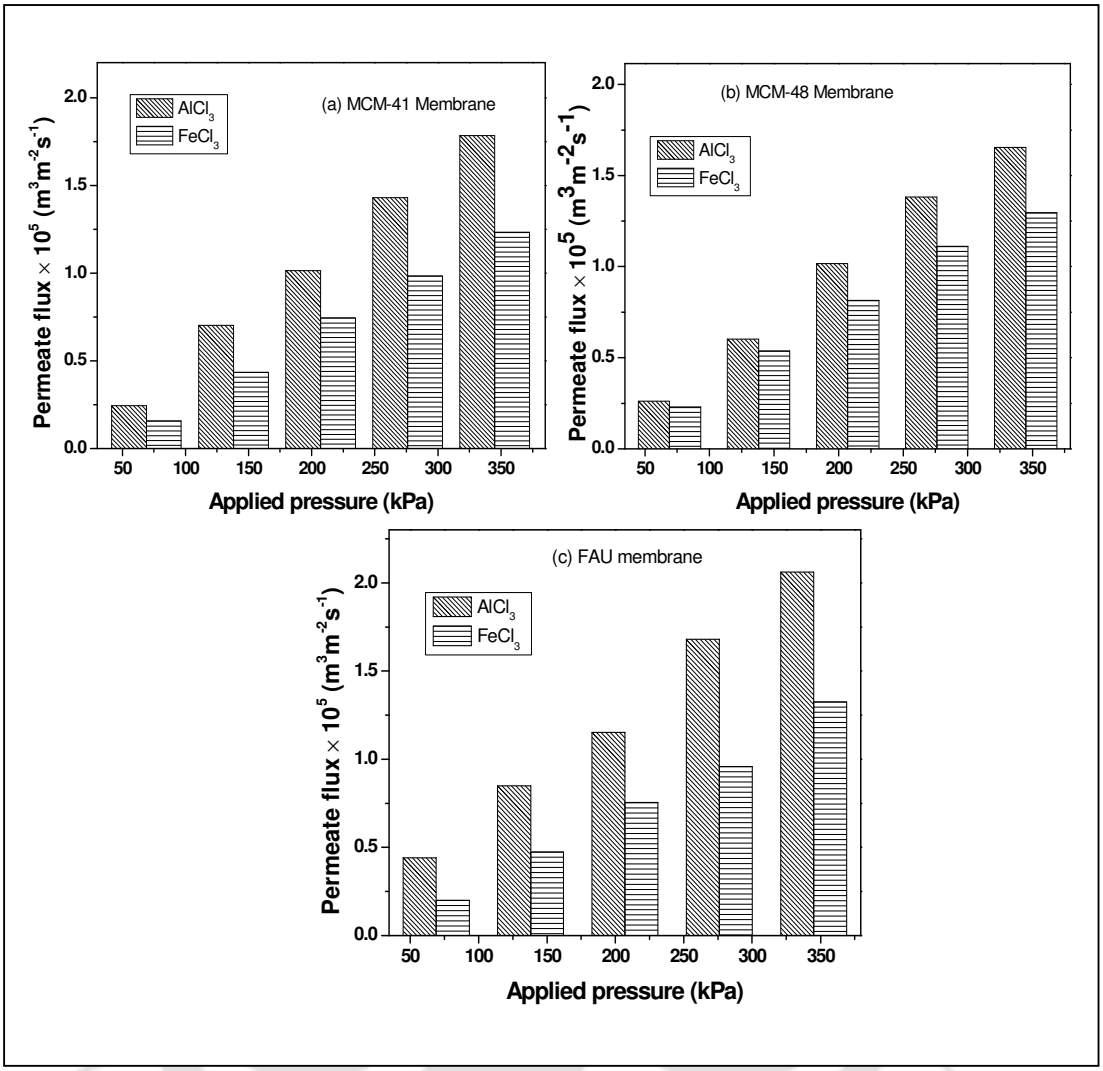

Fig. 5.9 Variation of permeate flux as a function of applied pressure for $AlCl_3$ and $FeCl_3$ using (a) MCM-41, (b) MCM-48 and (c) FAU membrane (feed concentration = 250 ppm, pH= 2.0)

The variation of percentage rejection of $AlCl_3$ and $FeCl_3$ using MCM-41, MCM-48 and FAU zeolite composite membranes with time at different applied pressures for a fixed cross flow rate of 1.11×10^{-7} m^3s^{-1} is presented in Fig. 5.10(a-c). For all the zeolite membranes, the rejection of trivalent metal ions slightly increases with the duration of the process for all the studied pressure. This is possibly due to due to building up of the concentration polarization till steady state is reached at the membrane surface (Danis and Keskinler 2009). The rejection

also augments with increasing applied pressure for all the composite membranes. The convective transport becomes more important than the diffusive transport with increasing applied pressure, and hence, the retention will increase. Thus the rejection of trivalent metal ions increases with enhancing pressure due to the dilution effect; as the higher transport solvent flux would result in a dilution of permeate. Therefore, maximum rejection is obtained at an elevated pressure (Rashdi *et al*. 2015). The maximum rejection of 88, 87 and 86% is accomplished with FAU, MCM-48 and MCM-41 zeolite composite membrane, respectively at a higher applied pressure (345 kPa) for the removal of $FeCl_3$. In case of $AlCl_3$ retention, 84%, 83% and 82% is achieved using FAU, MCM-48 and MCM-41 zeolite membranes at an applied pressure of 345 kPa.

Figure 5.11(a-c) illustrates the rejection of $AlCl_3$ and $FeCl_3$ as a function of applied pressure for MCM-41, MCM-48 and FAU zeolite membranes. One can clearly see that the rejection of $AlCl_3$ and $FeCl_3$ increases with an increase in the applied pressure (Danis and Keskinler 2009). Generally, the surface charge of the membrane plays a vital role in determining the separation efficiency of the membrane with ionic solution and it differs with pH of the solution. The diffusion coefficient of $AlCl_3$ and $FeCl_3$ also affects the retention behavior of metal ions (Schaep *et al*., 1998). $AlCl_3$ (5.5×10^{-9} m^2s^{-1}) has a higher diffusion coefficient than $FeCl_3$ (1.4×10^{-9} m^2s^{-1}), which results in lower rejection of $AlCl_3$ with zeolite membranes (Jafarian *et al.*, 2006; Haarberg and Keppert 2008). It is documented in literature (Peeters *et al*. 1998) that the salt, which has lower diffusion co-efficient displays a higher retention efficiency. The amount of FAU zeolite deposition (1.26 g) on ceramic support is more than that of MCM-41 (0.89 g), whereas zeta potential value of MCM-41 (18.25 mV) is higher than the FAU (4.8 mV) zeolite, and both membranes have almost similar IEP value. However, the rejection of FAU zeolite composite membrane is found to be higher when compared to MCM-41 membrane and this may be due to more hydrophilic nature of FAU

zeolite membrane. Among the three zeolite membranes, the rejection of FAU membrane is marginally higher as it has almost equal amount of deposition with MCM-48 and its hydrophilicity is also greater than that of other two composite membranes.

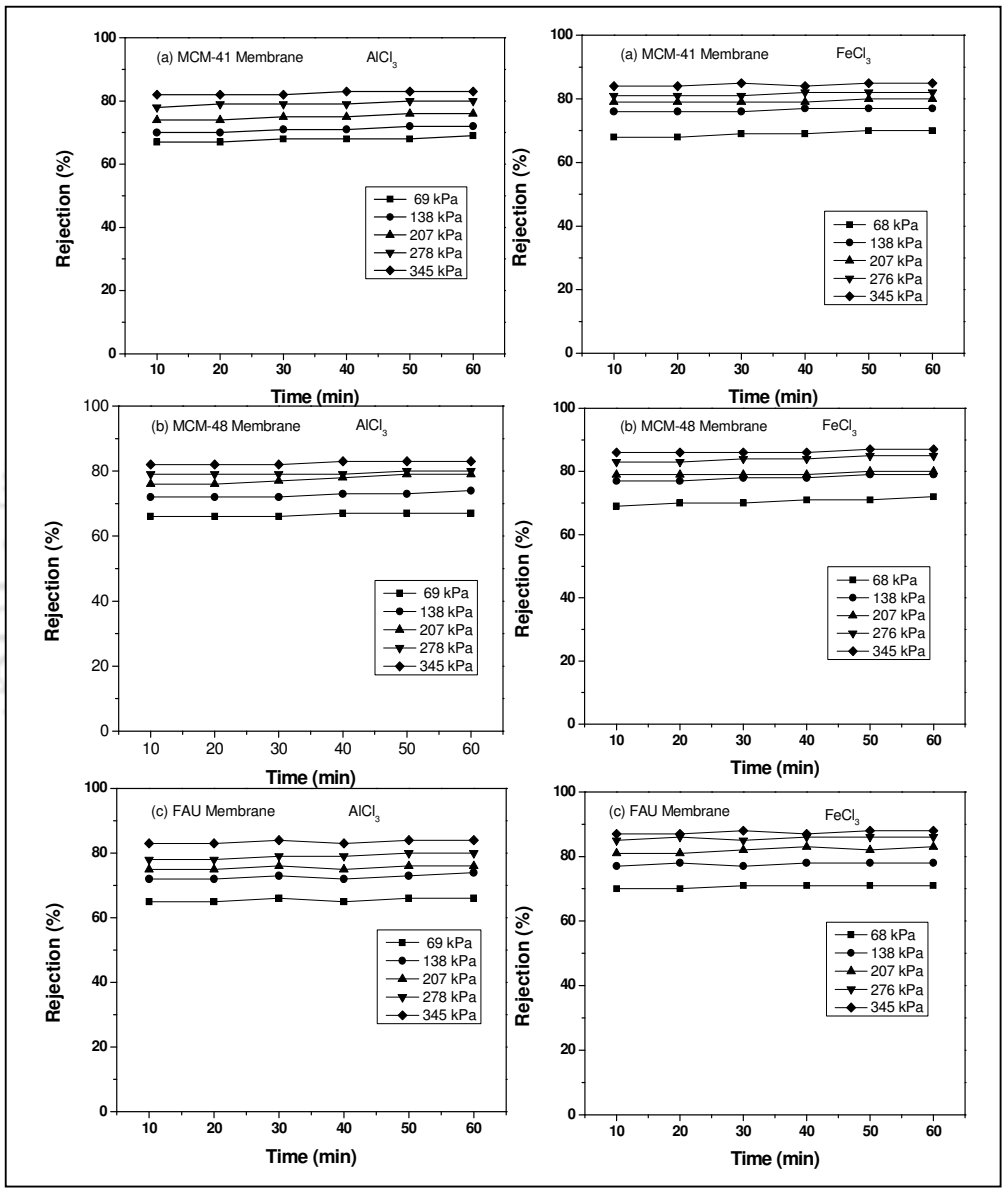

Fig. 5.10 Variation of rejection for $AlCl_3$ and $FeCl_3$ with time at different applied pressures using (a) MCM-41, (b) MCM-48 and (c) FAU (feed concentration = 250 ppm, pH~ 2.0)

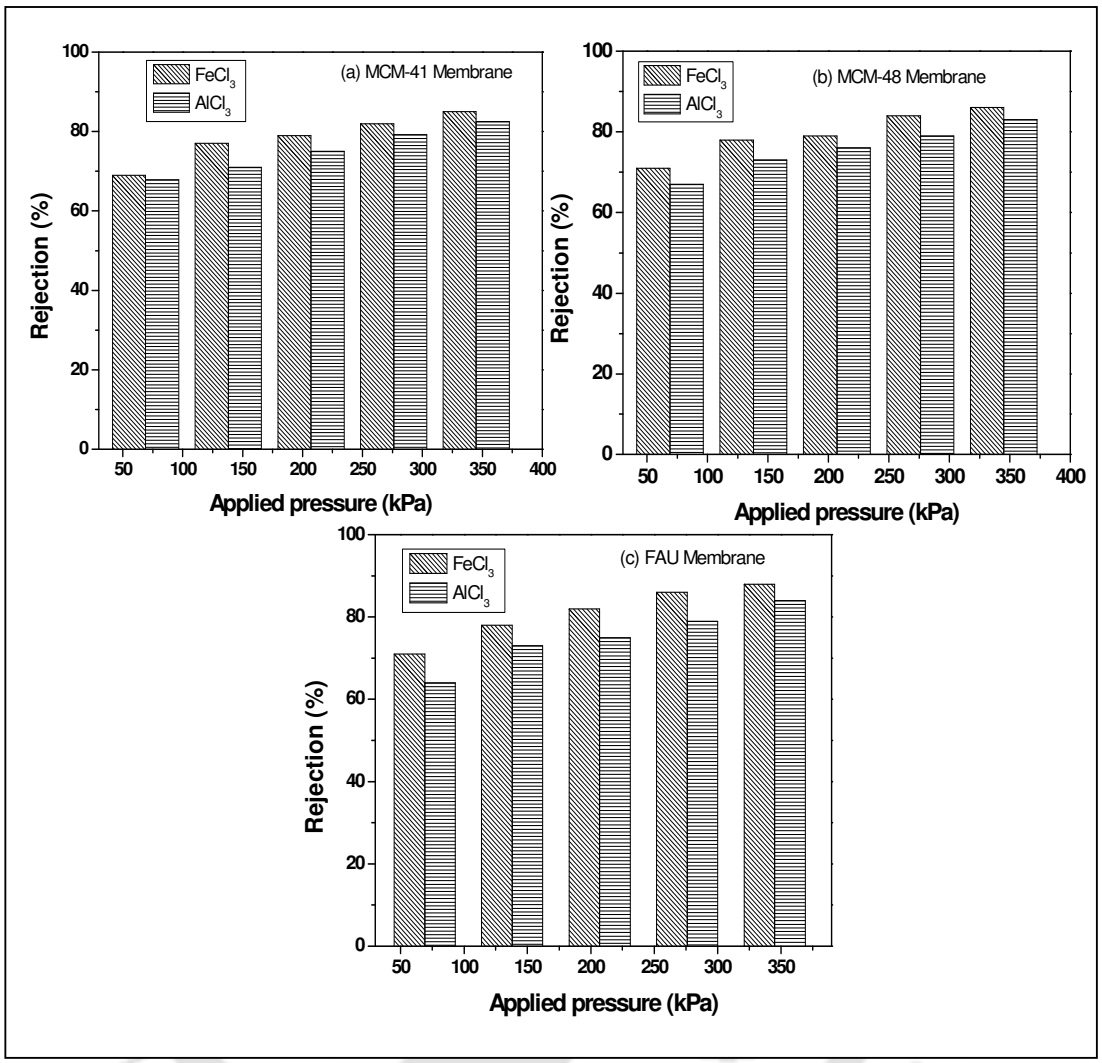

Fig. 5.11 Variation of rejection as a function of applied pressure for $AlCl_3$ and $FeCl_3$ using (a) MCM-41, (b) MCM-48 and (c) FAU membrane (feed concentration = 250 ppm, pH= 2.0)

Table 5.1 Comparative analysis of Cr (VI) removal in a batch and cross flow mode for MCM-41, MCM-48 and FAU zeolite composite membranes.

Composite membrane	Feed conc. (ppm)	Water permeability ($m^3m^{-2}s^{-1}kPa^{-1}$)		Solute flux (ms^{-1}) at applied pressure of 345 (kPa)		Rejection (%)	
		batch setup	cross flow	batch setup	cross flow	batch mode	cross flow mode
MCM-41	1000	6.05×10^{-8}	6.0×10^{-8}	2.30×10^{-5}	2.20×10^{-5}	73	75
MCM-48	1000	4.18×10^{-8}	4.54×10^{-8}	1.00×10^{-5}	1.79×10^{-5}	77	77
Faujasite	1000	6.09×10^{-8}	5.98×10^{-8}	2.00×10^{-5}	2.1×10^{-5}	70	82

5.4 Summary

Chromium and trivalent metal ions can be efficiently removed using zeolite composite membranes (MCM-41, MCM-48 and FAU) in a cross flow ultrafiltration. It is apparent that the prepared zeolite composite membranes do not have the tendency of fouling and cake layer deposition on the surface of the membrane in the removal of Cr (VI) and trivalent metal ions. FAU zeolite composite membrane displays higher rejection compared to other two membranes. The fabrication cost of FAU membrane is lower due to shorter synthesize time and lower temperature, and no calcination process required as surfactant is not used as a templating agent in the development of FAU zeolite membrane. With increasing applied pressure, the rejection of Cr (VI) enhances for all the zeolite composite membranes and maximum rejection is observed to be 75, 77 and 82% for MCM-41, MCM-48 and FAU zeolite membranes, respectively. When the cross flow rate increases, the permeate flux increases and the rejection declines slightly. The maximum rejection is observed for $FeCl_3$ separation when compared to $AlCl_3$ with all the zeolite membranes and no flux decline trend is noticed during the entire period of filtration study. This indicates that these membranes could be utilized for longer duration without frequent regeneration of the membrane.

Chapter 6

Processing and Characterization of Analcime-C Zeolite-Ceramic Composite Membrane and Its Performance Assessment by Separation of Cr (VI) from Aqueous Solution

Processing and Characterization of Analcime-C Zeolite-Ceramic Composite Membrane and Its Performance Assessment by Separation of Cr (VI) from Aqueous Solution

This chapter addresses the synthesis of analcime-C zeolite membrane on a ceramic support by in-situ hydrothermal crystallization. A circular shaped ceramic support was firstly fabricated using low cost raw materials by uni-axial pressing method and sintering process. The zeolite composite membrane was prepared with the repeated coating of analcime-C on the ceramic support. The synthesized zeolite composite membrane was characterized by X-ray diffraction (XRD), Field emission scanning electron microscopy (FESEM), porosity, average pore size and pure water permeability. Finally, the separation performance of three times coated zeolite membrane was evaluated by removal of Cr (VI) from aqueous solution using dead-end ultrafiltration (UF) set up at various operating conditions (applied pressure, concentration and pH).

6.1 Experimental

6.1.1 Materials

Hydrochloric acid, triethanolamine (TEA), aluminium fine powder and chromium (VI) oxide were purchased from Merck (I) Ltd., Mumbai. Sodium hydroxide was procured from Loba Chemie (Laboratory Reagents & Fine Chemicals), Mumbai, India. Fumed silica (Aerosil 200) was procured from CDH, Laboratory Reagents, Mumbai. Water used in this work was taken from the Millipore water system (ELIX-3).

6.1.2 Fabrication of analcime-C zeolite-ceramic composite membrane

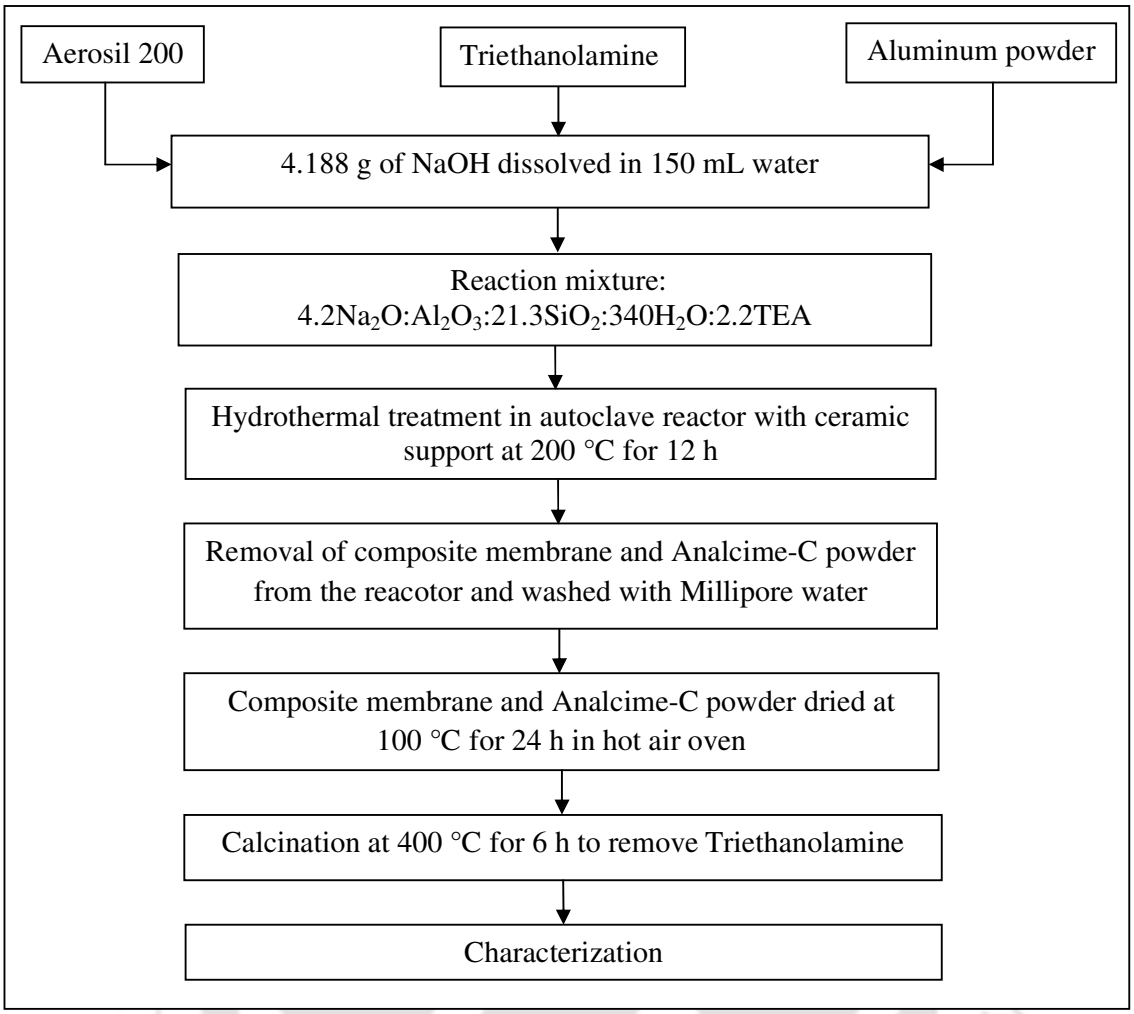

Fig. 6.1 Flow chart for the fabrication of Analcime-C zeolite composite membrane.

The protocol used for the synthesis of ceramic support and its composition were elaborated in chapter 2 (section 2.3). The mixture for hydrothermal reaction was prepared by dissolving 4.188 g of sodium hydroxide in 150 mL of Millipore water. Then aluminium metal powder (0.6607 g) was slowly added into the NaOH solution, after which an estimated amount of Aerosil 200 (fumed silica) and triethanolamine (TEA) were added and then the reaction mixture was stirred. The molar composition of the final gel was $4.2Na_2O:Al_2O_3:21.3SiO_2:340H_2O:2.2TEA$. A flat ceramic support was placed in a Teflon coated stainless steel autoclave reactor and the above prepared reaction mixture was transferred to the reactor. The

hydrothermal crystallization was carried out at 200 ^{o}C for 12 h. During hydrothermal crystallization, the zeolite particles precipitated inside the pores of ceramic support. After the synthesis, the zeolite membrane was carefully washed several times with Millipore water and dried at 100 ^{o}C for 24 h followed by calcined at 400 ^{o}C for 6 h in an air atmosphere during which triethanolamine (TEA) was removed. The flow chart for the preparation of analcime-zeolite membrane was shown in Fig. 6.1.

6.2 Characterization

The X-Ray diffraction of zeolite powder under air at room temperature was performed using a machine (Bruker AXS instrument) with a Cu Kα radiation source. The patterns were obtained in the 2θ range of 2 to 80^{o} with a scan speed of 0.05^{o}s^{-1}. The FTIR analysis was performed using a Shimadzu IRAffinity-1 model spectrometer in the wave number range of 4000-450 cm^{-1}. Samples of zeolite powder were prepared in the form of KBr tablets and the spectra were taken at room temperature and atmospheric pressure. Thermogravimetric analysis (TGA) of Analciome-C zeolite powder was carried out with Netzsch TG 209F1 Libra at an air atmosphere. The sample was heated from 30 °C to 950 °C at the heating rate of 10 °C/min. Nitrogen adsorption/desorption isotherm of MCM-41 powder samples were measured using a Quantachrome ® Asiqwin TM-Automated Gas Sorption (Version 3.0). The samples were degassed at 150 °C for 3 h prior to adsorption/desorption analysis. The specific surface area was evaluated using a multipoint BET method. The pore size distribution was calculated using a BJH method from the adsorption branch of nitrogen isotherm. The pore volume was estimated at a relative pressure, P/P_0 of 0.99, assuming full surface saturation with nitrogen. In order to determine point of zero charge (PZC) of the composite membrane, the solid addition method was employed to determine the point of zero charge (Silva *et al.*, 2012). 50 mg of the solid sample was treated in 50 mL of 0.001 M NaCl solutions at various

pH (2-12) for 24 h in a shaking bath. The initial pH (pHi) of the solution was adjusted using 0.1 M HCl or NaOH. Then the suspensions were shaken and allowed to equilibrate for 24 h. After that, the pH value of the supernatant for each flask was measured. The difference between the final and initial pH ($\Delta pH = pH_f - pH_i$) was calculated and the graph was plotted between ΔpH and pH_i. In the plot, the point of intersection of the resulting curve at which $\Delta pH = 0$ was the pH_{PZC} value of the composite membrane. Field Emission Scanning Electron Microscope (FESEM, JEOL JSM-5600LV) was used to look into the surface properties of prepared composite membrane. A small size of the sample was fixed onto the stub and coated with gold using a JEOL JFC-1300 auto fine coater prior to morphology assessment. The porosity of the membrane was calculated according to Archemides principle explained in chapter 2 (section 2.2).

6.2.1 Water flux and chromium removal

The water permeability and separation potential of the composite membranes were measured using an in-house made dead end UF setup given in section 2.3 of chapter 2. The water flux was calculated at different applied pressures. At each applied pressure, the first 50 mL of water collected was disposed and the time taken for the collection of the following 50 mL of water was used for the determination of water flux.

The performance of the composite membrane in the removal of Cr (VI) was tested using the UF setup filled with 100 mL of the feed solution. The Cr (VI) solution was prepared with Millipore water and the concentration was measured using a conductivity cell (Eutech Instruments, Model: CON 2700). In order to determine the permeate flux at a fixed applied pressure, the first 10 mL of the permeate collection was discarded and the time taken for collection of the second 10 mL was noted. The observed rejection was calculated using the following expression:

$$R(\%) = \left[1 - \frac{C_p}{C_f}\right] \times 100 \qquad (6.1)$$

where, C_f is the concentration of the feed solution, C_p is the concentration of permeate solution and R is the observed rejection (%). After every experimental run, the membrane was thoroughly cleaned by flushing with Millipore water at a higher pressure to regain the original pure water flux.

6.3 Results and discussion

6.3.1 Characterization of analcime-C zeolite powder

Analcime-C zeolite powder (before and after calcination) was subjected to analyze for its structure and purity verification by a means of XRD patterns as shown in Fig. 6.2. The obtained XRD patterns closely match with ICDD (COD 9008207 Al_2 H_4 Na_2 $O1_4$ Si_4 analcime) and the standard pattern of analcime (Intaraprasit and Kongkachuichay 2011). The main crystalline phase identified corresponds to the ANA-type structure, although a few extra lines reveal the occurrence of traces of anatase and ilmenite. Moreover, there are no significant changes in the peak position and intensities of the zeolite before and after calcination. Fig. 6.3 shows the FTIR spectra of analcime-C zeolite powders (as-synthesized and calcined). The bands (antisymmetric and symmetric) for the stretching vibration of hydroxyl groups appear in the wave number range of 3610-3550 cm^{-1} and exhibit high intensity (Stuart 2004). The H-O-H bending vibration appears at 1630 cm^{-1}. The bands of antisymmetric stretching vibration with the variable intensity of the tetrahedral T-O (T = Si, Al) appear in the wavenumber range between 1050 and 810 cm^{-1} (Stuart 2004, Pechar and Rykl 1983). The bands observed at 780-660 cm^{-1} are attributed to the symmetric stretching

vibration of T-O bonds. The bending vibration of the tetrahedral bonds exhibited in the region of 615-450 cm^{-1} (Stuart, 2004; Pechar and Rykl 1983).

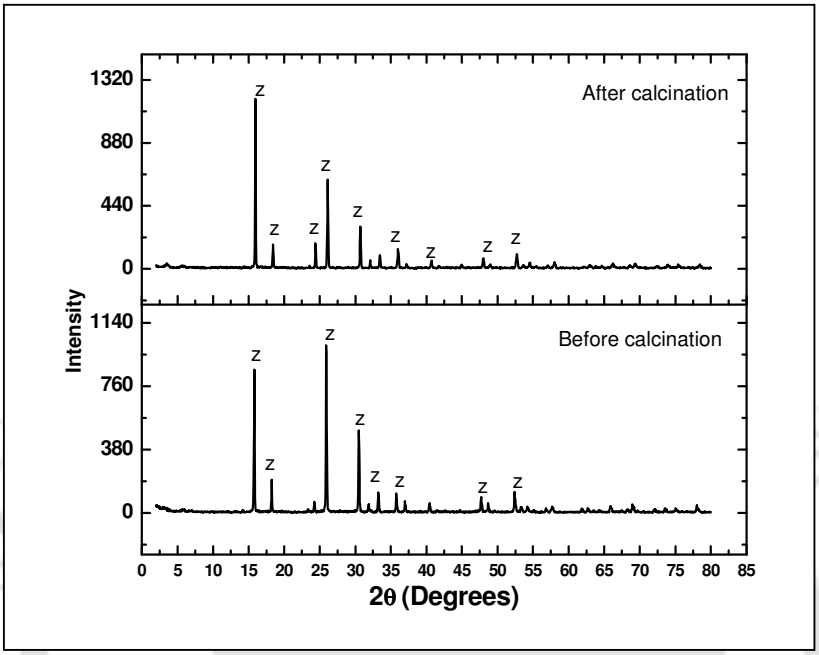

Fig. 6.2 XRD pattern of analcime-C zeolite powder formed during hydrothermal crystallization reaction

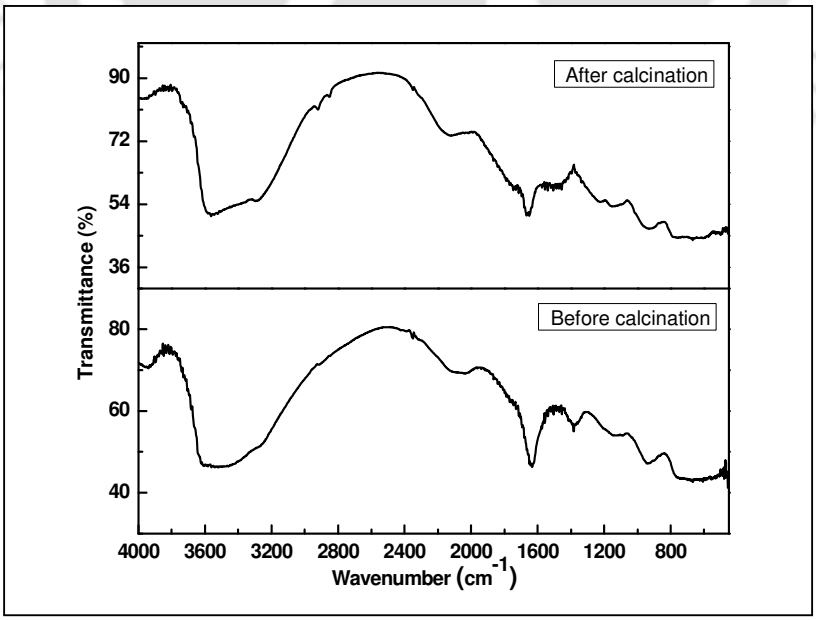

Fig. 6.3 FTIR spectra of synthesized analcime-C zeolite powder.

Figure 6.4 depicts the TGA curve of the synthesized analcime-C zeolite particles. The total weight loss is estimated to be approximately 8%. The weight loss at the temperature below 150 ^{o}C is owing to removal of the unbounded moisture that was absorbed by the sample. The weight loss at higher temperature is due to the removal of structural hydroxyl groups. Moreover, the weight loss of the particles after 400 ^{o}C is found to be insignificant. Therefore, it can be inferred from the graph that the minimum calcination temperature after coating should be above 400 ^{o}C. During calcination at 400 ^{o}C, TEA is burnt to leave an open pore zeolite framework. The N_2 adsorption/desorption isotherm of the analcime-C zeolite powder is presented in Fig. 6.5. The obtained isotherm demonstrates that the adsorbed volume increases with increasing relative pressure and it gives an isotherm of type III. The pore size distribution of the zeolite is calculated by the adsorption isotherm using the BJH model as depicted in Fig. 6.6. This plot proves that the pore size of zeolite is in the mesoporous range. It is observed that the maximum pores are below 20 nm (around 80%). BET surface area and the pore volume of analcime-C zeolite are determined to be 0.329 m^2g^{-1} and 0.0420 mL g^{-1}, respectively.

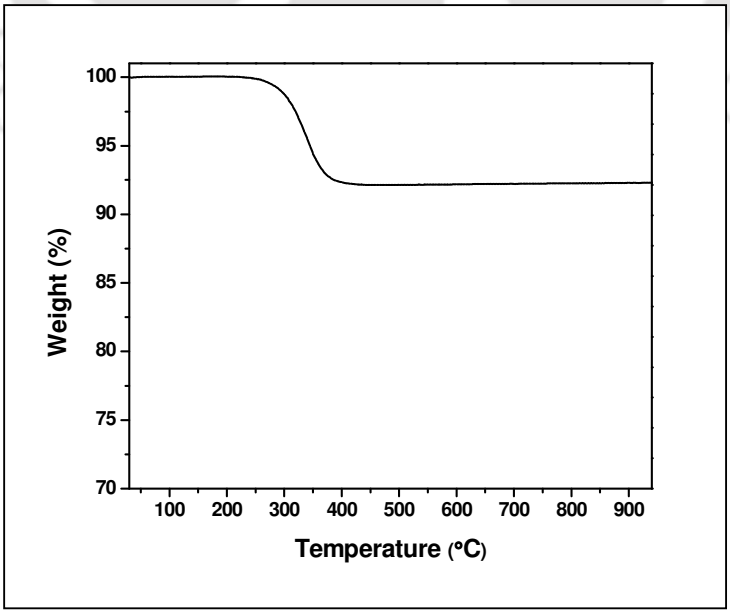

Fig. 6.4 Thermogravimetric analysis of as synthesized analcime-C zeolite powder.

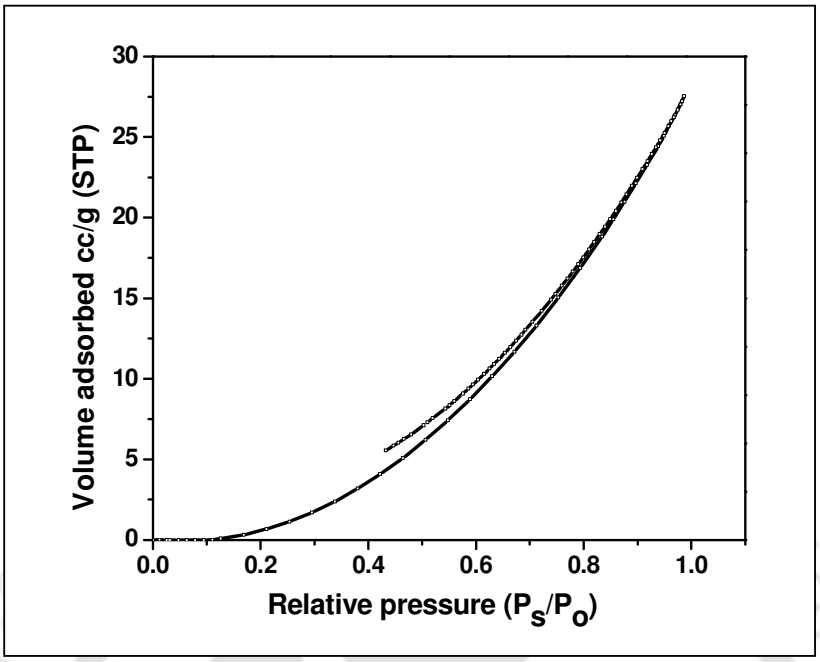

Fig. 6.5 N_2 adsorption-desorption isotherm of analcime-C zeolite powder.

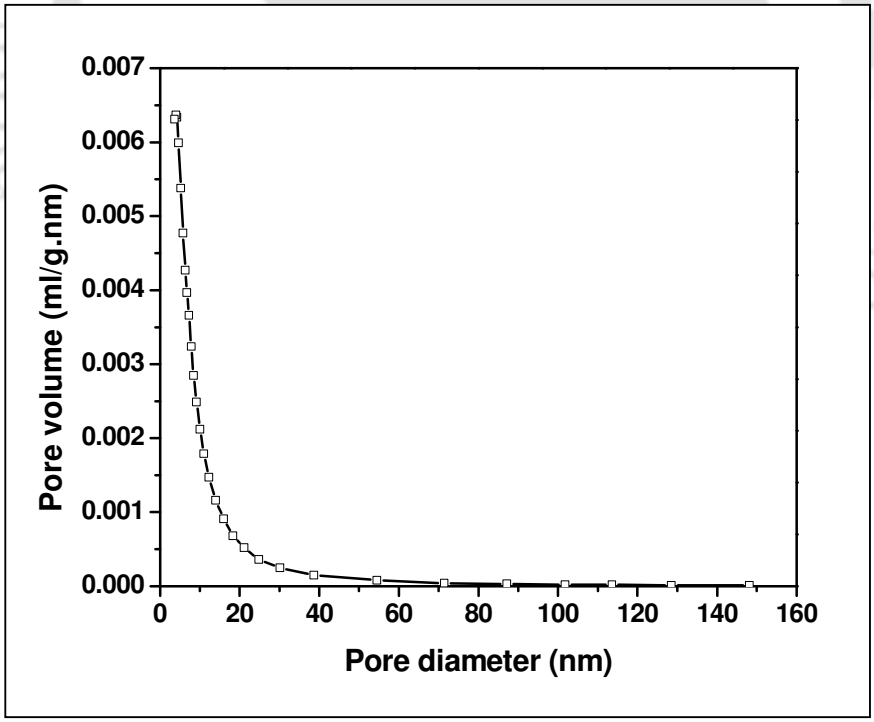

Fig. 6.6 BJH pore size distribution of analcime-C zeolite powder

6.3.2 Characterization of analcime-C zeolite membrane

The point of zero charge measurement of the composite membrane was performed at various pH (2-12) and the obtained result is illustrated in Fig. 6.7. The surface of the membrane changes its polarization according to the pH of the solution and the pH_{PZC} of the composite membrane. In the present work, the PZC of the composite membrane is found to be pH 5.6. At pH values below the point of zero charge (pH_{PZC}), the membrane surface is positively charged and the pH values higher than the (pH_{PZC}), the membrane surface is negatively charged.

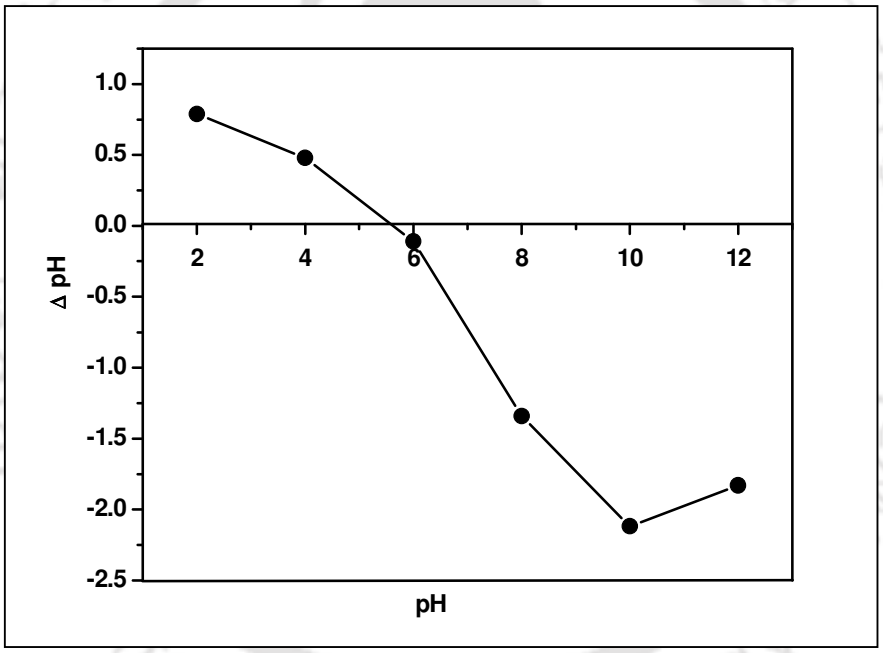

Fig. 6.7 Point of zero charge measurement for composite membrane.

Figure 6.8 (a) shows the FESEM image of the fabricated membrane support and it is apparent that the membrane support is highly porous and crack free. Fig. 6.8(b) demonstrates that the zeolite crystals are spherical in shape with sizes ranging between 15 and 20 µm. Fig. 6.8(c-e) depicts the surface images of analcime-C zeolite ceramic composite membranes with multiple cycle of coatings (1-3). It is evident that the zeolite particles adhered more with repeated coatings. Fig. 6.8(f) displays the cross-sectional view of the zeolite membrane. It

indicates that the pores of the ceramic support are roofed with a dense film of zeolite and the typical structure of the zeolite is observable at higher magnification. Hence, it can be concluded that the analcime-C is formed on the surface of membrane support.

The hydraulic permeability is estimated from the fundamental theory of porous membranes. Further, the average pore radius of the membrane is determined using the following expression (Vasanth, 2011):

$$r = \left[\frac{8 \mu l L_h}{\varepsilon} \right]^{0.5} \tag{6.2}$$

where, μ is the viscosity of water, l is the pore length, L_h is the permeability of the membrane, and ε is the porosity of the membrane. Table 6.1 presents the characterization results of analcime-C zeolite ceramic composite membranes with different coatings. As expected, the membrane porosity decreases with increasing the number of coatings. The sequential reduction in pore size of the membrane is because of deposition of zeolite on the membrane surface. The deposition gradually decreases with an increase in the number of coating cycles (Table 6.1). After third coating, there was no significant amount of weight increment. Therefore, coating was stopped and the prepared membrane was applied for the removal of Cr (VI).

Table 6.1 Characterization results of analcime-C ceramic composite membranes

Membranes	Porosity	Average pore size (µm)	Water permeability ($m^3m^{-2}.s^{-1}.kPa^{-1}$)	Weight increment (g)
Ceramic support	47	1.00	3.63×10^{-6}	-
Coating 1	38	0. 285	2.18×10^{-7}	1.058
Coating 2	26	0. 170	5.88×10^{-8}	1.668
Coating 3	24	0. 155	4.53×10^{-8}	1.883

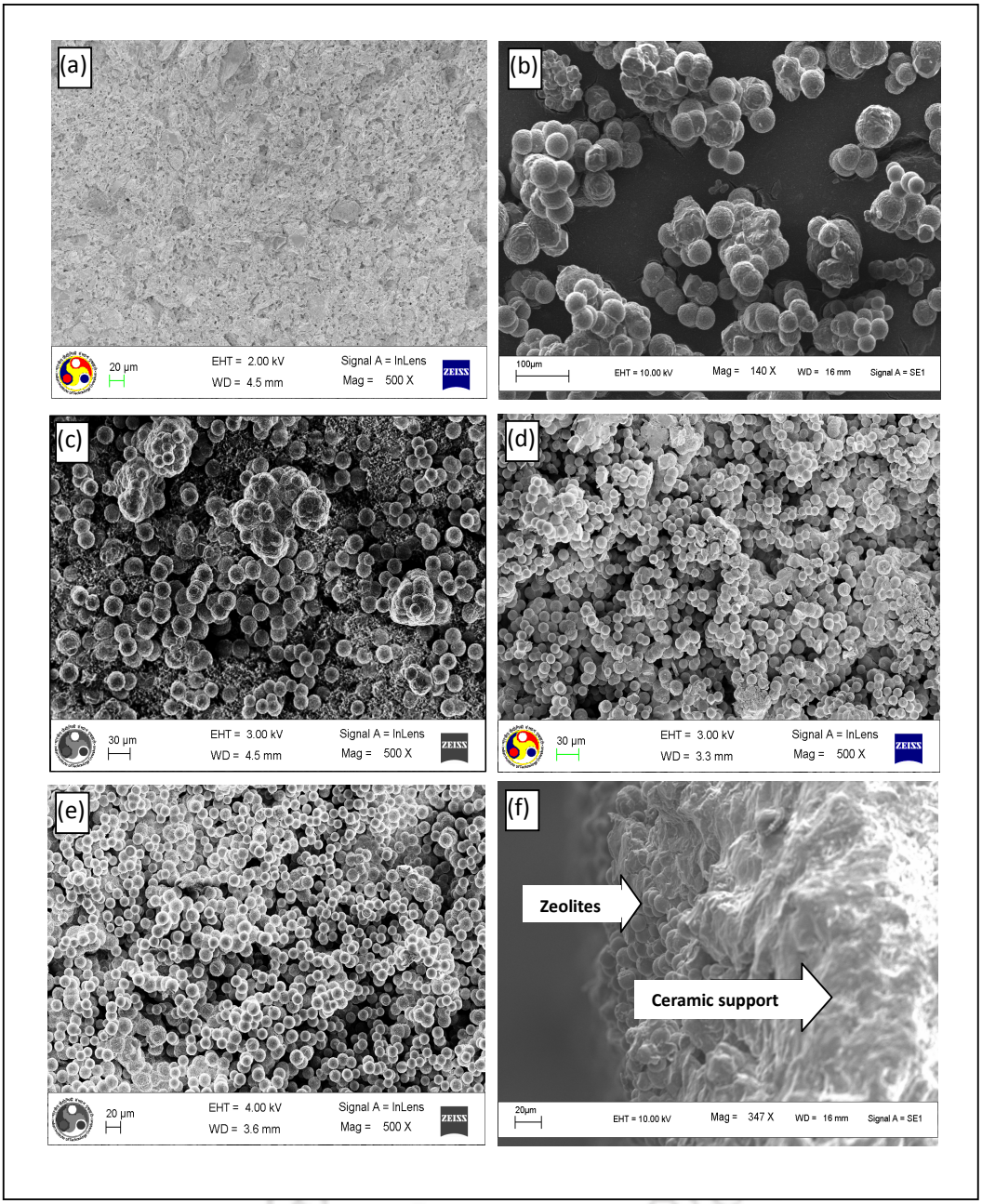

Fig. 6.8 (a) Ceramic support, (b) analcime-C zeolite particles, (c-e) Images of the prepared composite membrane with different coating (1-3), and (f) Cross sectional view of analcime-C zeolite composite membrane.

Figure 6.9 depicts the variation of water flux with applied pressure for the support and zeolite membranes. As expected, the water flux increases linearly with an increase in the applied pressure for all the membranes. It is also observed that the water flux of the composite

membrane decreases with increasing the number of coatings. This illustrates the reduction in pore size and porosity (Table 6.1), which results in decreased hydraulic permeability of analcime-C zeolite composite membrane. The pure water permeability of support, the once-coated, twice-coated and thrice-coated composite membrane is found to be 3.63×10^{-6}, 2.18×10^{-7}, 5.88×10^{-8}, and 4.53×10^{-8} $m^3m^{-2}.s^{-1}.kPa^{-1}$, respectively.

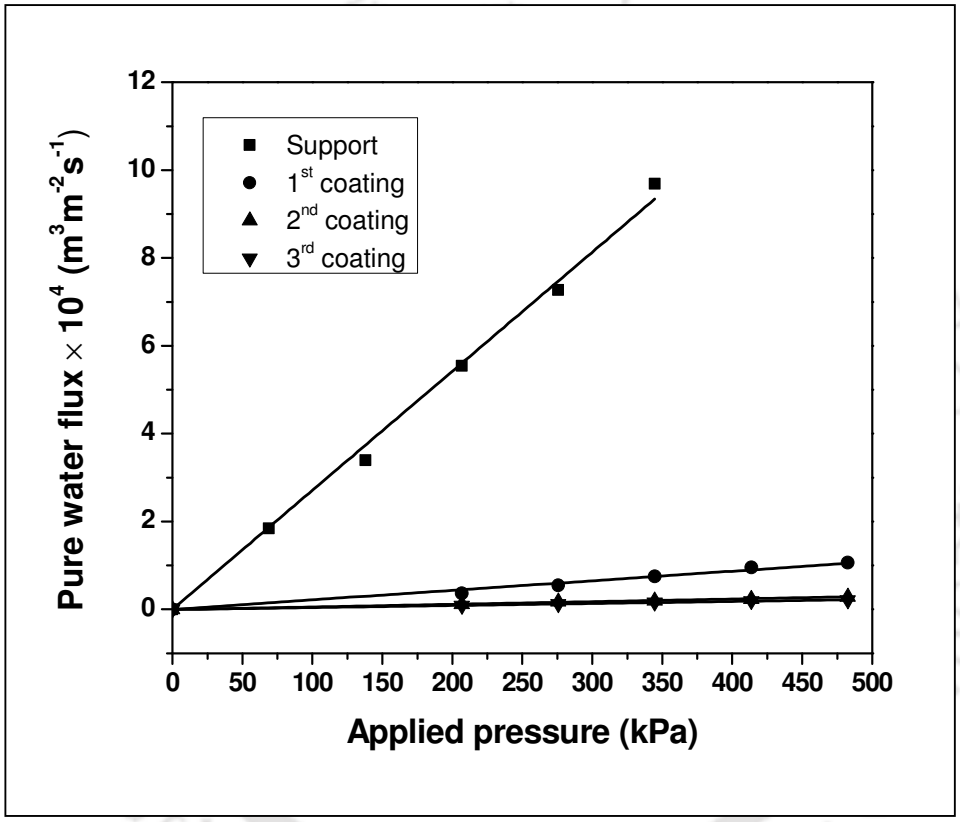

Fig. 6.9 Variation of water flux for ceramic support and zeolite ceramic composite membranes with respective coatings

6.3.3 Chromium removal from aqueous solution

Studies on Cr (VI) removal using the synthesized, thrice-coated membrane demonstrate that the applied pressure, Cr (VI) concentration, solution pH and membrane charge have significant influence on the separation efficiency.

6.3.3.1 Effect of applied pressure

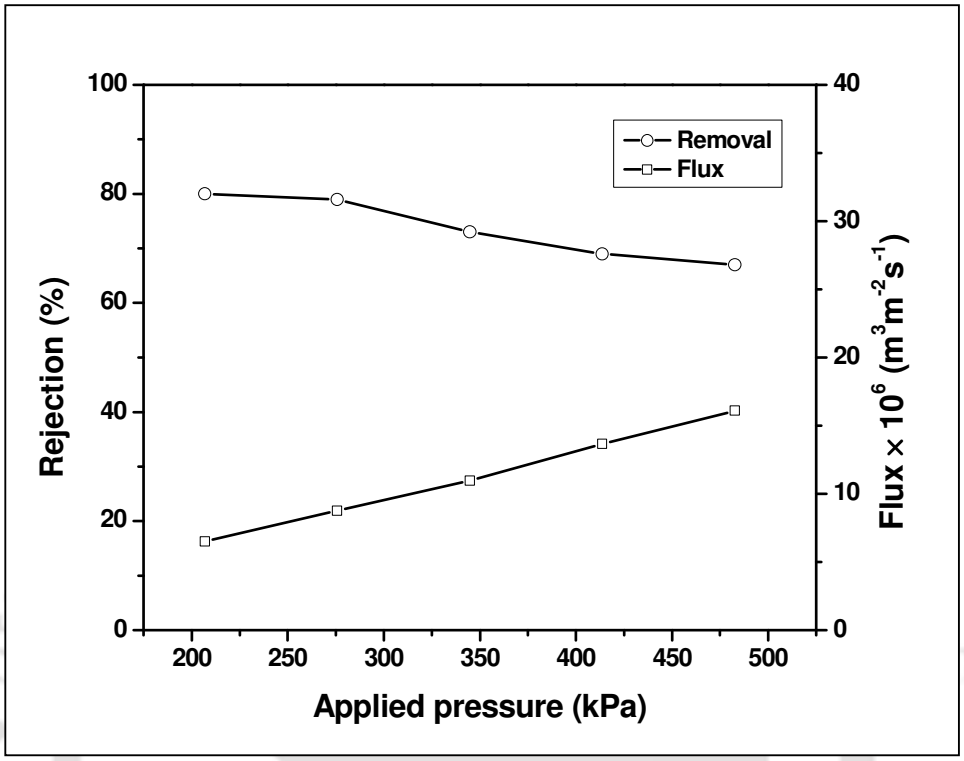

Fig. 6.10 Effect of applied pressure on the permeate flux and rejection of Cr (VI) (Feed concentration = 1000 ppm, pH = 2.35).

The flux and retention behavior of Cr (VI) with applied pressure are shown in Fig. 6.10. Concentration and pH of the Cr (VI) solution used in this study are 1000 ppm and 2.35, respectively. The effect of applied pressure on the permeate flux and Cr (VI) removal was studied in the range of 207-483 kPa. It can be seen that the permeate flux increases with increasing applied pressure. However, the permeate flux is lower than that of pure water flux. This indicates that the existence of chromate ions causes an extra restriction (concentration polarization) to the flow of solvent. The observed rejection decreases with increasing applied pressure. This shows that the concentration polarization effect is a large and substantial loss of efficiency (Shukla and Kumar 2007). Apart from applied pressure, other parameters such as charge density, solute concentration and interaction of membrane

surface charges with ionic solutes, play an important role in determining the rejection. However, concentration polarization effects cannot be ignored and can lead to a considerable loss.

6.3.3.2 Effect of feed concentration

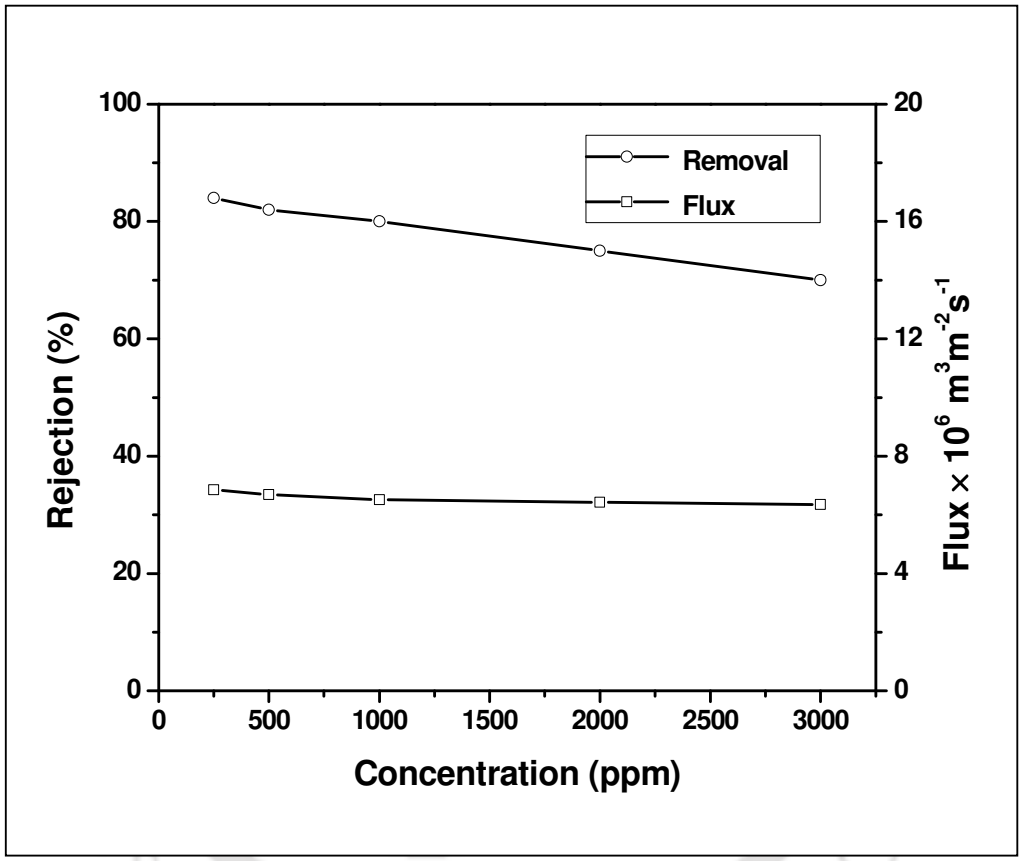

Fig. 6.11 Effect of concentration on the permeate flux and rejection of Cr (VI) (applied pressure = 207 kPa; pH = 2.35).

The effect of feed concentration of Cr (VI) on the permeate flux and rejection was measured at a constant pressure of 207 kPa and pH of 2.35. It is evident from the Fig. 6.11 that the flux declines to some extent with an increase of feed concentration. This is due to the concentration polarization and partial plugging of the membrane at higher concentration. The rejection values obtained at these concentrations also demonstrate that the observed rejection

decreases with increasing the feed concentration. This is a typical characteristic of charged membranes, for which Donnan exclusion plays a vital role (Cabatingan 2001). With increasing Cr (VI) concentration, the effect of Donnan exclusion declines and also the surface concentration increases, which leads to the harsh concentration polarization. Consequently, the solute permeation by diffusion increases and hence the permeate concentration also raises.

6.3.3.3 Effect of pH

Generally, chromium exits in two oxidation forms, Cr (VI) and Cr (III). In aqueous solution, Cr (VI) species are dissociated in following forms (Benhamou *et al*., 2013):

$$H_2CrO_4 + H_2O \rightleftharpoons HCrO_4^- + H_3O^+ \qquad pK_1 = -0.5$$

$$HCrO_4^- + H_2O \rightleftharpoons CrO_4^{2-} + H_3O^+ \qquad pK_2 = 5.8$$

$$2HCrO_4^- \rightleftharpoons Cr_2O_7^{2-} + H_2O \qquad pK_3 = 2.2$$

$HCrO_4^-$ dominates in the pH range of 0 to 5.8 except that above a certain Cr (VI) concentration (~10^{-3} M) it coexists with $Cr_2O_7^{2-}$; at pH > 8, Cr (VI) exists only as CrO_4^{2-}.

In general, the surface charge of the membrane depends on the pH of the solution (Chung *et al*., 2005). It is especially a key factor to recognize the efficiency of a membrane separation process during removal of ionic species. In this context, the rejection was measured over the range of pH (2.3-11) for a fixed concentration of Cr (VI) (1000 ppm), at an applied pressure of 207 kPa. Fig. 6.12 depicts the observed rejection as a function of pH. The result shows that the removal is strongly dependent on the working pH and the highest rejection is obtained at pH = 2.3. Since the point of zero charge (PZC) of the composite membrane is 5.6 (see Fig. 6.7), the membrane is positively charged at pH < 5.6 and negatively charged at pH > 5.6. While the charged membrane is in contact with chromium solution, the concentration of ions

with the same charge as the membrane will be lower at near the surface of the membrane than that in the solution, and the other ions, which have the opposite charge, have a higher concentration in the membrane than in the solution. On account of this concentration difference, a potential difference is generated at the interface between the membrane and the solution to maintain electrochemical equilibrium between solution and membrane. With this potential, the membrane repels the ions with same charge as the membrane (Chung *et al*., 2005). When the pH of the solution increases from 2 to 5.6, the magnitude of membrane charges (positive) declines and this is evidenced from the decrease of ΔpH value as shown in Fig. 6.7. As a result, the repulsion between the positively charged membrane and positive species (H_3O^+) decreases and the rejection reduces from 80%. Because the cation and anion cannot act independently, hence, $HCrO_4^-$ is also rejected to maintain electroneutrality. Upon increasing the pH of the solution from 5.6 to 11 by adding NaOH, OH^- ions are accumulated on the membrane surface. Accordingly, the membrane acquires a greater negative charge while in contact with the feed. It is noteworthy to mention that when the pH increases, the CrO_4^{2-} concentration also increases compared to $HCrO_4^-$. As the pH increases from 5.6 to 11, the magnitude of membranes charge (negative) also increases as evidenced from Fig. 6.7 and hence, the higher surface charge (negative) leads to increase the intensity of the electrostatic repulsion between ions present in the solution (CrO_4^{2-}, $Cr_2O_7^{2-}$) and the membrane surface. This explains an increase of rejection with increasing pH from 5.6 to 11.

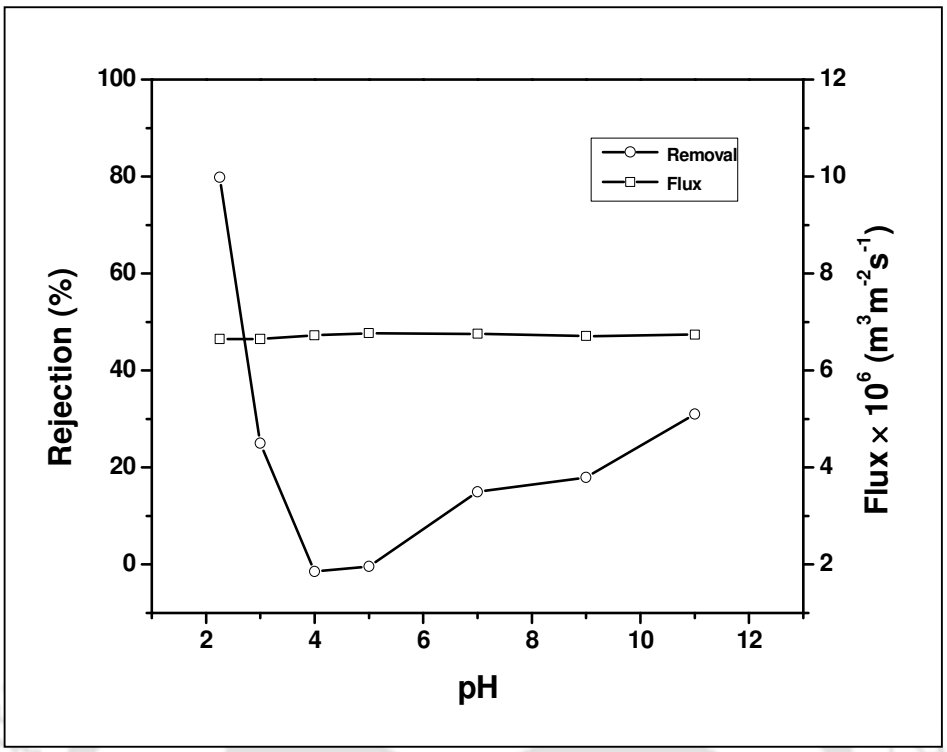

Fig. 6.12 Effect of pH on the permeate flux and rejection of Cr (VI) (applied pressure = 207 kPa; concentration = 1000 ppm).

6.3.3.4 Performance comparison of the prepared membrane with other membranes

It is apparent from Table 6.2, that the rejection (80%) reported in this work at a lower applied pressure of 207 kPa with Cr (VI) concentration of 1000 ppm is comparable or even better than those described in literature. Moreover, a maximum rejection of 84% is obtained with Cr (VI) concentration of 250 ppm at 207 kPa. In the work reported by Pugazhenthi *et al.*, (2005), the carbon composite membrane demonstrated 96% rejection of Cr (VI) with permeate flux of 1.464×10^{-8} ($m^3m^{-2}s^{-1}$) for a chromium concentration of 1000 ppm (Table 6.2). In other work by Sachdeva *et al.*, (2008), around 90% rejection with 1.464×10^{-8} ($m^3m^{-2}s^{-1}$) permeate flux was obtained for styrene acrylonitrile composite membrane. In comparison with results described in the literature, the permeate flux of the membrane (5.96×10^{-6} $m^3m^{-2}s^{-1}$) is higher

even at lower operating pressure of 207 kPa. From the comparison study, it can be concluded that the synthesized membrane is better than the other membranes reported in the literature.

Table 6.2 Rejection comparison of other membranes with prepared membrane

Membrane Material	Pore size	Feed concentration (ppm)	Solute permeability (ms^{-1})	Rejection (%)	Reference
PMMA–EGDM	8.5 kDa	1000	5.96×10^{-10}	68	Neelakandan *et al.*, 2003
Zeolite-clay membrane	30 nm	1000	2.73×10^{-6}	66	Shukla and Kumar 2007
Styrene acrylonitrile	55 nm	1000	2.38×10^{-6}	90	Sachdeva and Kumar 2008
Clay-carbon	2 nm	1000	1.46×10^{-8}	96	Pugazhenthi *et al.*, 2005
Analcime-C Ceramic	**155 nm**	**1000**	**5.96×10^{-6}**	**80**	**Present work**

6.4 Summary

An analcime-C zeolite composite membrane has been successfully fabricated through an in situ hydrothermal crystallization technique over a ceramic support. FESEM images show that the zeolite particles adhere more on the surface of the membrane with repeated coatings. The porosity, average pore size and water permeability of the composite membrane (3 times coated) are found to be 24%, 155 nm and 4.53×10^{-8} $m^3m^{-2}s^{-1}$.kPa, respectively. Overall results suggest that membrane morphology, porosity, average pore size, and pure water permeability of the prepared zeolite membrane vary significantly by the repeated coating on ceramic support. The thrice-coated membrane has been used for the chromium removal with in-house made dead end UF setup at room temperature and the performance of the membrane has been investigated for the effect of several parameters: applied pressure, feed concentration and pH. The highest separation (84%) is achieved for pH 2.35 with the

permeate flux of 6.85 × 10^{-6} $m^3m^{-2}s^{-1}$ at 207 kPa and feed concentration of 250 ppm. The separation test displays that the membrane has high removal efficiency for Cr (VI) from an aqueous solution and is comparable to those reported in literature.

Chapter 7

Conclusions and Scope for Future Work

Conclusions and Scope for Future Work

This chapter summarizes the inference drawn from the present research work and provides some suggestion towards future direction of research. The main theme of this thesis is the fabrication and characterization of zeolite-ceramic composite membranes for the separation of metal ions from aqueous solution. The prepared zeolite composite membranes possessed desired characteristics for liquid phase separation applications. The performance of zeolite composite membranes was investigated by the separation of chromium and trivalent metals from aqueous solution. In the study, a number of remarkable issues have been explored that are associated with materials and surface science. These observations are highlighted in the following section.

7.1 Conclusions

- A facile uniaxial compaction method was employed to fabricate circular shaped ceramic support using cheaper clay materials.
- MCM-41, MCM-48, FAU and Analcime-C zeolite ceramic composite membrane are successfully synthesized on a low cost circular shaped ceramic support by hydrothermal crystallization method.
- Porosity and pore size of the ceramic support are reduced from 47 to 23, 22, 33, 24% and 1.0 to 0.173, 0.142, 0.153, 0.155 μm by the deposition of MCM-41, MCM-48, FAU, Analcime-C zeolite, respectively.
- Solvent permeation studies confirm that permeation of solvents through the zeolite composite membranes is influenced by chemical nature of the solvents.

- Fabricated zeolite composite membranes are investigated for the separation of Cr (VI) from aqueous solution using both batch and cross flow filtration set-up. Highest rejection of 80, 81, 83 and 80% is observed with MCM-41, MCM-48, FAU and Analcime-C zeolite composite membranes in dead-end flow mode at an applied pressure of 207 kPa for the feed concentration of 1000 ppm and pH 2. The prepared composite membranes have two to four order of higher solute flux in comparison with other membranes reported in literature. This confirms that the composite membranes have the potential for liquid phase separation applications.

- There is no concentration polarization and permeate flux decline trend observed in the cross flow mode operation for the removal of Cr (VI) by zeolite membranes. Highest Cr (VI) rejection of 82% is observed with FAU zeolite composite membrane in the cross flow operation. MCM-48 and MCM-41 zeolite composite membrane display the maximum Cr (VI) rejection of 77 and 75%, respectively.

- In the batch filtration study, the maximum rejection of $AlCl_3$ is found to be 82 and 81% for MCM-41 and MCM-48-ceramic composite composite membranes, respectively at an applied pressure of 276 kPa with feed concentration of 250 ppm and pH 1.5. For $FeCl_3$ separation, the highest rejection of 83 and 85% is observed with MCM-41 and MCM-48 membrane, respectively at an applied pressure of 276 kPa for the feed concentration 250 ppm and pH 2. FAU zeolite composite membrane demonstrates 81 and 75% rejection for $FeCl_3$ and $AlCl_3$, respectively at an applied pressure of 276 kPa for the feed concentration of 250 ppm and pH 2.

- In cross flow ultrafiltration, the flux decline is not observed during the separation of $AlCl_3$ and $FeCl_3$ with MCM-41, MCM-48, and FAU zeolite composite membranes. FAU zeolite membrane displays the utmost rejection of 88 and 83% for $FeCl_3$ and

$AlCl_3$, respectively in the cross flow ultrafiltration with the feed concentration of 250 ppm and pH 2. The MCM-48 membrane demonstrates 87 and 83% rejection of $FeCl_3$ and $AlCl_3$, respectively, whereas the rejection of MCM-41 membrane is found to be 86 and 82% for $FeCl_3$ and $AlCl_3$, respectively for the feed concentration of 250 ppm.

- Among the investigated zeolite composite membranes (MCM-41, MCM-48, FAU and Analcime-C), FAU zeolite composite membrane is the best due to the following advantages: higher separation efficiency, requirement of lesser synthesize time (24 h) and temperature (75 °C), no calcination step required and the cost of raw materials used is lower, that leads to the reduction of fabrication cost.

7.2 Future scope

Based on the outcome of this thesis work, some recommendations for the future direction of research in this field are presented as follows:

- This work can be extended for the separation of other heavy metals such as lead, zinc, nickel, cadmium from aqueous solution in cross flow mode of operation and also can be extended for the treatment of real industrial effluent.

- Development of tubular shaped ceramic support by extrusion technique and synthesis of zeolite layers on the support and its application in the removal of protein and heavy metals.

Agrafiotis, C. and Tsetsekou, A., 2002. Deposition of Mesoporous γ-Alumina Coating on ceramic Honeycomb by Sol-Gel Methods, *Journal of the European Ceramic Society*, **22,** 423-434**.**

Aksay, I. A., Trau, M., Honma, I., Yao, N., Zhou, L., Fenter, P., Eisenberger, P. M. and Grunner, S. M., 1996. Biomimetic Pathways for Assembling Inorganic Thin Films, *Science,* **273** 892-898.

Alem, A., Sarpoolaky, H. and Keshmiri, M., 2009. Sol-Gel Preparation of Titania Multilayer Membrane for Photocatalytic Applications, *Ceramic International*, **35** 1837-1843.

Almandoz, M. C., Marchese, J., Pradanos, P., Palacio, L. and Hernandez, A., 2004. Preparation and Characterization of Non-Supported Microfiltration Membranes from Aluminosilicates, *Journal of Membrane Science*, **241** 95-103.

Alonso, A. I., Urtiaga, A. M., Irabien, A. and Ortiz, M. I., 1994. Extraction of Cr (VI) with Aliquat 336 in Hollow Fiber Contactors: Mass Transfer Analysis and Modeling, *Chemical Engineering Science*, **49** 901-909.

Al-Rashdi, B. A. M., Johnson, D. J. and Hilal, N., 2013. Removal of Heavy Metal Ions by Nanofiltration, *Desalination*, **315** 2-17.

Amanipour, M., Safekordi, A., Babakhani, E. G., Zamaniyan, A. and Heidari, M., 2012. Effect of Synthesis Conditions on Performance of a Hydrogen Selective Nano-Composite Ceramic Membrane, *International Journal of Hydrogen Energy*, **37**, 15359-15366.

Anderson, M. A., Gieselmann, M. J. and Xu, Q., 1998. Titania and Alumina Ceramic Membranes, *Journal of Membrane Science*, **39** 243-258.

Aroua, M. K., Zuki, F. M. and Sulaiman, N. M., 2007. Removal of Chromium Ions from Aqueous Solutions by Polymer Enhanced Ultrafiltration, *Journal of Hazardous Materials*, **147** 752-758.

References

Arthanareeswaran, G., Thanikaivelan, P., Jaya, N., Mohan, D. and Raajenthiren, M., 2007. Removal of Chromium from Aqueous Solution using Cellulose Acetate and Sulfonated Poly (Ether Ether Ketone) Blend Ultrafiltration Membranes, *Journal of Hazardous Materials*, **139** 44-9.

Baker, R. H., 2004. Membrane Technology and Applications, Second Edition, John Wiley and Sons Ltd, Chichester, England.

Beck, J. S., Vartuli, J. C., Roth, W. J., Leonowicz, M. E., Kresge, C. T., Schmidtt, K. D., Chu, C. T. W., Olson, D. H., Sheppard, E. W., McCullen, S. B., Higgins, J. B. and Schlenker, J. L., 1992. A new Family of Mesoporous Molecular Sieves Prepared with Liquid Crystal Templates, *Journal of American Chemical Society*, **114** 10834-10843.

Benhamou, A., Basly, J. P., Baudu, M., Derriche, Z. and Hamacha, R., 2013. Amino-Functionalized MCM-41 and MCM-48 for the Removal of Chromate and Arsenate, *Journal of Colloid and Interface Science*, **404** 135-139.

Bhanushali, D., Kloos, S., Kurth, C. and Bhattacharyya, D., 2001. Performance of Solvent-Resistant Membranes for Non-Aqueous System: Solvent Permeation Results and Modeling, *Journal of Membrane Science*, **189** 1-21.

Bissett, H., Zah, J. and Krieg, H. M., 2008. Manufacture and Optimization of Tubular Ceramic Membrane Supports, *Powder Technology*, **181** 57-66.

Bouzerara, F., Harabi, A., Achour, S. and Larbot, A, 2006. Porous Ceramic Supports for Membranes Prepared from Kaolin and Doloma Mixtures, *Journal of the European Ceramic Society*, **26** 1663-1671.

Bowen, W. R. and Mukhtar, H., 1997. Characterization and Prediction of Separation Performance of Nanofiltration Membranes, *Journal of Membrane Science*, **112** 263-274.

Burggaraaf, A. J. and Cot, L., 1996, Fundamentals of Inorganic Membranes, Elsevier, Amsterdam, The Netherlands.

Cabatingan, L. K., Agapay, R. C., Rakels, J. L. L., Ottens, M. and Wielen, L. A. M. V., 2001. Potential of Biosorption for the Recovery of Chromate in Indusrial Wastewaters, *Industrial Engineering Chemical Research,* **10** 2302-2309.

Cassano, A., Drioli, E., Molinari, R. and Bertolutti, C., 1996. Quality Improvement of Recycled Chromium in Tanning Operation by Membrane Process, *Desalination*, **108** 193-203.

Chen, J., Li, J., Han, X. and Chen, C., 2010. Effect of PEG Additives on properties and Morphologies of Polytherimide Membranes Prepared by Phase Inversion, *Frontiers of Chemical Engineering in China*, **4** 300-306.

Cheryan, M., 1998, Ultrafiltration and Microfiltration Handbook, Technomic Publishing Co. Inc. Lancaster, Pennsylvania.

Choksi, P. M. and Joshi, V. Y., 2007. Adsorption Kinetic Study for the Removal of Nickel (II) and Aluminum (III) from an Aqueous Solution by Natural Adsorbents, *Desalination,* **208,** 216-231.

Chowdhury, S. R., Schmuhl, R., Keizer, K., Elshof, J. E., T. and Blank, D. H. A., 2003. Pore Size and Surface Chemistry Effects on the Transport of Hydrophobic and Hydrophilic Solvents through Mesoporous γ-Alumina and Silica MCM-48, *Journal of Membrane Science*, **225** 177-186.

Chung, C. V., Buu, N. Q. and Chau, N. H., 2005. Influence of Surface Charge and Solution pH on the Performance Characteristics of a Nanofiltration Membrane, *Science and Technolology of Advance Materirals*, **6** 246-250.

Çifci, C. and Kaya, A., 2010. Preparation of Poly(Vinyl Alcohol)/Cellulose Composite Membranes for Metal Removal from Aqueous Solutions, *Desalination*, **253**, 175-179.

Covarrubias, C., Garcia, R., Arriagada, R., Yanez, J., Ramanan, H., Lai, Z. and Isapatsis, M., 2008. Removal of Trivalent Chromium Contaminant from Aqueous Media using FAU-type Zeolite Membranes, *Journal of Membrane Science*, **312** 163-173.

Cui, J., Zhang, X., Liu, H., Liu, S. and Yeung, K. L., 2008. Preparation and Application of Zeolite/Ceramic Microfiltration Membranes for Treatment of Oil Contaminated Water, *Journal of Membrane Science*, **325** 420-426.

Çulfaz, P. Z., Çulfaz, A. and Kalıpçılar, H., 2006. Preparation of MFI type Zeolite Membranes in a Flow System with Circulation of the Synthesis Solution, *Microporous and Mesoporous Materials*, **92** 134-144.

Danis, U. and Keskinler, B., 2009. Chromate Removal from Wastewater using Micellar Enhanced Crossflow Filtration: Effect of Transmembrane Pressure and Cross Flow Velocity, *Desalination*, **249** 1356-1364.

Das, D. P., Parida, K. M. and De, B. R., 2006. Photo Catalytic Reduction of Hexavalent Chromium in Aqueous Solution over Titania Pillared Zirconium Phosphate and Titanium Phosphate under Solar Radiation, *Journal of Molecular Catalysis A: Chemical,* **245** 217-224.

Deere, J., Magner, E., Wall, J. G. and Hodnett, B. K., 2002. Mechanistic and Structural Features of Protein Adsorption onto Mesoporous Silicates, *Journal of Physical Chemistry B*, **106** 7340-7347.

Dong, Y., Feng, X., Dong, D., Wang, S., Yang, J., Gao, J., Liu, X. and Meng, G., 2007. Elaboration and Chemical Corrosion Resistance of Tubular Macro-Porous Cordierite Ceramic Membrane Supports, *Journal of Membrane Science*, **304** 65-75.

Fabiani, C., Ruscio, F., Spadoni, M. and Dizzichini, M., 1996. Chromium (III) Salts Recovery Process from Tannery Wastewater, *Desalination*, **108** 183-191.

Falamaki, C., Afarani, M. S. and Aghaie, A., 2004. Initial Sintering Stage Pore Growth Mechanism Applied to the Manufacture of Ceramic Membrane Supports, *Journal of the European Ceramic Society*, **24** 2285-2292.

Frenzel, I., Holdik, H., Stamatialis, D. F., Pourcelly, G. and Wessling, M., 2005. Chromic Acid Recovery by Electro-Electrodialysis. I. Evaluation of Anion-Exchange Membrane, *Journal of Membrane Science*, **261** 49-57.

Galan, B., Castaneda, D. and Ortiz, I., 2005. Removal and Recovery of Cr(VI) from Polluted Ground Waters: A Comparative Study of Ion-Exchange Technologies, *Water Research*, **39** 4317-4324.

Gao, L., Xu, W., Chen, L. and Xiao, G., 2014. In-Situ Synthesis of MCM-41 on Ceramic Membranes and its Application in Transesterification as Catalyst Support for P-Toluenesulfonic Acid, *Journal of Porous Materials*, **21** 667-675.

Garg, V. K., Gupta, R., Kumar, R. and Gupta, R. K., 2004. Adsorption of Chromium from Aqueous Solution on Treated Sawdust, *Bioresource Technology,* **92** 79-81.

Georgiev, D., Bogdan B., Angelova, K., Markovska, I. and Hristov, Y., 2009. Synthetic Zeolites-Structure, Classification, Current Trends in Zeolites Synthesis Review, *International Science conference*, Stara Zagora, Bulgaria.

Ghaderi, M. J., Afarani, M. S. and Roudini, G., 2013. Synthesis of Alumina Porous Supports via different Compaction Routes: Vibration and Pressing, *Journal of Chemical Technology and Metallurgy*, **48** 289-295.

Gherasim, C. V. and Mikulasek, P., 2014. Influence of Operating Variables on the Removal of Heavy Metal Ions from Aqueous Solutions by Nano Filtration, *Desalination*, **343** 67-74.

Golder, A. K., Chanda, A. K., Samanta, A. N. and Ray, S., 2011. Removal of Hexavalent Chromium by Electrochemical Reduction-Precipitation: Investigation of Process Performance and Reaction Stoichiometry, *Separation and Purification Technology*, **76** 345-350.

Guillou, F., Rouleau, L., Pirngruber, G. and Valtchev, V., 2009. Synthesis of FAU-type Zeolite Membrane: An Original in Situ Process Focusing on the Rheological Control of Gel-like Precursor Species, *Microporous and Mesoporous Materials*, **119** 1-8.

Gzara, L. and Dhabi, M., 2001. Removal of Chromic Anions by Micellar-Enhanced Ultrafiltration using Cationic Surfactants, *Desalination*, **137** 241-250.

Haarberg, G. M. and Keppert, M., 2008. Diffusion Kinetics for the Electrochemical Reduction of Fe (III) Species in Molten NaCl-$FeCl_3$, *The Electrochemical Society*, **2**(49) 3000.

Hafez, A. and Maharawy, S.-El., 2004. Design and Performance of Two-Stage/Two-Pass RO Membrane System for Chromium Removal from Tannery Wastewater. Part 3, *Desalination*, **165** 141-151.

Hafiane, A., Lemordant, D. and Dhabi, M., 2000. Removal of Hexavalent Chromium by Nanofiltration, *Desalination*, **130** 305-312.

Hamad, B., Alshebani, A., Pera-Titus, M., Wang, S., Torres, M., Albela, B., Bonneviot, L., Miachon, S. and Dalmon, J. A., 2008. Synthesis and Characterization of Nanocomposite MCM-41 ('LUS') Ceramic Membranes, *Microporous and Mesoporous Materials*, **115** 40-50.

Han, X., Shan, Y., Ming, W., Wong, H. and Tam, N. F. Y., 2007. Biosorption and Bioreduction of Cr (VI) by a Microalgal Isolate, Chlorella Miniata, *Journal of Hazardous Material*, **146**, 65-72.

Hao, Y., Li, J., Yang, X., Wang, X. and Lu, L., 2004. Preparation of ZrO_2-Al_2O_3 Composite Membranes by Sol-Gel Process and their Characterization, *Material Science and Engineering*, A **367**, 243-247.

Hasegawa, Y., Abe, C., Nishioka, M., Sato, K., Nagase, T. and Hanaoka, T., 2010. Formation of High Flux CHA-type Zeolite Membranes and their Application to the Dehydration of Alcohol Solutions, *Journal of Membrane Science*, **364** 318-324.

Hsieh, H. P., 1996, Inorganic Membranes for Separation and Reaction, Elsevier, Amsterdam, The Netherlands.

Huang, A., Wang, N. and Caro, J., 2012. Seeding-Free Synthesis of Dense Zeolite FAU Membranes on 3-Aminopropyltriethoxysilane-Functionalized Alumina Supports, *Journal of Membrane Science*, **389** 272-279.

Huang, B., Liu, Q., Caro, J. and Huang, A., 2014. Iso-Butanol Dehydration by Pervaporation using Zeolite LTA Membranes Prepared on 3-Aminopropyltriethoxysilane-Modified Alumina Tubes, *Journal of Membrane Science*, **455** 200-206.

Hui, K. S. and Chao, C. Y. H., 2006. Synthesis of MCM-41 from Coal Fly Ash by a Green Approach: Influence of Synthesis PH, *Journal of Hazardous Materials*, *B* **137** 1135-1148.

Iglesia, O., Pedernera, M., Mallada, R., Lin, Z., Rocha, J., Coronas, J. and Santamaria, J., 2013. Synthesis and Characterization of MCM-48 Tubular Membrane, *Journal of Membrane Science*, **280** 867-875.

Intaraprasit, N. and Kongkachuichay, P., 2011. Preparation and Properties of Sulfonated Poly(ether ether ketone)/Analcime Composite Membrane for a Proton Exchange Membrane Fuel Cell (PEMFC), *Journal of Taiwan Institute of Chemical Engineering*, **42** 190-195.

Jafari, M., Bayat, A., Mohammadi, T. and Kazemimoghadam, M., 2013. Dehydration of Ethylene Glycol by Pervaporation using Gamma Alumina/NaA Zeolite Composite Membrane, *Chemical Engineering Research and Design*, **91** 2412-2419.

Jafarian, M., Mahjani, M. G., Gobal, F. and Danaee, I., 2006. Electrodeposition of aluminum from molten $AlCl_3$-NaCl-KCl mixture, *Journal of Applied Electrochemistry*, **36** 1169-1173.

Jeong, B. H., Hasegawa, Y., Sotowa, K. I., Kusakabe, K. and Morooka, S., 2002. Separation of Mixtures of Benzene and n-Alkanes using an FAU-type Zeolite Membrane, *Journal of Chemical Engineering Japan,* **35** 167-172.

Jeong, B. H., Hasegawa, Y., Sotowa, K.-I., Kusakabe, K. and Morooka, S., 2003. Permeation of Binary Mixtures of Benzene and Saturated C_4-C_7 Hydrocarbons through an FAU-type Zeolite Membrane, *Journal of Membrane Science*, **213** 115-124.

Jia, M. D., Chen, B., Noble, R. D. and Falconer, J. L., 1994. Ceramic-Zeolite Composite Membranes and their Application for Separation of Vapor/Gas Mixtures, *Journal of Membrane Science*, **90** 1-10.

Jia, M. D., Peinemenn, K. V. and Behling, R. D., 1993. Ceramic Zeolite Composite Membranes: Preparation, Characterization and Gas Permeation, *Journal of Membrane Science*, **82** 15-26.

Judd, S. and Jefferson, B. (Eds.), 2003. Membranes for Industrial Wastewater Recovery and Reuse, Elsevier, 102-131.

Kaya, C., He, J. Y., Gu, X. and Butler, E. G., 2002. Nanostructured Ceramic Powders by Hydrothermal Synthesis and their Applications, *Microporous and Mesoporous Materials*, **54** 37-49.

Khemakhem, S., Amar, R. B. and Larbot, A., 2007. Synthesis and Characterization of a New Inorganic Ultrafiltration Membrane Composed Entirely of Tunisian Natural Illite Clay, *Desalination*, **206** 210-214.

Kim, H. J., Jang, K.-S., Galebach, P., Gilbert, C., Tompsett, G., Conner, W. C., Jones, C. W. and Nair, S., 2013. Seeded Growth, Silylation, and Organic/Water Separation Properties of MCM-48 Membranes, *Journal of Membrane Science*, **427** 293-302.

Kim, S. J., Jones, C. W., Nair, S., Liu, Y., Moore, J. S., Dixit, R. S., Pendergast J., J. G. and Sarsani, S., 2015. Ion Exchange of Zeolite Membranes by a Vacuum 'Flow-through' Technique, *Microporous and Mesoporous Materials*, **203** 170-177.

Kimbrough, D. E., Cohen, Y., Winer, A. M., Creelman, L. and Mabuni, C., 1999. A Critical Assessment of Chromium in the Environment, *Critical Review on Environmental Science and Technology*, **29** 1-46.

Kir, E., Cengeloglu, Y. and Ersoz, M., 2005. The effect of chelating agent on the separation of Fe(III) and Ti(IV) from binary mixture solution by cation-exchange membrane, *Journal of Colloid and Interface Science*, **292** 498-502.

Kishore, N., Sachan, S., Rai, K. N. and Kumar, A., 2003. Synthesis and Characterization of a Nanofiltration Carbon Membrane Derived from Phenol-Formaldehyde Resin, *Carbon*, **41** 2961-2972.

Kita, H., Inoue, T., Asamura, H., Tanaka, K. and Okamoto, K., 1997. NaY Zeolite Membrane for the Pervaporation Separation of Methanol-Metylert-Butyl Ether Mixtures, *Chemical Communication*, 45-46.

Koros, W. J., Ma, Y. H. and Shimidzu, T., 1996. Terminology for Membranes and Membrane Processes, *Pure and Applied Chemistry*, **68** 1479-1489.

Kozlowski, C. A. and Walkowiak, W., 2002. Removal of Chromium (VI) from Aqueous Solutions by Polymer Inclusion Membranes, *Water Research*, **36** 4870-4876.

Kresge, C. T., Leonowicz, M. E., Roth, W. J., Vartuli, J. C. and Beck, J. S., 1992. Ordered Mesoporous Molecular Sieves Synthesized by a Liquid-Crystal Template mechanism, *Nature*, **359** 710-712.

Kumar, D., Schumacher, K., Fresne von Hohenesche, C. du, Grün, M. and Unger, K. K., 2001. MCM-41, MCM-48 and Related Mesoporous Adsorbents: their Synthesis and Characterization, *A: Physicochemicl and Engineering Aspects*, **187-188** 109-116.

Kumar, M., Agarwal, S., Pugazhenthi, G., Shukla, A. and Kumar, A., 2006. Preparation and Characterization of Iron Salt Embedded Electrodialysis Analcime-C Zeolite Clay Composite Membrane, *Journal of Membrane Science*, **275** 110-118.

Kumar, P., Ida, J., Guliants, V. V., 2008. High Fflux Mesoporous MCM-48 Membranes: Effects of Support and Synthesis Conditions on Membrane Permeance and Quality, *Microporous and Mesoporous Materials*, **110,** 595-599.

Kumar, P., Ida, J., Kim, S., Guliants, V. V., and Lin, J. Y. S., 2006. Ordered Mesoporous Membranes: Effects of Support and Surfactant Removal Conditions on Membrane Quality, *Journal of Membrane Science*, **279** 539-547.

Lakshminarayanaih, N. 1984. Equations of Membrane Biophysics, Academic Press, New York.

Lakshmipathiraj, P., Bhaskar Raju, G., Raviatul Basriya, M., Parvathy, S. and Prabhakar, S., 2008. Removal of Cr (VI) by Electrochemical Reduction, *Separation and Purification Technology,* **60** 96-102.

Lambert, J., Rakib, M., Durand, G. and Rodriguez, M. A., 2006. Treatment of Solutions Containing Trivalent Chromium by Eletrodialysis, *Desalination*, **191** 100-110.

Li, Y., Chen, H., Liu, J. and Yang, W., 2006. Microwave Synthesis of LTA Zeolite Membranes Without Seeding, *Journal of Membrane Science*, **277** 230-239.

Likhar, M. C. and Shivramwar, M. V., 2013. Removal of Chemical Oxygen Demand (COD) and Color from Dye Manufacturing Industry by Coagulation, *International Journal of Engineering Research and Applications,* ISSN: 2248-9622, **3** 1116-1118.

Lima, P. D. L., Leite, D. S., Vasconcellos, M.C., Cavalcanti, B. C., Santos, R. A., Costa-Lotufo, L. V., Pessoa, C., Moraces, M. O. and Burbano, R. R., 2007. Genotoxic Effects of Aluminum Chloride in Cultural Human Lymphocytes Treated in Different Phases of Cell Cycle, *Food and Chemical Toxicology*, **45** 1154-1159.

Ling, W. S., Thian, T. C. and Bhatia, S., 2011. Synthesis, Characterization and Pervaporation Properties of Microwave Synthesized Zeolite A Membrane, *Desalination*, **277** 383-389.

Liou, T. H., 2011. A Green Route to Preparation of MCM-41 Silicas with Well-Ordered Mesostructure Controlled in Acidic and Alkaline Environments, *Chemical Engineering Journal*, **171** 1458-1468.

Liu, B. S., Tang, D. C. and Au, C. T., 2005. Fabrication of Analcime Zeolite Fibers by Hydrothermal Synthesis, *Microporous and Mesoporous Materials*, **86** 106-111.

Liu, C., Wang, L., Ren, W., Rong, Z., Wang, X. and Wang, J., 2007. Synthesis and Characterization of a Mesoporous Silica (MCM-48) Membrane on a Large-Pore α-Al_2O_3 Ceramic Tube, *Microporous and Mesoporous Materials*, **106** 35-39.

Loganathan, S., Tikmani, M. and Ghoshal, A. K., 2013. Novel Pore-Expanded MCM-41 for CO_2 Capture: Synthesis and Characterization, *Langmuir*, **29** 3491-3499.

Machado, D. R., Hasson, D. and Semiat, R., 1999. Effect of Solvent Properties on Permeates Flow through Nanofiltration Membranes, Part I: Investigation of Parameters Affecting Solvent Flux, *Journal of Membrane Science*, **163** 93-102.

Machado, D. R., Hasson, D. and Semiat, R., 2000. Effect of Solvent Properties on Permeate Flow through Nanofiltration Membranes. Part II: Transport Model, *Journal of Membrane Science*, **166** 63-69.

Maghsoudi, H. and Soltanieh, M, 2014. Simultaneous Separation of H_2S and CO_2 from CH_4 by a High Silica CHA-type Zeolite Membrane, *Journal of Membrane Science*, **470** 159-165.

Majhi, A., Monash, P. and Pugazhenthi G., 2009. Fabrication and Characterization of γ-Al_2O_3-Clay Composite Ultrafiltration Membrane for the Separation of Electrolytes from its Aqueous Solution, *Journal of Membrane Science*, **340** 181-191.

Masmoudi, S., Larbot, A., Feki, H. E. and Amar, R. B., 2007. Elaboration and Characterization of Apatite Based Mineral Supports for Microfiltration and Ultrafiltration Membranes, *Ceramic International*, **33** 337-344.

Matsufuji, T., Nishiyama, N., Matsukata, M. and Ueyama, K., 2000. Separation of Butane and Xylene Isomers with MFI-type Zeolitic Membrane Synthesized by a Vapor-Phase Transport Method, *Journal of Membrane* Science, **178** 25-34.

McCool, B. A., Hill, N., DiCarlo, J. and DeSisto, W. J., 2003. Synthesis and Characterization of Mesoporous Silica Membranes via Dip-Coating and Hydrothermal Deposition Techniques, *Journal of Membrane Science*, **218** 55-67.

Mehiguene, K., Garba, Y., Taha, S., Gondrexon, N., Dorange, G., 1999. Influence of operating conditions on the retention of copper and cadmium in aqueous solutions by nanofiltration: experimental results and modeling, *Separation and Purification Technology*, **15**, 181-187.

Mohammed, T. J., Hashim, M., Eman, H. Z. and Abideen, A. L., 2007. Treatment of Oily Wastewater, *Engineering & Technology,* **25** 407-421.

Mohapatra, P., Samantaray, S. and Parida, K. M., 2005. Photocatalytic Reduction of Hexavalent Chromium in Aqueous Solution over Sulphate Modified Titania, *Journal of Photochemistry and Photobiology A: Chemistry*, **170** 189-194.

Monash, P. and Pugazhenthi, G., 2010. Investigation of Equilibrium and Kinetic Parameters of Methylene Blue Adsorption onto MCM-41, *Korean Journal of Chemical Engineering*, **27** 1184-1191.

Monash, P. and Pugazhenthi, G., 2011. Development of Ceramic Supports Derived from Low-Cost Raw Materials for Membrane Applications and its Optimization Based on Sintering Temperature, *International Journal of Applied Ceramic Technology*, **8** 227-238.

Monash, P. and Pugazhenthi, G., 2011. Effect of TiO_2 Addition on the Fabrication of Ceramic Membrane Supports: A Study on the Separation of Oil Droplets and Bovine Serum Albumin (BSA) from its Solution, *Desalination*, **279** 104-114.

Mulder M., 1991, Basic Principles of Membrane Technology, Kluwer Academic Publishers, Dordrecht.

Muthukrihna, M. and Guha, B. K., 2008. Effect of pH on Rejection of Hexavalent Chromium by Nanofiltration, *Desalination*, **219** 171-178.

Namasivayam, C. and Yamuna, R. T., 1995. Adsorption of Cr (VI) by a Low Cost Adsorbent: Biogas Residual Slurry, *Chemosphere*, **30** 561-578.

Nandi, B. K., Uppaluri, R. and Purkait, M. K., 2008. Preparation and Characterization of Low Cost Ceramic Membranes for Micro-Filtration Applications, *Applied Clay Science*, **42** 102-110.

Nataraj, S. K., Hosamani, K. M. and Aminabhav, T. M., 2007. Potential Application of an Electrodialysis Pilot Plant Containing Ion-Exchange Membranes in Chromium Removal, *Desalination,* **217,** 181-190.

Nazzal, F. F. and Wiesner, M. R., 1994. pH and Ionic Strength Effects on the Performance of Ceramic Membranes in Water Filtration, *Journal of Membrane Science*, **93** 91-103.

Neelakandan, C., Pugazhenthi, G. and Kumar, A., 2003. Preparation of NOx Modified PMMA-EGDM Composite Membrane for the Recovery of Cromium (VI), *European Polymer Journal*, **39** 2383-2391.

Nishiyama, N., Koide, A., Egashira, Y. and Ueyama, K., 1998. Mesoporous MCM-48 Membrane Synthesized on a Porous Stainless Steel Support, *Chemical Communication*, 2147-2148.

Nishiyama, N., Park, D. H., Egashira, Y. and Ueyama, K., 2003. Pore Size Distributions of Silylated Mesoporous Silica MCM-48 Membranes, *Separation and Purification Technology*, **32** 127-132.

Nishiyama, N., Park, D. H., Koide, A., Egashira, Y. and Ueyama, K., 2001. A Mesoporous Silica (MCM-48) Membrane: Preparation and Characterization, *Journal of Membrane Science*, **182** 235-244.

Noble, R. D. and Falconer, J. L., 1995. Silicate-1 Zeolite Composite Membranes, *Catalysis Today*, **25**, 209-212.

Nunes S. P., Peinemann K. V. (Eds), 2001. Membrane Technology in the Chemical Industry, Wiley-VCH Verlag GmbH.

Ochando-Pulido, J. M., Victor-Ortega, M. D. and Martínez-Ferez, A., 2015. On the Cleaning Procedure of a Hydrophilic Reverse Osmosis Membrane Fouled by Secondary-Treated Olive Mill Wastewater, *Chemical Engineering Journal*, **260,** 142-151.

Oh, Y., Lee, S., Elimelech, M., Lee, S. and Hong, S., 2014. Effect of Hydraulic Pressure and Membrane Orientation on Water Flux and Reverse Solute Flux in Pressure Assisted Osmosis, *Journal of Membrane Science*, **465** 159-166.

Okubo, T., Haruta, K., Kusakabe, K. and Morooka, S., 1991. Preparation of a Sol-Gel Derived Thin Membrane on a Porous Ceramic Hollow Fiber by the Filtration Technique, *Journal of Membrane Science*, **59** 73-80.

Oonkhanond, B. and Mullins, M. E., 2001. The Preparation and Analysis of Zeolite ZSM-5 Membranes on Porous Alumina Supports, *Journal of Membrane Science*, **194** 3-13.

Pabby, A. K., Rizvi, S. S. and Sastre, A. M. (Eds.), 2008. Handbook of Membrane Separations: Chemical, Pharmaceutical, Food, and Biotechnological Applications. CRC press 3-40.

Pan, X. L., Stroh, N., Brunner, H., Xiong, G. X., Sheng, S. S., 2003. Deposition of Sol-Gel Derived Membranes on α-Al_2O_3 Hollow Fibers by a Vacuum-Assisted Dip-Coating Process, *Journal of Membrane Science*, **226**, 111-118.

Parks, G. A., 1965. The Isoelectric Points of Solid Oxides, Solid Hydroxides, and Aqueous Hydroxo Complex Systems, *Chemical Review*, **65** 177-198.

Parmar, N., Upadhyay, K., 2013. Treatability Study of Pharmaceutical Wastewater by Coagulation Process, *International Journal of Chem Tech Research*, **5**, 2278-2283.

Patterson, V. A, Krieg, H. M, Kriek, R. J. and Bisset, H., 2006. Direct Synthesis of a Titania Membrane on a Centrifugally Casted Tubular Ceramic Support, *Journal of Membrane Science*, **285** 1-3.

Pechar, F. and Rykl, D., 1983. A Complex Study of Vibrational Spetra of Natural Analcime, *Chemical Papers,* **6** 757-765.

Pedernera, M., Iglesia, O. de la, Mallada, R., Lin, Z., Rocha, J., Coronas, J. and Santamaria, J., 2009. Preparation of Stable MCM-48 Tubular Membranes, *Journal of Membrane Science*, **326** 137-144.

Peeters, J. M. M., Boom, J. P., Mulder, M. H. V. and Strathmann, H., 1998. Retention measurements of nanofiltration membranes with electrolyte solutions, *Journal of Membrane Science*, **145** 199-209.

Porter, M. C., 1989, Handbook of Industrial Membrane Technology, Noyes Publications, Westwood, New Jersey, U.S.A.

Potdar, A., Shukla, A. and Kumar, A., 2002. Effect of Gas Phase Modification of Analcime Zeolite Composite Membrane on Separation of Surfactant by Ultrafiltration, *Journal of Membrane Science*, **210** 2009-225.

Praptowidodo, V. S., 2005. Influence of Swelling on Water Transport through PVA-Based Membrane, *Journal of Molecular Structure*, **739**, 207-212.

Pugazhenthi, G., Sachan, S., Kishore, N. and Kumar, A., 2005. Separation of Chromium (VI) using Modified Ultrafiltration Charged Carbon Membrane and its Mathematical Modeling, *Journal of Membrane Science*, **254** 229-239.

Qi, H., Fan, Y., Xing, W. and Winnubst, L., 2010. Effect of TiO_2 Doping on the Characteristics of Macroporous Al_2O_3/TiO_2 Membrane Supports, *Journal of European Ceramic Society*, **30** 1317-1325.

Qin, Q., Ma, J. and Liu, K., 2009. Adsorption of Anionic Dyes on Ammonium-Functionalized MCM-41, *Journal of Hazardous Materials*, **162** 133-139.

Reed, J. S., 1989. Introduction to the Principles of Ceramic Processing, Wiley, New York.

Religa, P., Kowalik, A. and Gierycz, P., 2011. Application of Nanofiltration for Chromium Concentration in the Tannery Wastewater, *Journal of Hazardous Materials*, **186** 288-292.

Ren, X., Zhao, C., Du, S., Wang, T., Luan, Z., Wang, J. and Hou, D., 2010. Fabrication of Asymmetric Poly (m-Phenylene Isophthalamide) Nanofiltration Membrane for Chromium (VI) Removal, *Journal of Environmental Science*, **22** 1335-1341.

Sachdeva, S. and Kumar, A., 2008. Synthesis and Modeling of Composite Poly (Styrene-Co-Acrylonitrile) Membrane for the Separation of Chromic Acid, *Journal of Membrane Science*, **307** 37-52.

Sacmaci, S., Kartal, S., Yilmaz, Y., Sacmaci, M. and Soykan, C., 2012. A new Chelating Resin: Synthesis, Characterization and Application for Speciation of Chromium (III)/ (VI) Species, *Chemical Engineering Journal*, **181-182** 746-753.

Saffaj, N., Alami Younssi, S., Albizane, A., Messouadi, A., Bouhria, M., Persin, M., Cretin, M., Larbot A., 2004. Elaboration and Properties of TiO_2-$ZnAl_2O_4$ Ultrafiltration Membranes Deposited on Cordierite Support, *Separation and Purification Technology,* **36**, 107-114.

Sahinkaya, E., Altun, M., Bektas, S. and Komnitsas, K., 2012. Bioreduction of Cr (VI) from Acidic Wastewaters in a Sulfidogenic ABR, *Minerals Engineering,* **32** 38-44.

Sakamoto, Y., Kaneda, M., Terasaki, O., Zhao, D. Y., Kim, J. M., Stucky, G., Shin, H. J. and Ryoo, R., 2000. Direct Imaging of the Pores and Cages of Three-Dimensional Mesoporous Materials, *Nature*, **408** 449-453.

Salgado-Gómez, N., Macedo-Miranda, M. G. and Olguín, M. T., 2014. Chromium VI Adsorption from Sodium Chromate and Potassium Dichromate Aqueous Systems by Hexadecyltrimethylammonium-Modified Zeolite-Rich Tuff, *Applied Clay Science,* **95** 197-204.

Sanchez, J. and Rivas, B. L., 2011. Cationic Hydrophilic Polymers Coupled to Ultrafiltration Membranes to Remove Chromium (VI) from Aqueous Solution, *Desalination*, **279** 338-343.

Sarma, A. and Battacharya, K. G., 2005. Adsorption of Chromium (VI) on Azadirachta Indica (Neem) Leaf. Powder, *Adsorption*, 1**0** 327-338.

Sato, K., Sugimoto, K., and Nakane, T., 2008. Synthesis of Industrial Scale NaY Zeolite Membranes and Ethanol Permeating Performance in Pervaporation and Vapor Permeation up to 130 °C and 570 kPa, *Journal of Membrane Science*, **310** 161-173.

Sato, K., Sugimoto, K., Sekine, Y., Takada, M., Matsukata, M. and Nakane, T., 2007. Application of FAU-type Zeolite Membranes to Vapor/Gas Separation Under High Pressure and High Temperature upto 5 MPa and 180 °C, *Microporous and Mesoporous Materials*, **101** 312-318.

Schaep, J., Bruggen, B. V. D., Vandecasteele, C. and Wilms, D., 1998. Influence of ion size and charge in nanofiltration, *Separation and Purification Technology*, **14** 155-162.

Schumacher, K., Grün, M. and Unger, K. K., 1999. Novel Synthesis of Spherical MCM-48, *Microporous and Mesoporous Materials*, **27** 201-206.

Seshadri, S. K. and Lin, Y. S., 2011. Synthesis and Water Vapor Separation Properties of Pure Silica and Aluminosilicate MCM-48 Membranes, *Separation and Purification Technology*, **76** 261-267.

Shukla, A. and Kumar, A., 2004. Analysis of Separation of Chromic Acid by Zeolite-Clay Composite Membrane using Space-Charge Model, *Journal of Membrane Science*, **237** 119-130.

Shukla, A. and Kumar, A., 2005. Characterization of Chemically Modified Zeolite-Clay Composite Membranes using Separation of Trivalent Cations, *Separation and Purification Technology*, **41** 83-89.

Shukla, A. and Kumar, A., 2007. Separation of Cr (VI) by Zeolite-Clay Composite Membranes Modified by Reaction with NOx, *Separation and Purification Technology*, **52** 423-429.

Silva, M. M. F., Oliveira, M. M., Avelino, M. C., Fonseca, M. G., Almeida R. K.S. and Filho, E. C. S., 2012. *Chemical Engineering Journal,* **203** 259-268.

Sondhi, R. Lin, Y. S. and Alvarez, F., 2000. Crossflow Filtration of Chromium Hydroxide Suspension by Ceramic Membranes: Fouling and its Minimization by Backpulsing, *Journal of Membrane Science*, **174** 111-122.

Stuart, B. H., 2004. Infrared Spectroscopy: Fundamentals and Applications, John Wily & Sons, England, ch. 3, pp. 46-47.

Su, F., Lu, C., Kuo, S. C. and Zeng, W., 2010. Adsorption of CO_2 on Amine-Functionalized Y-type Zeolites, *Energy Fuels*, **24** 1441-1448.

Takagi, R., Larbot, A., Cot, L. and Nakagaki, M., 2000. Effect of Al_2O_3 Support on Electrical Properties of TiO_2/Al_2O_3 Membrane Formed by Sol-Gel Method, *Journal of Membrane Science*, **177** 33-40.

Tansel, B., Sager, J., Rector, T., Garland, J., Strayer, R. F., Levine, L., Roberts, M., Hummerick, M. and Bauer, J., 2006. Significance of hydrated radious and hydration shells on ionic permeability during nanofiltration in dead end and cross flow modes, *Separation and Purification Technology*, **51** 40-47.

Treacy, M. M. J. and Higgins, J. B., 2007. Collection of Simulated XRD Powder Diffraction Pattern for Zeolites, fifth revised ed., Elsevier, Amsterdam.

Udayakumar, S., Pandurangan, A. and Sinha, P. K., 2005. Mesoporous Material as Catalyst for the Production of Fine Chemical: Synthesis of Dimethyl Phthalate Assisted by Hydrophobic nature MCM-41, *Journal of Molecular Catalyst A: Chemical*, **240** 139-154.

Vasanth, D., Pugazhenthi, G. and Uppaluri, R., 2011. Fabrication and Properties of Low Cost Ceramic Microfiltration Membranes for Separation of Oil and Bacteria from its Solution, *Journal of Membrane Science*, **379** 154-163.

Vasanth, D., Pugazhenthi, G. and Uppaluri, R., 2012. Biomass Assisted Microfiltration of Chromium (VI) using Baker's Yeast by Ceramic Membrane Prepared from Low Cost Raw Materials, *Desalination*, **285** 239-244.

Wang, Y. H., Zhang, Y., Liu, X. Q. and Meng, G. Y., 2006. Microstructure Control of Ceramic Membrane Support from Corundum-Rutile Powder Mixture, *Powder Technology,* **168** 125-133.

Wang, Z., Ma, J. and Wang, P., 2011. Optimization of Membrane Structure using the Spin-Coating Method, *Desalination and Water Treatment*, **34** 197-203.

Weh, K., Noack, M., Hoffmann, K., Schroder, K.-P. and Caro, J., 2002. Change of Gas Permeation by Photoinduced Switching of Zeolite-Azobenzene Membranes of type MFI and FAU, *Microporous and Mesoporous Materials*, **54** 15-26.

Wirawan, S. K., Creaser, D., Lindmark, J., Hedlund, J., Bendiyasa, M. and Sediawan, W., B., 2011. H_2/CO_2 Permeation through a Silicalite-1 Composite Membrane, *Journal of Membrane Science*, **375** 313-322.

Wirnsberger, G., Scott, B. J. and Stucky, G. D., 2001. pH Sensing with Mesoporous Thin Films, *Chemical Communication*, 119-120.

Workneh, S. and Shukla, A., 2008. Synthesis of Sodalite Octahydrate Zeolite-Clay Composite Membrane and its use in Separation of SDS, *Journal of Membrane Science*, **309** 189-195.

Wu, S., Yang, J., Lu, J., Zhou, Z., Kong, C. and Wang, J., 2008. Synthesis of Thin and Compact Mesoporous MCM-48 Membrane on Vauum-Coated α-Al_2O_3 Tube, *Journal of Membrane Science*, **319** 231-237.

Yan, Y., Davis, M. E. and Gavalas, G. E., 1997. Preparation of Highly Selective Zeolite ZSM-5 Membranes by a Post-Synthetic Coking Treatment, *Journal of Membrane Science*, **123** 95-103.

Zhang, C., Hong, Z., Chen, J., Gu, X., Jin, W. and Xu, N., 2012. Catalytic MFI Zeolite Membranes Supported on α-Al_2O_3 Substrates for m-Xylene Isomerization, *Journal of Membrane Science*, **389** 451-458.

Zhu, G., Li, Y., Zhou, H., Liu, J. and Yang, W., 2008. FAU-type Zeolite Membranes Synthesized by Microwave Assisted in Situ Crystallization, *Materials Letters*, **62** 4357-4359.

Zhu, G., Li, Y., Zhou, H., Liu, J. and Yang, W., 2009. Microwave Synthesis of High Performance FAU-type Zeolite Membranes: Optimization, Characterization and Pervaporation Dehydration of Alcohols, *Journal of Membrane Science,* **337** 47-54.

List of Publications

International Journals:

1. Ashim Kumar Basumatary, R. Vinoth Kumar, Aloke Kumar Ghoshal and G. Pugazhenthi, Synthesis and characterization of MCM-41-ceramic composite membrane for the separation of chromic acid from aqueous solution, **Journal of Membrane Science**, 475 (2015) 521-532.

2. R. Vinoth Kumar, Ashim Kumar Basumatary, Aloke Kumar Ghoshal and G. Pugazhenthi, Performance assessment of analcime-C zeolite-ceramic composite membrane by separation of Cr (VI) from aqueous solution, **RSC Advances**, 5 (2015) 6246-6254.

3. Ashim Kumar Basumatary, P. Vikram Singh, R. Vinoth Kumar, Aloke Kumar Ghoshal and G. Pugazhenthi, Development and characterization of MCM-48 ceramic composite membrane for the removal of Cr (VI) from aqueous solution, **ASCE Journal of Environmental Engineering**, 0733-9372 (2015) C4015013-11.

4. Ashim Kumar Basumatary, Aloke Kumar Ghoshal and G. Pugazhenthi, Performance assessment of MCM-48 ceramic composite membrane by separation of $AlCl_3$ from aqueous solution, **Ecotoxicology and Environmental Safety** (In Press).

5. Ashim Kumar Basumatary, Partha Pratim Adhikari, Aloke Kumar Ghoshal and G. Pugazhenthi, Fabrication and performance evaluation of Faujasite (FAU) zeolite composite ultrafiltration membrane by separation of trivalent ions from aqueous solution, **Environmental Progress & Sustainable Energy** (Revised Manuscript Submitted).

6. Ashim Kumar Basumatary, R. Vinoth Kumar, Aloke Kumar Ghoshal and G. Pugazhenthi, Cross flow Ultrafiltration of Cr (VI) using MCM-41, MCM-48 and Faujasite (FAU) zeolite ceramic composite membranes, **Chemosphere** (Revised Manuscript Submitted).

7. Ashim Kumar Basumatary, Kunal Pant, R. Vinoth Kumar, Aloke Kumar Ghoshal and G. Pugazhenthi, Ceramic supported Faujasite (FAU) zeolite composite membrane for the

removal of Cr (VI) from aqueous solution, **Chemical Engineering Research and Design** (Under Review).

8. Ashim Kumar Basumatary, Aloke Kumar Ghoshal and G. Pugazhenthi, Removal of $FeCl_3$ from aqueous solution by ultrafiltration using mesoporous MCM-48 ceramic composite membrane, **Separation Science and Technology** (Under Review).

9. Ashim Kumar Basumatary, R. Vinoth Kumar and G. Pugazhenthi, Removal of trivalent metal ions from aqueous solution via crossflow ultrafiltration system using zeolite membranes, **Asia-Pacific Journal of Chemical Engineering**, (Under Review).

10. Ashim Kumar Basumatary, R. Vinoth Kumar, Partha Pratim Adhikari, Aloke Kumar Ghoshal and G. Pugazhenthi, Ultrafiltration of $FeCl_3$ from aqueous solution using MCM-41 ceramic composite membrane, **Journal of Membrane Science and Research**, (Under Review).

Conferences:

1. Ashim Kumar Basumatary, Partha Pratim Adhikari, A. K. Ghoshal and G. Pugazhenthi, Removal of $AlCl_3$ from Aqueous Solution with MCM-41-Ceramic Composite Membrane**, National Conference on Sustainable Development of Environmental Systems,** 20-21 June 2014, IIT Guwahati, Assam, India.

2. Ashim Kumar Basumatary, A. K. Ghoshal and G. Pugazhenthi, Performance Assessment of MCM-48 Ceramic Composite Membrane by Separation of $AlCl_3$ from Aqueous Solution, **International Conference on Green Technology for Environmental Pollution Prevention and Control (ICGTEPC 2014),** 27-29 September 2014, National Institute of Technology Tiruchirappalli (NITT), India.

3. Ashim Kumar Basumatary, Partha Pratim Adhikari, A. K. Ghoshal and G. Pugazhenthi, Development and Performance Evaluation of MCM-41-Ceramic Composite Membrane by Separation of $AlCl_3$ from Aqueous Solution, **International Conference on Advances in Chemical Engineering & Technology (ICACE '14)**, 16-18 October 2014, Thangal Kunju Musaliar College of Engineering, Kollam, Kerala.

4. Ashim Kumar Basumatary, Partha Pratim Adhikari, R. Vinoth Kumar, A. K. Ghoshal and G. Pugazhenthi, Synthesis of FAU-type Inorganic Ultrafiltration Membrane, **National Seminar on Recent trends in Fundamental and Applied Chemical Sciences (RTFACS-2014)**, 19-21 November 2014, Department of Chemistry, Dibrugarh University, Dibrugarh, Assam.

5. Ashim Kumar Basumatary, A. K. Ghoshal and G. Pugazhenthi, Preparation and Evaluation of MCM-48 Ceramic Composite Membrane by Separation of $FeCl_3$ from Aqueous Solution, **Frontiers in Chemical Sciences (FICS 2014),** 4-6 December 2014, IIT Guwahati, Assam.

6. Ashim Kumar Basumatary, R. Vinoth Kumar, Partha Pratim Adhikari, Aloke Kumar Ghoshal and G. Pugazhenthi, Ultrafiltration of $FeCl_3$ from aqueous solution using MCM-41 ceramic composite membrane, **International Conference on Environment (ICENV 2015),** Penang, Malaysia, 18-19 August 2015.